Interfacial rheology of polymers in the molten state/ experimental and fundamental aspects

Younes El Omari

N°d'ordre NNT : 2022ISAL0109

THESE de DOCTORAT DE L'INSA LYON,
Membre de l'Université de Lyon

Ecole Doctorale N° 34
Ecole Doctorale de Matériaux de Lyon

Spécialité/ discipline de doctorat : Matériaux Polymères

Soutenue publiquement le 02/12/2022, par :
Younes EL OMARI

Interfacial rheology of polymers in the molten state/ experimental and fundamental aspects

---

Devant le jury composé de :

ANDERSON Patrick	Professor (Université de Technologie d'Eindhoven)	Rapporteur
BENYAHIA Lazhar	Professeur (Université du Maine)	Rapporteur
EL KISSI Nadia	Directrice de Recherche, HDR (Université Grenoble Alpes)	Examinatrice
MARCHAL Philippe	Ingénieur de recherche, HDR (Université de Lorraine)	Examinateur
MAAZOUZ Abderrahim	Professeur (INSA LYON)	Directeur de thèse
DUCHET-RUMEAU Jannick	Professeur (INSA LYON)	Co-Directrice de thèse
YOUSFI Mohamed	Maître de conférences (INSA LYON)	Co-Encadrant

Département FEDORA – INSA Lyon - Ecoles Doctorales

SIGLE	ECOLE DOCTORALE	NOM ET COORDONNEES DU RESPONSABLE
CHIMIE	CHIMIE DE LYON https://www.edchimie-lyon.fr Sec. : Renée EL MELHEM Bât. Blaise PASCAL, 3e étage secretariat@edchimie-lyon.fr	M. Stéphane DANIELE C2P2-CPE LYON-UMR 5265 Bâtiment F308, BP 2077 43 Boulevard du 11 novembre 1918 69616 Villeurbanne directeur@edchimie-lyon.fr
E.E.A.	ÉLECTRONIQUE, ÉLECTROTECHNIQUE, AUTOMATIQUE https://edeea.universite-lyon.fr Sec. : Stéphanie CAUVIN Bâtiment Direction INSA Lyon Tél : 04.72.43.71.70 secretariat.edeea@insa-lyon.fr	M. Philippe DELACHARTRE INSA LYON Laboratoire CREATIS Bâtiment Blaise Pascal, 7 avenue Jean Capelle 69621 Villeurbanne CEDEX Tél : 04.72.43.88.63 philippe.delachartre@insa-lyon.fr
E2M2	ÉVOLUTION, ÉCOSYSTÈME, MICROBIOLOGIE, MODÉLISATION http://e2m2.universite-lyon.fr Sec. : Bénédicte LANZA Bât. Atrium, UCB Lyon 1 Tél : 04.72.44.83.62 secretariat.e2m2@univ-lyon1.fr	Mme Sandrine CHARLES Université Claude Bernard Lyon 1 UFR Biosciences Bâtiment Mendel 43, boulevard du 11 Novembre 1918 69622 Villeurbanne CEDEX sandrine.charles@univ-lyon1.fr
EDISS	INTERDISCIPLINAIRE SCIENCES-SANTÉ http://ediss.universite-lyon.fr Sec. : Bénédicte LANZA Bât. Atrium, UCB Lyon 1 Tél : 04.72.44.83.62 secretariat.ediss@univ-lyon1.fr	Mme Sylvie RICARD-BLUM Institut de Chimie et Biochimie Moléculaires et Supramoléculaires (ICBMS) - UMR 5246 CNRS - Université Lyon 1 Bâtiment Raulin - 2ème étage Nord 43 Boulevard du 11 novembre 1918 69622 Villeurbanne Cedex Tél : +33(0)4 72 44 82 32 sylvie.ricard-blum@univ-lyon1.fr
INFOMATHS	INFORMATIQUE ET MATHÉMATIQUES http://edinfomaths.universite-lyon.fr Sec. : Renée EL MELHEM Bât. Blaise PASCAL, 3e étage Tél : 04.72.43.80.46 infomaths@univ-lyon1.fr	M. Hamamache KHEDDOUCI Université Claude Bernard Lyon 1 Bât. Nautibus 43, Boulevard du 11 novembre 1918 69 622 Villeurbanne Cedex France Tél : 04.72.44.83.69 hamamache.kheddouci@univ-lyon1.fr
Matériaux	MATÉRIAUX DE LYON http://ed34.universite-lyon.fr Sec. : Yann DE ORDENANA Tél : 04.72.18.62.44 yann.de-ordenana@ec-lyon.fr	M. Stéphane BENAYOUN Ecole Centrale de Lyon Laboratoire LTDS 36 avenue Guy de Collongue 69134 Ecully CEDEX Tél : 04.72.18.64.37 stephane.benayoun@ec-lyon.fr
MEGA	MÉCANIQUE, ÉNERGÉTIQUE, GÉNIE CIVIL, ACOUSTIQUE http://edmega.universite-lyon.fr Sec. : Stéphanie CAUVIN Tél : 04.72.43.71.70 Bâtiment Direction INSA Lyon mega@insa-lyon.fr	M. Jocelyn BONJOUR INSA Lyon Laboratoire CETHIL Bâtiment Sadi-Carnot 9, rue de la Physique 69621 Villeurbanne CEDEX jocelyn.bonjour@insa-lyon.fr
ScSo	ScSo* https://edsciencessociales.universite-lyon.fr Sec. : Mélina FAVETON INSA : J.Y. TOUSSAINT Tél : 04.78.69.77.79 melina.faveton@univ-lyon2.fr	M. Bruno MILLY Université Lumière Lyon 2 86 Rue Pasteur 69365 Lyon CEDEX 07 bruno.milly@univ-lyon2.fr

*ScSo : Histoire, Géographie, Aménagement, Urbanisme, Archéologie, Science politique, Sociologie, Anthropologie

Remerciements

Je souhaite exprimer ma sincère gratitude envers de nombreuses personnes qui m'ont apporté leur aide et leur soutien tout au long de ma thèse durant les trois dernières années.

Je tiens à exprimer ma sincère reconnaissance envers mes encadrants, le Prof. Abderrahim Maazouz, le Prof. Jannick Duchet Rumeau et le Dr. Mohamed Yousfi dont l'aide et les conseils ont été indispensables pour la réalisation de cette thèse. Leur soutien constant et leur **imp**lication ont été des éléments clés de sa réussite. J'ai eu la chance d'être membre de leur groupe de recherche. Les discussions avec eux m'ont toujours donné des inspirations pour aller de l'avant.

Je souhaiterai remercier les membres du jury chargés d'évaluer mes travaux de thèse, en particulier Messieurs Lazhar Benyahya et Patrick Anderson, en leurs qualité de rapporteurs, ainsi que Madame Nadia EL Kissi et Monsieur Philipe Marchal, examinateurs. Merci à eux pour leur temps consacré à la lecture de ce manuscrit, mais aussi pour les discussions intéressantes qui ont suivi la soutenance de cette thèse.

Je remercie le Ministère français de l'enseignement supérieur, de la Recherche et de l'innovation (MESRI) pour le financement de ce projet.

Du côté du laboratoire, je souhaite remercier l'ensemble du personnel, permanent et non permanent. Plus particulièrement Isabelle, Mallou, Sylvain, Fernande, Laura, Vivien et Raph pour leur sympathie et leur assistance dans diverses problématiques organisationnelles et techniques.

Plus directement, ceux sans qui l'aventure de la thèse serait bien fade : les doctorants, les post-doctorants, et les amis qu'on se fait, qui restent, et qu'on veut toujours garder.

A mes co-bureaux bien aimés, Liutong (LT), Yiping (Bro), Celso (Ciyealso) et Raissa (The president) : merci pour votre soutien quotidien, votre écoute bienveillante et votre amitié en or.

Merci aux **IMP**otes :

Merci Charlotte pour ta positivité et pour ton amour du fromage.

Merci Laurent pour toutes les invitations, les jeux de société mais aussi pour m'avoir appris l'expression « c'est moche ! ».

Gam sa hap ni da Morgane pour toutes les longues discussions sur les coréens et sur la rhéologie interfaciale. Merci pour les petits morceaux joués à la guitare (Way Back Home & Without You).

Muito obrigado Gabriel pour être un frère. Merci d'avoir été un excellent partenaire à la salle de sport. Merci pour toutes les discussions intéressantes et pour ta passion pour la chimie.

Merci à mon équipe de foot du laboratoire : Raouhi, Mathieu, Théophile, Barthélemy, Gabriel, Celso et Okba. Merci pour les bonnes passes que j'ai traduit en superbes buts.

Je remercie également les nouveaux doctorants et post-docs. Un merci particulier à Camille pour sa gentillesse, son aide pendant la période de la soutenance et pour ses corrections de mon français.

Merci pour les bons moments passés ensemble au laboratoire, mais aussi en dehors (WE **IMP**, **goûters, …)**.

C'est aussi le moment d'avoir une pensée pour ceux qui nous ont quittés. Ma tante Mireille et mes grand-mères Khayti et Hemma. Vous me manquez énormément.

Je terminerai en remerciant mes amis, ma famille en France (Aziz, Myriam, Mehdi, Guillaume et Rose), au Maroc, mes parents Najat et Bouazza et mon frère Achraf et ma sœur Imane. Merci d'avoir toujours cru en moi.

Encore, je vous remercie sincèrement pour tout !

Amicalement

Younes EL OMARI

Résumé

Les travaux de cette thèse portent sur la rhéologie interfaciale en cisaillement et en dilatation/compression de systèmes polymères. Dans un premier temps, notre choix a porté sur l'étude de systèmes modèles à base de PIB poly (isobutylene) et PDMS poly (dimethylsiloxane). Ces polymères présentent l'avantage d'être liquides à température ambiante. Les propriétés de surface et d'interface ont été sondées à l'aide d'une nouvelle cellule interfaciale développée pendant ce projet. Elle présente l'avantage de réaliser des mesures à des températures élevées pouvant atteindre 200°C. L'effet de la masse molaire et de la température sur les propriétés interfaciales ont été étudiées selon les régimes, permanent et oscillatoire. Ces études ont été transposées ensuite sur des polymères semi-cristallins fondus tels que le PEG poly (éthylène glycol) et le PCL poly(caprolactone). Dans un deuxième temps, nous avons étudié et analysé les propriétés rhéologiques interfaciales en élongation des systèmes modèles, au moyen de la rhéologie interfaciale en dilatation / compression en utilisant la méthode de la goutte pendante oscillante. De plus, la relaxation des surfaces / interfaces a été sondée par la méthode de « pulse », d'une part, et en utilisant un rhéomètre extensionnel à rupture capillaire (CaBER), d'autre part. Les grandeurs rhéologiques interfaciales en élongation/compression des systèmes modèles de différentes masses molaires et sous différentes températures ont été obtenues. Elles ont ensuite été comparées à celles mesurées en cisaillement et analysées selon le rapport de Trouton interfacial. Dans la dernière partie de la thèse, nous avons montré que la rhéologie interfaciale en cisaillement permet de sonder les réactions chimiques aux interfaces d'un système polymère fondu : PEgMA, Poly (Ethylène Greffé Anhydride Maléique) / PDMS-($PropNH_2$)$_2$, Poly (DiMethyl Siloxane, terminé Amino Propyle). En outre, l'étude de la tension interfaciale dynamique a permis le suivi de la cinétique de la réaction interfaciale des systèmes réactifs de différentes masses molaires et à différentes températures. Enfin les études de rhéologie interfaciale s'avèrent très pertinentes pour sonder *in-situ* les interfaces et/ou interphases de systèmes polymères liquides. Les méthodologies ainsi établies et utilisées sont très innovantes et font sauter des verrous scientifiques et technologiques majeurs.

Mots clés : polymères liquides, surface, interface, rhéologie interfaciale, bicone, goutte pendante oscillante.

Abstract

The work of this thesis deals with the interfacial rheology in shear and in extension of polymeric systems. Initially, we chose to study model systems based on PIB poly (isobutylene) and PDMS poly (dimethylsiloxane). These polymers have the advantage of being liquid at room temperature. For this purpose, a cell for measuring interfacial properties has been developed in our laboratory. It allows to study the surface and interface properties at high temperatures up to 200 °C. Thus, we were able to study the interfacial properties according to the steady and oscillatory regime of these model systems by highlighting the influence of the molar mass and the temperature. These studies were then transposed to semi-crystalline molten polymers such as PEG poly (ethylene glycol) and PCL poly (caprolactone). In a second step, we studied and analyzed the interfacial elongational rheological properties of the model systems, by means of interfacial dilational rheology via the oscillating pendant drop method. In addition, the relaxation of surfaces / interfaces was studied by the "pulse" method and using the capillary breakup extensional rheometer (CaBER). The interfacial rheological quantities in elongation of model systems of different molar masses and under different temperatures were obtained. They were then compared with those measured in shear and analyzed according to the interfacial Trouton ratio. In the last part of the thesis, we have shown that the interfacial shear rheology allows to probe the chemical reaction at the interfaces of a polymeric melt system : PEgMA Poly (Ethylene Grafted Maleic Anhydride) / PDMS-(PropNH_2)$_2$, Poly (Dimethyl Siloxane Amino Propyl terminated). In addition, the study of the dynamic interfacial tension allowed the monitoring of the kinetics of the interfacial reaction of the reactive systems of different molar masses and at different temperatures. Finally, the studies of interfacial rheology are very relevant to probe *in-situ* the interfaces and/or interphases of molten polymer systems. The methodologies thus established and used are very innovative and overcome major scientific and technological barriers.

Keywords: liquid polymers, surface, interface, interfacial rheology, bicone, oscillating pendant drop.

Table of Contents

List of Figures

List of Tables

General Introduction

Nowadays, polymers have become the most ubiquitous materials in different fields such as electronics, aeronautics, automotive technology and biomedical applications. They are often assembled with other polymers and additives in the molten state to design new products with improved functional properties. Thus, the study of multiphase polymer/polymer systems has garnered a great deal of interest over the last few decades, covering a broad segment of research in both the academic and industrial communities. These systems can be polymer blends, coextruded multilayer films, foams or emulsions. All of these entities have the ability to organise and form multi-scale structures during their development. This often takes place in the molten state, under high temperatures and/or under radiation (laser, UV, etc.).

The surface (air/polymer) and interface (polymer/polymer) might sometimes behave differently from the bulk; their properties can affect the whole system and thus change the final properties in a straightforward manner. The interface or surface can be characterised by its "interfacial tension," but this is not the only interfacial property. The interface could have its own response to an applied stress or strain, depending on the nature of the deformation (shear or dilation/compression). It can be viscous, elastic or viscoelastic. In other words, we are referring to the interfacial rheology. This particular branch of rheology is a direct way of probing interfaces.

Interfaces and surfaces of high flow-rate liquid systems (emulsions, foams, etc.) have been the subject of studies in many fields, but molten polymer/polymer interfaces have not been studied before. This thesis project aimed to apply the basics of interfacial rheology to investigate the interfacial properties of melt polymer systems. This has required an understanding of the theoretical aspects of interfacial rheology, as well as an adaptation of the existing measuring tools and the development of a new setup to make this measurement possible. All of these issues have been systematically studied in this PhD thesis.

In Chapter I, we provide an overview of the theoretical basics of interfacial rheology. First, we start with interfacial shear rheology. To perform this type of measurement, a special geometry is placed at the interface. We are particularly interested in the Double Wall Ring (DWR), the bicone, the Du Noüy ring and the oscillating needle (ISR). The measurement requires a consideration of the bulk contributions to the measured stress. Therefore, we have highlighted the methodologies used to correct the apparent data. Second, we report the theory and principle of the interfacial dilational rheology. Here the surface/interface is stretched or compressed by changing the volume of a coexisting phase, or mechanically by using a particular tool. The Langmuir trough method, the oscillating spinning drop and the oscillating pendant drop techniques are investigated. Some pioneering works on interfacial shear and dilational rheology in the literature are also presented. On the other hand, the limit of each technique is also given, and the possibility of using it to study polymer/polymer interfaces is critiqued

in this chapter. This bibliographic review has been published recently in "**Polymers**" (http://dx.doi.org/10.3390/polym14142844).

Chapter II is dedicated to the study of the interfacial shear rheology of different polymer systems. The bicone and the Double Wall Ring (DWR) geometries are the most common interfacial rheological setups (IRS) used in the field of rheology to measure the interfacial viscoelastic properties. However, performing interfacial measurements on melt polymer systems is not commonplace. In addition, in today's commercial rheometers, interfacial experiments must be made below 70 °C to ensure a stable, homogeneous temperature at the interface. On the other hand, the limitations of the current IRS devices, such as the high inertia and relatively low Boussinesq number of the bicone geometry, as well as the mechanical fragility of the DWR, do not allow the probing of the interfaces of highly viscous systems in the molten state. For these reasons, a new interfacial biconical setup has been developed. A novel high-temperature heating system was added to the interfacial rheology cell, allowing interfacial rheology measurements up to 200 °C. Moreover, the current stainless steel-based biconical geometry was replaced by a lighter titanium-based one, enabling a more sensitive measurement of the interfacial rheological properties. Second, the surface/interfacial properties of various model polymers with different well-known molecular and viscoelastic characteristics have been investigated to validate this new setup. To achieve these objectives, two model polymers were chosen: poly(dimethylsiloxane) (PDMS), poly(isobutene) (PIB) and Boger fluids. The effects of molecular weight and temperature were highlighted. Finally, the interfacial rheology of molten semi-crystalline polymer systems has been characterised for the first time, using poly(caprolactone) (PCL) and poly(ethylene glycol) (PEG). The measured apparent interfacial shear properties in both oscillatory and steady flow modes were carefully corrected, considering the contribution of the bulk subphases during the treatment of the numerical data. The obtained interfacial rheological properties were interpreted based on the microscopy, the tensiometry and the modelling of the solubility parameters to understand the physical phenomena behind the interfacial property data. The main results of this chapter have been published in "***Polymer Testing***" (http://dx.doi.org/10.1016/j.polymertesting.2021.107280).

In Chapter III, the rising oscillating drop method was used to probe the interfacial and surface dilational properties of poly(isobutylene) (PIB) and poly(dimethylsiloxane) (PDMS) model polymers. First, the interfacial properties of the PIB/PDMS systems in both oscillatory and static drop experiments were measured. The apparent dilational moduli were carefully corrected, considering the inertial and viscous effects of the subphases. The effect of molecular weight and temperature on the resulting interfacial properties was also examined. The migration of PIB chains to the PDMS matrix occurred from a specific viscosity, in accordance with the data already provided in the literature. Second, the surface/interfacial elongational properties of different PIB/PDMS systems were studied as

well, and a new method was developed to extract their characteristic elongational relaxation times using a straightforward relaxation test called a "pulse." The experimental data of the evolution of surface or interfacial tension as a function of time were well fitted by a stretched exponential model. The effect of the temperature and viscosity of co-existing components on the surface/interfacial relaxation behaviour was highlighted. The data obtained by the dilational oscillating technique were compared to the surface/interfacial shear rheology and the capillary breakup extensional rheology (CaBER) method. Finally, the link between shear and dilational surface properties was investigated using the interfacial Trouton ratio relationship. The results of this chapter have been published in ***"Rheologica Acta"*** (http://dx.doi.org/10.1007/s00397-022-01364-x).

Chapter IV provides an effective rheological approach for studying the interfacial reaction of polymer systems encountered in different fields, including reactive extrusion and multilayer reactive polymers. The approach developed in this study aimed to probe reactive polymer interfaces in a direct manner and to investigate the reaction/diffusion phenomena in-situ. The present work has assessed polymer/polymer interfaces resulting from reactive molten polymers. Poly(dimethylsiloxane) trimethyl siloxy terminated, poly(dimethylsiloxane) aminopropyl terminated, and polyethylene grafted maleic anhydride (PE-g-MA) were chosen. First, the chemical reaction at the interface between the different melts was followed by different techniques such as dynamic rheology, FTIR spectroscopy and DSC. Then, the interfacial reaction was revealed by the interfacial shear rheology using a homemade and in-house-developed biconical setup. Second, the dynamic interfacial tension method was used to examine *in-situ* the extent of chemical reaction between the co-existing phases. The effect of molecular weight and temperature on the interfacial reaction kinetics was highlighted. This part of the thesis has been published in ***"Materials Today Communication"*** (https://doi.org/10.1016/j.mtcomm.2023.105640)**.**

NB: The manuscript of this thesis presents two general introductions, one in English and one in French, followed by a synthesis of major results. Then four chapters are presented in the form of publications followed by a general conclusions and perspectives in English.

Introduction générale

De nos jours, les matériaux polymères sont omniprésents dans des domaines aussi variés que l'électronique, l'aéronautique, l'automobile, le biomédical, etc. Ils sont souvent assemblés ou formulés avec d'autres polymères et additifs à l'état fondu pour concevoir de nouveaux produits avec des propriétés fonctionnelles améliorées. Ainsi, l'étude des systèmes polymère/polymère couvre actuellement une grande partie des travaux de recherche, académique et industrielle. Ces systèmes peuvent être des mélanges de polymères, des films multicouches coextrudés, des mousses ou des émulsions. Toutes ces entités ont la capacité de s'organiser et former des structures multi-échelles lors de leur élaboration. Cette structure a souvent eu lieu à l'état fondu, sous des températures élevées et/ou sous rayonnement (laser, UV, ...). Souvent, les propriétés de l'interface sont généralement caractérisées par la mesure de la tension interfaciale. En revanche, la maitrise des processus d'élaboration de ces systèmes et les propriétés fonctionnelles qui en découlent (mécaniques, thermiques, etc.) nécessite la connaissance de leurs comportements rhéologiques. En effet, l'interface est souvent sollicitée mécaniquement (cisaillement ou compression/élongation) à l'état fondu au cours d'un procédé de transformation. Une réponse rhéologique en volume n'est pas suffisante pour décrire l'ensemble du comportement rhéologique et les propriétés finales du matériau. L'étude des propriétés rhéologiques interfaciales de ces systèmes ainsi que la modélisation du lien étroit entre les paramètres physiques sous-jacents (viscosité, tension de surface, tension interfaciale, etc.) permet une meilleure compréhension des propriétés interfaciales et en masse « bulk » de ces matériaux.

La rhéologie interfaciale permet d'étudier et de sonder directement les surfaces et les interfaces en ayant son application dans différents domaines telles que la biologie, la pharmacie ou la pétrochimie…. De telles études ont été menées à l'ambiante sur des systèmes de faible viscosité. Ces études sont souvent menées selon deux concepts : i) la rhéologie interfaciale en cisaillement qui nécessite l'utilisation d'un rhéomètre équipé de cellules de mesures de géométries spécifiques (anneau à double parois, bicone, anneau Du-Nouÿ ou aiguille oscillante), ces dispositifs sont placés à la surface ou à l'interface de deux fluides. ii) La rhéologie interfaciale en dilatation / compression qui utilise la méthode de la goutte pendante/montante oscillante ou la balance de Langmuir. Les aspects théoriques de ces deux concepts de la rhéologie interfaciale seront étudiés et analysés dans le **premier chapitre** qui décrit « Etat de l'art ».

Les études des propriétés de surface/ interface à l'état liquide sont souvent basées sur des méthodes indirectes basées sur des mesures de l'angle de contact sur substrat en corrélation avec les propriétés rhéologiques. D'autres travaux se focalisent sur la modélisation rhéologique et morphologique pour remonter à la tension interfaciale (Modèle de Palierne) ou au module viscoélastique (Modèle de Lee et Park). Cependant l'extraction des propriétés interfaciales via ces

méthodes indirectes nécessitent plusieurs expériences complémentaires qui pourrait être source de l'élargissement de la barre d'erreur relative à la grandeur physique obtenue.

L'objectif majeur de ces travaux de thèse consiste en l'étude des aspects théoriques et expérimentaux de la rhéologie interfaciale en utilisant des méthodes directes pour sonder les interfaces à des systèmes polymère/polymère à l'état liquide. A cet effet des méthodologies originales seront développées. En préliminaire, une étape de développement/ adaptation des techniques de mesure (actuelles) de la rhéologie interfaciale pour les systèmes polymères à l'état liquide, a été soigneusement mise en œuvre. L'étude des interfaces en cisaillement, une nouvelle cellule de mesure sous forme de bicone a été développée, afin de réduire l'inertie de la géométrie. Cette dernière a été équipée d'un système de chauffage pouvant atteindre 200°C. En outre, la détermination des propriétés interfaciales élongationnelles a nécessité l'adaptation de la méthode de la goutte pendante/montante. Cette méthode permet de mesurer la tension de surface et interfaciale en régime statique. Aussi la viscosité et l'élasticité interfaciale en régime dynamique oscillatoire peuvent être déterminées.

Les travaux menés pour la compréhension des phénomènes interfaciaux des systèmes polymères à l'état fondu, notamment la diffusion interfaciale ou la réaction chimique aux interfaces peuvent être présentés en deux parties majeures :

La première partie concerne l'étude des surfaces/interfaces dites « vierges » sans présence de groupements chimiques réactifs aux interfaces. Cette partie est divisée en deux sous parties dont les objectifs sont les suivants :

- Etude de la rhéologie interfaciale en « Cisaillement » de systèmes polymères liquides. L'effet de la masse molaire moyenne et de la température sera élucidé. Elle est décrite comme un **deuxième chapitre** basé sur un article que nous avons publié dans le journal « Polymer Testing ».
- Etude de la rhéologie interfaciale en « dilatation/compression » de systèmes polymères fondus en faisant varier la masse molaire moyenne en masse et la température s. Cette sous partie est reportée dans le troisième **chapitre** qui a fait l'objet d'un article récemment publié dans le journal « Rheologica Acta »

L'étude a été menée sur deux grandes familles de polymères :

i) Des fluides modèles ont été étudiés à température ambiante. Ainsi un lien étroit entre les propriétés rhéologiques et interfaciales résultantes a été établi. Des polymères à base de PDMS, Poly (DiMéthyle Siloxane) et de PIB, Poly (IsoButène) de différentes masses molaires ont été choisis comme fluides modèles. Ce système PIB-PDMS a beaucoup été étudié dans la littérature, cependant, la compatibilité entre ces deux polymères fait débat. Certaines études considèrent qu'ils sont immiscibles et incompatibles. D'autres font état

d'une miscibilité partielle entre le PIB et PDMS. Quant à nous, nous avons déployé différentes méthodes pour étudier la compatibilité d'un tel système en utilisant les paramètres de solubilité, la rhéologie des mélanges, la microscopie…

ii) Systèmes polymères thermoplastiques semi-cristallins à base de PCL Poly (CaproLactone) et le PEG Poly (Ethylène Glycol) de différentes viscosités ont été sélectionnés. Ces derniers présentent l'avantage d'être stables d'avoir des températures de fusion modérées et stables aux températures légèrement plus élevées.

De tels systèmes polymère/polymère présentent la caractéristique de pouvoir créer une réaction chimique aux interfaces. Les travaux de cette partie sont reportés dans le **quatrième chapitre**. Ils font l'objet d'une publication publiée dans « Materials Today Communication ». Ainsi nous avons pu étudier et comparer les propriétés interfaciales de deux systèmes ;

i) Système non réactif de PDMS/ PEgMA (Poly Ethylène Greffé Anhydride Maléique).

ii) Interphase entre un PDMS fonctionnalisé (PDMS-(PropNH_2)$_2$) Poly (DiMethyl Siloxane, terminé Amino Propyle) et le PEgMA. L'effet de la température et la masse molaires sur les propriétés interfaciales a été mise en évidence.

NB : Le manuscrit de cette thèse présente deux introductions générales, une en anglais et l'autre en français, suivies d'une synthèse de résultats majeurs. Ensuite quatre chapitres sont présentés sous forme de publications avec une conclusion et des perspectives en anglais et dont les résultats majeurs sont résumés en français ci-dessous.

Synthèse des résultats majeurs obtenus

Chapitre I. Progrès récents de la rhéologie interfaciale en cisaillement et en dilatation des systèmes polymères : Du fondamental aux applications

Après une introduction sur l'historique de l'origine de l'interface et de ses propriétés, thermodynamique et rhéologique, ce chapitre présente les aspects théoriques et techniques expérimentales de la rhéologie interfaciale (en cisaillement et en dilatation). De nombreux travaux de la littérature ont été reportées, permettant ainsi de positionner l'originalité de ce projet de thèse.

Chapitre II. Etude de la rhéologie interfaciale en « Cisaillement » de systèmes polymères fondus : Effet de la masse molaire et de la température sur les propriétés interfaciales.

- Développement d'une cellule interfaciale du bicone travaillant sous hautes températures (200 °C). Elle est adaptée à l'étude de polymères de hautes masses molaires moyennes et ayant éventuellement de hauts points de fusion.

Les techniques de mesure de la rhéologie interfaciale en cisaillement, commercialisées aujourd'hui, ne sont pas adaptées aux systèmes polymère/polymère. Leur rigidité mécanique n'est pas suffisante pour étudier des polymères hautement viscoélastiques qui présentent une haute résistance aux déformations élevées. Nous avons alors choisi la géométrie de cisaillement bicone pour sa plus grande robustesse. Cependant, cette géométrie a un inconvénient, en l'occurrence sa propre inertie. La conception d'une nouvelle géométrie de bicone (Ti-Bicone) a été effectuée avec un matériau à base de Titane moins dense que l'acier. On réduit ainsi l'inertie tout en améliorant la sensibilité des mesures.

L'autre inconvénient des cellules interfaciales commerciales est leur limitation en température ne pouvant guère monter au-dessus de 70°C. les systèmes polymères étudiés dans la littérature présentent des températures de fusion supérieures à 100°C. Pour cette raison, un nouveau système de chauffage a été intégré. Il peut atteindre 200°C avec une très bonne régulation en température ($\Delta T = \pm 1°C$).

Pour étudier l'effet de la viscosité et l'élasticité des sous phases sur les propriétés des interfaces, nous avons choisi des fluides modèles visqueux (PIB et PDMS) dont la viscosité varie entre 0.002 et 300 Pa.s. Ces polymères présentent la même viscosité mais avec des masses molaires différentes (système axisymétrique avec une énergie d'activation en masse du PIB 5 fois supérieure à celle du PDMS). Les masses molaires des PDMS dépassent la masse critique d'enchevêtrement Mc, alors que celles des PIB choisis dans ce travail sont inférieures à la Mc (Oligomère). Deux fluides modèles de Boger (BF) ont été préparés en vue d'étudier l'effet de leurs élasticités sur les propriétés des surfaces/interfaces. Ces études sur des polymères modèles seront ensuite transposées aux polymères thermoplastiques liquides (amorphes ou semi-cristallins). Parallèlement nous avons étudié les interfaces PIB- PDMS et BF-PDMS ainsi que les surfaces air-PIB, air-PDMS et air-BF.

- *Relation entre la tension de surface et la masse molaire des polymères*

Dans un premier temps, la tension de surface des différents fluides modèles a été mesurée à l'aide de la méthode de la goutte pendante à différentes températures. Les tensions de surface du PDMS et du PIB diminuent avec la température et la masse molaire Dans ce dernier cas, on assiste à l'apparition d'un palier à partir d'une masse molaire critique.

- *Rhéologie de surface en cisaillement : étude des surfaces (Air-PIB, Air-PDMS et Air-BF)*

Dans cette partie, nous avons effectué deux types d'expériences qui consistent en un test d'écoulement et un balayage de fréquence. L'objectif est de déterminer le comportement rhéologique des surfaces des polymères newtoniens. Ces surfaces sont visqueuses, le module élastique apparent surfacique G'_s était très faible. Après avoir effectué les corrections numériques pour enlever la contribution des sous phases, la valeur de G'_s corrigé est devenue très faible ou nulle. La viscosité en régimes, dynamique $|\eta_s|^*(\omega)$ et stationnaire $\eta_s(\dot{\gamma})$ sont indépendantes respectivement de la fréquence angulaire ω ou la vitesse de cisaillement $\dot{\gamma}$. Il s'agit d'un phénomène caractéristiquedes surfaces newtoniennes.

Les effets de la masse molaire et de la température sur les propriétés des surfaces (viscosités et modules viscoélastiques) ont été évalués. L'augmentation de la température provoque une diminution de la viscosité de surface. Cette dernière augmente, à son tour avec la viscosité de « bulk » selon une loi polynomiale. Boussinesq a envisagé la surface comme une superposition de feuillets de densités variables qui fournit au fluide la force nécessaire à son maintien dans un domaine fixe. Dans le cas des systèmes air-polymère, la surface est formée à partir du volume « bulk », elle est composée de chaînes macromoléculaires avec une conformation spécifique en contact avec les molécules d'air. Les propriétés du volume (bulk) peuvent avoir des effets sur les propriétés des surfaces. Ainsi, les viscosités newtoniennes des surfaces ont été déterminées avant et après les corrections.

- *Rhéologie interfaciale en cisaillement : étude des interfaces (PIB-PDMS et BF/PDMS)*

Nous avons procédé avec la même méthodologie que celle déployée pour l'étude des surfaces. L'anneau à double parois DWR a été utilisé pour sonder les interfaces entre les sous-phases de faibles valeurs de viscosités allant jusqu'à 3 Pa.s, tandis que le bicone a été employé pour étudier les autres interfaces de systèmes ayant des viscosités pouvant aller jusqu'à 300 Pa.s.

Les études en écoulement en régime permanant et en balayage de fréquences ont permis de tirer les enseignements suivants :

- La viscosité interfaciale augmente avec celle du bulk.
- Dans le cas d'interfaces de deux polymères de masses molaires moyennes faibles, l'augmentation de la température conduit à une diminution de la viscosité interfaciale.

- Dans le cas d'interfaces de deux polymères de masses molaires moyennes élevées, l'augmentation de la température conduit à une augmentation de la viscosité interfaciale. Aussi, la diffusion des chaînes du PIB vers le PDMS à travers l'interface est d'autant plus rapide que la température augmente.

Selon la littérature, les chaînes de PIB sont plus petites (donc plus mobiles) et peuvent diffuser vers le PDMS à travers l'interface, on parle d'une interface dynamique [1, 2]. Cette diffusion a été mise en évidence par des études en microscopie optique qui ont permis de suivre la variation du diamètre d'une goutte de PIB dans une matrice de PDMS [3]. Ce diamètre diminue avec le temps jusqu'à atteindre un palier. Cette expérience a été effectuée sur un système PIB-PDMS de haute viscosité dont les résultats seront présentés dans le chapitre III.

Une étude préliminaire de compatibilité entre ces deux polymères a été menée en utilisant deux méthodes :

- *Un calcul théorique des paramètres de solubilité via le logiciel HSPiP*

Le logiciel HSPiP n'est pas réduit au calcul et à la visualisation des paramètres de solubilité de Hansen (HSP) en 3D. Il dispose également d'un optimiseur de solvant, d'un calculateur de polymère, d'un calculateur HSP et d'un puissant modélisateur de diffusion. La simulation théorique à l'aide de ce logiciel, prédit une miscibilité partielle entre le PIB et le PDMS. Cette dernière diminue avec l'augmentation de la masse molaire des polymères et augmente, en revanche avec la température.

- *La rhéologie volumique des mélanges PIB-PDMS (10/90, 50/50 et 90/10 wt%)*

Les courbes de *Van-Gurp Palmen* représentées par le déphasage δ en fonction du module complexe $|G|^*$ à différentes températures montrent que : i) à faible taux de PIB dans le mélange (10/90 wt%) les courbes sont superposables prouvant une certaine miscibilité entre les phases. ii) Dans le cas des compositions 50/50 wt% et 90/10 wt%, elles ne le sont pas. Ainsi, PIB et PDMS ne sont pas complétement miscibles.

Ces deux approches basées sur des outils expérimentaux et de simulation couplés à la rhéologie interfaciale ont mis en évidence le phénomène de la diffusion à l'interface et l'effet de la masse molaire et de la température sur ce dernier.

Chapitre III. Etude de la rhéologie interfaciale en « dilatation » des systèmes polymères fondus : Effet de la masse molaire et de la température sur les propriétés interfaciales.

- *Etude de l'effet de la masse molaire et la température sur la tension interfaciale et le module dilatationnel obtenu par la méthode de la goutte pendante oscillante.*

La tension de surface/interfaciale statique a été déterminée via la méthode de la goutte pendante, dans ce cas la loi de Young-Laplace est valable. En d'autres termes, les forces gravitationnelles

agissant sur la goutte sont en équilibre avec les forces interfaciales. Cependant, dans le cas de mesures oscillatoires, la surface interfaciale change pendant le temps de l'expérience. Dans ce cas, des forces d'inertie et des forces visqueuses apparaissent et modifient la forme de la goutte/bulle. Par conséquent, la loi de Young-Laplace n'est plus valable, ce qui restreint l'exploration des fréquences élevées. [4, 5].

Pour quantifier les forces inertielles et visqueuses, Il faut connaître : i) nombre capillaire Ca, défini comme étant le rapport entre les forces visqueuses et capillaires : le nombre de Weber We, défini comme le rapport entre les forces inertielles et capillaires. Les relations qui définissent ces deux nombres sont les suivantes [4] :

$$\mathbf{Ca} = \frac{\Delta \eta \omega \Delta V}{\gamma {R_c}^2} \qquad \textbf{(S.III-1)}$$

$$\mathbf{We} = \frac{\Delta \rho \omega^2 \Delta V^2}{\gamma R_c^3} \qquad \textbf{(S.III-2)}$$

La gamme des valeurs de ces deux nombres influence non seulement les paramètres opératoires (l'amplitude ΔV, la fréquence ω) mais aussi le choix des propriétés des matériaux étudiés. Nous avons préparé trois PIB et trois PDMS afin d'avoir la même viscosité newtonienne à 25°C ce qui induit la réduction des valeurs du nombre Ca. Ces mélanges à base de PIB et de PDMS ont été préparés séparément à partir de fluides modèles commerciaux, en utilisant une loi de mélange. Ainsi, différentes surfaces de polymères et interfaces polymère/polymère ont été étudiées en faisant varier les viscosités des sous phases.

- *Etudes des propriétés interfaciales en régime statique et dynamique :*

La tension interfaciale des différents systèmes PIB/PDMS a été mesurée avec la méthode de la goutte montante. La mesure a été effectuée à 25, 45 et 60°C. On constate que la tension interfaciale entre le PDMS et le PIB diminue avec la diminution de leur masse molaire moyenne. Legrand et Gaines [6] ont remarqué la même tendance en utilisant des systèmes polymères similaires. D'autre part, il a été observé que pour les systèmes de plus faible viscosité, la tension interfaciale augmente légèrement avec la température. Dans le cas de polymères de viscosité plus élevée, la tension interfaciale diminue avec l'augmentation de la température. Ceci pourrait être expliqué par la diffusion des chaînes de PIB vers l'interface, se comportant dans ce cas comme des tensioactifs qui baissent la tension interfaciale. Ce phénomène est apparu à partir d'une masse molaire moyenne en masse spécifique des sous-phases, et accéléré par l'augmentation de la température.

Avant de réaliser l'expérience de balayage de fréquence, il est important de mentionner que les nombres sans dimension (nombres de Bond, Weber et capillaire) ont été soigneusement vérifiés afin de réaliser correctement ces mesures de dilatation pour chaque système PIB/PDMS à différentes températures.

Pour tous les systèmes PIB/PDMS, l'absence du module de perte interfacial a été remarquée. Il est utile de mentionner que dans notre cas, les interfaces sondées sont vierges (pas de particules ou de surfactants présents sur l'interface), ce qui induit des valeurs d'angle de phase très faibles entre les oscillations de l'aire interfaciale et les variations de la tension interfaciale. Cela signifie que le module de conservation E' est beaucoup plus grand que le module de perte E" [7].

On observe qu'à température constante, le module élastique interfacial E' est d'autant plus important que la viscosité des phases coexistantes augmente. Pour le système de plus faible viscosité, le module élastique interfacial E' augmente lorsque la température diminue. Cependant, en augmentant la viscosité des phases coexistantes, la tendance inverse a été observée. Le module d'élasticité interfacial diminue lorsque la température augmente, ce qui est en accord avec nos observations lors des mesures de gouttes pendantes statiques.

- *Etude de la relaxation des surfaces / interfaces avec la méthode des « Pulses » et la méthode de « CaBER »*

Les temps de relaxation des surfaces et interfaces ont été déterminés par la méthode des pulses. Elle consiste à former une goutte de PIB dans le PDMS. Après atteinte de l'équilibre de la tension de surface (ou interfaciale), une amplitude constante (ΔV) est appliquée pendant un temps $\Delta t = t_2 - t_1$. L'évolution de la tension de surface (ou interfaciale) permet de caractériser la relaxation de chaque surface ou interface en fonction de la température. L'évolution de la tension de surface / interfaciale a été ajustée par le modèle de l'équation S.III-3.

$$\gamma(t) = \gamma_0 + \Delta\gamma . \exp\left(\frac{-t}{3\tau}\right) \qquad \textbf{(S.III-3)}$$

- Temps de relaxation des surfaces (Pulses) :

On constate que les temps de relaxation de dilatation des surfaces augmentent avec la viscosité des phases coexistantes, alors qu'ils diminuent lorsque la température augmente.

- Temps de relaxation des interfaces (Pulses) :

Dans le cas des interfaces PDMS/PIB, les temps de relaxation interfaciale caractéristiques augmentent avec la viscosité des phases coexistantes, En revanche, ils diminuent avec l'augmentation de la température. De plus, les temps de relaxation interfaciale sont plus élevés que ceux des surfaces. Ce phénomène peut être expliqué par les degrés de liberté élevés des chaînes macromoléculaires à la surface par rapport aux interfaces. La relaxation des systèmes PIB/PDMS ayant une grande viscosité à 25 et 45 °C était lente, le temps de relaxation tend vers une valeur infinie. Ce phénomène pourrait être expliqué par la viscosité élevée de ces polymères.

- Temps de relaxation des surfaces (CaBER) :

Le rhéomètre extensionnel à rupture capillaire (CaBER) est basé sur le positionnement d'un volume de polymère à l'état liquide entre deux plateaux parallèles, un est fixe, l'autre est mobile. Une force axiale est appliquée pour former un filament dont le diamètre varie avec le temps suivant la relation décrite par l'équation S.III-4 permettant la détermination des temps de relaxation. Ce filament de polymère à surface libre, maintenu par la tension superficielle entre deux surfaces solides est placé dans une situation instable qui conduit à sa rupture en deux volumes distincts de fluide. Cette rupture est un écoulement en élongation dont la dynamique dépend uniquement de la tension superficielle et de la viscosité du fluide.

$$\mathbf{D(t) = \alpha e^{-\frac{t}{3\tau}} - \beta t + \delta} \qquad \textbf{(}\text{S.III-4}\textbf{)}$$

La variation des temps de relaxation élongationnelle avec la température pour toutes les viscosités apparentes des phases coexistantes a été déterminée. Il a été clairement observé que les temps de relaxation élongationnelle pour le PIB et le PDMS augmentent avec la masse molaire moyenne en masse et diminuent avec la température. Pour les fluides de faible viscosité et à haute température, la rupture du filament est instantanée, et les données enregistrées ne sont pas suffisantes pour réaliser l'ajustement des variations du diamètre avec le temps (seulement trois ou quatre points).

On constate que les temps de relaxation extensionnelle obtenus à partir des mesures CaBER sont très proches des temps de relaxation dilatationnelle obtenus avec la méthode "pulse" (plusieurs secondes dans les deux cas en fonction de la viscosité et de la masse molaire moyenne en masse du polymère). On pense alors que la migration des chaînes courtes de la surface vers la masse/volume « bulk » lors de l'amincissement est préférentielle. Ce phénomène se manifeste de la même manière pour le filament de polymère que pour la goutte montante ou pendante.

Nous avons également analysé l'évolution des viscosités newtoniennes obtenues par la rhéologie interfaciale cisaillement (Bicone) et celle des temps de relaxation élongationnelle déterminés par le test de relaxation par la méthode de « pulse ». On remarque que les viscosités de surface augmentent avec le temps de relaxation élongationnelle. Cette dépendance suit une loi de type puissance. Alors l'existence d'une relation directe entre les propriétés interfaciales en cisaillement et les propriétés en élongation dans nos systèmes air/PIB et air/PDMS est plausible. Elle est décrite généralement par un rapport de Trouton interfacial ou de surface.

Chapitre IV. Rhéologie interfaciale utilisée comme sonde du suivi de la réaction chimique *in situ* aux interfaces de systèmes polymères fondus : effet de la masse molaire et de la température.

L'étude des interfaces réactives est le sujet de ce chapitre. Grâce à la rhéologie interfaciale en cisaillement et les mesures de la tension interfaciale, l'effet de la masse molaire et de la température sur la réaction interfaciale à l'état fondu a été investigué. La cinétique de ce processus est contrôlée

par la dualité diffusion/réaction chimique et peut être affectée par la température et la viscosité des espèces réactives.

Deux types d'interfaces et/ou interphases ont été étudiés et analysés, la première est non réactive et concerne le système PDMS/PEgMA et la deuxième est réactive et concerne le système PDMS-$(PropNH_2)_2$/PEgMA.

- *Rhéologie en volume*

Une étude préliminaire a concerné l'étude rhéologique de chaque polymère à différentes températures allant de 120 à 140 °C.

La rhéologie dynamique a été employée aussi pour mettre en évidence la réaction chimique entre ces matériaux à l'état fondu. L'évolution de la viscosité d'un mélange de 50/50 wt% de chaque système a été suivie dans le régime permanent à une vitesse de cisaillement constante de $5s^{-1}$. Il a été constaté que la viscosité du mélange a augmenté dans le temps. Ceci est dû à la formation d'un copolymère à l'interface. En revanche, la viscosité du mélange non-réactif n'a pas changé dans le temps.

- *Rhéologie interfaciale en cisaillement*

La rhéologie interfaciale est un moyen puissant pour caractériser la moindre modification des propriétés rhéologiques des interfaces. Dans notre cas, la formation d'une interphase se traduit par une rigidification de l'interface (caractère viscoélastique). Ce phénomène se traduit par une augmentation du couple ou de la viscosité interfaciale mesurés. Pour les systèmes réactifs, la viscosité interfaciale augmente puis atteint un palier. La vitesse à laquelle on atteint ce palier dépend de la température et de la masse molaire. La cinétique de la réaction chimique interfaciale est d'autant plus lente que la température est basse et que la masse molaire moyenne en masse est élevée.

- *Mesures de la tension interfaciale*

La variation de la tension superficielle / interfaciale dans le temps, est principalement le résultat de phénomènes interfaciaux, tels que l'adsorption ou la désorption d'une entité à l'interface, qui conduira à une diminution (adsorption) ou une augmentation (désorption) de la tension superficielle / interfaciale. Nous avons ainsi mesuré l'évolution de la tension interfaciale pendant le temps où le volume de la goutte est constant.

Pour les interfaces réactives PDMS-$(PropNH_2)_2$/PEgMA, la tension interfaciale a diminué, tendant vers une valeur faible. Ceci est lié à la diffusion de chaînes courtes vers les interfaces, suivie d'une réaction chimique. Ces deux processus se poursuivent jusqu'à saturation de l'interface par la formation d'une couche interfaciale (copolymère) responsable de la réduction de la tension interfaciale et permettant la comptabilisation des deux phases coexistantes. La cinétique de la dualité diffusion / réaction est devenue plus rapide après l'augmentation de la température. Néanmoins, elle diminue

après l'augmentation de la masse molaire de PDMS-($PropNH_2$)$_2$ car les macromolécules deviennent plus longues. Par conséquent, la diffusion / réaction pourrait être plus lente. D'autre part, la tension interfaciale des systèmes PDMS/PEgMA non réactifs a atteint une valeur d'équilibre en une minute et est ensuite restée constante. Nous notons que la tension interfaciale a diminué lorsque la température a augmenté, et lorsque l'état d'équilibre a été atteint, la goutte est restée accrochée au capillaire, contrairement à ce qui a été observé dans les systèmes réactifs PDMS-($PropNH_2$)$_2$/PEgMA.

Références

[1] G. W. Peters, A. N. Zdravkov, and H. E. Meijer, "Transient interfacial tension and dilatational rheology of diffuse polymer-polymer interfaces," *The Journal of chemical physics*, vol. 122, no. 10, p. 104901, 2005.

[2] T. Shi, V. E. Ziegler, I. C. Welge, L. An, and B. A. Wolf, "Evolution of the interfacial tension between polydisperse “immiscible” polymers in the absence and in the presence of a compatibilizer," *Macromolecules*, vol. 37, no. 4, pp. 1591-1599, 2004.

[3] S. Guido, M. Simeone, and M. Villone, "Diffusion effects on the interfacial tension of immiscible polymer blends," *Rheologica acta*, vol. 38, no. 4, pp. 287-296, 1999.

[4] E. Freer, H. Wong, and C. Radke, "Oscillating drop/bubble tensiometry: effect of viscous forces on the measurement of interfacial tension," *Journal of colloid and interface science*, vol. 282, no. 1, pp. 128-132, 2005.

[5] E. Santini, L. Liggieri, L. Sacca, D. Clausse, and F. Ravera, "Interfacial rheology of Span 80 adsorbed layers at paraffin oil-water interface and correlation with the corresponding emulsion properties," *Colloids and Surfaces a-Physicochemical and Engineering Aspects*, vol. 309, no. 1-3, pp. 270-279, Nov 2007, doi: 10.1016/j.colsurfa.2006.11.041.

[6] D. LeGrand and G. Gaines Jr, "Immiscibility and interfacial tension between polymer liquids: dependence on molecular weight," *Journal of Colloid and Interface science*, vol. 50, no. 2, pp. 272-279, 1975.

[7] J. Lucassen and M. Van den Tempel, "Longitudinal waves on visco-elastic surfaces," *Journal of Colloid and Interface Science*, vol. 41, no. 3, pp. 491-498, 1972.

Chapter I. State of the Art

I.1. Abstract

The study of the viscoelastic properties of polymer systems containing huge internal two-dimensional interfacial areas, such as blends, foams and multilayer films, is of growing interest and plays a significant role in a variety of industrial fields. Hence, interfacial rheology can represent a powerful tool to directly investigate these complex polymer–polymer interfaces. First, the current review summarizes the theoretical basics and fundamentals of interfacial shear rheology. Particular attention has been devoted to the double-wall ring (DWR), bicone, Du Noüy ring and oscillating needle (ISR) systems. The measurement of surface and interfacial rheological properties requires a consideration of the relative contributions of the surface stress arising from the bulk sub-phases. Here, the experimental procedures and methodologies used to correct the numerical data are described considering the viscoelastic nature of the interface. Second, the interfacial dilational rheology is discussed, starting with the theory and underlying principles. In particular, the Langmuir trough method, the oscillating spinning drop technique and the oscillating pendant drop technique are investigated. The major pioneering studies and latest innovations dedicated to interfacial rheology in both shear and dilatation–compression are highlighted. Finally, the major challenges and limits related to the development of high-temperature interfacial rheology at the molten state are presented. The latter shows great potential for assessing the interfaces of polymer systems encountered in many high-value applications.

Keywords: interfacial shear rheology; interfacial dilational rheology; double-wall ring; bicone; oscillating drop tensiometry

I.2. Introduction

Polymers are rarely miscible because of their high viscosity. When two immiscible polymers meet, a surface called an “interface” is defined. This surface is thermodynamically created due to the positive free enthalpy of mixing (Gibbs) related to the structural properties of the polymers. In particular, it is due to the low entropy of the macromolecular chains (low number of possible mixed configurations) and the poor chemical affinity (repulsive interactions) between the polymer constituents. The “interface” can be described as an “interphase,” which is a tridimensional entity. We make must a distinction between a physical interphase and a chemical interphase. A physical interphase is created when the two coexisting polymers are fully or partially miscible, or when prepared by forced assembly in the molten state, resulting in a physical intra-entanglement as in the coextrusion process [1]. A chemical interphase is created when a chemical reaction occurs at the interface of these two polymers, forming an interfacial copolymer [2].

The interfacial properties in multiphase polymer systems can control their morphology (e.g., a dispersion of one polymer phase within another polymer phase, coalescence) [3], their stability (e.g., emulsions [4], foams [5], polymer solutions [6]), their reinforcement (e.g., polymer/clay nanocomposites [7]) and their healing degree (e.g., multi-layered polymers [8]). Interfacial rheology is, thus, a powerful way to probe the polymer systems in different fields, including crude oil recovery [9], plastic processing [10], cosmetics [11], biomedical applications [12] and foods [13].

Interfacial rheology directly investigates the viscoelastic responses of the interface under the application of a stress or strain (i.e., the same formalism and techniques developed in bulk rheology). This two-dimensional area possesses properties that differ from those of the two sub-phases. This interface can be considered the third phase and is characterized not only by its interfacial tension but also by its rheological properties. The latter can affect the overall system [14].

The extensive state-of-the-art research reveals that most experimental studies devoted to interfacial rheology have concerned high flow rate liquid systems (suspensions, emulsions, etc.). However, reports investigating the particular case of high molecular weight polymer systems are not plentiful. This is related to the constraints that occur during the study of polymers, such as the viscosity, high inertia or fragility of the interfacial fixtures and the temperature limit (measurements are often made below 80 °C to ensure a stable, homogeneous temperature at the interface). Developing new interfacial rheological setups is a subject of increasing interest in the industrial and academic communities.

Hence, a large section of the present chapter is dedicated to these issues. First, the sufficient theoretical models and concepts related to the interfacial rheology during shear and dilatation or compression have been reviewed.

A good deal of the first part of this thesis manuscript details the methods of correction of the apparent measured interfacial properties in both oscillatory and steady-flow modes, taking into account the contributions of the sub-phases during the gathering of the numerical data.

Finally, this review ends by summarizing the major pioneering studies, experimental techniques and related applications of the interfacial rheology of polymer systems.

I.3. History

The term “rheology”, invented by Bingham in 1928, refers to the study of material movement and deformation in both fluid and solid states. In other words, it is the analysis of deformations under the impact of applied stress. In particular, rheologists have studied the rheology of different kinds of fluids, such as molten polymers, to better understand their processability and to monitor their industrial-scale implementation.

The study of multiphase systems is of great importance in academia, as well as in industry. From this perspective, it has been extremely valuable to study the deformation of their interfaces through interfacial rheology, i.e., the study of the stress–strain relationships taking place within interfaces, in the two-dimensional area located just between the two immiscible fluids, such as the interfacial layer of the surfactant or in the solid particles.

The term “interfacial viscosity” was introduced by Plateau in 1869 [15] to explain the slowing of the oscillation of a needle on the surface of water (gas–water surface). In the beginning, Plateau thought that he had used pure water, but this was not the case. The origin of these findings was related to the presence of impurities that remained on the surface of the water. He also described the surface gradient mechanisms that can be at the origin of convection movement, now known as the “Marangoni effect” [16].

Next, Rayleigh [17] confirmed Plateau’s assumption. He positioned a ring of thin brass wire on the surface of water dusted over with fine sulfur and set the system into rotation using an external magnet, namely a magnetized sewing needle (Figure I-1a). He found no noticeable movement on the surface around the ring and argued that an ordinary water surface does not appreciably resist the shear. Then, he slightly modified the apparatus by adding a material diameter of the same brass wire to the ring (Figure I-1b) and found that the sulfur indicated that the entire water surface included within the semicircles now shared in the motion. In this case, Marangoni’s assumptions were also shown to be correct.

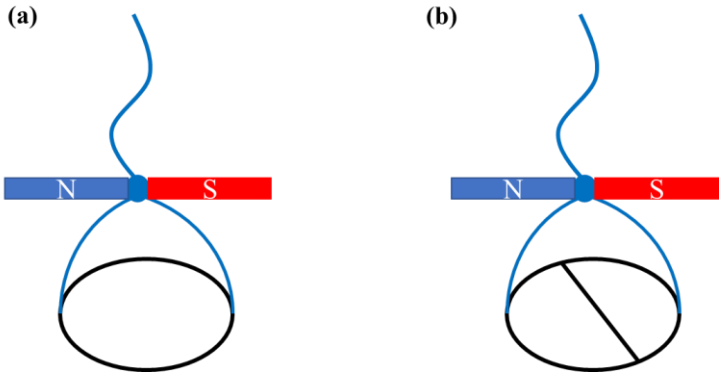

Figure I-1. (**a**) Rayleigh's experiment involving a ring of thin brass wire placed on the surface of the water and dusted over with fine sulfur. The system was magnetically rotated using a magnetized sewing needle (NS). (**b**) A material diameter of the same brass wire was added to the ring [17].

In 1913, Boussinesq [18] used the term "surface viscosity" to explain the measured drop in velocity of a drop of mercury in castor oil, which differs from that predicted by the theory when the dissipation of the interface is neglected. Many models have described the interface between two immiscible liquids, such as those proposed by Boussinesq [18], Kasperski [19] and Shikhmurzaev [20]. Here, we present the Boussinesq model. In the static equilibrium, the isotropy in the volume is maintained by molecular agitation and results in the presence of a pressure field. Boussinesq imagined the surface as a superposition of layers with variable density (ρ_0, ρ_1, ρ_2) (Figure I-2). This density gradient gives enough force to the fluid to maintain it within a fixed range [21].

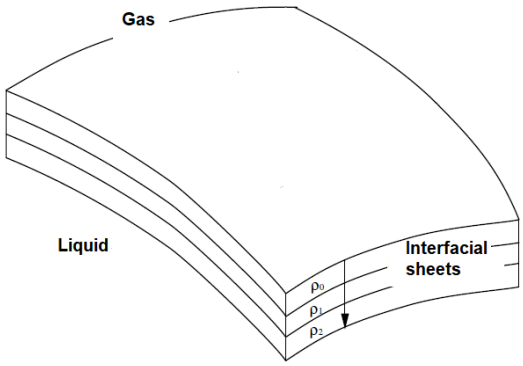

Figure I-2. The Newtonian interface according to the Boussinesq model: pressure equalization by the density gradient.

I.4. Vectors and Tensors on Interfaces

The flow in the liquid phases that establish the interface is described by conservation equations for the mass (continuity equation, Equation (I-1)), momentum (Navier–Stokes equation, Equation (I-2)) and energy.

$$\frac{\partial \rho}{\partial t} + \nabla.(\rho \mathbf{v}) = 0 \qquad \text{(I-1)}$$

$$\rho\left(\frac{\partial \mathbf{v}}{\partial t} + \mathbf{v}.\nabla\mathbf{v}\right) = -\nabla p + \eta_b \nabla^2 \mathbf{v} + \mathbf{f} \qquad \text{(I-2)}$$

where ρ is the density, t is the time, v is the velocity, p is the pressure, η_b is the bulk viscosity and f is the external body force.

The question that one might ask now is the position of the interface. The location of the dividing surface is not unique. Gibbs described an interface as a two-dimensional dividing area embedded in a 3D space that is located between two bulk liquids. We can refer to this as a sharp interface (few nanometer ~nm) [22]. Figure I-3 shows that the bulk properties are extrapolated up to this surface, and any excess quantity that is not accounted for by the bulk is assigned to the interface. The most transparent approach is to set the location of the interface by considering $\rho_s = 0$.

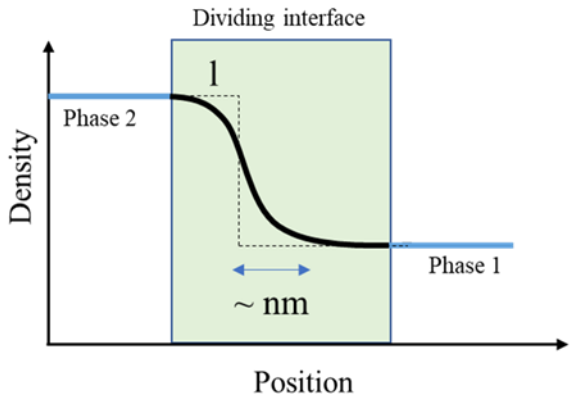

Figure I-3. Schematic plot of the density ρ as a function of position ***x*** crossing the interface.

The properties of the interface are important parameters to define. According to the studies by Boussinesq, in addition to the surface tension γ, the interfacial stress τ_s (Equation (I-3)) is a function of another intrinsic property of the interface, τ_e, which is the extra stress corresponding to the interfacial rheological properties.

$$\boldsymbol{\tau_s} = \gamma.\mathbf{I_s} + \boldsymbol{\tau_e} \qquad \text{(I-3)}$$

In addition to the kinematic condition, the free surface must satisfy the conditions of continuity of the velocity and stress across the interface. The excess momentum balance equation is obtained by collecting all of the forces that act on interfacial element A (Figure I-4) and identifying them as sources of momentum, starting with the interfacial inertia (left side of Equation (I-4)), the bulk stress (τ_1 and τ_2) and the interfacial stress (right side of Equation (I-4)) [23].

$$\iint_A \rho_s \frac{\mathbf{D_s v}}{\mathbf{Dt}}\,\mathbf{dA} = \iint_A (\boldsymbol{\tau_2} - \boldsymbol{\tau_1}).\mathbf{n}\mathbf{dA} + \iint_A \nabla_s.\boldsymbol{\tau_s}\mathbf{dA} \qquad \text{(I-4)}$$

where $\frac{D_s()}{Dt}$ is the time derivative.

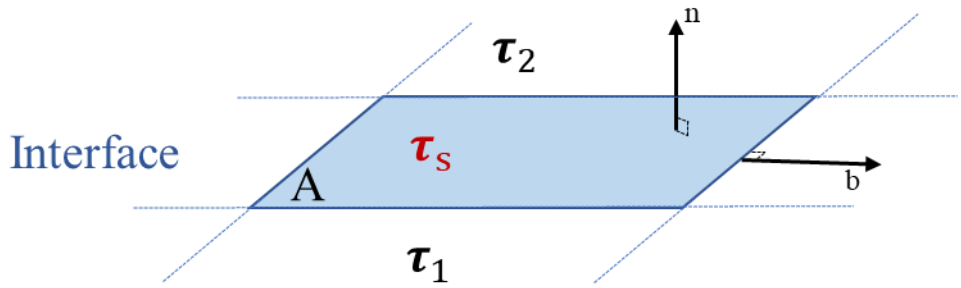

Figure I-4. The surface element *A* separated two fluids denoted 1 and 2. The unit vectors normal and tangential to the surface are denoted by ***n*** and ***b***, respectively.

The interfacial inertia is generally neglected in the case of a sharp interface (ρ_s=0). By substituting the expression for the interfacial stress tensor into Equation (I-4), we obtain the following equation:

$$(\boldsymbol{\tau_1} - \boldsymbol{\tau_2}).\mathbf{n} = \boldsymbol{\nabla_s \gamma} - \boldsymbol{\gamma}(\boldsymbol{\nabla_s}.\mathbf{n})\mathbf{n} + \boldsymbol{\nabla_s}.\boldsymbol{\tau_e} = \mathbf{0} \qquad \textbf{(I-5)}$$

representing the bulk stress, Marangoni stress, and extra-capillarity surface stress.

Equation (I-5) links the transport phenomena (equation of state, i.e., $\gamma(\Gamma(t,x,y,z))$ with the interfacial and bulk rheology (constitutive equations).

In 1959, Scriven [24] proposed a constitutive model describing the response of a purely Newtonian interface based on the Newton–Cauchy–Poisson law. This interface has thermodynamic properties corresponding to the surface (or interfacial) tension and rheological properties based on the interfacial dilatational viscosity (Pa.s.m) and the interfacial shear viscosity (Pa.s.m). This constitutive equation is known as the generalized Boussinesq–Scriven surface fluid model. This model describes the surface (or interfacial) stress tensor τ_s (with units of force per unit length) as a linear function of the surface rate of the deformation tensor $\overline{D_s}$ and can be expressed as:

$$\boldsymbol{\tau_e} = [(\eta_d - \eta_s)\, \mathrm{div}_s\, \overline{V}_s].\, \mathbf{I_s} + 2\eta_s\, \overline{\mathbf{D_s}} \qquad \textbf{(I-6)}$$

$$\overline{\mathbf{D_s}} = \frac{\boldsymbol{\nabla_s}\overline{\mathbf{V}}_s.\mathbf{I_s} + \mathbf{I_s}.(\boldsymbol{\nabla_s}\overline{\mathbf{V}}_s)^{\mathbf{T}}}{\mathbf{2}} \qquad \textbf{(I-7)}$$

This constitutive equation includes η_d, the surface dilatational viscosity; η_s, the surface shear viscosity; $\boldsymbol{\gamma}$, the thermodynamic (equilibrium) surface (or interfacial) tension; I_s, the surface unit tensor; τ_e, the extra stress component due to the deformation tensor; $\overline{V}_s$, the surface (or interfacial) velocity vector; div_s, the surface (or interfacial) divergence operator; ∇_s, the surface (or interfacial) gradient operator; and $\overline{D_s}$, the tensor of the surface deformation rate. Note that $\overline{V}_s$ has normal and tangential components to the interface. The Boussinesq–Scriven model describes a Newtonian interface. It has limited functionality for non-Newtonian interfaces, because they exhibit a complex, non-linear stress–strain relationship.

The behavior of a solid-like elastic surface can be described by a linear elastic model [24, 25] identical to Equation (I-6), which is valid for infinitely small deformations.

$$\tau_e = [(K_s - G_s)\, div_s\, \bar{V}_s].\, I_s + 2G_s\overline{U_s} \qquad \textbf{(I-8)}$$

$$\overline{U_s} = \frac{\nabla_s \bar{V}_s . I_s + I_s . (\nabla_s \bar{V}_s)^T}{2} \qquad \textbf{(I-9)}$$

where K_s is the interfacial dilatational modulus, G_s is the interfacial shear modulus, v_s is the displacement vector on the interface and U_s is the interfacial infinitesimal strain tensor. Note that these two constitutive equations describe the behavior of purely viscous and purely elastic plane interfaces. Another tensor projection P onto the interface needs to be performed for the general case of a curved interface with regular components in the interfacial velocity or displacement [26]. Pepicelli et al. [27] recently developed a "neo-Hookean" constitutive equation from a strain energy function, which separates the dilatational or compressional contributions from the contributions related to shear deformations, yielding the interfacial or surface elastic stress tensor. With all of these equations, as in 3D rheology, developing a modeling equation as well as numerical methods for a complex interface becomes possible and remains a task in progress [23, 26, 28-33].

From an experimental point of view, a sinusoidal deformation is often applied in order to characterize viscoelastic interfaces, because in rheology, time becomes an essential variable in the experiment. The principle and interpretation of the interfacial analysis depend on the type of stress applied (shear or dilatation) and on the nature of the deformation (constant speed deformation or sinusoidal deformation). In the current review, particular attention has been dedicated to summarizing the theoretical basics and principles of the devices used to study interfacial shear and dilational rheology.

I.5. Interfacial Shear Rheology

This analysis consists of deforming the interface (without changing its area) by moving an object with variable geometry (needle, bi-cone, ring, etc.). The resistance of the interface is recorded by the sensor of the rheometer. The solicitation mode (force or torque) makes it possible to determine the interfacial stress τ_s ($N.m^{-1}$ or Pa.m). However, the object movement analysis makes it possible to determine the interfacial deformation ε_s (dimensionless magnitude) and the rate of the interfacial deformation $\dot{\varepsilon}_s$ (s^{-1}), which gives a rheogram $\tau_s = f(\dot{\varepsilon}_s)$.

I.5.1. Interfacial Rheological Magnitudes

I.5.1.1. With imposed stress (or creep measurement)

In static measurements, a constant stress τ_0 is applied, and the compliance J(t) (in m/N) is measured as:

$$J(t) = \frac{\varepsilon(t)}{\tau_0} \qquad \textbf{(I-10)}$$

where $\varepsilon(t)$ is the interfacial deformation.

In harmonic measurements, a sinusoidal stress with magnitude τ_0 is applied, and the complex compliance $J^*(\omega)$ is measured with:

$$J^*(\omega) = J' - i J'' \qquad \text{(I-11)}$$

I.5.1.2. With imposed strain (or relaxation measurement)

In static measurements, a constant strain ε_0 is applied, and the interfacial shear modulus G (t) (in N m) is measured:

$$G(t) = \frac{\tau(t)}{\varepsilon_0} \qquad \text{(I-12)}$$

where $\tau(t)$ is the interfacial stress.

In harmonic measurements, on the other hand, a sinusoidal strain with magnitude ε_0 is applied, and the complex interfacial shear modulus $G^*(\omega)$ is measured:

$$G^*(\omega) = G'(\omega) + iG''(\omega) = |G^*| e^{i\delta(\omega)} = -i\omega\eta^*(\omega) \qquad \text{(I-13)}$$

The G* modulus is expressed via its real and imaginary components, which depend on the oscillation frequency. In this case, the dimension of the components of the complex modulus is also N/m or Pa.m. The real component G', which is in phase with the applied deformation profiles, characterizes the elastic properties, while the imaginary component G'', which is out of phase with the applied deformation profiles, describes the viscous properties of the interface.

Viscoelastic interfaces can be also described by the complex viscosity η^*(Pa.s.m) and phase angle δ (°), where:

$$\eta^*(\omega) = \eta'(\omega) - i\eta''(\omega) \qquad \text{(I-14)}$$

And:

$$\tan\delta = \frac{G''(\omega)}{G'(\omega)} \qquad \text{(I-15)}$$

I.5.2. Positioning of the Shear Geometry at the Interface

Presently, there are two methods for positioning the shear geometry at the interface. In the first method, the geometry can be positioned at the interface using a technique called normal force assistance (Figure I-5). The geometry is lowered from a known gap toward the surface while the rheometer measures the axial force. The normal force increases dramatically upon contact with the sub-phase surface of greater density.

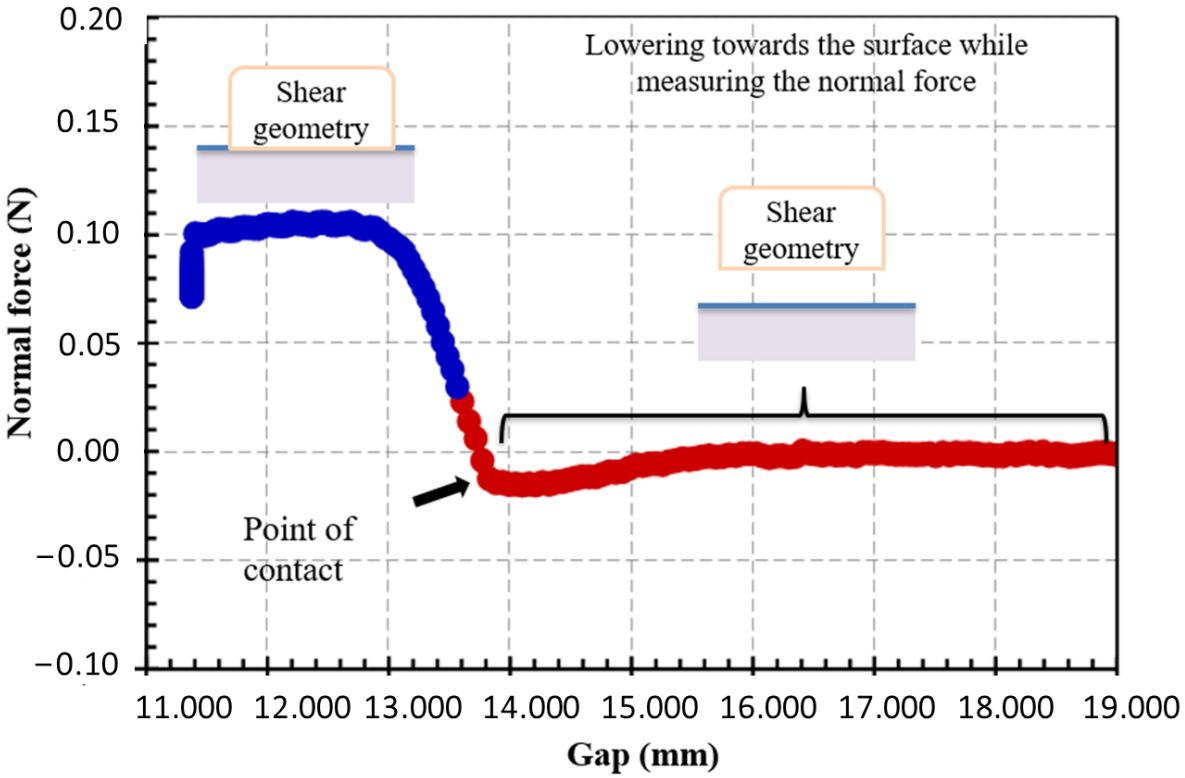

Figure I-5. Positioning of the object at the interface with normal force assistance.

In the second method, the geometry can be positioned at the interface by means of a visualization system (Figure I-6) [34] that is used to ensure that the edge of the geometry is precisely located at the interface.

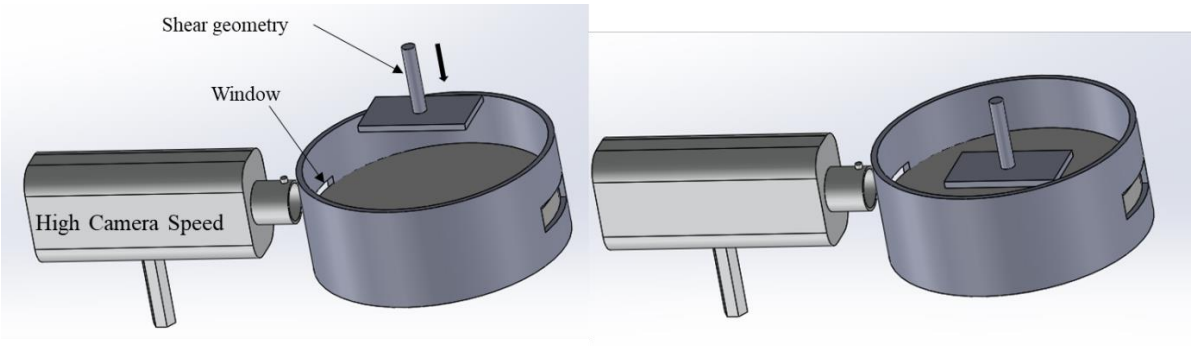

Figure I-6. Positioning of the object at the interface using a visualization system [35].

In addition to the difficulty of positioning the shear geometry at the interface, making accurate measurements is not straightforward. This is related to the sensitivity of the instrument employed, i.e., the contact surface between the geometry and the interface. In general, the interfaces are very thin, making the measurement difficult due to the low interfacial measured torque T (a few mN.m), which is usually very close to the limits of the rheometer and is affected by the inertia of the instrument and of the geometry [36].

I.5.3. The Boussinesq Number

In surface rheology measurements, it is very important to realize that the rheometer is going to measure the total response (stress or strain), including the responses of the interface and the sub-phases. The measurement of the interfacial rheological properties makes it necessary to consider the relative contributions of the interfacial stress and the stress resulting from the bulk liquid. The ratio of these two stresses is described by the Boussinesq number (Bo) [37].

In other words, the Bo allows us to foresee if the effects of the sub-phases can be neglected with respect to the interfacial effect. The Boussinesq number can be expressed as follows (Equation (I-16)):

$$\mathbf{Bo} = \frac{\text{surface drag force}}{\text{sub-phases drag forces}} = \frac{\eta_s . P . \frac{V}{L_S}}{\eta_v . A . \frac{V}{L_V}} = \frac{\eta_s}{l . \eta_v} \qquad \textbf{(I-16)}$$

where η_s (Pa.s.m) is the surface viscosity in a steady shear flow that is calculated from the geometry adopted in the interfacial rheological measurements and from the measured torque; η_v is the bulk viscosity (Pa.s) = (η_1+ η_2), with η_1 and η_2 representing the viscosities of sub-phases 1 and 2, respectively; V is the characteristic velocity (m/s); L_s and L_v are the characteristic length scales over which the characteristic velocity decays at the interface and in the sub-phases, respectively (m); P is the contact perimeter between the shear geometry and the interface (m); A is the contact area between the geometry and the surrounding sub-phases (m^2).

The Boussinesq number is dimensionless. It is a product of two parts: the first one is a material part that is the ratio between the interfacial and bulk viscosities. The more viscous the sub-phases are, the higher their drag forces become. The second part is a geometrical one that depends on the ratio 1/1, which has units of length and defines a characteristic length scale ‘‘l’’ associated with the measurement techniques.

In practice, as ‘‘l’’ is mainly determined by the ratio of A to P, the Boussinesq number is simplified to:

$$\mathbf{Bo} = \frac{\eta_s . P}{\eta_v . A} \qquad \textbf{(I-17)}$$

The interface and sub-phases can independently show non-Newtonian behavior. The sub-phases or the interface can have a shear-rate-dependent viscosity, such as in a generalized Newtonian fluid or a non-linear viscoelastic fluid. In the case of oscillatory measurements, the viscosities will depend on the frequency and the Boussinesq number will turn into a complex number Bo* [38, 39].

$$\mathbf{Bo^*} = \frac{\eta_s^*}{l . \eta_v^*} = \frac{G_s^*}{-l . \omega . i . \eta_v^*} = \frac{G''(\omega) - iG'(\omega)}{l . \omega . \eta_v^*} \qquad \textbf{(I-18)}$$

According to the value of Bo, there are two cases, as below.

If the Bo value is high (Bo >> 1), the contribution of the sub-phases to the interfacial flow is very negligible (i.e., very little fluid viscosity). This is true when the interface is rigid (high viscosity η_s) or when the geometric ratio (1/1) is high (low contact area between the geometry and the interface).

If the Bo value is low (Bo << 1), the interfacial rheological properties could be overestimated due to the high contributions of the flow in the sub-phase. In such instances, specific numerical corrections need to be carried out to the measurable magnitudes [36, 40].

I.5.4. Correction for the Contributions of the Sub-Phases

The velocity profiles v in the sub-phases and at the interface need to be calculated for different Boussinesq numbers in the cylindrical coordinate system (r, θ, z) in order to solve the Navier–Stokes equation (Figure I-7) [36]. Supposing that the inertial effects are neglected; the interfaces are planar, incompressible and of very low Reynolds numbers; and the stress–deformation behavior of the liquid interface may be represented by the generalized Boussinesq surface fluid model (described above), then the velocity profiles can be obtained from the Navier–Stokes equation (based on the fundamental principle of dynamics (FDP)).

Approximations and boundary conditions:

- Boundary conditions:

No sliding at the walls of the tank and maximum speed at the walls of the geometry:

v_s (Cup boundary) = 0 and v_s (Geometry boundary) = max

Zero speed along z: v (z) = 0;

Boussinesq–Scriven model (balance of tangential stress) at the interface.

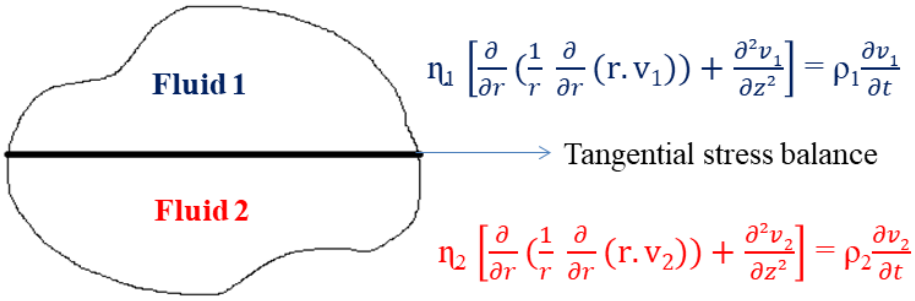

Figure I-7. Tangential stress balance.

- The tangential stress balance condition is as follows (under steady-state conditions):

$$\eta_1 \frac{\partial v_1}{\partial z} - \eta_2 \frac{\partial v_2}{\partial z} = \pm \eta_s \frac{\partial}{\partial r}\left(\frac{1}{r}\frac{\partial}{\partial r}(r.vs)\right) \quad \textbf{(I-19)}$$

The ± sign refers to the condition for the inner and outer gaps, respectively.

The surface viscosity η_s should be replaced by the complex number η_s^* for oscillatory flow.

- Separation of variables:

$$v_j = a_j(r,z).\Omega \quad \textbf{(I-20)}$$

$$\Omega = \theta_0.i.\omega.e^{i\omega t} \quad \textbf{(I-21)}$$

where v_j is the velocity in phase j; a_j is the amplitude of the velocity, which is a function of r and z; Ω is the angular velocity; ω is the frequency; and θ_0 is the angular velocity amplitude.

An iterative system that is based on the calculation of the velocity profiles is used for the subtraction of the contribution of the sub-phases. In the first step of the iteration, the authors calculate the initial value of the interfacial viscosity, based particularly on the formulas of equivalent geometry known as the double-wall ring [36] or the biconical bob geometry [40].

This often happens by evaluating a test inside a loop and imposing a convergence condition. The following steps share a common structure for the loop, starting with the first measured value of interfacial viscosity, called the "seed":

- Enter the "seed" interfacial viscosity;
- Compute the drag force and solve the Navier–Stokes equation, respecting the previously mentioned approximations and boundary conditions;
- Extract the new value of the interfacial viscosity;
- Check the convergence condition;
- If the convergence condition is verified, end the loop; if not, go back to the first step by using the first corrected value of the interfacial viscosity as a seed value.

All of these steps allow the computation of the corrected value of the torque T_C and the interfacial viscosity for a steady flow using this equation:

$$\eta_s^{k+1} = \eta_s^k . \frac{T_A}{T_C} \quad \textbf{(I-22)}$$

where T_A refers to the measured torque and k to the iteration step. The iteration is repeated until the deviation of the interfacial viscosity between two successive iterations is lower than 0.05% [40].

It is useful to mention that at high frequencies, the effect of fluid inertia (Reynolds number, Re) also needs to be taken into account in the corrections according to the methodology developed by Reynaert et al. [38].

Nowadays, in the rheometer market, many geometries allow the characterization of the interfacial rheological properties; these geometries are divided into two categories with two different measurement principles, namely translation and rotation. We are particularly interested here in three commercially available geometries: the oscillating needle, the bicone and the ring.

I.5.5. Interfacial Translational Rheometers

I.5.5.1. Oscillating Needle

The use of the oscillating needle as an interfacial rheological fixture was first proposed by Shahin [41]. The operating principle of the interfacial translational rheometer is practically the same as that of the bulk rheology. A magnetized needle is set up on the interface and oscillates longitudinally (Figure I-8). This needle is aligned along with the flow cell (silanized hydrophobic glass capillary). The sheared interface is the horizontal surface between the needle and the edge of the capillary [41]. A gradient in the magnetic field is generated by applying a different current through the two Helmholtz coils, which drives (translates or oscillates) the magnetic needle along the glass channel, with the resulting needle position being captured by a camera [42].

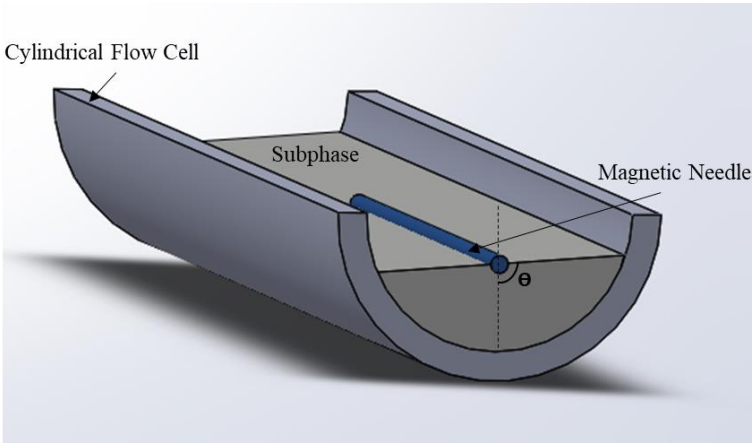

Figure I-8. Schematic diagram of the oscillating needle device used for interfacial rheology.

The first oscillating needle was manufactured by Plateau [15]. Currently, it is marketed under the name of the Interfacial Shear Rheometer (ISR) (Figure I-9). It can operate in two different modes: the static or harmonic regime.

In this case, the Boussinesq number can be expressed as:

$$\mathbf{Bo} = \frac{P\eta_s}{A\,\eta_v} = \frac{(2L + 4a)\eta_s}{2(\pi-\theta)aL\eta_v} = \frac{\eta_s}{a(\pi-\theta)\eta_v} \qquad \textbf{(I-23)}$$

where η_s is the surface viscosity, η_v is the viscosity of the bulk fluids, P is the perimeter of the probe in contact with the interface, A is the area of the probe in contact with the sub-phase, θ is the contact angle of the liquid on the probe, L is the length of the rod and a is the radius.

The interfacial viscosity is calculated from the shearing velocity (Figure I-9) of the magnetic needle (analogy with the rheology of the bulk).

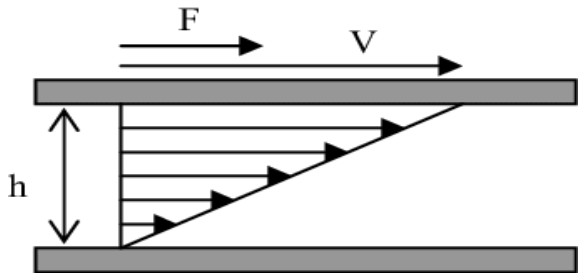

Figure I-9. Shear between two parallel flat plates: one is fixed and the other is mobile.

$$\dot{\varepsilon} = \frac{V}{h} \qquad \textbf{(I-24)}$$

$$\tau_S = \frac{F}{2L} \qquad \textbf{(I-25)}$$

$$\eta_S = \frac{\tau_s}{\dot{\varepsilon}} \qquad \textbf{(I-26)}$$

The complex interfacial modulus is calculated as follows:

$$\tau_s = \frac{F}{2L} = G^*_s \frac{z}{R-a} \qquad \textbf{(I-27)}$$

$$G_S^* = \frac{F}{z}\frac{R-a}{2L} = \frac{\tau_s}{\varepsilon_0} e^{i\tau(\omega)} = G'(\omega) + iG''(\omega) \qquad \textbf{(I-28)}$$

with

$$G'(\omega) = \left(\frac{\tau_s}{\varepsilon_0}\right).\cos(\delta) \qquad \textbf{(I-29)}$$

and

$$G''(\omega) = \left(\frac{\tau_s}{\varepsilon_0}\right).\sin(\delta) \qquad \textbf{(I-30)}$$

where F is the amplitude of the total drag force exerted on the needle; V, L and a are respectively the velocity, the length of the needle and the radius of the needle; R is the distance between the axis of the needle and the semi-cylindrical glass cell; and z is the amplitude of displacement of the needle.

The magnetic needle rheometer can produce a very high Boussinesq number due to its low surface contact with the interface. If the geometrical factor is not sufficient to compensate for the drag forces of the sub-phases, corrections must be applied as explained above (Section 4.4). The algorithm is

described in [36], and the implemented codes are available for download (https://softmat.mat.ethz.ch/opensource.html; last accessed July 08, 2022).

It is important to note that this technique is widely used in interfacial rheological studies, particularly in biology, to measure the surface (gas–liquid) tension and viscosity. This is the most sensitive technique among the interfacial shear measurements (the measured interfacial viscosity covers a wide range, from 10^{-6} to 10^{-1} Pa.s.m.); it is, however, more delicate to control because it is sometimes complicated to control the flotation of the needle, which relies on the surface tension (when the surface tension is too low, the needle sinks). This geometry is not appropriate for the study of interfacial rheological properties of viscous systems at low and high temperatures, such as polymer systems, because of their high viscosity and high melt temperature.

I.5.5.2. Pioneering Studies on the ISR

Based on the sensitivity of the ISR, there exist many studies that use this geometry to characterize interfaces. Here, we mention several studies on the ISR. The field of biology is the most studied with this geometry. Hermans and Vermant [43] focused on the study of the surface rheological properties of a phospholipid, DPPC (dipalmitoylphosphatidylcholine), on the air–water surface. They performed a complete temperature and surface pressure analysis of the interfacial shear rheology of DPPC, showing that the monolayer behaves as a viscoelastic liquid with a structure domain.

In another work [44], Hermans et al. studied the mechanisms affecting the stability of thin layers loaded with surfactants during their diffusion, using the drainage flows of a hemispherical dome. They concluded via the ISR that the presence of pulmonary surfactant replacement layers and DPPC monolayers at the air–fluid interface can improve the stability of thin films.

Gavranovic et al. [45] studied Langmuir monolayers of mixtures of straight and branched-chain hexadecanol forms using surface pressure isotherms on the ISR, at the air–water interface. The addition of branched molecules leads to a non-monotonic increase in surface viscosity.

Leiske et al. [46] studied the main components of the lipid layer of the tear film, referred to as the meibomian lipids. Using the ISR, they concluded that the interfacial meibum films were highly viscoelastic at 17 °C, but when the films were heated to 30 °C, the surface moduli decreased by more than two orders of magnitude.

Reynaert et al. [38] studied a purely viscous interface of known viscosity, produced by spreading thin silicon oil films onto a water layer, and a time-dependent viscoelastic interface was generated via the surface gelation of a lysozyme solution.

Freer et al. [47] studied protein adsorption at fluid–fluid interfaces after long-term exposure to produce interfacial gel-like networks. They used the ISR to examine the structure of a globular protein, lysozyme, and a disordered protein, α-casein, and to study the kinetics of the network formation at the

hexadecane–water interface. For lysozyme, the shear moduli grow with interfacial aging, indicating a transition from fluid-like behavior at early stages to network formation (solid-like behavior). Conversely, the interfacial shear moduli of α-casein change very little with interfacial aging.

I.5.6.6 Interfacial Rotational Rheometers

The principle of the interfacial rotational rheometer is based on a two-dimensional Couette geometry, in which the rotor with a radius of R_1 rotates inside the stator with a radius of R_2 [48]. The following equations can be used to compute the interfacial viscosity:

$$\tau_{int} = \frac{1}{4\pi} \frac{R_2^2 - R_1^2}{R_1^2 R_2^2} T \quad \text{(I-31)}$$

$$\varepsilon_{int} = \frac{R_2^2 + R_1^2}{R_2^2 - R_1^2} \varphi \quad \text{(I-32)}$$

$$\dot{\varepsilon}_{int} = \frac{R_2^2 + R_1^2}{R_2^2 - R_1^2} \Omega \quad \text{(I-33)}$$

$$\eta_{int} = \frac{\tau_{int}}{\dot{\varepsilon}_{int}} \quad \text{(I-34)}$$

$$\eta_{int} = \frac{1}{4\pi} \left(\frac{1}{R_1^2} - \frac{1}{R_2^2}\right). \frac{T}{\Omega} \quad \text{(I-35)}$$

where T, φ and Ω respectively represent the torque applied to the rotor, the angle of rotation of the rotor and the angular velocity of the rotor. These equations are rigorously valid only for Newtonian liquids or in the case of a narrow air gap $(R_2-R_1)/R_1 << 1$ (sufficiently high Bo).

I.5.6.1. Du Noüy Ring

In the beginning, this method was used for measuring the surface tension of a liquid. It is based on the same principle as the Wilhelmy plate method. Then, it was used for interfacial rheological measurements [49]. A horizontal ring is placed at the interface (or on the surface) and rotates or oscillates around its axis of rotation. This ring has a circular section, and a schematic profile of this geometry is displayed in Figure I-10.

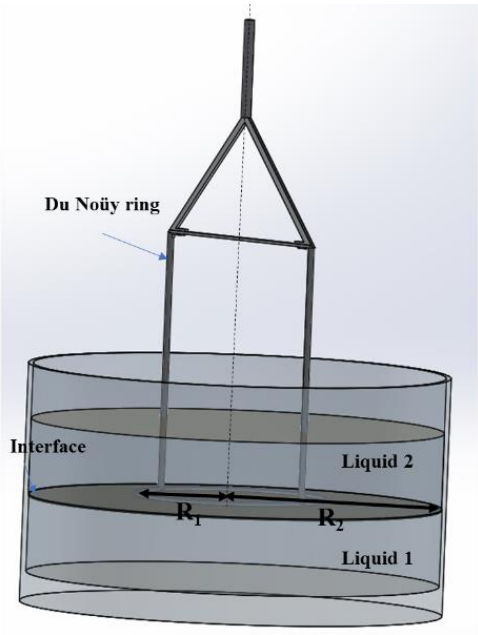

Figure I-10. Profile section of the Du Noüy ring device.

To measure the shear viscoelastic modulus, the applied equations are similar to the equations corresponding to the bidimensional cylindrical Couette geometry (they can be applied directly). The interfacial viscosity can be calculated by using the previous formulas of η_{int} (Equation (I-35)).

Noting that R_1 is the radius of the ring and R_2 is the radius of the cup containing the sub-phases, M and Ω respectively represent the torque applied to the rotor and the angular velocity of the rotor.

In this case, the Boussinesq number can be expressed as:

$$\mathbf{Bo} = \frac{\eta_{int}}{\eta_1+\eta_2}\frac{P}{A} = \frac{\eta_{int}}{\eta_1+\eta_2}\frac{(4\pi R_1)}{(2\pi^2 R_1 D)} = \frac{\eta_{int}}{\eta_1+\eta_2}\frac{2}{(\pi D)} \qquad \textbf{(I-36)}$$

where D is the diameter of the wire of the ring (0.36 mm), and η_1 and η_2 are respectively the viscosities of sub-phases 1 and 2.

The Du Noüy ring has a very light geometry with a low moment of inertia, which allows the measurement of interfacial properties. Furthermore, the geometrical factor $2/\pi D$ is very high, so the surface contact with the interface is low, leading to a high Boussinesq number. Nevertheless, if the geometrical factor is not enough to compensate for the drag forces of sub-phases (in other words, when Bo << 1), a numerical correction must be made to consider the effects of the sub-phases [36].

Despite this advantage, the Du Noüy ring also has some disadvantages, such as its fragility. It is easy to twist it during measurement (parts of the ring will be inside a sub-phase and not within the interface), which will lead to an erroneous calculation. Therefore, it is unsuitable for characterizing rigid interfaces (high interfacial viscosity ηs) or high-viscosity sub-phases (for instance, polymers). Another inconvenience of this geometry is the way the Du Noüy ring is placed in the interface. This is

related to its low contact area with the interface and its wetting properties (square section). Hence, the variation of the normal force is undetectable [49].

I.5.6.2. Bicone

I.5.6.2.1. Description

The bicone [40] is a robust geometry used to probe surfaces and interfaces. It is a two-dimensional projection of the Couette geometry used in bulk rheology. It is significantly tapered at its end (Figure I-11). The densest liquid is poured first, and then the bicone is placed at the surface.

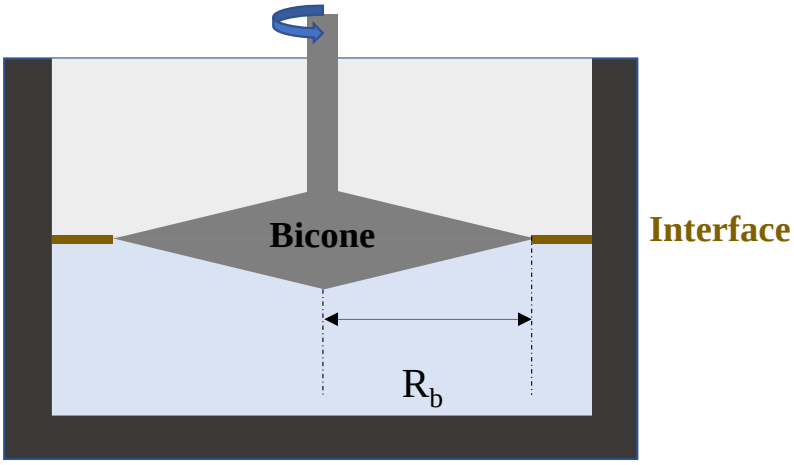

Figure I-11. Profile section of the bicone device.

The edges of the bicone need to be located exactly at the interface between the two immiscible liquids. This geometry is marketed by TA Instruments and Anton Paar. It can easily be attached to a rheometer and performs both the steady and oscillating tests. The bicone Boussinesq number is expressed as:

$$\mathbf{Bo} = \frac{\eta_{int}}{\eta_1+\eta_2}\frac{\mathbf{1}}{\mathbf{R_b}} \qquad \textbf{(I-37)}$$

where R_b is the radius of the bicone.

Independently of the ratio of the viscosities ($\frac{\eta_{int}}{\eta_1+\eta_2}$) of the studied system, the value of the Boussinesq number will decrease due to the geometrical factor ($\frac{1}{R_b}$) being low. This geometry is not often used to characterize fragile interfaces (with very low interfacial viscosity) and is rarely used for viscous sub-phases because the drag forces produced on the bicone are sometimes non-negligible.

When Bo << 1, a numerical correction based on an iterative method of the apparent data needs to be made to consider the effects of the sub-phases and to define the corrected value of the measured torque T_c (see the previous expressions). The implemented routine is available for download (https://data.mendeley.com/datasets/4tmy9k4ys3/1; last accessed July 08, 2022).

Soo-Gun and Slattery [48] demonstrated an exact solution of the velocity profiles in the two sub-phases and at the interface. The authors made assumptions for the sub-phases as well as for the interface. First, they supposed that the mass and momentum were conserved for the sub-phases. Second, they assumed that there was a jump in mass balance at the interface, i.e., that the velocity was continuous at the interface, which means that the dynamics of each of the two fluids were driven by the continuity and Navier−Stokes equations.

$$\mathbf{div\ v_\theta = 0\ with\ v_\theta = \bar{V}_s}\ \text{(in the above Equation (I-6))} \qquad \textbf{(I-38)}$$

where v_θ is the interfacial velocity vector.

Moreover, the authors defined a jump in momentum balance at the interface; in other words, the balance between the pressure and bulk viscous stress jumps through the interface, the stress generated by the interfacial viscosity and elasticity and the stress resulting from the dynamic interfacial tension, which includes the equilibrium interfacial tension, the Marangoni effect and Gibbs elasticity.

$$\boldsymbol{\tau_1.n_1 + \tau_2.n_2 + div(\tau) + \rho_s.g = 0} \qquad \textbf{(I-39)}$$

where τ is the interfacial stress tensor given in the Scriven–Boussinesq equation (Equation (I-6)), n_1 and n_2 are the normal vectors perpendicular to the interface pointing into phases 1 and 2, ρ_s is the mass density of the interface and g is the gravity per unit mass.

Finally, Soo-Gun and Slattery imposed a few boundary conditions. (a) Both of the sub-phases, as well as the interface, are incompressible and Newtonian. (b) The velocity of the sub-phases on the top, bottom and side of the walls is zero, while at the edge of the rotating bicone it is equal to the velocity of the bicone. (c) Supposing that the interface is flat, the shape and velocity distribution of the interface are stationary (steady flow). (d) The interfacial deflection is ignored. Therefore, the usual stress jump does not involve Laplace pressure. The research assumes a low Reynolds number and neglects the secondary flows. (e) The interfacial mass balance simplifies the surface divergence term. There are no Marangoni effects in the tangential stress balance.

Once this distribution of velocities is known, the reduced torque ($\overline{T}$) exerted by both liquids on the bicone and the interface (Figure I-12) is determined according to:

$$\overline{\mathbf{T}} = \overline{\mathbf{R_c}}\mathbf{3\ Bo}\frac{\partial}{\partial \bar{r}}\left(\frac{\overline{v_\theta}}{\bar{r}}\right)\Big|_{\bar{r}=\overline{R_c}} - \int_0^{\overline{R_c}} \frac{\partial \bar{v}_\theta^1}{\partial \bar{z}}\Big|_{\bar{z}=\overline{H_1}} \overline{r2}\ \bar{r}\ dr + \frac{1}{Y}\int_0^{\overline{R_c}} \frac{\partial \bar{v}_\theta^2}{\partial \bar{z}}\Big|_{\bar{z}=\overline{H_1}} \overline{r2}\ \bar{r}\ dr \qquad \textbf{(I-40)}$$

$$\mathbf{Y} = \frac{\eta_1}{\eta_2};\ \overline{\mathbf{r}} = \frac{\mathbf{r}}{\mathbf{R_1}};\ \bar{\mathbf{z}} = \frac{\mathbf{z}}{\mathbf{R_1}};\ \overline{\mathbf{H_1}} = \frac{\mathbf{H_1}}{\mathbf{R_1}};\ \bar{\mathbf{v}}_\theta^{\mathbf{j}} = \frac{\mathbf{v}_\theta^{\mathbf{j}}}{\mathbf{R_1\Omega - \bar{r}}} \qquad \textbf{(I-41)}$$

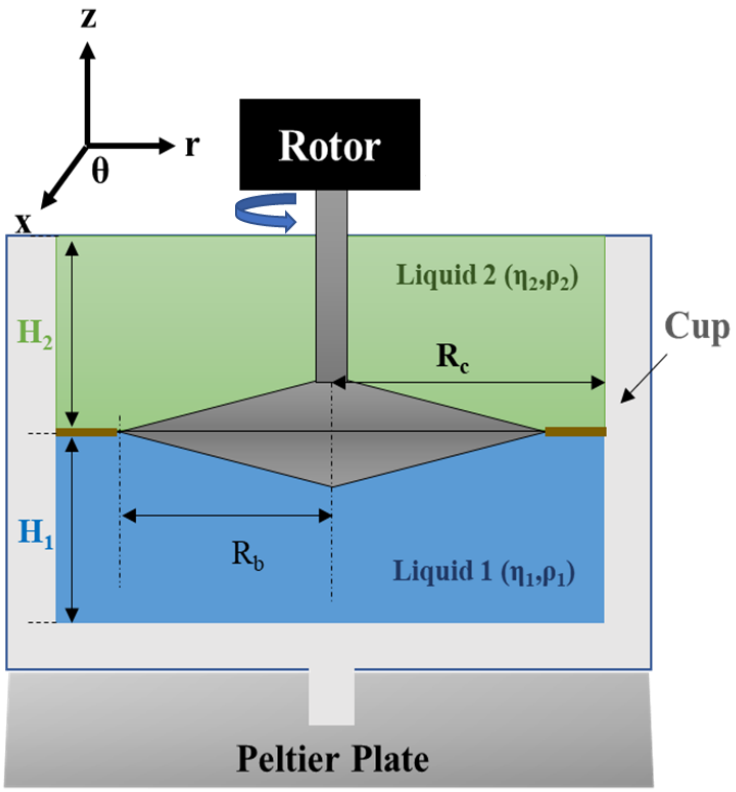

Figure I-12. Schematic diagram of the rotating biconical bob rheometer [50].

The exact solution of the reduced torque $\overline{T}$ proposed by Soo-Gun and Slattery is:

$$\overline{T} = \frac{T}{2\pi\Omega R_b{}^3(\eta_1+\eta_2)} \qquad \textbf{(I-42)}$$

In this case, T is replaced by $\overline{T}$ in the expression of the interfacial viscosity (Equation (I-30)).

$$\eta_{int,corr} = \frac{1}{4\pi}\left(\frac{1}{R_b 2} - \frac{1}{R_c 2}\right).\frac{\overline{T}}{\Omega} \qquad \textbf{(I-43)}$$

Soo-Gun and Slattery [48] have shown that the graphs of reduced torque as a function of Bo (Figure I-13) are represented by curves that depend on the ratio of the volume viscosities. These curves all converge toward the same linear asymptote for high values of Bo according to the following relation:

$$\overline{T} = \frac{2R_b 2}{R_c 2 - R_b 2}\,Bo \qquad \textbf{(I-44)}$$

(Line equation when Bo >>1)

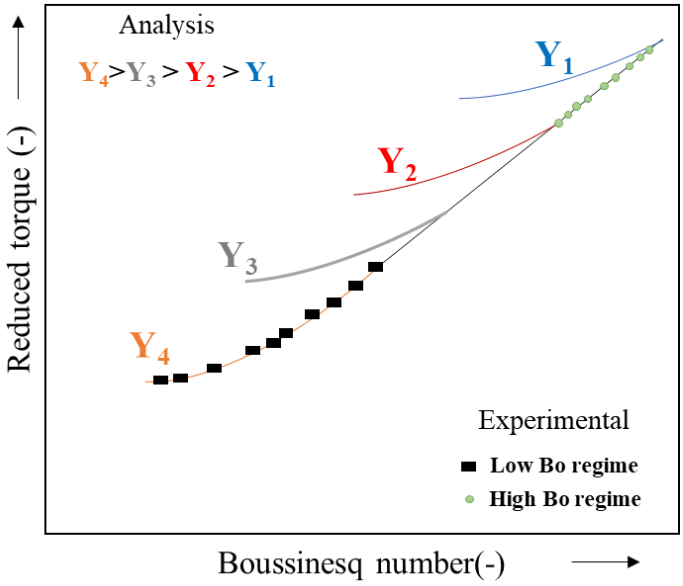

Figure I-13. Reduced torque evolution as a function of the Boussinesq number at different bulk viscosity ratios [50].

When the studied interface is rigid and the Boussinesq number is high, the interfacial stress must be calculated when R_c/H_1 and R_c/R_b tend toward 0. The interfacial viscosity will be expressed as:

$$\eta_{int} = \frac{T - \frac{8}{3} R_c^3 (\eta_1 + \eta_2) \Omega}{4\pi R_c^2 \Omega} \qquad \textbf{(I-45)}$$

It should be noted that interfacial rheology measurements are not straightforward, especially when performed at the rheometer's torque limit. The biconical geometry has a high weight (high momentum inertia); after extracting the inertia of the geometry and correcting for the effects of the sub-phases, the measured interfacial torque is very low or sometimes non-measurable, which makes the bicone less sensitive in this case and leads to less information from the collected data, particularly in the oscillating test, where the inertia is much more significant compared to the steady test. For this purpose, it is often used to characterize the viscoelastic properties of rigid interfaces (high interfacial viscosity). Probing the interfaces between two viscous polymers requires the adoption of a rigid, sturdy geometry in order to avoid deformation due to the high mechanical resistance of the polymers. In this thesis project, developed a novel biconical setup a gives the possibility of studying a wide range of molten polymer systems [51]. All details will be discussed in the chapter II.

I.5.6.2.2. Pioneering Studies on the Bicone

The bicone is infrequently used in interfacial rheology because of its inertia and its average sensitivity. Here, we highlight some examples of pioneering studies. In the field of biology, Erni et al. [50] studied steady shear and oscillatory experiments, as well as creep recovery and stress relaxation tests

at both oil–water and air–water interfaces with the adsorbed films of a globular protein (ovalbumin) and spread films of a surfactant (sorbitan tristearate).

The authors used the bicone in another work [52] to study the shear rheology of condensed interfacial layers (sorbitan tristearate) at the air–water interface. They defined the viscoelastic regime before performing shear experiments to avoid the destruction of the sample. By combining the interfacial rheology with microscopy, they concluded that interfacial films are both viscoelastic and fragile and are subject to fracture under small deformations, as shown by Brewster's angular microscopy method performed in situ in rheological experiments to record surface morphology.

Ruhs et al. [53] studied the interfacial shear rheology of three systems: β-lactoglobulin fibrils, peptides and monomers adsorbed at the water–MCT (medium-chain triglycerides) interface at pH 2 through a time sweep at constant frequency and deformation. The amplitude sweeps were performed after 16 h, and no differences between these systems could be observed at pH = 2. The interfacial elastic and viscous moduli increased when the pH increased.

It is useful to emphasize that this geometry can be efficient for probing rigid interfaces. Fan et al. [54] used the biconical geometry to study the interfacial shear rheology of asphaltenes (molecular substances that are found in crude oil) at the oil–water interface and their relation to the emulsion stability. They obtained a rigid interfacial film with a cross-linked structure due to the dispersion of the asphaltenes above a critical concentration in 20 h.

Ligiero et al. [55] studied the stability of oil–water emulsions by examining the interfacial films of surfactants already present in the crude oil. The authors used the bicone cell to define the shear interfacial rheological properties. They concluded that a perfect correlation with the emulsion stability and stronger mechanical properties lead to a more stable water–oil emulsion.

El Omari et al. [51] used a new bicone to study the interfacial properties at the interface of the two model fluids, polydimethylsiloxane (PDMS) and polyisobutylene (PIB). The authors also probed the interface of the immiscible molten polymers polycaprolactone (PCL) and polyethylene glycol (PEG). The apparent interfacial shear properties were measured in both oscillatory and steady flow modes. The contribution of the bulk sub-phases was corrected during the processing of the data, and the effects of the temperature and the molecular weight were also highlighted.

I.5.6.3. Double-Wall Ring (DWR)

I.5.6.3.1. Description

The double-wall ring (DWR) combines the advantages of the Du Noüy ring, which is lightweight (less inertia), and the bicone (the contact area is more important than the Du Noüy ring). It is a

geometry developed by TA Instruments [35]. Thus, just like the double-gap cylindrical Couette geometry, the double-wall ring has two gaps in which the interface is sheared (Figure I-14).

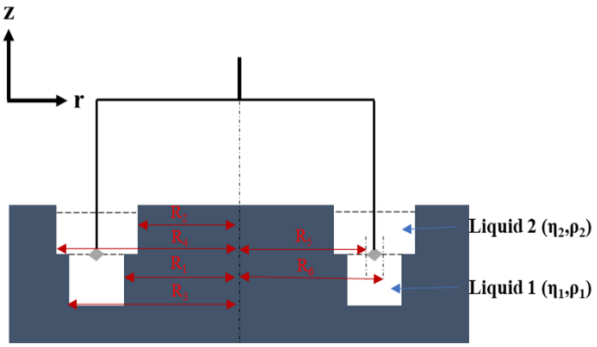

Figure I-14. Schematic diagram of the double-wall ring (DWR) device.

It consists of a thin ring and a cup (in Delrin®, Teflon or metal) with a rounded channel. The segment of the ring resembles a square (with a precise edge in contact with the interface (Figure I-15)) and is denoted a, which allows a better "grip" of the interface to the ring, in contrast to the rounded segment in the Du Noüy ring.

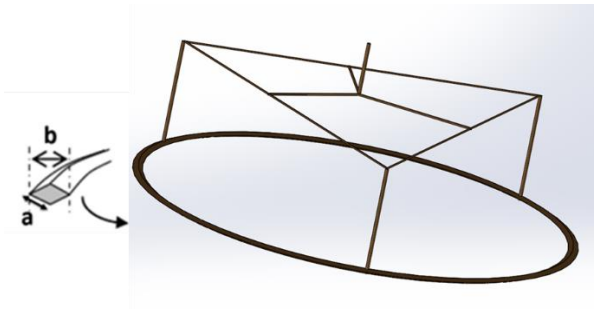

Figure I-15. Schematic diagram of the square section of the ring (DWR).

In order to benefit from the chemical inertness as well as the ease of cleaning and wettability, the ring and support feet are made of a platinum/iridium (Pt/Ir) material.

The double-wall ring (DWR) geometry is used to characterize interfacial thin films at both the gas–liquid surfaces and liquid–liquid interfaces. It helps to measure viscous as well as viscoelastic interfaces in the continuous shear and oscillatory experiments. The DWR can be attached to two types of rheometer: a CMT (combined motor transducer) and an SMT (separate motor transducer). The ring rotates or oscillates on the CMT rheometer, whereas on the SMT rheometer the cup rotates or oscillates [56].

In this case, the expression of the Boussinesq number is:

$$\mathbf{Bo} = \frac{\eta_{int}}{\eta_1+\eta_2}\frac{\mathbf{1}}{\mathbf{a}} \qquad \textbf{(I-46)}$$

where a is the diameter of the wire of the ring.

The interfacial stress can be expressed as:

$$\tau_{int} = \frac{T}{2\pi(R_5^2+R_6^2)} \quad \textbf{(I-47)}$$

The rate of interfacial deformation is given by:

$$\dot{\varepsilon}_{int} = \left[\frac{1}{\left(\frac{R_5}{R_1}\right)^2-1} + \frac{1}{1-\left(\frac{R_6}{R_1}\right)^2}\right]\Omega \quad \textbf{(I-48)}$$

The expression of the interfacial viscosity using the DWR is:

$$\eta_{int} = \frac{T}{2\Omega\,\pi(R_5^2+R_6^2)\left[\frac{1}{\left(\frac{R_5}{R_1}\right)^2-1}+\frac{1}{1-\left(\frac{R_6}{R_1}\right)^2}\right]} \quad \textbf{(I-49)}$$

The geometrical factor $\frac{1}{a}$ is beneficial for obtaining a high Boussinesq number. If the Bo is low, i.e., if the interfaces are sensitive (when the interfacial viscosity is low), numerical corrections can be carried out. The velocity profiles in the sub-phases can be determined using the Navier–Stokes equation in the cylindrical coordinates (r, θ, z). The boundary conditions [35] are listed below.

The no-slip condition at the inner and outer walls of the DWR:

$$v_1(R_1) = v_2(R_2) = v_1(R_3) = v_2(R_4) = 0 \quad \textbf{(I-50)}$$

The no-slip condition at the moving ring surface:

$$v_j(R_5) = R_5.\Omega \quad \textbf{(I-51)}$$

$$v_j(R_6) = R_6.\Omega \quad \textbf{(I-52)}$$

Moreover, the stress condition at the interface is ruled by the balance of the tangential stress (Boussinesq–Scriven equation) at the interface (see Equation (I-19)).

As mentioned previously, the determination of the corrected interfacial viscosity is based on an iterative approach using the numerical computation of the velocity profiles (see Equation (I-13)) [35]. In this context, the expression of the calculated torque is given by:

$$Tc = 2.\pi.\eta_{int}.R_5^3 \frac{d}{dr}\left(\frac{v_{int}}{r}\right)\Big|r = R_5 - 2.\pi.\eta_{int}.R_6^3 \frac{d}{dr}\left(\frac{v_s}{r}\right)\Big|r = R_5 - 2.\pi.\eta_1.\int_{R_5}^{R_r}\frac{dv_1}{dp_1} r_2.dr - 2.\pi.\eta_1.\int_{R_r}^{R_6}\frac{dv_1}{dp2} r_2.dr - 2.\pi.\eta_2.\int_{R_5}^{R_r}\frac{dv_2}{dp_3} r_2.dr - 2.\pi.\eta_2.\int_{R_r}^{R_6}\frac{dv_2}{dp_4} r_2.dr \quad \textbf{(I-53)}$$

The algorithm is described in [36], and the implemented codes are available for download at https://softmat.mat.ethz.ch/opensource.html (last accessed July 08, 2022).

It should be noted that the DWR presents some disadvantages, such as the fragility of the ring. Moreover, the temperature range of the measurements is restricted because of the heating system, which is not thermally insulated (much of the heat is exchanged with the ambient air outside). To conclude, a large range of polymers cannot be studied with this technique; this includes polymers with a high melting point and high viscosity. This geometry was used in the present work to probe surfaces and interfaces of low viscosity polymer systems (Chapter II).

I.5.6.3.2. DWR and Controlled Surface Pressure

The double-wall ring can also be used for measurements under pressure [35]. In such cases, the measuring cell is modified; the idea is to merge the Langmuir balance (explained in the next section covering the interfacial dilatational rheology) and the DWR and to homogenize the pressure inside and outside the ring. The geometry of the ring is changed to achieve this kind of manipulation by adding three 5 mm openings to the ring (Figure 11 in [35]). The temperature can be controlled by a fluid bath. The surface pressure is controlled using a Wilhelmy plate in both the Langmuir trough and the DWR cup during the compression–expansion cycle.

I.5.6.3.3. DWR and Dilatational Measurements

In interfacial rheology, the shear and expansion measurement techniques are examined separately. Verwijlen et al. [57] designed a new geometry by modifying the DWR cell to make it sinusoidal, referring to it as the DWSR (Figure 1 in reference [57]), to simultaneously monitor both the expansion and the shear of the interface based on the following constitutive equation:

$$\boldsymbol{\tau_s = [\sigma+(\eta_d-\eta_s)div_s.v_s+(K-G)\ div.u_s]I+2\eta_sD_s+2GU_s} \qquad \textbf{(I-54)}$$

where u_s is the surface displacement vector (m), U_s is the surface strain tensor for small deformation, and K and G are respectively the surface dilatational elasticity and shear elasticity (Pa.m).

This equation adds an elastic contribution to the Boussinesq–Scriven constitutive law. Due to the design of this geometry, the surface can be exposed and sheared, leading to a mixed flow. The elastic effect can be determined from the torque measurements.

In order to measure the complex dilatational interfacial viscosity from the torque measurements, a highly sensitive rotational rheometer is required, as well as a complex fluid interface whose torque is measurable in the sensitive region, with sensitivity values $|\Theta|$ between 20 and 2000.

The limitation of the torque is mainly affected by the shear surface viscosity, and the measured values are affected very little by interfacial rheology during dilatation (they are about 25 times more affected

by interfacial shear). It should be noted that the interpretation of the raw data requires knowledge of linear interfacial shear rheology as well as a high Boussinesq number. In other words, it is necessary to perform a manipulation of the interfacial shear rheology with the different geometries we previously explained (DWR, ISR, bicone) before interpreting the DWSR raw data.

I.5.6.3.4. Pioneering Studies on the DWR

Vandebril et al. [35] were the first scientists who tried to study interfaces using a DWR cell. They probed the behavior of complex interfaces such as the interface of poly(octadecylmethacrylate) (PODMA)–water, an interfacial layer of lysozyme (protein) on the air–water surface and a commercial lung surfactant on the air–water surface.

In another application, the DWR was also used to study the role of the interface in coalescence in polymer blends using nanoparticles as compatibilizing agents. Vandebril et al. [3] demonstrated that the nanoparticles mainly affect the surface rheological properties between an immiscible system, e.g., polydimethylsiloxane (PDMS)–polyisobutylene (PIB). Based on the frequency sweep at a fixed strain on a layer of an ellipsoidal particle at the PIB–PDMS interface, they concluded that increasing the particle volume fraction suppresses the coalescence more efficiently. For highly loaded polymer blends, the microstructure even becomes independent of the shear rate and no coalescence happens.

One of the fields most studied using the DWR is biology. For instance, Sharma et al. [58] combined bulk and interfacial rheology to study the behavior of surfactant-free bovine serum albumin (BSA) solutions. They used the interfacial flow sweep to demonstrate that the origin of this yield-like behavior, which is manifested as a highly shear-thinning bulk rheological response, lies in the formation of a film of adsorbed protein formed at the solution–gas interface.

This conclusion was confirmed in another work by Jaishankar et al. [59] by comparing the interfacial rheological measurements with the corresponding interface; they demonstrated that the apparent yield strength presented by these solutions comes from the presence of a viscoelastic layer formed by the adsorption of protein molecules at the air–water interface.

Wang et al. [60] studied the behavior of the interfacial viscoelastic natural silk fibroin (protein) at both the air–water and oil–water interfaces. This natural multiblock copolymer forms a stable film at these interfaces. This interfacial layer presents a rheologically complex behavior with strong surface elastic moduli that is only slightly frequency-dependent.

The DWR has also been used in the study of foams and emulsions. Barman et al. [34] utilized the DWR to study the stability of foams and Pickering emulsions through the particle-laden interfaces (PLI) adsorbed on an air–water or oil–water interface. The bulk rheology and the stability of these foams and emulsions depend on the interfacial rheology of the PLI. This study required the correlation

of the rheology with the microstructure by modifying the DWR cell to allow real-time, simultaneous interfacial visualization and shear rheology measurements. They demonstrated that the interfacial viscosity increases with increasing PLI concentrations and presents a shear thinning behavior.

Felix et al. [61] studied the dynamics of heterogeneous food products such as emulsions. These can be significantly affected by the interfacial properties of their interfaces. Proteins are widely used to increase the stability of these food products. This work compared the interfacial properties of a model protein (whey protein isolate, WPI) and silkworm pupae (SLW) adsorbed at the oil–water interface. A natural aldehyde (cinnamaldehyde, CNM) was used for both protein systems to promote protein–protein interactions. The results obtained from interfacial shear tests showed that the use of CNM resulted in the development of more robust interfaces, with higher values for the surface storage moduli and a lower loss tangent.

I.5.6.4. Comparison between the Different Geometries

Here, we give a simple comparison between the geometrical factor that depends on the $\frac{1}{l}$ ratio of each geometry to give an idea of the Boussinesq number (Table I-1):

Table I-1. Geometrical ratios of interfacial shear geometries.

Geometry	DWR (TA Instruments)	Bicone (Anton Paar)	ISR (KSV)
$\frac{1}{l}$ (m^{-1})	1,428.57	0.03	55.55

I.6. Interfacial Dilatational Rheology

In contrast to the interfacial shear analysis, in interfacial dilational rheology, the test consists of measuring the surface or interfacial tension when the area of the interface changes [39]. In the expansion–compression tests, the viscoelastic properties of the interface are characterized by the 2D elastic modulus E_d and the 2D dilatational viscosity η_d:

$$\mathbf{E}\boldsymbol{d} = \mathbf{A_0}\frac{\mathbf{d\gamma}}{\mathbf{dA}} = \frac{\mathbf{d\gamma}}{\mathbf{dlnA}} \qquad \textbf{(I-55)}$$

and

$$\boldsymbol{\eta_d} = \frac{\mathbf{d\gamma}}{\mathbf{dlnA/dt}} \qquad \textbf{(I-56)}$$

where A_0 is the initial interface area, γ is the surface tension and A is the interface area at time t. In the case of oscillatory measurements (harmonic testing of the interface at a frequency ω), a sinusoidal change in the surface tension can be observed with the presence of a phase shift. This can be explained

by the viscoelastic nature of the interface. With low-amplitude surface deformation, the response of the interface (surface tension variation) is linear. It can be expressed as follows:

$$\gamma = \gamma_0 + \Delta\gamma \sin(\omega t + \delta) \quad \text{(I-57)}$$

$$A = A_0 + \Delta A \sin(\omega t) \quad \text{(I-58)}$$

where ΔA and $\Delta\gamma$ are respectively the amplitude of the interfacial area and surface tension, while A_0 and γ_0 are respectively the interfacial area and surface tension just before the oscillatory deformation. In this case, we define the dilatational complex modulus E_d^* with a real part, the elastic modulus E', presenting the stored and recoverable energy, and an imaginary part, the viscous modulus E'', referring to the energy dissipated by the system:

$$E_d^* = E' + iE'' = |E_d|\cos\delta + i|E_d|\sin\delta \quad \text{(I-59)}$$

Before performing a frequency sweep, it is mandatory to define the linear region. In other words, we need to define the critical deformation in order to study the viscoelastic properties of the surfaces (or interfaces) in their reversible equilibrium state without any change to their structure. Therefore, an amplitude sweep experiment at a specific frequency needs to first be performed. When the interfacial viscoelastic modulus begins to decrease at the highest strain amplitude, we refer to the non-linear regime.

Another alternative to this classic strain sweep representation can be found in Lissajous–Bowditch plots (often referred to as Lissajous plots). This model was used extensively for bulk rheology and subsequently has been transposed for shear [62, 63] and dilatational [63] deformations of the interface. Lissajous plots are graphically presented for surface (or interface) shear experiments by plotting the stress responses versus the shear rate or strain amplitude, and for dilational rheology by plotting the complex modulus E* or surface tension (or alternatively surface pressure) versus the deformation [64]. Figure I-16 presents specific curves enabling the prediction of the linear (1) and non-linear (2) viscoelastic behaviors of the interfaces. In the case of linear dilatational interfacial rheology, the Lissajous plots are symmetrical, the variation of the dilatational modulus is independent of the applied strain and the variation of the interfacial tension follows a perfect sinusoidal curve, unlike the non-linear region.

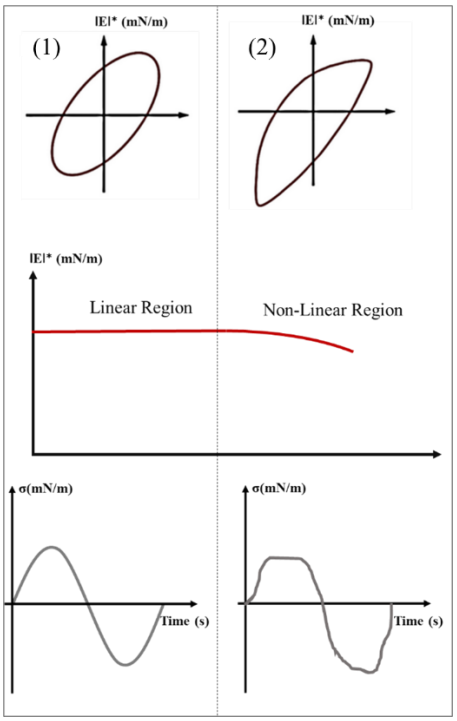

Figure I-16. Lissajous plots in interfacial rheology: (1) the behavior in the linear domain and (2) the behavior in the non-linear region.

Concerning the experimental part, there are two techniques that can be used to measure the interfacial dilational rheological properties. The first one is a direct measurement that consists of measuring the surface pressure (Langmuir balance). The second one is based on an optical contour analysis (oscillating pendant drop and spinning drop).

I.6.1. Langmuir Balance (or Langmuir Trough)

I.6.1.1. Description

The Langmuir balance uses the Wilhelmy plate (Figure I-17). The latter is a perfectly clean blade with a constant thickness e and length L (e << L) connected to a precise balance and immersed in a liquid. The liquid exerts an attractive force on the Wilhelmy plate, which depends on the nature of the liquid and the length of the blade [35].

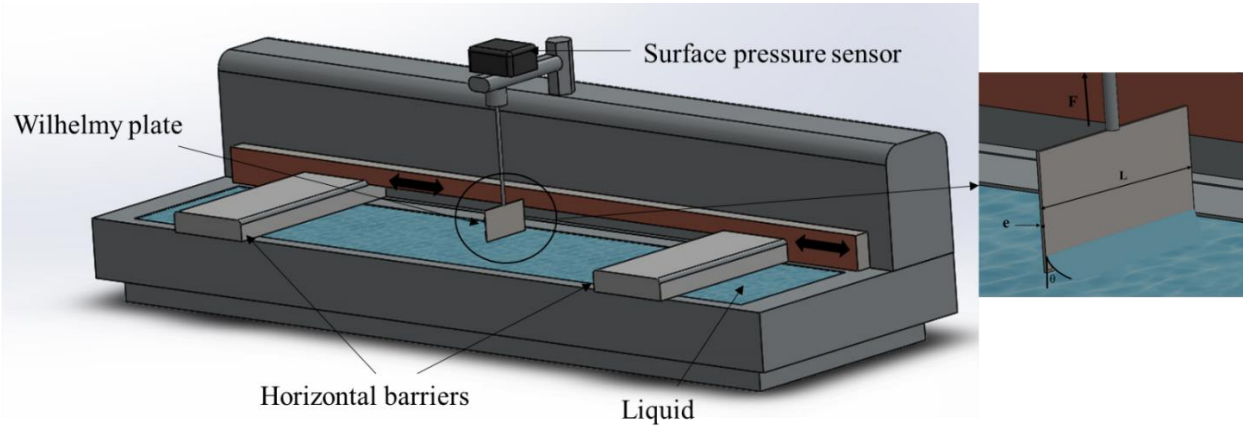

Figure I-17. Schematic diagram of the Langmuir balance.

When the Wilhelmy plate is immersed in a liquid, a meniscus is formed along the perimeter of the blade. The force exerted on the blade (blade pull-out force) is related to the surface tension by:

$$F = P\,\gamma\cos\theta \qquad \text{(I-60)}$$

where P is the perimeter of the blade, γ is the surface tension and θ is the contact angle.

The machine contains two barriers allowing the compression of the surface, while a pressure sensor above the tank allows the measurement of the surface pressure as a function of time and the area between the barriers. The two types of measurements are defined as described below.

I.6.1.2. Compression at Constant Velocity Followed by Relaxation

Here, we measure the variation of the surface pressure:

$$\Delta P = \Delta Pe + \Delta Pt \qquad \text{(I-61)}$$

where ΔPe is the variation of the equilibrium pressure:

$$\Delta Pe = E_e\frac{\Delta A}{A_0} \qquad \text{(I-62)}$$

while ΔP_t is the transient pressure (dissipated energy):

$$\Delta P_t = E_t\frac{\Delta A.\tau}{A_0}\left(1-\exp\left(\frac{-t}{\tau}\right)\right) \qquad \text{(I-63)}$$

and ΔP_t is monitored as a function of time.

I.6.1.3. Harmonic Stress (Oscillation) at a Frequency ω

In the methods involving a Langmuir trough, the deformation is a combination of shear and dilatation. For this reason, Pepicelli et al. [27] designed another custom radial surface compression system, in

which the deformation field is noticeably simpler, purely comprising dilation or compression. An elastic barrier is used to control the compression. Twelve fingers are used to apply uniform deformation to a radially shaped cup to facilitate a fluid mechanics analysis (Figure I-18).

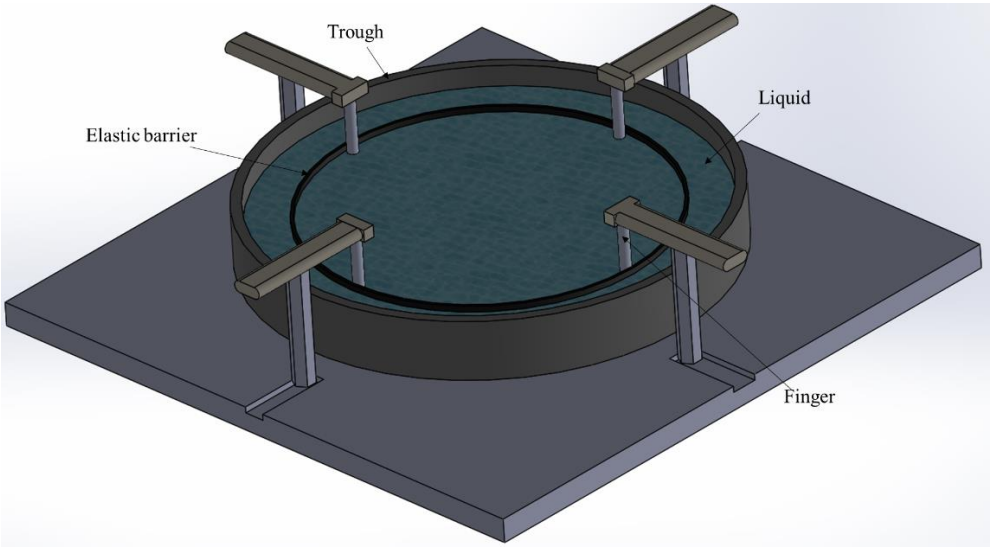

Figure I-18. Schematic diagram of the radial trough setup composed of a circular Teflon trough with an elastic barrier and aluminum fingers, controlled by a stepper motor, adapted from [27].

Note that the Langmuir balance allows an understanding of the dilatational rheological properties of surfaces of low-viscosity sub-phases. The design of this device does not permit measurements to be performed at high temperatures and equipping this instrument with a heating system can help overcome this limitation.

I.6.2. Oscillating Drop Tensiometry

I.6.2.1. Description of the Pendant Drop Method

The oscillating drop tensiometry method is based on the study of the shape of a liquid (or gaseous) pendant drop (or a rising drop) at the end of a capillary within another liquid or gaseous phase (Figure I-19).

The shape of the drop depends on the interfacial tension, which tends to make the drop spherical, and the difference between the density of the two fluids (gravitational effects), which tends to expand the drop and changes its spherical shape. The drop then takes on the form of a “bulb” [65].

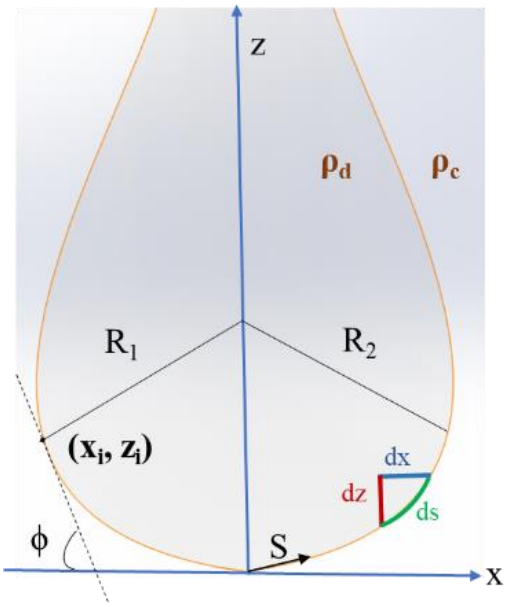

Figure I-19. Schematic diagram of the characteristics of the pendant drop.

In theoretical terms, at equilibrium, the drop (or bubble) obeys the Young–Laplace equation linking the Laplace pressure to both the radius of the curvature and the interfacial tension:

$$\gamma\left(\frac{1}{R_1}+\frac{1}{R_2}\right)=\Delta P=\Delta P_0-\Delta\rho gz \qquad \textbf{(I-64)}$$

where γ is the surface (or interfacial) tension, R_1 and R_2 are respectively the first and second principal radii of curvature, and $\Delta P = P_{in} - P_{out}$ is the Laplace pressure, which is the pressure difference across the interface.

Here, ΔP_0 is a reference pressure at $z = 0$, whereas $\Delta\rho gz$ is the hydrostatic pressure.

$\Delta\rho = \rho_d - \rho_c$ is the density difference; ρ_d and ρ_c are respectively the density of the drop phase and the density of the continuous phase.

By fitting the drop contour, the surface (or interfacial) tension can be extracted from the images of the drop (Figure I-20).

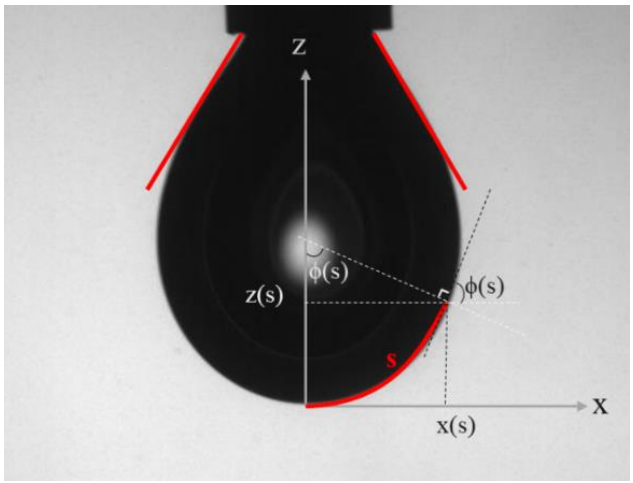

Figure I-20. A pendant drop image indicating the coordinate system used for determining the surface tension. The drop shape is fit to a solution of the Young–Laplace equation.

Another important parameter that needs to be well defined is the Bond number B_d (dimensionless) [65]. It represents the ratio between the gravitational forces and the interfacial tension. The shape of the drop depends on this number:

$$\mathbf{B_d} = \frac{\mathbf{g\Delta\rho R_{app}^2}}{\boldsymbol{\gamma}} \qquad \textbf{(I-65)}$$

The more the drop is spherical, the lower the Bond number becomes and the more the relative error of the measurement increases. By observing the expression of B_d, and in order to increase the accuracy of the measurement, it is recommended to increase the Bond number by increasing the radius of curvature (increasing the volume of the drop) or by increasing the difference in densities of the coexisting phases [50].

The Young–Laplace equation can be expressed in cylindrical coordinates r and x, according to differential equations in terms of the arc length s measured from the drop's apex, the Bond number Bd and the tangent angle ϕ in a curvilinear coordinate system of x(s) and z(s) (the smoothed solution of the Laplace equation).

$$\mathbf{R_1} = \frac{\mathbf{ds}}{\mathbf{d\phi}} \qquad \textbf{(I-66)}$$

$$\mathbf{R_2} = \frac{\mathbf{x}}{\mathbf{\sin\phi}} \qquad \textbf{(I-67)}$$

The first and second principal radii of curvature are defined as:

Considering the axisymmetry of the drop or bubble, the curvature at the apex is constant in all directions:

$$\mathbf{R_{apex} = R_1 = R_2} \qquad \textbf{(I-68)}$$

The reference pressure can be expressed as:

$$\mathbf{\Delta P_0 = \frac{2\gamma}{R_{apex}}} \qquad \textbf{(I-69)}$$

Therefore, Equation (I-64) can be obtained as a coupled set of differential equations in terms of the arc length x measured from the drop apex:

$$\mathbf{\frac{d\phi}{ds} = 2 - B_d z - \frac{\sin\phi}{x}} \qquad \textbf{(I-70)}$$

$$\mathbf{\frac{dx}{ds} = \cos\phi} \qquad \textbf{(I-71)}$$

$$\mathbf{\frac{dz}{ds} = \sin\phi} \qquad \textbf{(I-72)}$$

where R_{apex} is the radius of curvature of the surface.

Here, a comment needs to be added. The fitted Young–Laplace solution can also be used to give additional data, such as the drop volume V_d and drop surface area A_d, which are defined as:

$$\mathbf{V_d = \pi \int r^2 \sin\phi \, ds} \qquad \textbf{(I-73)}$$

and:

$$\mathbf{A_d = 2\pi \int r ds} \qquad \textbf{(I-74)}$$

These two relationships allow the extraction of other interesting interfacial data. For example, the percentage of evaporation of the pendant drop can be quantitatively determined by monitoring the variation over time of the volume of the drop (or bubble) [66].

I.6.2.2. Precision of the Pendant Drop Method: The Worthington Number

According to the Bond number expression, it is interesting to note that as the diameter of the needle decreases, the minimum Bond number value needed for an accurate calculation decreases. Berry et al. [65] introduced a universal solution independent of the needle diameter by using a dimensionless number, which represents the ratio of the drop volume V_d (calculated with Equation (I-73)) to the theoretical maximum drop volume V_{max}. Berry et al. [65] referred to this parameter as the Worthington number Wo (Figure I-21). It is expressed as follows:

$$\mathbf{Wo} = \frac{\mathbf{V_d}}{\mathbf{V_{max}}} \qquad \textbf{(I-75)}$$

where V_{max} is expressed as:

$$\mathbf{V_{max}} = \frac{\pi \mathbf{D_n} \gamma}{\Delta \rho \mathbf{g}} \qquad \textbf{(I-76)}$$

and D_n is the external diameter of the needle.

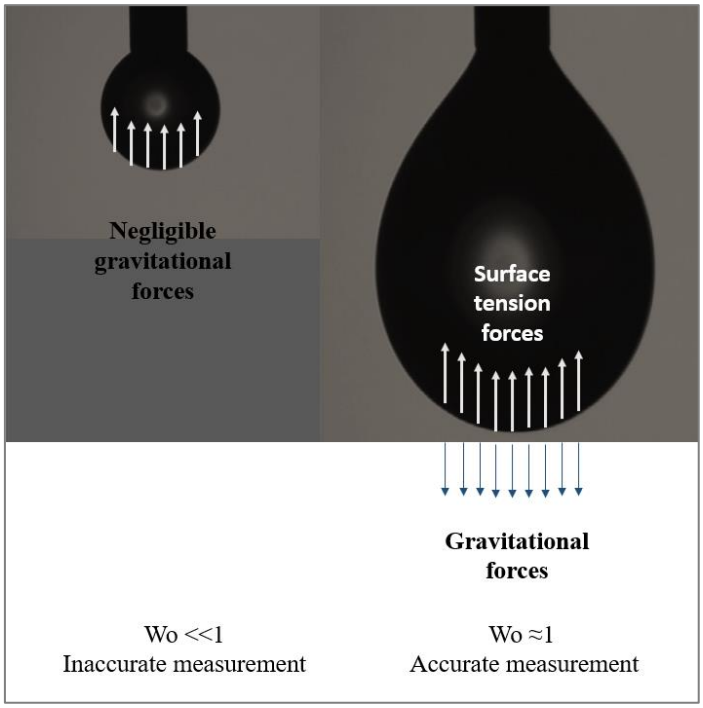

Figure I-21. Accuracy of the pendant drop method.

It should be noted that before launching the measurements, it is necessary to determine the volume corresponding to the detachment of the drop, V_{max}.

I.6.2.2. Rheological Measurements in the Harmonic Regime (Oscillation at a Given Frequency)

I.6.2.2.1. Description

The drop is subjected to a change in volume (through a piezoelectric or mechanical piston (Figure I-22)) with a sinusoidal deformation profile (Figure I-23), and the shape of the drop at each oscillation makes it possible to calculate the surface or interfacial tension via the Young–Laplace equation.

Since the pioneering articles that appeared in 1983 [67], developing the computational routines used for all available data of the pendant drop profile, which greatly increased the precision of the fitting methods, other papers have been published [65]; among these, we can cite the recent article by Kratz and Kierfeld [68].

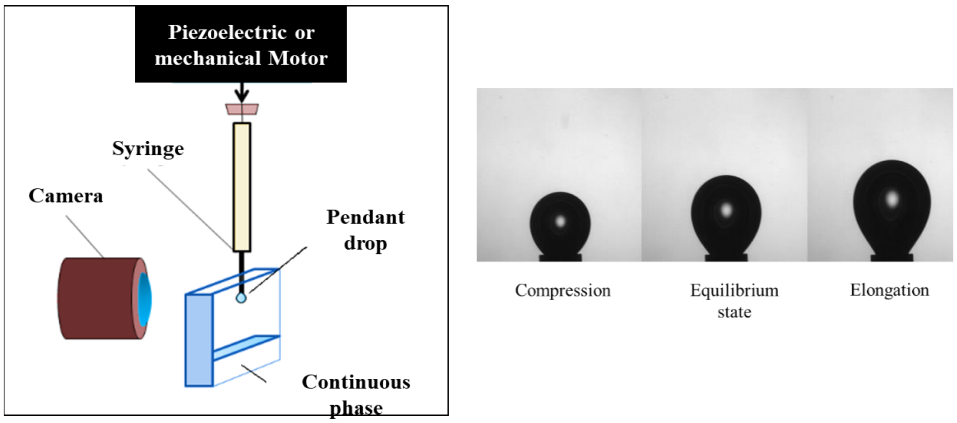

Figure I-22. Close-up views of an oscillating drop.

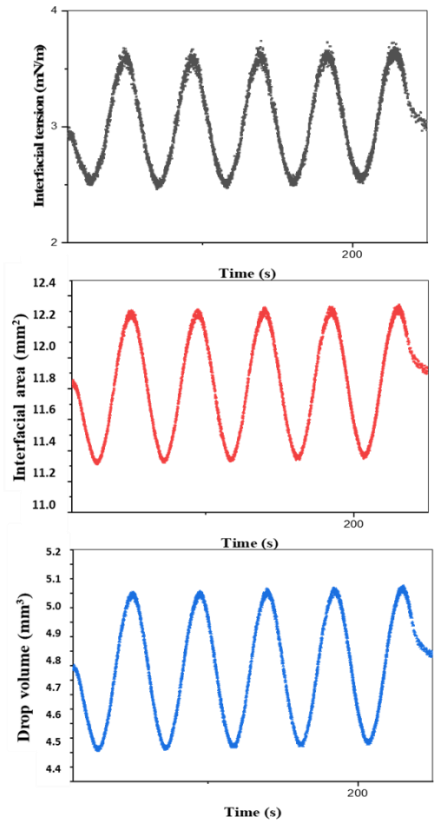

Figure I-23. The interfacial tension (mN/m), surface area A (mm^2) and drop volume V (mm^3) versus time t (s).

I.6.2.2.2. Influence of the Viscosity and Elasticity on the Interfacial Dilatational Measurements

I.6.2.2.2.1. Effect of the Continuous-Phase and Drop-Phase Viscosity

When measuring the static surface or interfacial tension with the pendant drop method, the gravitational effects acting on the drop or bubble are in equilibrium with the interfacial effects. In this case, the Young–Laplace equation is valid.

However, in the case of oscillatory measurements, other forces appear because of the change in the interfacial area during the experiment. In this instance, inertial and viscous forces modify the shape of the drop or bubble. Consequently, the Young–Laplace equation is invalid, and the measuring frequency range is restricted (the maximum frequency is limited) [69].

Other parameters need to be quantified in order to estimate the inertial and viscous forces [69]. They are the capillary number Ca, defined as the ratio of viscous to capillary forces, and the Weber number We, defined as the ratio of inertial to capillary forces:

$$\mathbf{We} = \frac{\Delta\rho\omega^2\Delta V^2}{\gamma R_c^3} \qquad \textbf{(I-77)}$$

$$\mathbf{Ca} = \frac{\Delta\eta\omega\Delta V}{\gamma R_c^2} \qquad \textbf{(I-78)}$$

where $\Delta\eta$ and $\Delta\rho$ are respectively the differences between the Newtonian viscosities and the densities of the drop and the continuous fluid, ω is the oscillation frequency of the drop, ΔV is the amplitude of volume oscillation, σ is the equilibrium interfacial tension and Rc is the radius of the capillary.

In the limits of Ca << 1 and We << 1, the drop shape is that of a static drop and is well described by the Young–Laplace equation.

To determine the dilatational behavior of viscous systems where the inertia is important, the principle of the time–temperature superposition is used to artificially extend the pulsation gap at a given temperature. Bouriat et al. [70] demonstrated that for a wide range of pulsations between 0.001 and 10 rad/s, the log–log curve of the elastic modulus E (expansion test) is a straight line, while the loss angle stays constant. Chambon and Winter [71] showed that for a crosslinking polymer system near its gelation point, the loss and storage moduli are parallel at the gel point, with a pulsation dependence of:

$$\mathbf{E' \propto E'' \propto \omega^n} \qquad \textbf{(I-79)}$$

where $0 < n < 1$ is a relaxation exponent. A gel with n approaching 1 is purely viscous, whereas for n approaching 0 it is purely elastic. The loss angle δ is related to n by:

$$\boldsymbol{\delta} = \frac{\mathbf{n\pi}}{\mathbf{2}} \qquad \textbf{(I-80)}$$

Abi Chebel et al. [72] demonstrated that for moderately aged crude oil droplets (≤ 5000 s), the elasticity and viscosity at a high frequency (10−80 Hz) could be extrapolated from low-frequency measurements (≤1 Hz) by the same power law of the frequency, ωn.

Main Physical Contributions to the Measured Signal and Calculated Surface Rheological Parameters

Regardless of the nature of the interface, the Laplace equation can be written for each point of the interface as:

$$\Delta P = P_{in} - P_{out} = \frac{T_1}{R_1} + \frac{T_2}{R_2} \qquad \textbf{(I-81)}$$

where T_1 and T_2 are respectively the surface tensions in two perpendicular directions along the interface (Figure I-24).

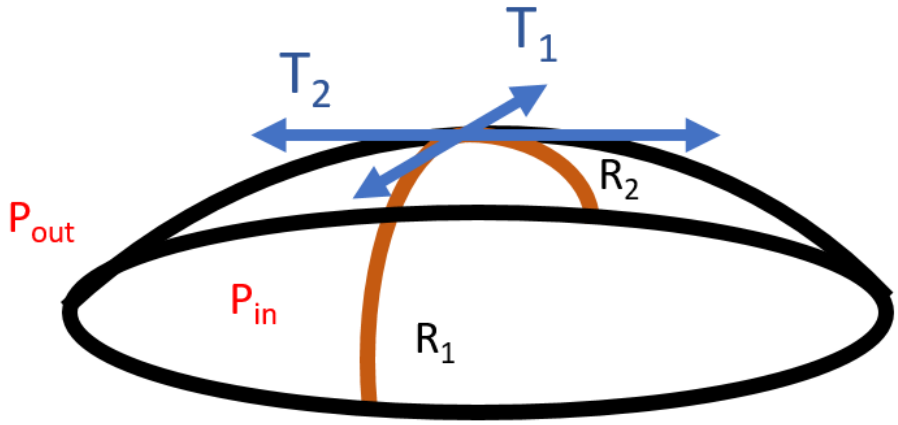

Figure I-24. Representation of the parameters defining the interface.

In static measurements, according to the Laplace equation, the surface (or interfacial) tension [73] varies linearly with the capillary pressure Pc. For reasons of symmetry, every direction is equivalent, so Equation (I-81) becomes:

$$\gamma = \frac{P_c \cdot R_{apex}}{2} \qquad \textbf{(I-82)}$$

However, in the dynamic measurements, P_{app}, the pressure applied to form the drop or bubble contains the capillary pressure (P_c) in addition to other contributions, such as the hydrostatic pressure, P_{hydr} (considered negligible), and P_{dyn}, the dynamic pressure (due to the deformation of the drop volume) [70].

$$P_{app} = P_{hydr} + P_{dyn} + P_c \qquad \textbf{(I-83)}$$

Note that in the static measurements, the dynamic pressure equals zero (mechanical equilibrium, where P_c = function (γ) and $P_{dyn} = 0$). In contrast to this case, during the oscillatory measurements, the capillary pressure is proportional not only to the surface tension but also to the viscous forces.

The complex interfacial modulus is obtained by replacing Equations (I-82) and (I-83) in the expression of the

$$E^* = \frac{d\gamma}{d\ lnA} = \gamma\left(1 - \frac{R_{s,eq}}{H_{s,eq}}\right) + \frac{R_{s,eq}}{2}\frac{d}{d\ lnA}(P_{app} - P_{hydr} - P_{dyn}) \qquad \textbf{(I-84)}$$

surface tension and generalizing Equation (8) from [74] to the following equation:

where $H_{s,eq}$ and $R_{s,eq}$ are respectively the initial drop height and the initial radius (apex) before starting the oscillation (the equilibrium value). Equation (I-84) can be written in a revised form:

$$E^* = E^*_0 - \frac{R_{s,eq}}{H_{s,eq}} \frac{dP_{dyn}}{d\ lnA}, \qquad \textbf{(I-85)}$$

$$E^*_0 \equiv \gamma \left(1 - \frac{R_{s,eq}}{H_{s,eq}}\right) + \frac{R_{s,eq}}{2} \frac{d}{d\ lnA}(P_{app}\text{-}P_{hydr}) \qquad \textbf{(I-86)}$$

Viscous and inertial contributions are included in P_{dyn}. For frequencies larger than 10 Hz, the inertial term in P_{dyn} becomes more significant (the inertial forces are neglected by using frequencies lower than 10 Hz). Hence, the viscous contribution in P_{dyn} consists of two parts.

The first part is the Poiseuille pressure (P_{Pois}) due to the flow in the capillary (Figure I-25); for a Newtonian fluid, P_{Pois} is given by the Poiseuille equation.

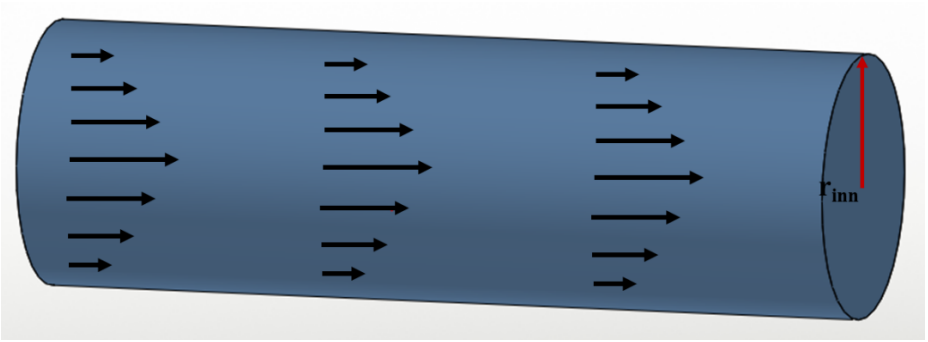

Figure I-25. The flow of a Poiseuille tube inside a needle.

$$P_{Pois} = \frac{8\eta_{inn} L}{\pi r_{inn}^4} \frac{dV}{dt} = 8 \frac{R^2_{s,eq} H_{s,eq}\ L}{r_{inn}^4} \frac{dlnA}{dt} \qquad \textbf{(I-87)}$$

where η_{inn} is the dynamic viscosity of the drop phase moving inside the capillary, L and r_{inn} are respectively the capillary length and its inner radius and dV/dt is the flow rate (the variation of the drop volume (cm^3/s) V, as a function of time).

The second part of the viscous contribution in P_{dyn} is the viscous pressure (P_{visc}) due to the bulk viscous forces acting from both adjacent phases on the drop surface. Two different methods are used to compute the P_{visc} [75]:

In the first place, by using the method of similarity and dimensional analyses in [76, 77], the following relationship for P_{visc} is obtained:

$$\mathbf{P_{visc} = \chi \frac{\eta_{out}}{r_c} \frac{dH_s}{dt} = \chi \frac{(\eta_{out} - \eta_{inn}) R_{s,eq}}{r_c} \frac{dlnA}{dt}} \qquad \textbf{(I-88)}$$

where r_c is the radius of the drop contact line, while the dimensionless parameter χ accounts for the drop geometry (χ should be a function of the ratio $\chi = H_s/r_c$).

In the second place, by theoretically solving the hydrodynamic problem of a dilatational or compressive spherical drop attached to a capillary in an outer fluid phase in [77], the hydrodynamic drag force (F_{visc}) can be calculated. When this force is applied in the circular section of the capillary, it creates pressure. This pressure can be expressed as follows:

$$\mathbf{P_{visc} = \frac{F_{visc}}{\pi r_c^2} \frac{\pi r_{inn}^2}{\pi r_c^2} = \frac{R^2_{s,eq} H_{s,eq} r_{inn}^2}{\pi r_c^5} [\eta_{inn} fa,0 + \eta_{out}(fab + fb)] \frac{dlnA}{dt}} \qquad \textbf{(I-89)}$$

As is obvious from Equations (I-88) and (I-89), the viscous stress contributions in P_{visc} depend on the rate of the surface deformation ($dlnA_s/dt$). They only contribute to the imaginary part of the complex interfacial modulus. Therefore, the expression of the dilatational elastic modulus (the real part of the complex modulus E*) (see Equation (I-86)) is:

$$\mathbf{E' = E'_0} \qquad \textbf{(I-90)}$$

while the dilatational loss modulus can be presented as:

$$\mathbf{E'' = E''_0 - E''_{Pois} - E''_{visc}} \qquad \textbf{(I-91)}$$

where E''_{Pois} and E''_{visc} are the dynamic corrections to the loss modulus due to the flow in the capillary and to the drop in dilatation or compression, respectively.

$$\mathbf{E''_{visc} = \chi \omega \frac{(\eta_{out} - \eta_{inn}) R2_{s,eq}}{r_c}} \qquad \textbf{(I-92)}$$

$$\mathbf{E''_{Pois} = 4\omega\eta_{inn} \frac{R^3_{s,eq} H_{s,eq} L}{r_{inn}^4}} \qquad \textbf{(I-93)}$$

$$\mathbf{E'' = E''_0 - \chi \omega \frac{(\eta_{out} - \eta_{inn}) R2_{s,eq}}{r_c} - 4\omega\eta_{inn} \frac{R^3_{s,eq} H_{s,eq} L}{r_{inn}^4}} \qquad \textbf{(I-94)}$$

Equation (94) shows that it is necessary to carry out the above for each correction of the dilatational loss modulus through the subtraction of the viscous and inertial contributions.

I.6.2.2.2.2. Effect of the Elasticity of the Interface

When the interface (or surface) is elastic, i.e., the interface can support a shear stress in the interfacial plane, the elasticity of the interface in the dilatational measurement is the sum of the interfacial tension γ and the interfacial elastic tensor. This is very often used in the study of interfacial membranes [78]

when the variation in the surface shear modulus reflects changes in the thermophysical properties of the interfacial film or the number density (cross-link density) of intermolecular interactions at the interface [79]. A neo-Hookean model was used to model the small deformation of the interface in this instance. The interfacial elastic tensor is given in Equation (4) from [79].

As mentioned earlier, a drop shape analysis or pressure tensiometry is used to extract the surface–material properties of these complex interfaces. The use of the Young–Laplace equation needs to be generalized to account for the extra and anisotropic stresses at the interface [80]. Shape-fitting methods, when combined with an adequate constitutive approach, do not perform well in defining the elastic stresses, especially for small deformations. Nagel et al. [81] used an additional measurement of the pressure or capillary pressure tensiometry to improve the sensitivity. This requires knowledge of the undeformed reference state (when the interfacial elastic tensor is negligible), which may be challenging to achieve in practice.

I.6.2.2.3. Operating Parameters That Can Disturb the Measurement

Many parameters can modify the measurements. Among these parameters, some may even disturb the measurements.

Vibration:

The first parameter that can disturb the measurements is the vibration due to the external environment (workplace insulation, sound, noise, etc.). To limit vibrations during the measurement, the box that contains the device should be equipped with rubber shock absorbers and placed on a stable support.

Verticality of the needle:

The symmetry of the drop and the balance of the forces exerted on the drop can be changed if the needle is not strictly vertical.

Impurities:

The presence of an impurity can disturb the measurements either by modifying the properties of the environment or by complicating the visualization of the drop, as well as the detection of the edges of the drop (or bubble). For example, air bubbles may be considered an impurity. To fix this problem, the samples should be degassed.

Drop configuration:

If the value of $\Delta\rho$ is positive ($\Delta\rho > 0$), we must use the pendant drop; if it is negative ($\Delta\rho < 0$), we must use the rising drop. In this case, the drop is formed upward at the tip of a U-bend (Figure I-26).

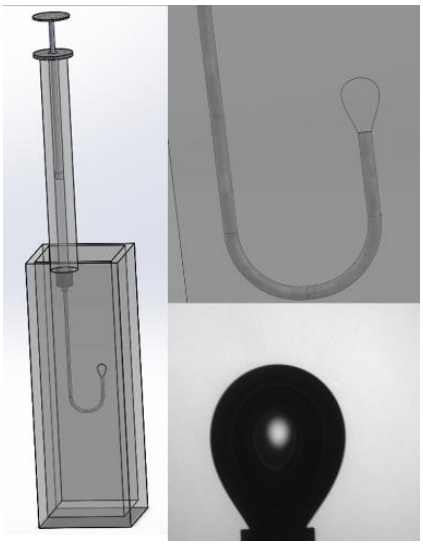

Figure I-26. Rising drop formed upward at the tip of a U-bend.

Stabilization time:

First, we form the drop, then the variation of the interfacial tension is monitored as a function of time until a constant value (plateau) is reached. Note that the experimental conditions should be constant, especially the parameters that most affect the interfacial (or surface) tension, such as the temperature and vibration.

Another issue that should be mentioned is the material characteristics, which could influence the accuracy of the measurement. For example, in the case of thermo-sensitive polymers, when the temperature increases and if the stabilization time to reach the equilibrium is long, the polymer may be degraded. Therefore, the measurements will be wrong. Taking this into consideration, the measurements should be made under an inert atmosphere.

The oscillating drop method is a potential technique that might allow the measurement of the dilatational rheological properties of polymer systems. This could be possible if some technical modifications based on the theoretical aspects of interfacial dilational rheology are applied. The details will be discussed in chapter III.

I.6.2.3. Some pioneering studies on dilational interfacial rheology based on the oscillating drop method

Ruhs et al. [77] performed oscillatory surface amplitude measurements with a pendant drop tensiometer to determine the linear regime of β-lactoglobulin fibrils and their derivatives. The deformation experiments combined with a frequency sweep of the interfacial films showed different surface rheological behaviors at high and low frequencies. These observed dilatational rheological responses were described using two different adsorption models, the Maxwell model and a modified Lucassen and van den Temple model.

Rühs et al. studied in another work [53] the static and dilatational responses of β-lactoglobulin fibrils and native β-lactoglobulin (monomers) at the water–air and water–oil interfaces at pH 2 using the pendant drop method. The resulting adsorption behavior and the viscoelasticity were dependent on the concentration and adsorption time. They observed that with higher concentrations, they achieved fast adsorption kinetics and slightly higher interfacial and surface pressures, but this did not lead to higher viscoelastic moduli.

Understanding the properties and behaviors of diluted bitumen–water interfaces under stresses is essential to find a solution to emulsion problems in bitumen production. Angle and Hua. [82] studied the interfacial dilational rheology of toluene-diluted mineral-free Athabasca bitumen. For all oscillation frequencies studied, they observed that the interfacial viscoelastic modulus of Athabasca bitumen in toluene reached a maximum at 0.865 g/L (0.1 wt%) bitumen, then declined as the bitumen concentration increased.

A recent work by Gimenez et al. [83] focused on escin (a natural mixture of triterpenoid saponins isolated from horse chestnut seeds). The stabilized air–water interfaces displayed a highly non-linear behavior during dilatation, as evidenced by the Lissajous plot method. The use of surface rheological measurements beyond the commonly measured linear domain has provided new insights into the behavior of these interfaces and their microstructure.

The oscillating pendant (or rising) drop is also present in the study of oil extraction. Ligiero et al. [73] explored the characterization of a crude oil interfacial film (IM) isolated from wet silica via the oscillating rising drop method at 30 °C. Dilatational rheology measurements revealed that successive IM extracts from crude oil are composed of molecules that behave increasingly like insoluble surfactants that aggregate at the water–oil interface. These surfactants would be responsible for hindering the mechanical characteristics of the interface.

Abi-Chebel et al. [72] evaluated the dilatational rheology of a pendant-shaped diluted crude oil within water with an interface that contained a significant amount of surfactant. At a low frequency, the fluid viscosity and inertia were negligible, which allowed a direct determination of the dilatational interfacial rheology. This interfacial film underwent a viscoelastic behavior, with the elastic moduli being larger than the viscous moduli.

I.6.3. Spinning Drop Method

Based on the same principle as the pendant drop method, spinning drop tensiometry uses the optical contour analysis of a drop to determine the minimal interfacial tensions (below 1 mN/m), which cannot be performed with the other interfacial tension devices. Instead of dosing a drop using a syringe and a needle, a drop of the less dense liquid is put inside another liquid of higher density. The drop is exposed to gravity and placed inside a rotating capillary tube. Due to the centrifugal forces, the

drop is deformed cylindrically toward the rotational axis (Figure I-27) and its interfacial area increases. The interfacial tension counteracts this increase in area and can, thus, be determined by analyzing the shape of the drop in the equilibrium state.

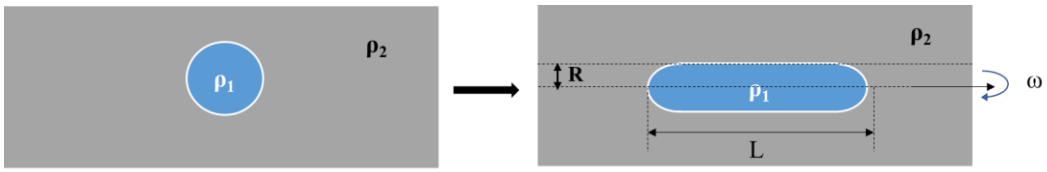

Figure I-27. Schematic diagram of the spinning drop principle.

This method was developed by Vonnegut [84]. The interfacial tension can be determined if the drop length is at least four times longer than the drop radius: L > 4R (Equation (I-95)).

$$\gamma = \frac{\Delta\rho \cdot R^3 \cdot \omega^2}{4} \qquad \textbf{(I-95)}$$

where ω is the angular velocity and R is the radius of the spinning drop.

To investigate the viscoelastic properties of systems with such low interfacial tension, the spinning drop is deformed with a known frequency instead of a steady rotational velocity, which directly results in a sinusoidal change of the interfacial area. In this instance, the interface elongation–compression is performed by oscillating the continuous phase. The calculation of the dilational modulus E_d and viscosity η_d is the same as explained previously.

The spinning drop method in oscillation was developed for the first time in 2018 by Zamora et al. [85], who used the oscillating spinning drop method to study surfactant-free systems, soluble surfactant systems and insoluble surface-active species (asphaltenes in a solvent–brine interface).

I.7. Conclusions and Perspectives

In this literature review, the theoretical and experimental aspects of interfacial rheology are highlighted. This specific branch of rheology has been used to study liquid–liquid or air–liquid systems with or without an active agent at the surface (or interface). In order to probe the interfacial viscoelastic properties and follow the same formalism as in bulk rheology, an interface must be deformed, either by shear force, in which the interfacial area remains constant, or by elongation, in which the interfacial area changes. Each type of deformation provides information about the surface (or interface), depending on the application studied.

As shown in the different parts of this report, interfacial shear rheology requires the use of a geometry positioned at the interface of the two sub-phases. The oscillating needle, the bicone and the double-wall ring (DWR) are the most common geometries used to probe the interface. Deforming an interface generates a flow at the sub-phase level, and the recorded response is the sum of the interfacial effects

and the bulk effects; hence, the interest in quantifying a unitless macroscopic number, the Boussinesq number, which represents the ratio of these two effects. At low Boussinesq numbers, the subtraction of the contribution of the sub-phases is accomplished numerically with an iterative method (DWR and oscillating needle) or directly using an exact solution (bicone).

When the interface (or surface) has to be expanded (or compressed), interfacial dilatational rheology is involved. Several studies have been based on the Langmuir balance or the oscillating pendant drop method. The principle of these techniques is to measure the change in interfacial tension after a change in interfacial area, either via imaging (rising or pendant drop) or by measuring the surface pressure (Langmuir balance). The correction of the viscoelastic moduli by subtracting the effects of the sub-phase viscosity and elasticity has also been documented.

The oscillating drop method has potential for the study of the interfacial expansion of molten polymers if it can be adapted, in the same way as discussed in the case of the shear force, using a heated closed cell and isolation with suitable syringes and needles (low-capillary and Weber numbers).

The interfacial rheology of polymer systems in the molten state has rarely been investigated due to the difficulty of manipulating these materials and due to their intrinsic properties, such as their viscosity and high melting points. On the other hand, current commercial interfacial rheological devices have not been designed to study molten polymer systems, which require an adaptation of these techniques.

Probing the interfaces between two molten polymers requires the overcoming of technical or material constraints. A heating system is essential to broaden the range of polymers studied, as well as an innovative shear geometry that is both robust mechanically, to deform viscous polymer interfaces, and also light with a high geometric factor (Boussinesq number), to reduce its inertia when performing experiments within the limits of current rheometers and tensiometers.

Contrary to the conventional indirect modeling methods used for the assessment of polymer–polymer interfacial properties, the application of interfacial rheology to molten polymer systems might allow the direct measurement of their interfacial behavior, which is predominant in the case of polymer blends, coextruded multilayer polymers and polymer foams. Additionally, interfacial rheology can be essential to study interdiffusion and interphase formation from one polymer to another in the case of reactive interfaces, such as reactive compatibilized immiscible polymer melts. For all these reasons, high-temperature interfacial rheology appears to be one of the most promising techniques that should be further developed in the near future to probe the different polymer–polymer interfaces encountered in the processing and formation of multiphase polymer systems.

The choice of the interfacial rheological instruments used in this thesis project to study polymers interfaces, their particular modifications/adaptations and the investigation of interfacial processes for polymer systems (interdiffusion, interfacial reaction…) will be discussed in the next chapters.

I.8. References

[1] R. Y. Liu, Y. Jin, A. Hiltner, and E. Baer, "Probing nanoscale polymer interactions by forced-assembly," *Macromolecular rapid communications*, vol. 24, no. 16, pp. 943-948, 2003.

[2] C. W. Macosko, H. K. Jeon, and T. R. Hoye, "Reactions at polymer–polymer interfaces for blend compatibilization," *Progress in Polymer Science*, vol. 30, no. 8-9, pp. 939-947, 2005.

[3] S. Vandebril, J. Vermant, and P. Moldenaers, "Efficiently suppressing coalescence in polymer blends using nanoparticles: role of interfacial rheology," *Soft Matter*, vol. 6, no. 14, pp. 3353-3362, 2010.

[4] D. Langevin, "Influence of interfacial rheology on foam and emulsion properties," *Advances in Colloid and Interface Science*, vol. 88, no. 1-2, pp. 209-222, Dec 2000, doi: 10.1016/s0001-8686(00)00045-2.

[5] S. Costa, R. Höhler, and S. Cohen-Addad, "The coupling between foam viscoelasticity and interfacial rheology," *Soft Matter*, vol. 9, no. 4, pp. 1100-1112, 2013.

[6] V. Kulichikhin, A. Y. Malkin, A. Maklakova, and A. Semakov, "Some Dynamic Properties of the Interface," *Russian Journal of General Chemistry*, vol. 92, no. 4, pp. 679-693, 2022.

[7] J. S. Hong and P. Fischer, "Bulk and interfacial rheology of emulsions stabilized with clay particles," *Colloids and Surfaces A: Physicochemical and Engineering Aspects*, vol. 508, pp. 316-326, 2016.

[8] A. Das, E. L. Gilmer, S. Biria, and M. J. Bortner, "Importance of Polymer Rheology on Material Extrusion Additive Manufacturing: Correlating Process Physics to Print Properties," *ACS Applied Polymer Materials*, vol. 3, no. 3, pp. 1218-1249, 2021.

[9] H.-Q. Sun, L. Zhang, Z.-Q. Li, L. Zhang, L. Luo, and S. Zhao, "Interfacial dilational rheology related to enhance oil recovery," *Soft Matter*, vol. 7, no. 17, pp. 7601-7611, 2011.

[10] C. D. Han, *Multiphase Flow in Polymer Processing. In: Astarita, G., Marrucci, G., Nicolais, L. (eds) Rheology. Springer, Boston, MA, 1980; pp. 121–128.*

[11] T. F. Tadros, "Fundamental principles of emulsion rheology and their applications," *Colloids and Surfaces A: Physicochemical and Engineering Aspects*, vol. 91, pp. 39-55, 1994.

[12] F. S. Ariola, A. Krishnan, and E. A. Vogler, "Interfacial rheology of blood proteins adsorbed to the aqueous-buffer/air interface," *Biomaterials*, vol. 27, no. 18, pp. 3404-3412, 2006.

[13] B. S. Murray and E. Dickinson, "Interfacial rheology and the dynamic properties of adsorbed films of food proteins and surfactants," *Food Science and Technology International, Tokyo*, vol. 2, no. 3, pp. 131-145, 1996.

[14] D. Wasan, J. McNamara, S. Shah, K. Sampath, and N. Aderangi, "The role of coalescence phenomena and interfacial rheological properties in enhanced oil recovery: an overview," *Journal of Rheology*, vol. 23, no. 2, pp. 181-207, 1979.

[15] J. Plateau, "Experimental and theoretical research into the figures of equilibrium of a liquid mass without weight," *Philosophical Magazine and Journal of Science*, vol. 38, no. 257, pp. 445-455, 1869, doi: 10.1080/14786446908640254.

[16] Y. Pawar and K. J. Stebe, "Marangoni effects on drop deformation in an extensional flow: The role of surfactant physical chemistry .1. Insoluble surfactants," *Physics of Fluids*, vol. 8, no. 7, pp. 1738-1751, Jul 1996, doi: 10.1063/1.868958.

[17] L. Rayleigh, "On the superficial viscosity of water," *Proceedings of the Royal Society of London*, vol. 48, pp. 127-140, 1890.

[18] M. Boussinesq, "Sur l'existence d'une viscosité superficielle dans la mince couche de transition séparant un liquide d'un autre fluide contigu," *Annales de chimie et de physique*, vol. 29, pp. 349-357, 1913.

[19] E. Chénier, C. Delcarte, G. Kasperski, and G. Labrosse, *Thermocapillary flows and vorticity singularity." Interfacial Fluid Dynamics and Transport Processes. Springer, Berlin, Heidelberg, 2003. 177-200.*

[20] Y. D. Shikhmurzaev, "The moving contact line on a smooth solid surface," *International Journal of Multiphase Flow*, vol. 19, no. 4, pp. 589-610, 1993.

[21] D. Lyubimov, T. Lyubimova, J. I. D. Alexander, and N. Lobov, "On the Boussinesq approximation for fluid systems with deformable interfaces," *Advances in Space Research*, vol. 22, no. 8, pp. 1159-1168, 1998.

[22] J. Gibbs, "On the equilibrium of heterogeneous substances, vol 1. Collected works," ed: Longmans, Green, and Co., New York, 1876.
[23] N. O. Jaensson, P. D. Anderson, and J. Vermant, "Computational interfacial rheology," *Journal of Non-Newtonian Fluid Mechanics*, vol. 290, p. 104507, 2021.
[24] L. Scriven, "Dynamics of a fluid interface equation of motion for Newtonian surface fluids," *Chemical Engineering Science*, vol. 12, no. 2, pp. 98-108, 1960.
[25] J. C. Slattery, L. Sagis, and E.-S. Oh, *Interfacial Transport Phenomena; Springer Science & Business Media: 2007, New York, USA*.
[26] N. Jaensson and J. Vermant, "Tensiometry and rheology of complex interfaces," *Current Opinion in Colloid & Interface Science*, vol. 37, pp. 136-150, Sep 2018, doi: 10.1016/j.cocis.2018.09.005.
[27] M. Pepicelli, T. Verwijlen, T. A. Tervoort, and J. Vermant, "Characterization and modelling of Langmuir interfaces with finite elasticity," *Soft Matter*, vol. 13, no. 35, pp. 5977-5990, 2017.
[28] M. Carrozza, M. Hulsen, and P. Anderson, "Benchmark solutions for flows with rheologically complex interfaces," *Journal of Non-Newtonian Fluid Mechanics*, vol. 286, p. 104436, 2020.
[29] M. Carrozza, M. Hütter, M. Hulsen, and P. Anderson, "Constitutive framework for rheologically complex interfaces with an application to elastoviscoplasticity," *Journal of Non-Newtonian Fluid Mechanics*, p. 104726, 2022.
[30] E. de Kinkelder, L. Sagis, and S. Aland, "A numerical method for the simulation of viscoelastic fluid surfaces," *Journal of computational physics*, vol. 440, p. 110413, 2021.
[31] L. M. Sagis, "Dynamic properties of interfaces in soft matter: Experiments and theory," *Reviews of Modern Physics*, vol. 83, no. 4, p. 1367, 2011.
[32] J. Gounley, G. Boedec, M. Jaeger, and M. Leonetti, "Influence of surface viscosity on droplets in shear flow," *Journal of Fluid Mechanics*, vol. 791, pp. 464-494, 2016.
[33] S. C. Ozan and H. A. Jakobsen, "Effect of surface viscoelasticity on the film drainage and the interfacial mobility," *International Journal of Multiphase Flow*, vol. 130, p. 103377, 2020.
[34] S. Barman and G. F. Christopher, "Simultaneous interfacial rheology and microstructure measurement of densely aggregated particle laden interfaces using a modified double wall ring interfacial rheometer," *Langmuir*, vol. 30, no. 32, pp. 9752-9760, 2014.
[35] S. Vandebril, A. Franck, G. G. Fuller, P. Moldenaers, and J. Vermant, "A double wall-ring geometry for interfacial shear rheometry," *Rheologica Acta*, vol. 49, no. 2, pp. 131-144, 2010.
[36] D. Renggli, A. Alicke, R. H. Ewoldt, and J. Vermant, "Operating windows for oscillatory interfacial shear rheology," *Journal of Rheology*, vol. 64, no. 1, pp. 141-160, 2020.
[37] D. A. Edwards, H. Brenner, D. T. Wasan, and A. M. Kraynik, "Interfacial transport processes and rheology," *PhT*, vol. 46, no. 4, p. 63, 1993.
[38] S. Reynaert, C. F. Brooks, P. Moldenaers, J. Vermant, and G. G. Fuller, "Analysis of the magnetic rod interfacial stress rheometer," *Journal of Rheology*, vol. 52, no. 1, pp. 261-285, Jan-Feb 2008, doi: 10.1122/1.2798238.
[39] S. Derkach, J. Krägel, and R. Miller, "Methods of measuring rheological properties of interfacial layers (Experimental methods of 2D rheology)," *Colloid journal*, vol. 71, no. 1, pp. 1-17, 2009.
[40] R. Nagarajan, S. I. Chung, and D. T. Wasan, "Biconical bob oscillatory interfacial rheometer," *Journal of Colloid and Interface Science*, vol. 204, no. 1, pp. 53-60, Aug 1998, doi: 10.1006/jcis.1998.5583.
[41] R. Miller, J. K. Ferri, A. Javadi, J. Krägel, N. Mucic, and R. Wüstneck, "Rheology of interfacial layers," *Colloid and Polymer Science*, vol. 288, no. 9, pp. 937-950, 2010.
[42] J. Ding, H. E. Warriner, J. A. Zasadzinski, and D. K. Schwartz, "Magnetic needle viscometer for Langmuir monolayers," *Langmuir*, vol. 18, no. 7, pp. 2800-2806, 2002.
[43] E. Hermans and J. Vermant, "Interfacial shear rheology of DPPC under physiologically relevant conditions," *Soft matter*, vol. 10, no. 1, pp. 175-186, 2014.
[44] E. Hermans, M. S. Bhamla, P. Kao, G. G. Fuller, and J. Vermant, "Lung surfactants and different contributions to thin film stability," *Soft Matter*, vol. 11, no. 41, pp. 8048-8057, 2015, doi: 10.1039/c5sm01603g.

[45] G. T. Gavranovic, R. E. Kurtz, K. Golemanov, A. Lange, and G. G. Fuller, "Interfacial rheology and structure of straight-chain and branched hexadecanol mixtures," *Industrial & engineering chemistry research,* vol. 45, no. 21, pp. 6880-6884, 2006.
[46] D. L. Leiske *et al.*, "Temperature-induced transitions in the structure and interfacial rheology of human meibum," *Biophysical journal,* vol. 102, no. 2, pp. 369-376, 2012.
[47] E. M. Freer, K. S. Yim, G. G. Fuller, and C. J. Radke, "Shear and dilatational relaxation mechanisms of globular and flexible proteins at the hexadecane/water interface," *Langmuir,* vol. 20, no. 23, pp. 10159-10167, 2004.
[48] O. Soo-Gun and J. C. Slattery, "Disk and biconical interfacial viscometers," *Journal of Colloid and Interface Science,* vol. 67, no. 3, pp. 516-525, 1978.
[49] B. Costello, P. Hodder, and A. Franck, "Use of the Du Nouy ring with a rotational rheometer to measure interfacial rheological properties," *ANNUAL TRANSACTIONS-NORDIC RHEOLOGY SOCIETY,* vol. 14, p. 209, 2006.
[50] P. Erni, P. Fischer, E. J. Windhab, V. Kusnezov, H. Stettin, and J. Lauger, "Stress- and strain-controlled measurements of interfacial shear viscosity and viscoelasticity at liquid/liquid and gas/liquid interfaces," *Review of Scientific Instruments,* vol. 74, no. 11, pp. 4916-4924, Nov 2003, doi: 10.1063/1.1614433.
[51] Y. El Omari, M. Yousfi, J. Duchet-Rumeau, and A. Maazouz, "Interfacial rheology testing of molten polymer systems: Effect of molecular weight and temperature on the interfacial properties," *Polymer Testing,* vol. 101, p. 107280, 2021.
[52] P. Erni, P. Fischer, and E. J. Windhab, "Sorbitan tristearate layers at the air/water interface studied by shear and dilatational interfacial rheology," *Langmuir,* vol. 21, no. 23, pp. 10555-10563, 2005.
[53] P. A. Rühs, C. Affolter, E. J. Windhab, and P. Fischer, "Shear and dilatational linear and nonlinear subphase controlled interfacial rheology of β-lactoglobulin fibrils and their derivatives," *Journal of Rheology,* vol. 57, no. 3, pp. 1003-1022, 2013.
[54] Y. Fan, S. Simon, and J. Sjöblom, "Interfacial shear rheology of asphaltenes at oil–water interface and its relation to emulsion stability: Influence of concentration, solvent aromaticity and nonionic surfactant," *Colloids and Surfaces A: Physicochemical and Engineering Aspects,* vol. 366, no. 1-3, pp. 120-128, 2010.
[55] L. M. Ligiero *et al.*, "Characterization of crude oil interfacial material isolated by the wet silica method. part 2: Dilatational and shear interfacial properties," *Energy & Fuels,* vol. 31, no. 2, pp. 1072-1081, 2017.
[56] A. Franck, "Double Wall Ring Geometry to Measure Interfacial Rheological Properties, APN031; 2015, pp. 1–9, Germany.."
[57] T. Verwijlen, P. Moldenaers, and J. Vermant, "A fixture for interfacial dilatational rheometry using a rotational rheometer," *The European Physical Journal Special Topics,* vol. 222, no. 1, pp. 83-97, 2013.
[58] V. Sharma, A. Jaishankar, Y.-C. Wang, and G. H. McKinley, "Rheology of globular proteins: apparent yield stress, high shear rate viscosity and interfacial viscoelasticity of bovine serum albumin solutions," *Soft matter,* vol. 7, no. 11, pp. 5150-5160, 2011.
[59] A. Jaishankar, V. Sharma, and G. H. McKinley, "Interfacial viscoelasticity, yielding and creep ringing of globular protein–surfactant mixtures," *Soft Matter,* vol. 7, no. 17, pp. 7623-7634, 2011.
[60] L. Wang *et al.*, "Interfacial rheology of natural silk fibroin at air/water and oil/water interfaces," *Langmuir,* vol. 28, no. 1, pp. 459-467, 2012.
[61] M. Felix, J. Yang, A. Guerrero, and L. M. Sagis, "Effect of cinnamaldehyde on interfacial rheological properties of proteins adsorbed at O/W interfaces," *Food Hydrocolloids,* vol. 97, p. 105235, 2019.
[62] M. E. Van Den Berg, S. Kuster, E. J. Windhab, L. M. Sagis, and P. Fischer, "Nonlinear shear and dilatational rheology of viscoelastic interfacial layers of cellulose nanocrystals," *Physics of Fluids,* vol. 30, no. 7, p. 072103, 2018.
[63] A. Bykov, L. Liggieri, B. Noskov, P. Pandolfini, F. Ravera, and G. Loglio, "Surface dilational rheological properties in the nonlinear domain," *Advances in colloid and interface science,* vol. 222, pp. 110-118, 2015.

[64] L. M. Sagis and P. Fischer, "Nonlinear rheology of complex fluid–fluid interfaces," *Current Opinion in Colloid & Interface Science,* vol. 19, no. 6, pp. 520-529, 2014.
[65] J. D. Berry, M. J. Neeson, R. R. Dagastine, D. Y. Chan, and R. F. Tabor, "Measurement of surface and interfacial tension using pendant drop tensiometry," *Journal of colloid and interface science,* vol. 454, pp. 226-237, 2015.
[66] E. M. Freer, H. Wong, and C. J. Radke, "Oscillating drop/bubble tensiometry: effect of viscous forces on the measurement of interfacial tension," *Journal of Colloid and Interface Science,* vol. 282, no. 1, pp. 128-132, Feb 2005, doi: 10.1016/j.jcis.2004.08.058.
[67] Y. Rotenberg, L. Boruvka, and A. Neumann, "Determination of surface tension and contact angle from the shapes of axisymmetric fluid interfaces," *Journal of colloid and interface science,* vol. 93, no. 1, pp. 169-183, 1983.
[68] F. S. Kratz and J. Kierfeld, "Pendant drop tensiometry: A machine learning approach," *The Journal of Chemical Physics,* vol. 153, no. 9, p. 094102, 2020.
[69] E. Santini, L. Liggieri, L. Sacca, D. Clausse, and F. Ravera, "Interfacial rheology of Span 80 adsorbed layers at paraffin oil-water interface and correlation with the corresponding emulsion properties," *Colloids and Surfaces a-Physicochemical and Engineering Aspects,* vol. 309, no. 1-3, pp. 270-279, Nov 2007, doi: 10.1016/j.colsurfa.2006.11.041.
[70] P. Bouriat, N. El Kerri, A. Graciaa, and J. Lachaise, "Properties of a two-dimensional asphaltene network at the water− cyclohexane interface deduced from dynamic tensiometry," *Langmuir,* vol. 20, no. 18, pp. 7459-7464, 2004.
[71] F. Chambon and H. H. Winter, "Linear viscoelasticity at the gel point of a crosslinking PDMS with imbalanced stoichiometry," *Journal of Rheology,* vol. 31, no. 8, pp. 683-697, 1987.
[72] N. Abi Chebel *et al.*, "Interfacial dynamics and rheology of a crude-oil droplet oscillating in water at a high frequency," *Langmuir,* vol. 35, no. 29, pp. 9441-9455, 2019.
[73] L. M. Ligiero *et al.*, "Characterization of crude oil interfacial material isolated by the wet silica method. Part 1: gel permeation chromatography inductively coupled plasma high-resolution mass spectrometry analysis," *Energy & Fuels,* vol. 31, no. 2, pp. 1065-1071, 2017.
[74] N. Alexandrov, K. G. Marinova, K. D. Danov, and I. B. Ivanov, "Surface dilatational rheology measurements for oil/water systems with viscous oils," *Journal of Colloid and Interface Science,* vol. 339, no. 2, pp. 545-550, Nov 2009, doi: 10.1016/j.jcis.2009.08.002.
[75] V. I. Kovalchuk *et al.*, "Rheological surface properties of C12DMPO solution as obtained from amplitude- and phase-frequency characteristics of an oscillating bubble system," *Journal of Colloid and Interface Science,* vol. 280, no. 2, pp. 498-505, Dec 2004, doi: 10.1016/j.jcis.2004.08.004.
[76] K. D. Danov, D. K. Danova, and P. A. Kralchevsky, "Hydrodynamic forces acting on a microscopic emulsion drop growing at a capillary tip in relation to the process of membrane emulsification," *Journal of Colloid and Interface Science,* vol. 316, no. 2, pp. 844-857, Dec 2007, doi: 10.1016/j.jcis.2007.08.061.
[77] P. A. Rühs, N. Scheuble, E. J. Windhab, and P. Fischer, "Protein adsorption and interfacial rheology interfering in dilatational experiment," *The European Physical Journal Special Topics,* vol. 222, no. 1, pp. 47-60, 2013.
[78] D. Carvajal, E. J. Laprade, K. J. Henderson, and K. R. Shull, "Mechanics of pendant drops and axisymmetric membranes," *Soft Matter,* vol. 7, no. 22, pp. 10508-10519, 2011.
[79] J. K. Ferri, P. A. Fernandes, J. T. McRuiz, and F. Gambinossi, "Elastic nanomembrane metrology at fluid–fluid interfaces using axisymmetric drop shape analysis with anisotropic surface tensions: deviations from Young–Laplace equation," *Soft Matter,* vol. 8, no. 40, pp. 10352-10359, 2012.
[80] S. Knoche *et al.*, "Elastometry of deflated capsules: Elastic moduli from shape and wrinkle analysis," *Langmuir,* vol. 29, no. 40, pp. 12463-12471, 2013.
[81] M. Nagel, T. A. Tervoort, and J. Vermant, "From drop-shape analysis to stress-fitting elastometry," *Advances in colloid and interface science,* vol. 247, pp. 33-51, 2017.
[82] C. W. Angle and Y. Hua, "Dilational interfacial rheology for increasingly deasphalted bitumens and n-C5 asphaltenes in toluene/NaHCO3 solution," *Energy & fuels,* vol. 26, no. 10, pp. 6228-6239, 2012.

[83] G. Giménez-Ribes, M. Habibi, and L. M. Sagis, "Interfacial rheology and relaxation behavior of adsorption layers of the triterpenoid saponin Escin," *Journal of colloid and interface science,* vol. 563, pp. 281-290, 2020.
[84] B. Vonnegut, "Rotating bubble method for the determination of surface and interfacial tensions," *Review of scientific instruments,* vol. 13, no. 1, pp. 6-9, 1942.
[85] J. M. Zamora, R. Marquez, A. M. Forgiarini, D. Langevin, and J.-L. Salager, "Interfacial rheology of low interfacial tension systems using a new oscillating spinning drop method," *Journal of colloid and interface science,* vol. 519, pp. 27-37, 2018.

Chapter II. Interfacial Shear Rheological properties of molten polymer systems: Effect of molar weight and temperature on the interfacial properties

II.1. Abstract

New interfacial rheological setups (IRS) for probing the interfacial viscoelastic properties of polymer systems are a subject of growing interest in the industrial and academic communities. Recently, biconical and double-wall Ring (DWR) devices that can easily be attached to standard rheometers have been marketed for this purpose, but measurements must be made below 70 ° C to ensure a stable homogeneous temperature at the interface. Meanwhile each device has its own limitation: the bicone has high inertia and a relatively low Boussinesq number, giving it a low signal-to-noise ratio, while the DWR is too fragile to probe the interfaces of high viscous systems in the molten state. First the stainless steel based biconical geometry was replaced by lighter titanium based one, enabling a more sensitive measurement of interfacial rheological properties. Also, we developed a novel high temperature resistant interfacial rheology cell equipped with an actively heated Peltier-temperature-controlled hood allowing interfacial rheology measurements up to 200 °C with temperature gradients of 1 °C at the sample interface. To validate this new setup, the surface/interfacial properties of different model fluids having different well-known structure and viscoelastic characteristics have been investigated. DWR was used to probe interfaces from high fluidity liquids. The effects of the molecular weight and the temperature were highlighted. Finally, the interfacial rheology of molten polymer systems has been characterized for the first time. The measured apparent interfacial shear properties in both oscillatory and steady flow modes were carefully corrected, considering the contribution of the bulk-subphases during processing of the numerical data.

Keywords: interfacial shear rheology, bicone, double-wall-ring, interfacial tension, interphase.

II.2. Introduction

The interfacial rheology of two immiscible fluids systems is probed by investigating the response of the interface to an applied stress or strain according to the same formalism and techniques developed in the field of the bulk rheology [1]. As explained before in the first chapter, in the two-dimensional rheology, we distinguish between interfacial shear rheology and dilatational interfacial rheology. The difference between the two tests lies in whether or not the probed surface or interfacial area undergoes a change. Interfacial shear rheological measurements (which are the main subject of this chapter) are often carried out using a rheometer and an interfacial geometry in order to shear the interface without modifying its area. The bicone [2, 3] is by far one of the most frequently used geometries for this purpose [4]. The bicone has mainly been used in biology [5] or in oil extraction for studying the stability of emulsions **[6]** or for investigating the behavior of rigid interfacial layers between two immiscible fluids [7, 8]. The second interfacial geometry that we will consider here is the double wall ring (DWR) developed by *Vandebril et al*. [9]. It is the most used interfacial shear rheology (ISR) geometry for measuring the interfacial viscoelasticity because of its low inertia and high sensitivity, especially for the study of low viscosity systems such as emulsions [10], and foams [11]. In the ISR measurements, the optimization of the interface-to-bulk signal ratio is based on the maximization of the Boussinesq number (B_o) (described in Chapter 1) [12].

At the time of their preparation, processed polymer systems have the capacity to organize and form multi-scale structures. In the past, such preparation procedures were often conducted in the molten state, under high temperatures, high shear rate or under radiation. Interfacial shear rheology might be an interesting way to understand the rheological behavior of polymers interface when this latter is sheared during the processing. However, the 2D rheology measurements are conducted at ambient temperature bellow a maximum of 70°C. The experimental interfacial devices currently in the market are not suitable for measurements at high temperature or in the presence of highly viscous polymers. Until now, the interfacial rheological properties measurements carried out in the melt state have been based only on indirect experimental methods [13]. Moreover, other works have been focused on morphological and rheological modeling for accessing viscoelastic interfacial properties [14].

In the present chapter, two categories of polymer systems are studied. The first systems investigated consist of the interface formed between different model fluids that are liquid at room temperature. The effect of viscosities and elasticities of the sub-phases on the interfacial shear viscosity and interfacial shear modulus has been investigated by varying the molecular weights and the viscoelastic nature of the bulk components. The thermal dependence of the interfacial rheological parameters has also been studied by varying the temperature of the medium. The second systems investigated consist of molten immiscible thermoplastic polymers having different bulk viscosities.

For the first time, a novel experimental interfacial setup dedicated to molten polymer systems is described. The interfacial rheological measurements at different temperatures are highlighted, and corrections of apparent data are considered and discussed.

II.3. Experimental

II.3.1. Materials

The model fluids chosen are PDMS (Polydimethylsiloxane) trimethylsiloxy terminated supplied from abcr (and Alfa Acesar for the PDMS 3), PIB (PolyIsobutene) supplied from INEOS and BF (Boger fluids). PDMS and PIB, used in the present work, present different molecular weights. Table II-1 shows the composition of each materiel.

Table II-1. Weight average molecular weight of the used PDMS and PIB.

Material	PDMS1	PDMS2	PDMS3	PDMS4	PDMS5	PIB1	PIB2	PIB3	PIB4	PIB5
Mw (g/mol)	5970	28000	63000	91700	204000	481	1333	1280	1440	3780

The linear formula of the used PDMS and PIB is shown on the figure II-1.

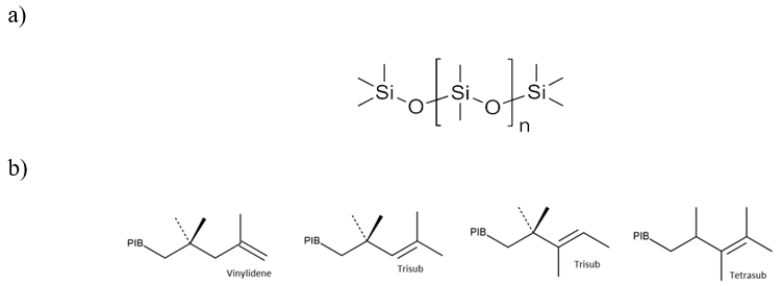

Figure II-1. Chemical Formula of PDMS (a) and PIB (b).

In this study, another grade of PDMS (From abcr, Mw= 410 g/mol)) and another grade of PIB (From INEOS, Mn=570 g/mol) have been used to sweep a very large range of PDMS and PIB viscosities.

The Boger fluids used in this report are elastic fluids with constant viscosities [15, 16]. They are dilute solutions obtained from a high molecular weight polymer and prepared with a suitable solvent. The mixture is sufficiently viscoelastic due to the presence of an amount of elasticity. In the present work, Boger fluids were prepared from a mixture of polybutene PB (a viscous liquid) and polyisobutylene PIB (an elastic solid). In order to study the effect of viscosity, the molecular weight of PB were varied. Kerosene is used here as a co-solvent of PB and PIB. Table II-2 shows the composition of each Boger fluid.

Table II-2. The composition of Boger fluids.

	BF1	BF2
Polybutene	92.8% (Mn=920 g/mol), Sigma Aldrich	92.8% (Mn=2300 g/mol), Sigma Aldrich
Polyisobutylene	0.22% (Mn=600000 g/mol), Sigma Aldrich	0.22% (Mn=600000 g/mol), Sigma Aldrich
Kerosene	6.98% (reagent grade), Sigma Aldrich	6.98% (reagent grade), Sigma Aldrich

There are three steps in the preparation of such Boger fluids. First of all, the PIB should be dissolved in kerosene. The stirring is performed using a magnetic rod. This first step takes about 24 to 48 hours depending on the amount of PIB to be dissolved. Next the PB is added and a stirring motor with a propeller is used to homogenize the solution. This step lasts from 14 to 21 days depending on both the initial quantity of PIB and the type of PB (high or low viscosity). The mixing is completed when the torque measured by the stirring motor reaches a stable value. Finally, the last step consists in removing the kerosene from the solution. The fluid is then placed under vacuum for three weeks.
For molten thermoplastic polymers, the PCL (polycaprolactone) and PEG (polyethylene glycol) are supplied from Sigma Aldrich and were chosen due to their low melting temperatures (around 70 °C). Different molecular weights of each polymer were used. Table II-3 summarizes the characteristics of the polymers studied.

Table II-3. The characteristics of the polycaprolactone (PCL) and the polyethylene glycol (PEG) used.

Material	PCL1	PCL2	PEG1	PEG2	PEG3
Mn (g/mol)	10000	45000	10000	20000	35000

II.3.2. Characterization Methods

II.3.2.1. DIFFERENTIAL SCANNING CALORIMETRY

The interfacial rheological measurements of the PEG-PCL systems should be made far from their crystallization temperatures. Thus, to measure the melting and crystallization temperatures of the PCL and PEG polymers, differential scanning calorimetry (DSC Q10 from TA Instruments) was performed. Samples were first heated for three minutes to the temperature of thermodynamic equilibrium (around 208°C) in order to melt any crystalline parts, and then they were cooled down to ambient temperature.

The following cycle was then applied in the DSC apparatus: heating from -70°C to 120°C at 10°C/min, cooling from 120°C to -70°C and finally second heating ramp under the same conditions.

II.3.2.2. BULK RHEOLOGICAL MEASUREMENTS

In order to determine the rheological properties of different bulk subphases and their effect on the interfacial rheological measurements, dynamic rheological measurements were performed.
The first rheological tests on the model fluids were carried out on a DHR-2 machine from TA Instruments. i.e. a combined motor-transducer (CMT) rotational rheometer [17]. A cone-plate geometry was chosen (diameter 40 mm, angle 1.994. °) and the heating system used was a Peltier Plate temperature system. Frequency sweeps were performed at angular frequencies decreasing from 100 to 0.1 rad.s^{-1}. The complex viscosity ($|\eta^*|$) were measured as a function of the angular frequency.

To obtain more rheological data at high shear rates, the time-temperature superposition principle was applied. The rheological curves obtained at different temperatures were superimposed on a reference curve (at a reference temperature T_0) by translating them using horizontal and vertical shift factors (log $a_{T/T0}$ and log $b_{T/T0}$ respectively). These factors depend mainly on the temperature T and the reference temperature T_0. In this study, the reference temperature chosen was 25°C. A strain sweep at an angular frequency of 100 rad/s was used to determine the linear viscoelastic range for each fluid.

The rheological behaviour of PCL and PEG polymers was characterized using an ARES-G2 apparatus from TA Instruments, i.e. a separated motor-transducer (SMT) rheometer [18] that can alloy to attain a high shear rate up to 628 rad/s with negligible inertia effect. A parallel-plate geometry (of diameter 20 mm) was chosen and the heating used was a forced convection oven (FCO).

Finally, in order to check the miscibility of PIB-PDMS and PCL-PEG, Van Gurp Palmen plot of 50/50 wt% of the highest viscosity system of PIB5-PDMS5 (at 25, 35, 45, 60, 75 and 90°C) and PEG3- PCL2 (at 90, 100, 110, 120, 130 and 140°C) samples were plotted to make correlation between rheology and the obtained miscibility.

II.3.2.3. SURFACE AND INTERFACIAL MEASUREMENTS

The surface and interfacial tension at different temperatures were measured using an automatic drop tensiometer (TRACKER-H from TECLIS Instruments, France). The main parts of the Tracker™ instrument are a light source, a CCD camera, a syringe holder system and a needle for drop formation. For an improved temperature control, a high temperature regulated view cell consisting of a stainless steel assembly with two sapphire windows was used. A thermocouple measures the temperature inside the cell. The entire assembly is surrounded by a plastic block made of PEEK (Figure II-2). The high-temperature view cell could withstand a maximum temperature of 200 °C and a maximum pressure of 200 bar.

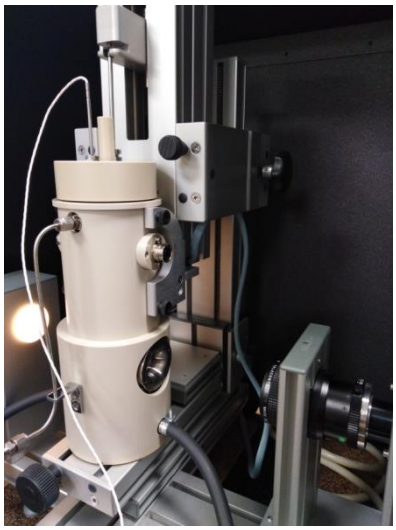

Figure II-2. Cell used for high-temperature measurements of surface and interfacial tension.

For low and high-viscosity model liquids (PDMS and PIB), the measurements were performed using a Hamilton glass syringe (1 mL) equipped with a Luer-lock fitting to a stainless-steel needle (14 Gauge).

For PDMS and PIB of high viscosity (up to 300 Pa.s), the liquids were preheated in an oil bath at 100 °C for 45 minutes to make them more fluid, and they were easily aspirated by a large syringe (50 mL) while the air was purged and were finally transferred to the quartz basin (30x30x70 mm^3).

Through the controlled movements of the syringe piston, which was driven by a step-by-step motor, the drop size was well controlled with a high accuracy during the entire experiment. From the digital analysis of a melt or liquid drop, the profile was acquired by a high-speed CCD camera and characteristic surface parameters (area, volume, surface tension) were determined in real time. Surface tension was determined from the Tracker™ software which uses a special algorithm to analyze the profile of the drop (either rising or pendant), and to fit it with models based on the Young-Laplace equation in order to determine surface tension, interfacial tension or contact angle [19, 20].

As described in the Chapter 1, the Bond number (Bd), which represents the ratio between the gravitational forces and the surface tension on an interface between two fluids, was carefully analysed prior to the measurements. To obtain high accuracy, the Bond number (Bd) was optimized that requiring an increase in the radius of curvature at the apex, which in turn, required an increase in the volume of the drop.

It is important to allow the drop liquid surface or fluid-fluid interfaces to achieve Laplace equilibrium before performing a measurement. When it comes to systems that are too liquid, this equilibrium is achieved rapidly (within a few seconds). On the contrary, when the polymer systems present a high bulk viscosity, the equilibrium state requires longer times (several hours).

II.3.2.4. MORPHOLOGICAL OBSERVATIONS

A polarized optical microscope (Zeiss, Germany) equipped with a sapphire hot stage was used to qualitatively probe the morphology of different PIB-PDMS and BF-PDMS model systems in isothermal conditions at 25 °C. The objective was to qualitatively check the compatibility of the studied systems. The preparation of PIB-PDMS and BF-PDMS blends (90/10 wt%) was performed using a dynamic rheometer (DHR2, TA Instruments) at a shear rate of 8 s^{-1} with a duration of 1250 seconds using a parallel-plate geometry (40mm) and a Peltier heating element to control the temperature at 25°C. High-quality images were taken with the aid of a scientific camera (Panthera 1M30).

To analyze the PEG-PCL morphology, scanning electron microscopy (SEM, HITACHI S-3500 N, Japan) was used at an accelerating voltage of 15 kV and a probe current of 130 pA. The PEG-PCL extrudates were cryofractured and coated with gold during 60 s at 2 kV before the SEM observations.

The immiscible PCL/PEG extrudate blends were prepared using a twin-screw DSM microcompounder. The temperature of melt mixing was 80°C, the screw velocity was 80 rpm and the residence time was five minutes.

II.3.2.5. NUMERICAL ASSESSMENT OF THE COMPATIBILITY OF THE POLYMER SYSTEMS STUDIED

To predict the compatibility of the systems studied, their Hansen's solubility parameters (HSP) were evaluated [21]. In the present work, we used HSPiP software (Louisville, Kentucky, USA) to evaluate the HSP. For the calculations, the software used a genetic algorithm optimization approach [22]. According to Hansen [23], the global solubility parameter is a combination of three components reflecting dispersive (London) (δ_D), polar (δ_P) and hydrogen bond (δ_H) interactions.

$$\boldsymbol{\delta^2 = \delta_{TOT}^2 = \delta_D^2 + \delta_P^2 + \delta_H^2} \qquad \textbf{(II-1)}$$

The determination of the Hansen solubility parameters of a polymer consists in testing the solubility of the polymer in different solvents with known solubility parameters using a sphere that encompasses the good solvents of the polymer in a 3D solubility diagram (δ_D, δ_P, δ_H), which defines as a solubility sphere with a radius R_0 [23, 24].

Polymers are expected to display a good mutual affinity when their HSPs are close and when the distance between the centres of their respective solubility spheres is low. The distance R_0 between centres of the solubility spheres of two components denoted 1 and 2 is given by:

$$\boldsymbol{R_0^2 = 4(\delta_{D1} - \delta_{D2})^2 + (\delta_{P1} - \delta_{P2})^2 + (\delta_{H1} - \delta_{H2})^2} \qquad \textbf{(II-2)}$$

We consider that two polymers would exhibit strong affinity in a presence of a very low value of Ra (inferior to R_0, the radius of the solubility sphere). However, when considering two different polymers, a value of R_{0min} = 8 $MPa^{1/2}$ is usually viewed as the upper limit for compatibility [23-25].

To assist the software in optimizing its analysis of the HSPs, different fluids were drawn, and the solubility of the fluids was tested in various solvents in order to find a good solvent. The software made it possible to obtain an optimized 3D solubility diagram for the studied system studied.

II.3.2.6. INTERFACIAL RHEOLOGY

II.3.2.6.1 Interfacial rheological measurements with a double-wall ring (DWR) geometry

The first interfacial rheological tests on the model fluids were carried out on a DHR2 apparatus (TA Instruments) using a double-wall ring (DWR) geometry (Figure II-3).

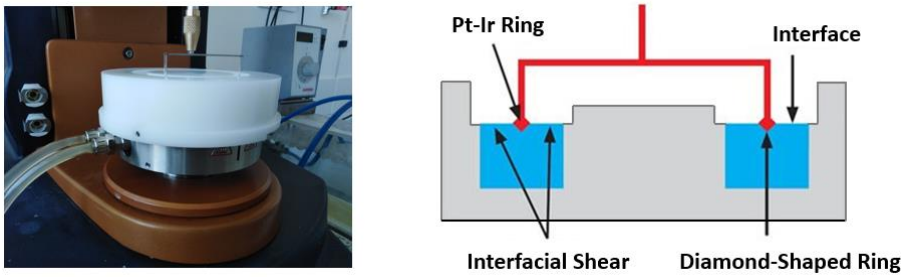

Figure II-3. Photograph (left) and schematic diagram (right) of the double wall-ring cell.

After cleaning and drying the ring and the cup, the gap is defined using only the geometry holder to avoid damaging the fragile ring. Thus, the geometry holder without the DWR is attached to the pull rod and the gap is reduced to zero by placing the mandrel of the geometry holder and the top of the cup into contact with each other.

Since the DHR2 is a combined motor transducer (CMT) type rheometer, the motor and the sensor are located in the upper part of the rheometer where the measured torque (T) is the sum of the instrument, geometry and sample torques (the interface in this case).

$$T_{measured} = T_{sample} + T_{instrument} + T_{geometry} \qquad \text{(II-3)}$$

First, we subtract from the measured torque the contribution of the instrument without geometry, then we subtract the contribution of the instrument with geometry, including inertia, friction and oscillatory mapping (six iterations in the "precision" mode). It is useful to mention that the calibration of the instrument to geometry in interfacial measurements is not only very important but is in fact crucial for obtaining reliable results without artefacts. Indeed, after the instrument and IRS inertia calibration, the raw phase angle was checked systematically. It must not exceed the critical

value of 170 °, if the interfacial rheological data obtained is to be valid and accurate. This is in complies with the manufacturer's stated limitations regarding the DHR-2 instrument.

In this study, a volume of 18.83 ml of the densest fluid was placed in the lower part of the cup. This volume corresponded to the internal air gap so that the possibility of having a meniscus was negligible. The ring was lowered at very low velocity until it came into contact with the surface of the first subphase, corresponding to an air gap of 12500 µm. This step was carried out either visually or using normal force (the detection of the surface normal force depends on the surface tension of the liquid). If it is low, the difference in the normal force between the surface and the air is not detectable. When the ring touches the interface, hanging is observed due to the metal/liquid surface tension effect (a wave rotates with the ring). The last step was to lower the ring by an another 500 µm (Figure II-4), add the second sub-phase (the less dense phase) and rotate the ring (by two or three turns) to homogenize the interface.

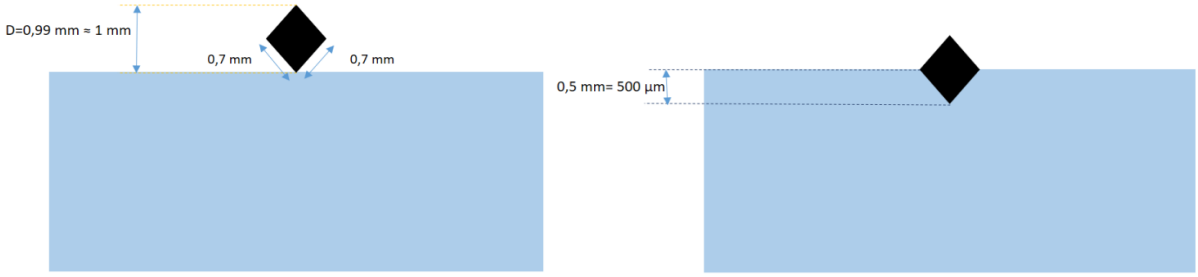

Figure II-4. Defining the gap in the case of the double-wall ring (DWR).

The geometrical characteristics of the DWR geometry (Figure II-5) are summarized in Table II-4.

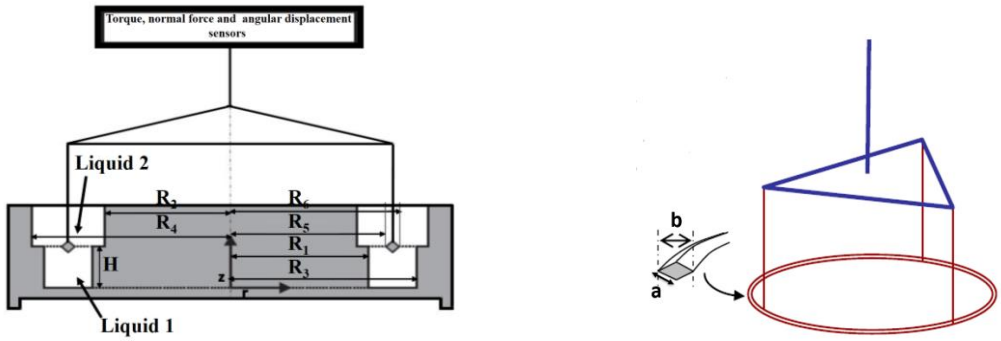

Figure II-5. Schematic of the double-wall ring (DWR) device (left) [26] and schematic of the square section of the ring (DWR) (right).

Table II-4. Dimensions of the DWR geometry.

R_1	R_2	R_3	R_4	R_5	R_6	b	a
(mm)	(mm)	(mm)	(mm)	(mm)	(mm)	(mm)	(mm)
31	34	35	39.5	34.5	35.5	1	0.7

Before starting the measurement with the DWR, a thin film of low viscous PDMS (η_{bulk} =0.002 Pa.s) was placed at the surface of water at 25°C. The theoretical surface viscosity $\eta_{s,th}$ is around 3.10^{-6} Pa.s.m (where $\eta_{s,th}=\eta_{bulk}*\frac{Bulk\ Volume}{surface\ Area}$). The purpose of this test is to compare this value to the measured experimental surface viscosity $\eta_{s,exp}$ in the steady flow from 1 to 10 s^{-1}.

Interfacial rheological measurements in steady flow and oscillation modes with DWR geometry are suitable for very fluid interfaces. However, this geometry has a limited usefulness for probing rigid interfaces or interfaces formed from highly viscous polymeric fluids. This is because the DWR geometry is a very fragile and can be deformed in the presence of rigid or very viscous materials. On the other hand, in the presence of such interfaces, a slip of the geometry with respect to the fixing rotation system is observed when the measured force increases sharply. For all these reasons, the interfacial rheological measurements for interfaces formed from high-viscosity fluids were performed using the biconical geometry which is much stiffer than DWR.

II.3.2.6.2 Interfacial rheological measurements with the biconical geometry

The bicone [5] is another geometry used in this work for performing viscoelastic interfacial measurements. As mentioned in the first chapter "State of the art", it mimics the Couette device but is very tapered at its end (Figure II-6) [27].

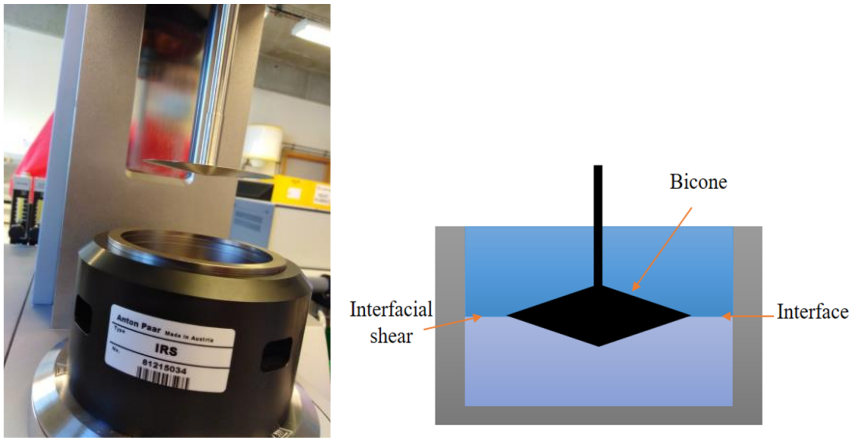

Figure II-6. Photograph of the bicone device (stainless steel) mounted onto the rotor of a rheometer used to measure the interfacial shear rheology at a temperature below 70°C (left). Profile section of the bicone device (right).

It is absolutely crucial to mention that characterizing a fluid interface (with low interfacial viscosity) is very difficult with the biconical geometry because the device is made from stainless steel; who suffers from high inertia and limited sensitivity.
For this reason, in this work, a novel biconical geometry was manufactured from titanium (Ti) instead of stainless steel. This titanium-based geometry is roughly half as dense as its stainless-steel equivalent but presents the same shape and dimensions.

This novel biconical geometry was designed by the Anton Paar Research and Development Service (Stuttgart, Germany) (D: 68.28 mm, angle 5°). Its composition of titanium material (ρ= 4.506 g/cm^3) made it less dense than the previous bicone (steel, ρ= 7.5 to 9 g/cm^3) and therefore provided it with the benefits of decreased inertia (denoted I) and increased its sensivity (Table II-5). This new Ti bicone which was attached to an MCR 302 rheometer was used for the very first time in this study.

Table II-5. Inertia of stainless steel and Titanium based bicone geometry.

Type of geometry	**Inertia (mN.m.s^2)**
Bicone machined from stainless steel	0.022733
Bicone machined from Titanium	0.01433

Note that in interfacial rheological measurements with low-viscosity fluids, the experiment is performed in the limit of rheometer performance (Torque limit). Thus, a small improvement in the inertia value is beneficial for accuracy of measurements.
As mentioned above, the geometric ratio of the DWR is high which in turns leads to a high value of Boussinesq number value compared to the bicone. That said, in the field of polymer, the Boussinesq number is not the only parameter we need to consider. Due to the high viscosity of polymers, the stiffness of the geometry is also an important variable to consider. For this reason, the Ti bicone was used for rigid systems, whereas the DWR was used for fluid systems.

In this study, PIB- PDMS and BF-PDMS interfaces in addition to air-PIB, air-PDMS and air-BF surfaces were investigated. The surfaces (air-fluid) and interfaces (fluid-fluid) that were studied are summarized in tables II-6 and II-7.

Table II-6. Model fluid surfaces studied.

Surfaces	Air-PDMS2	Air-PDMS3	Air-PDMS4	Air-PDMS5	Air-BF1
	Air-PIB2	Air-PIB3	Air-PIB4	Air-PIB5	Air-BF2

Due to the very low measured torque, surfaces Air-PDMS1 and Air-PIB could not be characterised by the bicone neither by the DWR.

Table II-7. Model fluid interfaces studied.

Interfaces	PIB1/PDMS 1	PIB2/PDMS 2	PIB3/PDMS 3	PIB4/PDMS 4	PIB5/PDMS 5	BF1/PDMS 4	BF2/PDMS 5

Note that the sub-phases have the same range viscosity values.

II.3.2.6.3 Novel experimental setup for interfacial rheological measurements of molten polymer systems

In order to study the interfaces between two molten polymers at high temperature, a new setup was manufactured. This novel interfacial rheology setup (IRS) is equipped with a Peltier Plate temperature device (P-PTD 200) combined with an Anton Paar patented actively heated hood (H-PTD200). The Peltier-temperature-controlled hood allows interfacial rheological measurements up to 200 °C and results in temperature gradients of 1 °C at the sample interface. The interfacial geometry is the biconical titanium–based measuring system described above which is used in conjunction with a novel homemade IRS cell.

To withstand high measurement temperatures, the cylindrical cup cell was manufactured entirely from stainless-steel contrary to the cup currently marketed by the Anton Paar Company. The latter consists of an assembly of a metallic, glass, thermoplastic polymers and elastomeric ring components (Figure II-7).

The steps performed prior interfacial rheological measurements are as follows:

The stainless-steel cup cell was heated at the set temperature using the Peltier Plate temperature device. The semi-crystalline polymers (PCL and PEG) were first melted at 100°C in a metallic container using an oil bath. Then the molten polymers were poured into the cup and degassed in an oven previously heated to 100 °C to remove air bubbles. Once the system had stabilized, the temperature near the interface was measured using a thermocouple. The measured temperature was found to be very close to the set point (± 1 °C).

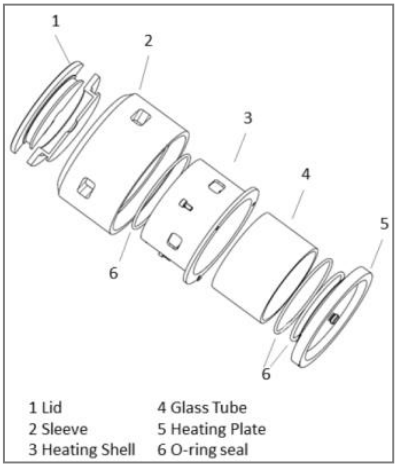

Figure II-7. Parts and assembly of the currently marketed biconical ISR [28].

The newly designed interfacial cylindrical cell has inner and outer diameters of 80 mm and 93 mm respectively. Its height is set at 57 mm. The interfacial cell contains a threaded hole with a sealed screw that allows the introduction of the upper subphase fluid into the cup (Figure II-8).

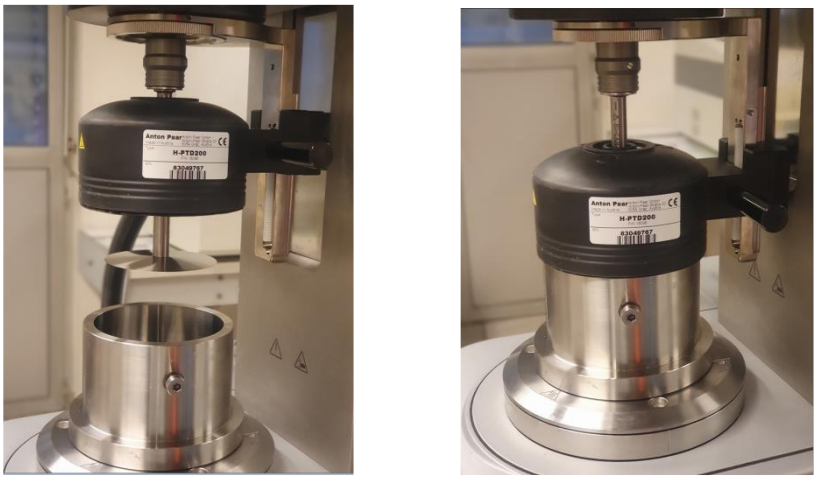

Figure II-8. The newly designed interfacial rheology setup, shown in open position (left) and in closed position (right).

A normal force assisted surface detection methodology (described in chapter I) was used to accurately position the titanium-based biconical geometry at the fluid-fluid interface. The rheometer's interfacial analysis software (RheoCompass), based on the unique Navier-Stokes solution of the full flow field for a biconical geometry (see details in the first chapter) was used to calculate of the corrected interfacial rheological properties.

II.4 Results

II.4.1. Model fluids investigation

II.4.1.1. Bulk rheological characterization

The bulk rheological data of different model fluids were evaluated from the master curves obtained using the time-temperature superposition principle. The main objective was to determine their rheological behaviour, over a large frequency domain. The latest data were used to define the viscous properties of PDMS, PIB and BF subphases and their effect on the interfacial rheological measurements. The master curves corresponding to each grade of PDMS, PIB and BF model fluids are presented in detail in Figures II-9, II-10 and II-11. It was observed that PIB, PDMS and BF fluids exhibit Newtonian behaviour until an angular frequency of 50 rad/s is reached. The Newtonian viscosities of the different model fluids are summarized in the Table II-8.

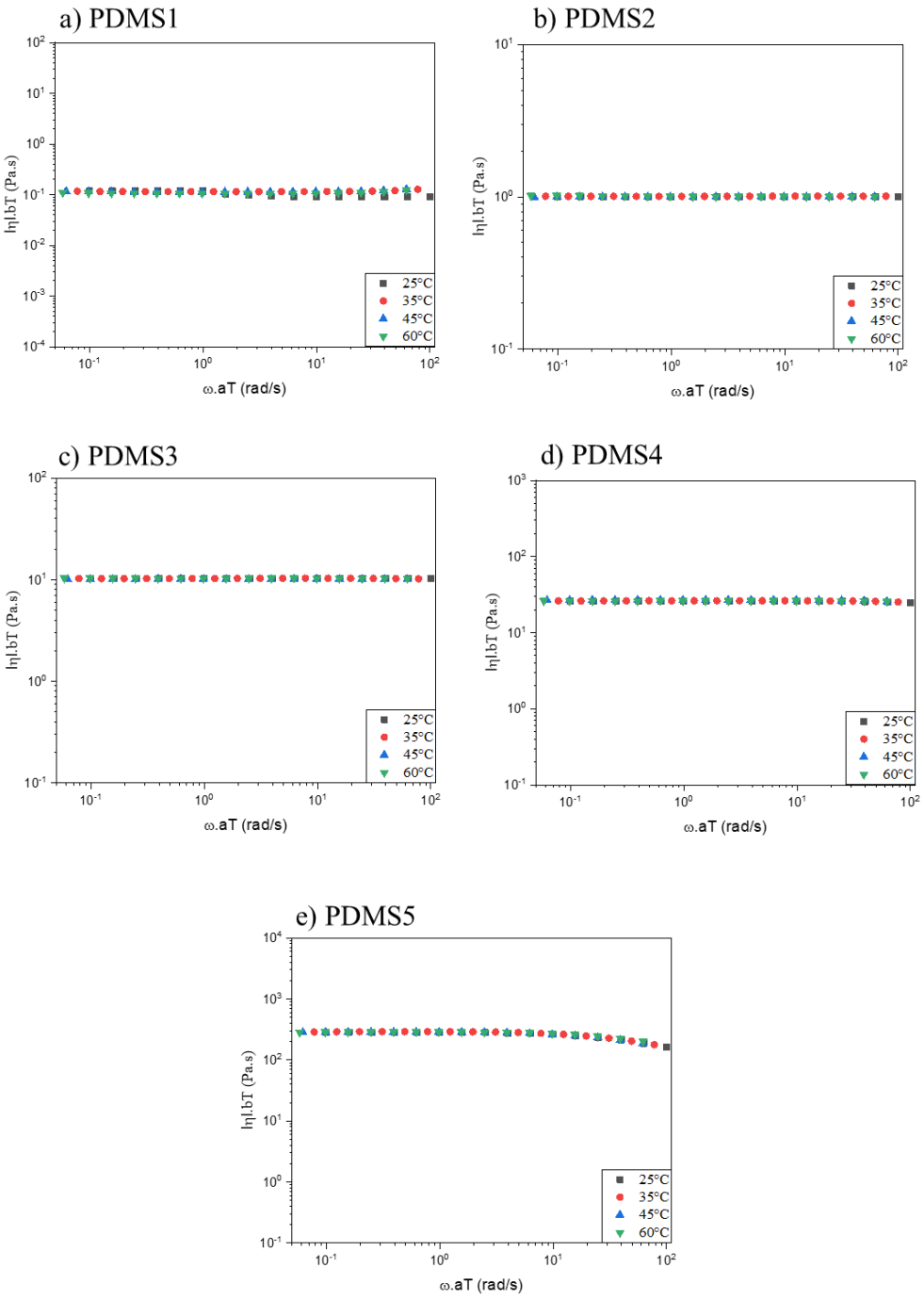

Figure II-9. Master curves of PDMS model fluids at 25 °C.

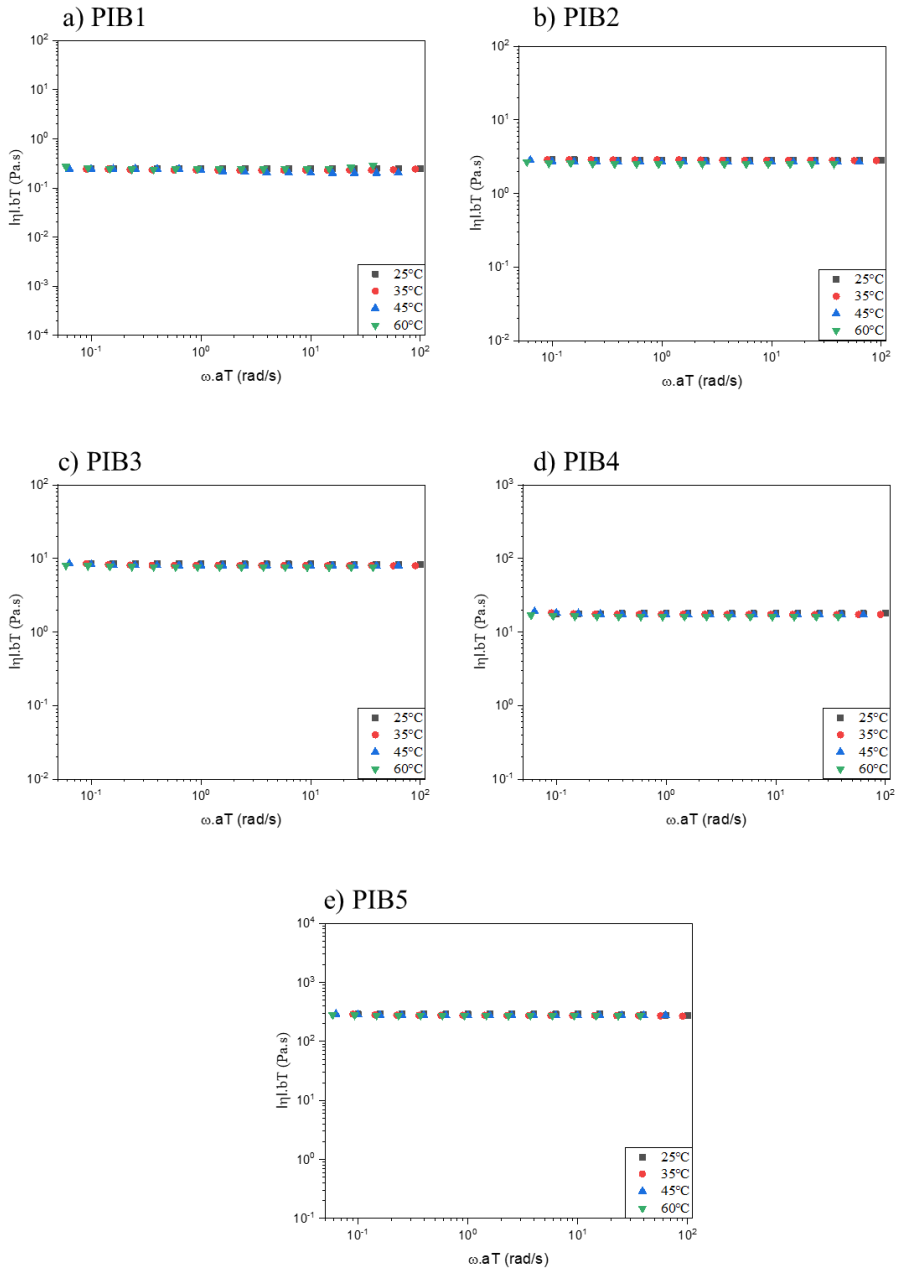

Figure II-10. Master curves of PIB model fluids at 25 °C.

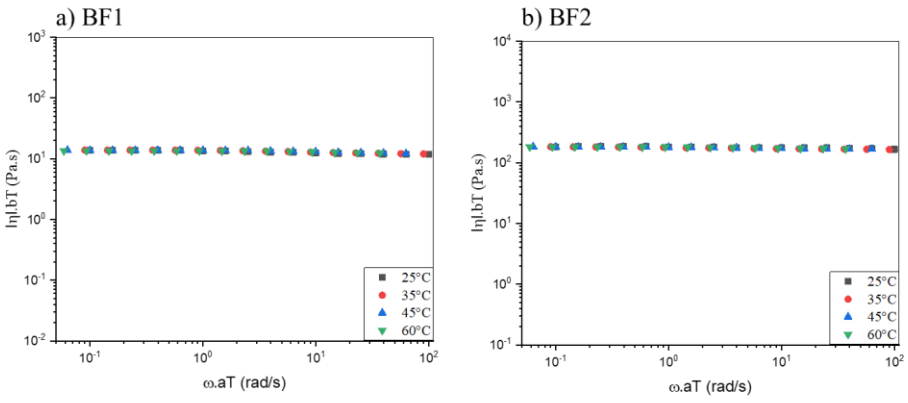

Figure II-11. Master curves of BF model fluids at 25 °C.

Table II-8. The zero-shear viscosity of the model fluids at 25°C.

Newtonian viscosity (Pa.s) at 25°C			
PIB1	0.2	**PDMS1**	0.1
PIB2	2.9	**PDMS2**	1.0
PIB3	8.9	**PDMS3**	10.3
PIB4	17.9	**PDMS4**	26.4
PIB5	289.5	**PDMS5**	269.7
BF1	13.7	**BF2**	193.9

It is useful to note that the zero-shear viscosities will be used to subtract the effects of the sub-phases effects. This information is used as input data to correct for the effects of the subphases.

The Van-Gurp-Palmen plot [29] (δ (°) as a function of the complex modulus $G^*(\omega)$) was used to probe the chain structure of the studied polymers.

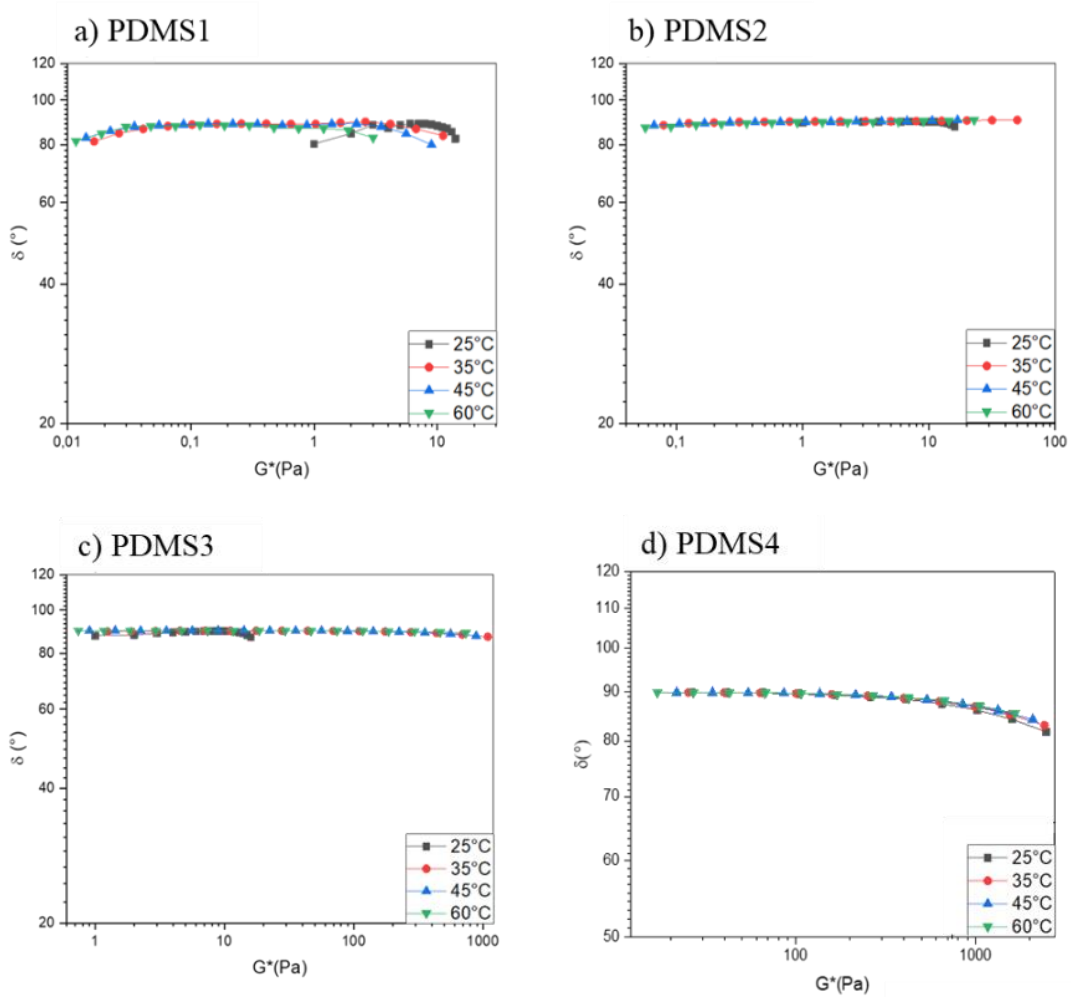

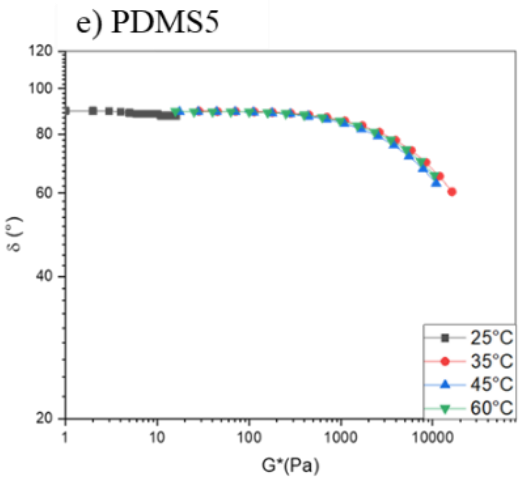

Figure II-12. Variation of the phase-shift angle as a function of the complex modulus for PDMS at 25, 35, 45 and 60°C.

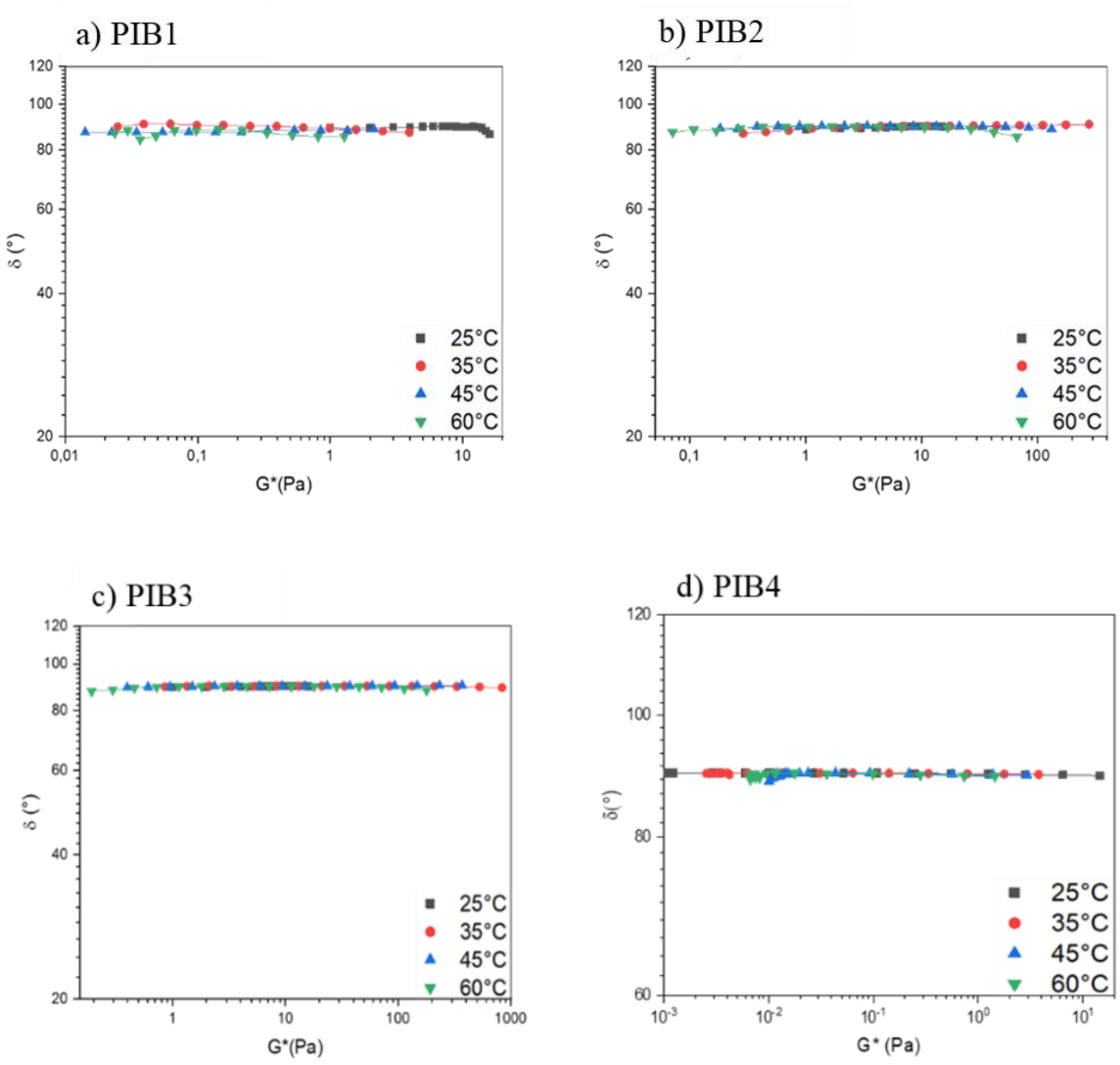

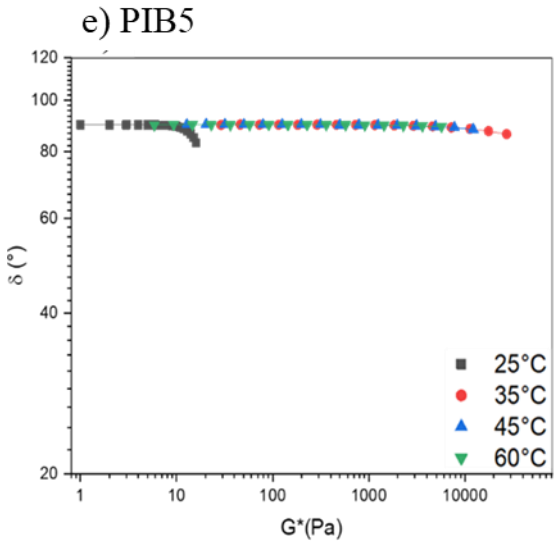

Figure II-13. Variation of the phase-shift angle as a function of the complex modulus for PIB at 25, 35, 45 and 60°C.

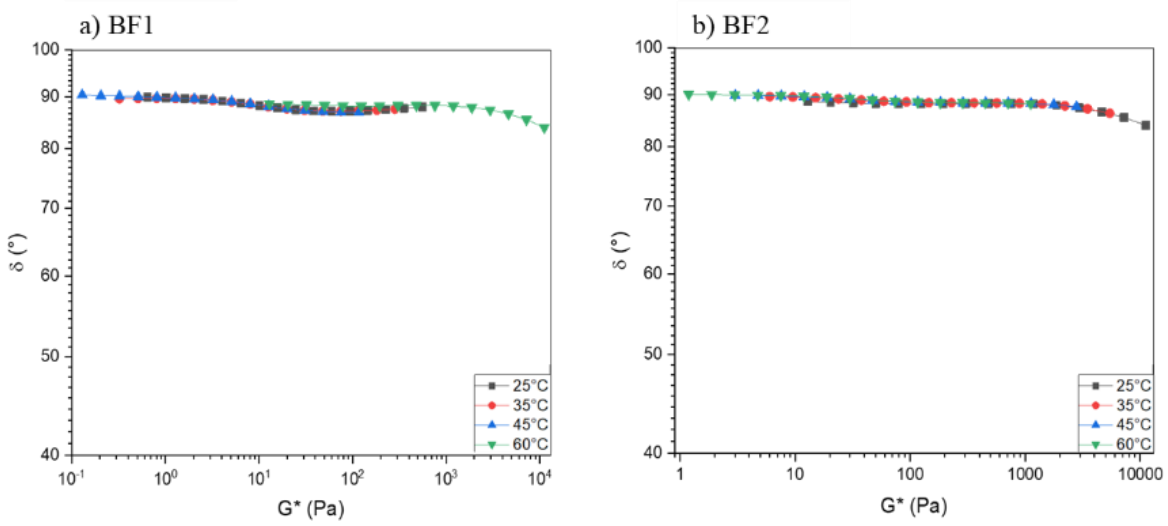

Figure II-14. Variation of the phase-shift angle as a function of the complex modulus for BF at 25, 35, 45 and 60°C.

From Figure II-12, II-13 and II-14 one can deduce that the variation of the phase-shift angle δ (°) as a function of the complex modulus $G^*(\omega)$ for the PDMS, PIB and BF is independent of the temperature for PDMS, PIB and BF. Therefore, these fluids are thermo-rheologically simple. These observations demonstrate the validity of the time-temperature superposition curves obtained. On the other hand, the Van-Gurp Palmen plots for the PDMS and PIB polymers display a classic shape that is generally expected for linear polymers with a plateau of the phase angle at 90° in the low frequency

zone, indicating viscous behaviour in this Newtonian zone. At higher frequencies or higher complex moduli, the phase angle decreases. *Trinkle et al*. [30] have obtained such typical plots for linear polyethylene.

For the 10/90, 90/10 and 50/50 wt% of PIB5/PDMS5, the Van-Gurp Palmen plots was plotted. Figure II-15 displays the variation of the phase-shift angle δ (°) as a function of the complex modulus $G^*(\omega)$ that is dependent of the temperature.

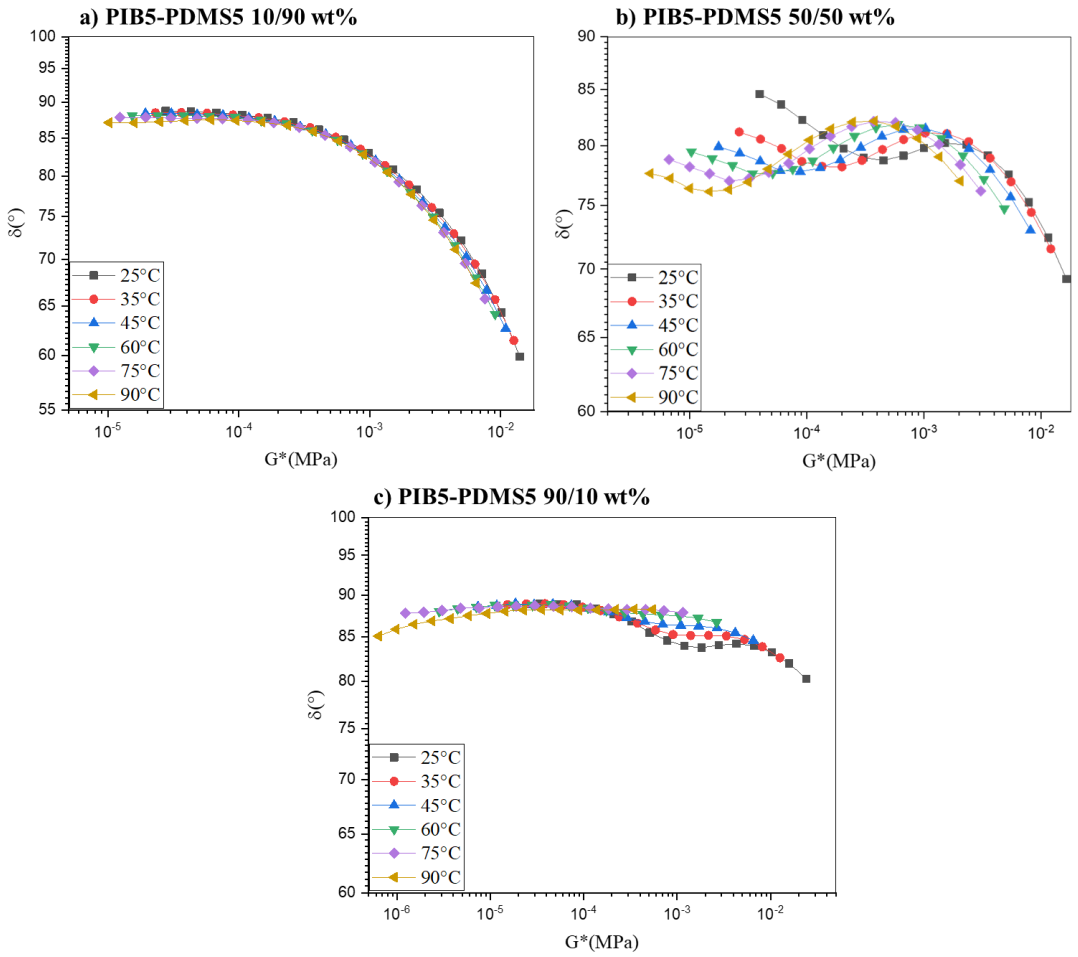

Figure II-15. Variation of the phase-shift angle as a function of the complex modulus for PIB5-PDMS5 blends at 25, 35, 45, 60, 75 and 90°C. (a) 10/90 wt%, (b) 50/50 wt% and 90/10 wt%.

Immiscible polymer blends will not obey TTS principle (Time Temperature Superposition) due to the different temperature dependencies of both components [31]. The Van-Gurp Palmen curves confirm that at low rates of PIB in PDMS (10/90 wt%), these curves are superimposable, which is not the case for the 50/50 and 90/10wt% formula. As a result, small partial miscibility might exist between PIB and PDMS. The same result was found for PEG-PCL system. The VGP curves are displayed in the supporting information section.

For the Boger fluids, the first normal tress difference (N_1) was estimated from the elastic modulus G' and loss modulus G" using the model of Laun [32] (Equation II-4).

$$N_1 = 2\,G'(\omega)\left[1+\left(\frac{G'(\omega)}{G''(\omega)}\right)^2\right]^{0.7} \qquad \textbf{(II-4)}$$

From Figure II-16, it can be seen that elasticity of the Boger fluids increases when the temperature decreases. The Boger Fluid BF2 presents higher elasticity than BF1 at the same temperature.

On the other hand, it is useful to mention that the Boger fluids prepared in this study have a fairly low elasticity that does not exceed 80 Pa at 25 ° C and 10 rad/s (for BF2). Since both first normal stress difference (N_1) and the viscosity increase with the amount of elasticity present in the Boger fluids, the low level of elasticity observed is chosen to avoid having high viscosities of the sub-phases, which makes the Boussinesq number very low and consequently it is possible to remain within the reliable accepted measurements.

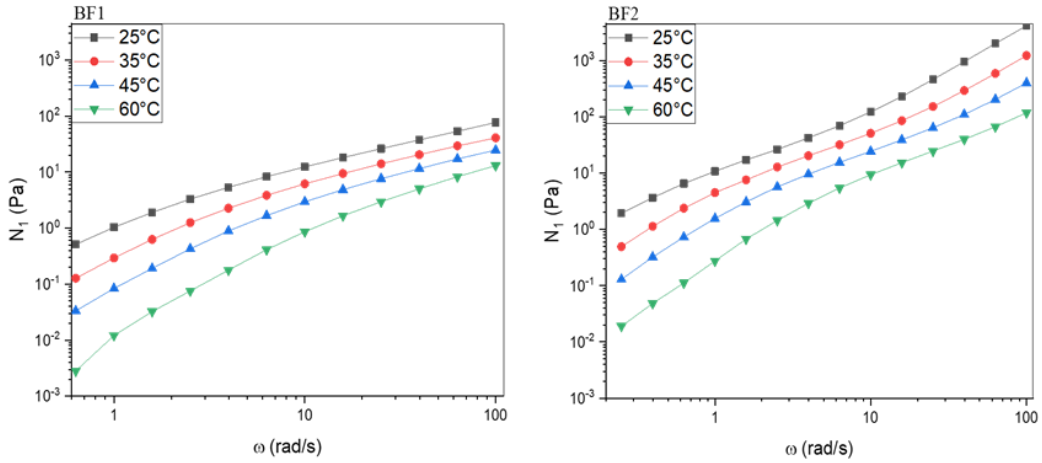

Figure II-16. Evolution of the first normal tress difference N_1 as a function of the frequency.

II.4.1.2. Surface tension

The experimental results for the measurements of surface tension obtained for the different grades of PDMS, PIB and BF are shown in Figure II-17.

It can be seen that the surface tension of the model fluids decreases when the temperature increases [33]. On the other hand, the surface tension increases with the growth of the viscosity. In fact, the more the viscosity increases the more material is cohesive and the more the energy of attraction between the macromolecules that oppose the surface break increases (more spherical drop shapes).

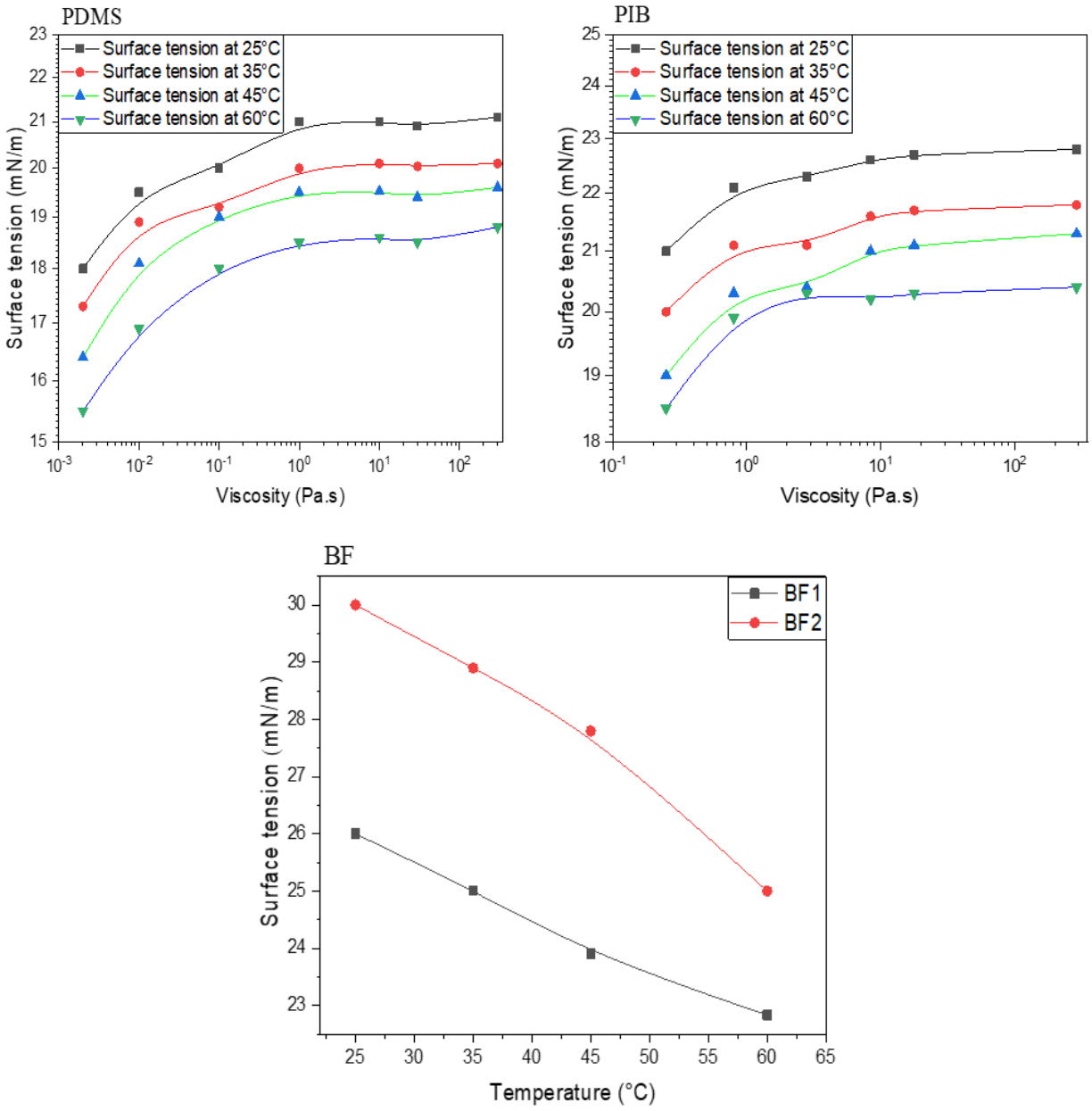

Figure II-17. Evolution of the surface tension of the model fluids as a function of temperature and viscosity.

The same tendency was found by *Cazaux et al*. [34] in the case of PA66. They observed that the surface tension decreases when the molecular weight decreases according to the LeGrand and Gaines model [35]. The authors found that the surface tensions of polymer liquids vary with molecular weight according to an empirical relationship:

$$\gamma = \gamma_{\infty} - \frac{k}{M^{\frac{2}{3}}} \qquad \textbf{(II-5)}$$

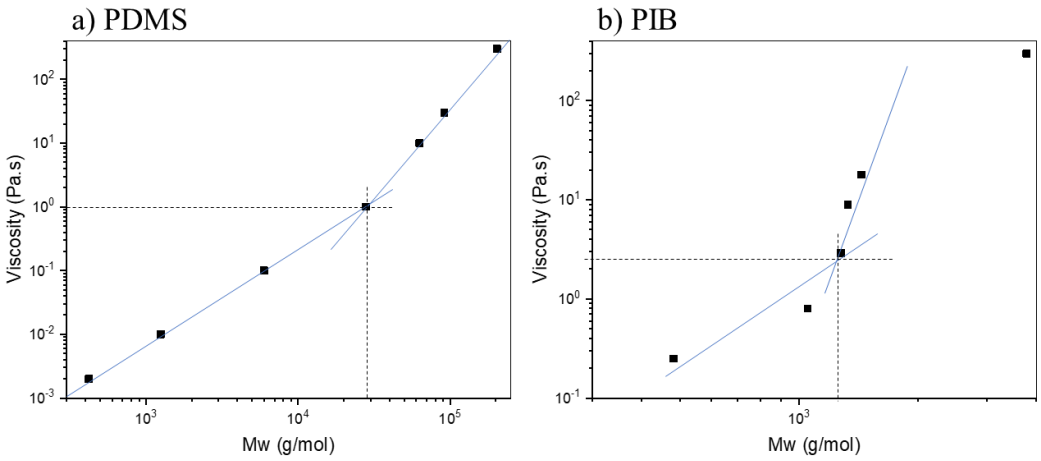

Figure II-18. Variation of the viscosity of PDMS (right) and PIB (left) at 25 °C as a function of their molecular weights.

We note that the sudden change in the trend of variation in surface tension as a function of viscosity (Figure II-17) is related to the M_c (critical entanglement molecular weight) for the PDMS and not for the PIB. The Mc of PDMS and PIB are 28000 and 15200 g/mol respectively [36, 37]. Indeed, Figures II-18 shows that the M_c corresponds to a viscosity of 1 Pa.s in PDMS samples. However, in the case of PIB, we were unable to obtain commercial grades with molar mass greater than Mc. Therefore, we cannot estimate the viscosity corresponding to Mc of PIB from Figure II-18.

On the other hand, the temperature coefficient of surface tension of PDMS and PIB varies with the viscosity along a similar trend to the surface tension and shows an abrupt change at a viscosity of 1 Pa.s (for PDMS) and 0.80 Pa.s (for PIB). After this molecular weight, the surface tension does not change, tending toward constant value γ_∞. These results could give important information about the cohesive energy of the material based on the definition of surface tension. This energy remains constant or varies very little from the critical mass of entanglement.

II.4.1.3. Optical microscopy

Figures II-19 and II-20 show the optical images of the model fluids studied. Droplets of PIB (and BF) in the PDMS matrix are clearly seen. A well-defined interface between the PIB nodules and the PDMS matrix as well as between the BF nodules and the PDMS continuous phase is clearly identified. The diameter of the PIB droplets increases when their viscosities increase, which reflect the behavior of immiscible or partially miscible liquids. Similar trends were found by Tong et al. in similar systems [38] in which PDMS and PIB were not miscible over the composition range investigated.

a) PIB-PDMS

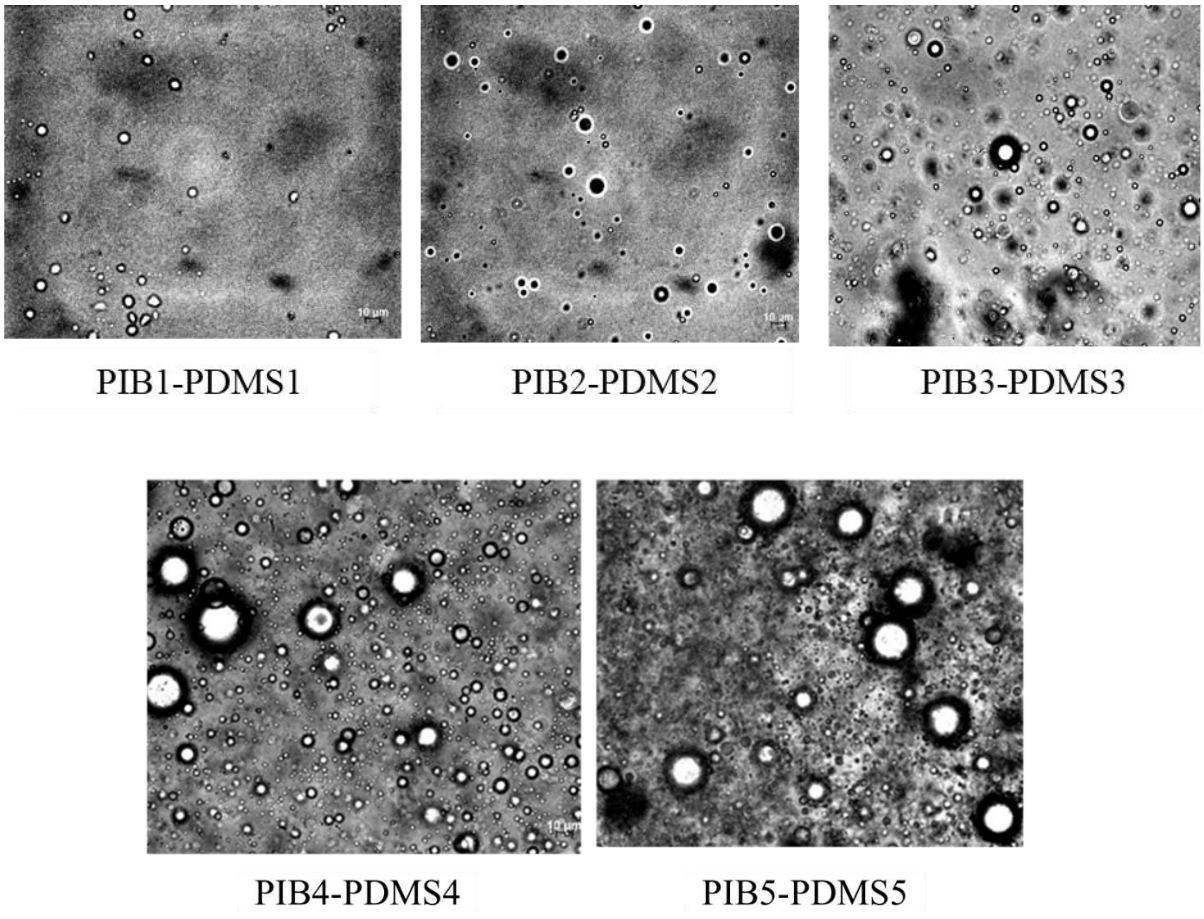

Figure II-19. Morphology corresponding to 10-wt.% PIB in PDMS matrix at a shear rate of 8 s^{-1} for 1250 s.

b) BF-PDMS

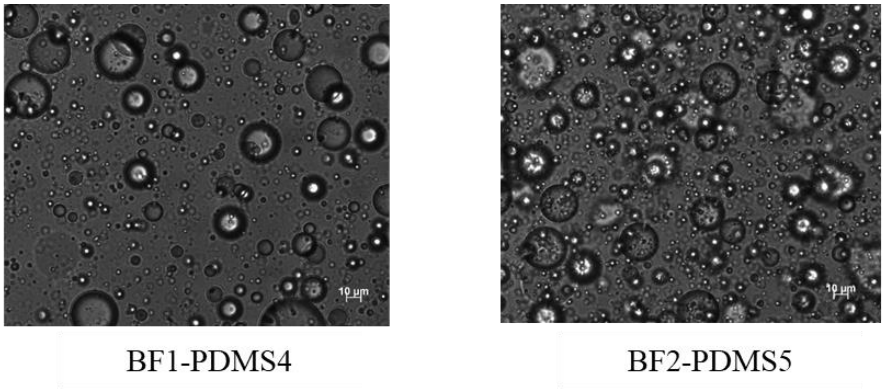

Figure II-20. Morphology corresponding to 10 wt.% BF in a PDMS matrix at a shear rate of 8 s^{-1} for 1250 s.

II.4.1.4. Solubility parameters

From the HSHiP software analysis, the Gibbs free energy of mixing is positive regardless of the polymer volume fraction (blue curve in the figure II-21). Also, the second derivative of the Gibbs free energy is negative (red curve). Furthermore, the distance R_a between the centres of the solubility

spheres is equal to 2.87 $MPa^{1/2}$ (3 $MPa^{1/2}$ for the PCL-PEG system) which is lower than the critical distance R_{0min}. Therefore, the systems studied could present a small partial miscibility, confirming the rheology, optical microscopy and SEM analysis results.

PIB-PDMS

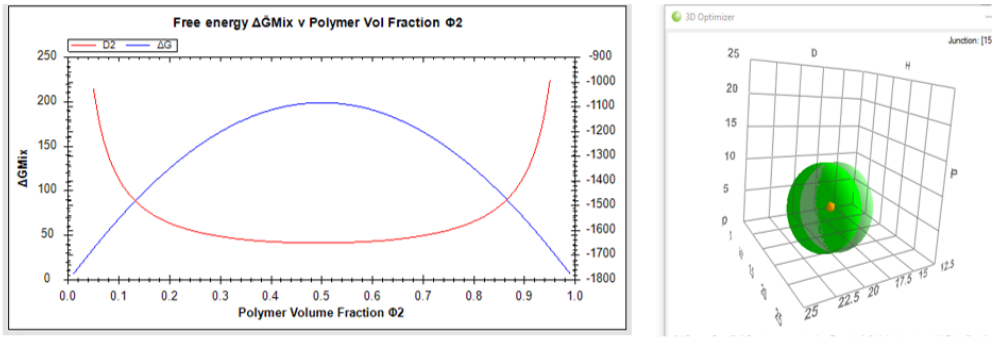

Figure II-21. the Gibbs free energy of mixing of the PIB-PDMS & PEG-PCL systems.

Table II-9. The theoretical solubility parameters of the studied materials obtained by HSHiP software.

	δ_D	δ_P	δ_H	Distance ($MPa^{1/2}$)
PDMS	14,9	0,4	0,8	2,87
PIB	16,3	0,3	0,2	

II.4.2. Interfacial rheology

II.4.2.1. Preliminary manipulation

Before performing measurement in the DWR setup, the experimental surface viscosity of a known viscosity film was compared to the theoretical value. The experimental and theoretical values were very close confirming (Figure II-22) the accuracy of the measurement for a low viscous surface (around 10^{-6} Pa.s.m)

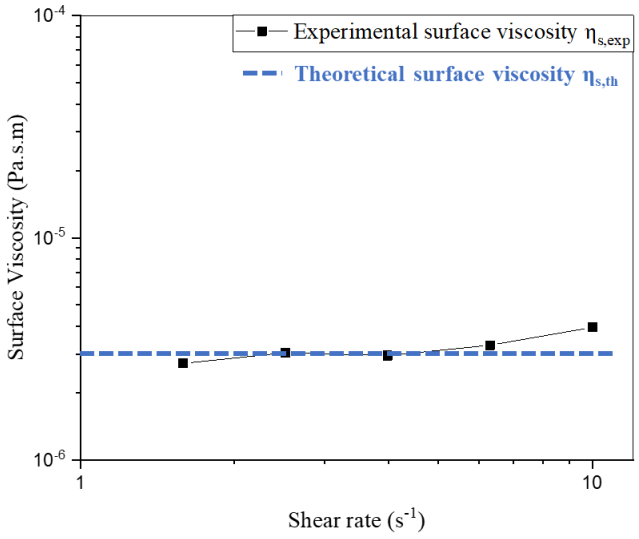

Figure II-22. Comparison between the theoritical and the experimental surface viscoisity in the steady flow at 25°C.

For each surface and interface, the experiments were performed as follows. First, the linear region was defined by an amplitude sweep experiment, and then the frequency and steady flow sweep tests were carried out. The effect of the temperature on the interfacial properties was also evaluated. Finally, a correction for the contribution of the sub-phases was performed to extract the real interfacial and surface properties.

II.4.2.2. Surface responses

The response of the air-PIB1 and air-PDMS1 surfaces were detected neither by the bicone nor by the DWR.

For the air-PDMS surface, we present just one system (air-PDMS4) using the test previously described (Figure II-23). For the other air-PDMS surfaces, the details are presented in the Supporting Information.

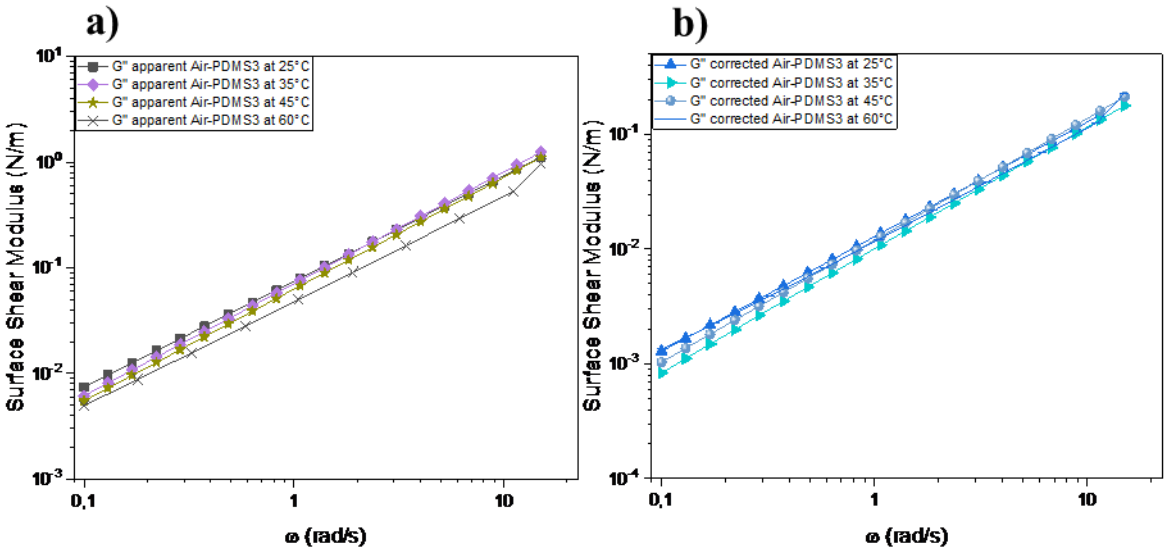

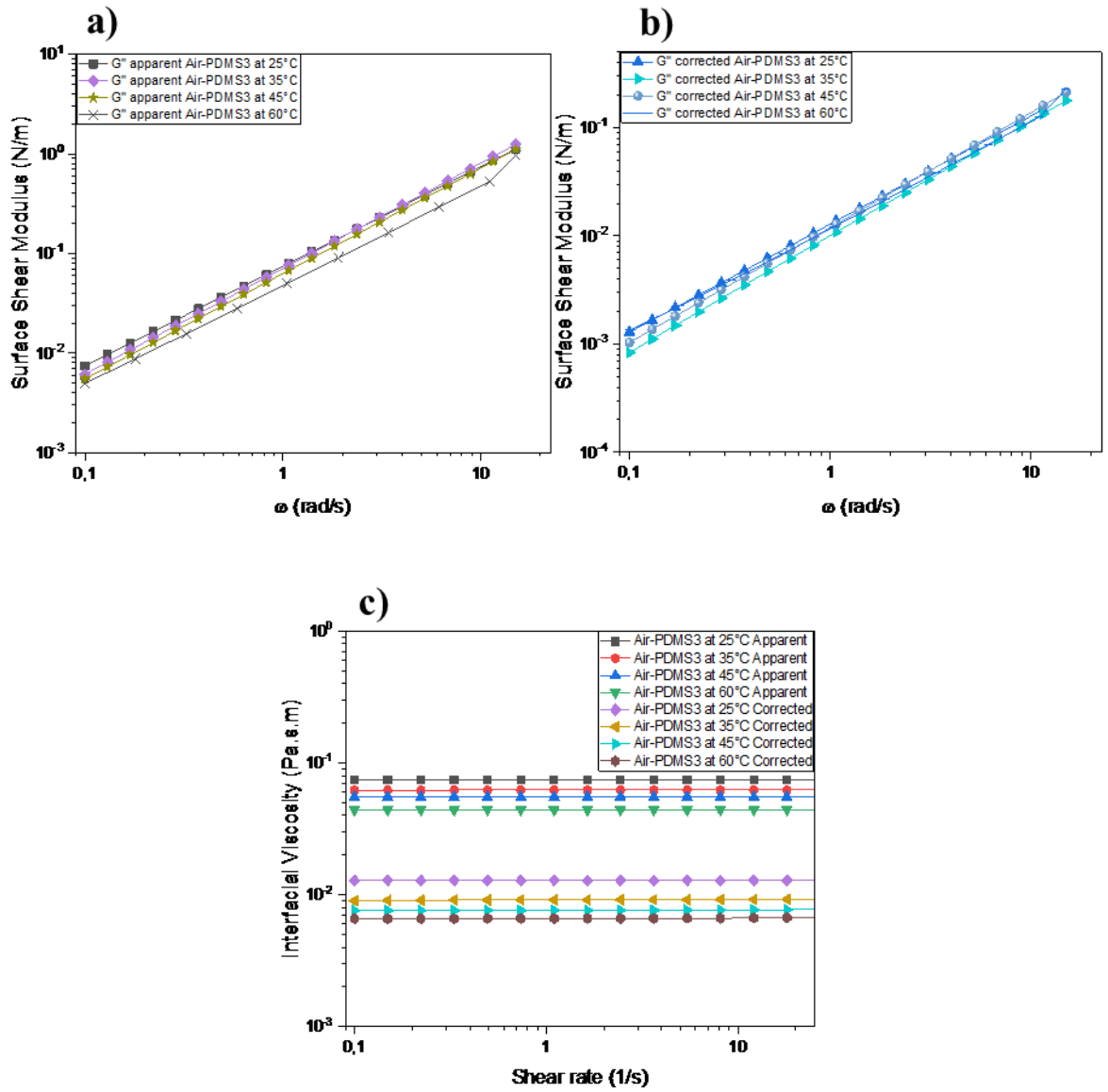

Figure II-23. Frequency sweep (apparent modulus (a), corrected modulus (b)) and the steady shear (c) experiments of air-PDMS3 surface.

From the frequency sweep test, it can be seen that the air-PDMS4 surface exhibits viscous behaviour because no elasticity is detected. When the temperature increases, the apparent surface loss modulus G" decreases as well. After the correction for the subphase effect in the oscillatory test, the same tendency is observed. There are no data collected at the temperature of 25°C due to the high inertia of the subphase and also due to the bicone inertia because of its high weight, and thus it was not straightforward to carry out a dynamic test (frequency sweep). For the flow sweep, we note that this surface is Newtonian. The corrected surface viscosity increases when the fluid bulk viscosity increases. The bicone could apply a permanent flow sweep (just a simple rotation contrary to the back and forth motion of the frequency sweep test). The same tendency was found for the other surfaces. Table II-10 summarizes the surface viscosities of the different surfaces at 60°C.

Table II-10. Interfacial shear properties of the air-PDMS surfaces at 60°C.

Surface	Apparent surface viscosity (Pa.s.m) at 60°C	Boussinesq Number at 60°C	Corrected surface viscosity (Pa.s.m) at 60°C	Temperature effect on the surface viscosity
Air-PDMS2	$4.1.10^{-3}$	0.20	$3.6.10^{-4}$	↓↓↓↓
Air-PDMS3	$4.4.10^{-2}$	0.21	$5.5.10^{-3}$	↓↓↓↓
Air-PDMS4	0.13	0.23	$2.0.10^{-2}$	↓↓↓↓
Air-PDMS5	1.3	0.62	0.69	↓↓↓↓

As shown in Table II-10, the Boussinesq numbers at 60°C are deficient because of the high viscosity of the subphases. Thus, carrying out these corrections is of primordial importance. We can also see that the viscosity of the surface increases when the viscosity of the subphases increases. This phenomenon is likely related to the cohesion of chain layers at the surface due to the viscosity effect which is in agreement with to the definition of the surface based on the Boussinesq approach [39]. The latter imagines the surface as a superposition of layers with variable density; this density gradient gives enough force to the fluid to maintain it in a fixed range. Similar trends were observed in the air-PIB and air-BF surfaces (Figure II-24).

For the air-BF1 surface, we notice the appearance of an elasticity at low frequency that disappearance after the correction. This elasticity comes from the contribution of subphase BF1, which is a Boger fluid that has an elasticity previously described in the rheological characterization of the model fluids. For the interfacial rheological measurements of the other air-PIB and air-BF surfaces at different temperatures, the plot details are presented in the Supporting Information.

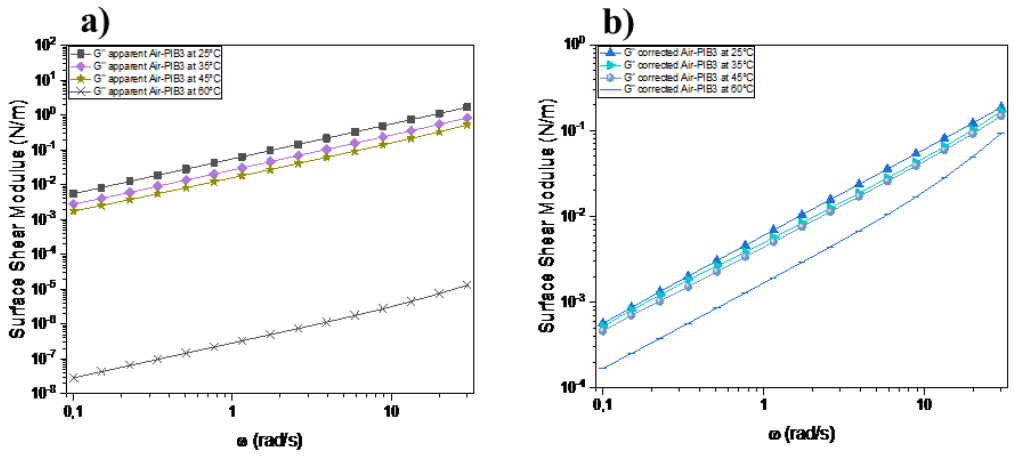

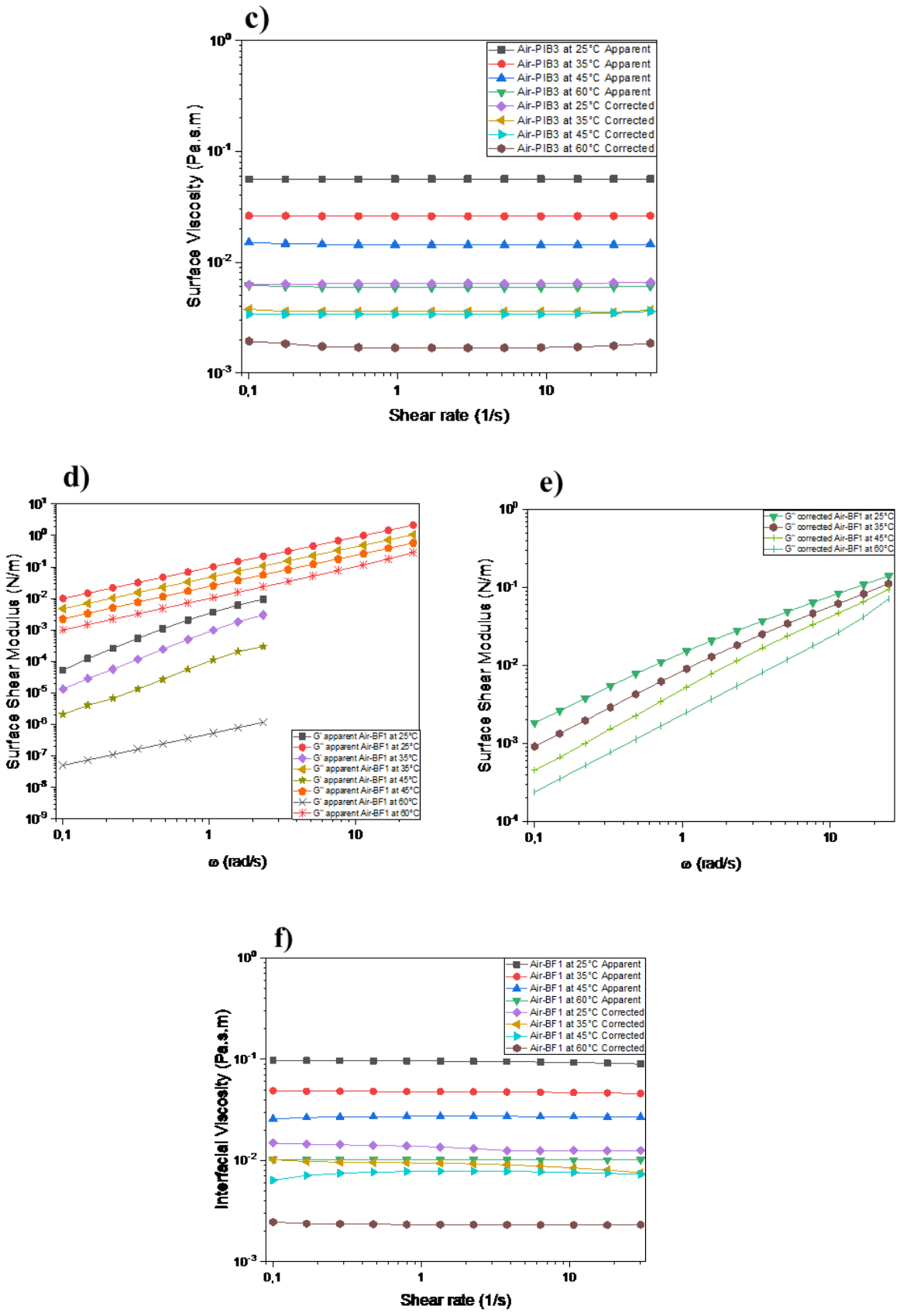

Figure II-24. Frequency sweep and steady shear experiments of air-PIB3 (a, b & c) and air-BF1 (d, e & f) surfaces.

Table II-11. The interfacial shear properties of Air-PIB & Air-BF surfaces at 60°C.

Surface	Apparent surface viscosity (Pa.s.m) at 60°C	Boussinesq Number at 60°C	Corrected surface viscosity (Pa.s.m) at 60°C	Temperature effect on the surface viscosity
Air-PIB2	$2.9.10^{-3}$	0.28	$1.9.10^{-4}$	↓↓↓↓
Air-PIB3	$6.1.10^{-2}$	0.30	$0.9.10^{-3}$	↓↓↓↓
Air-PIB4	$3.1.10^{-2}$	0.60	$4.9.10^{-2}$	↓↓↓↓
Air-PIB5	0.23	0.30	0.1	↓↓↓↓
Air-BF1	0.015	0.35	$0.25.10^{-2}$	↓↓↓↓
Air-BF2	0.127	0.22	$1.30.10^{-2}$	↓↓↓↓

To finish this section, we plot the variation of the surface viscosity as a function of the bulk viscosity (Figure II-25).

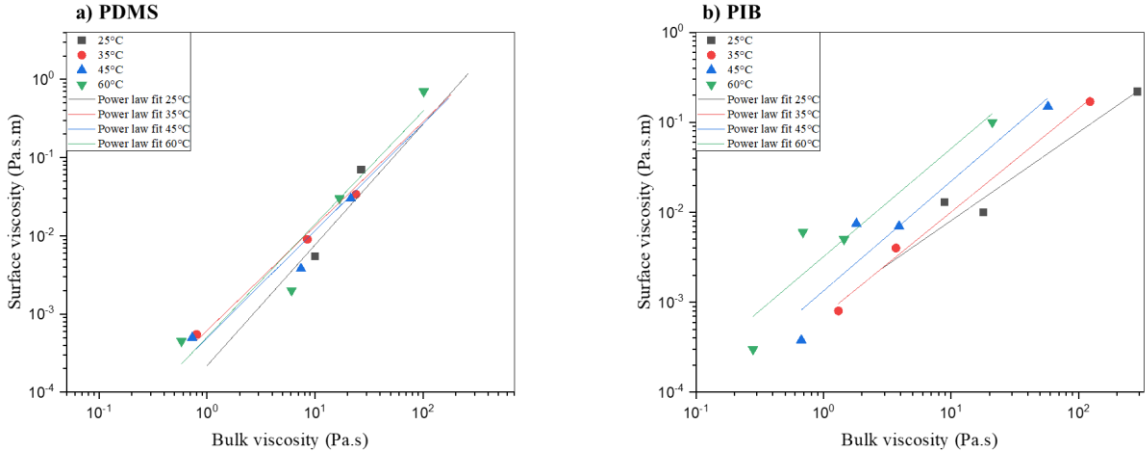

Figure II-25. Correlation between surface viscosities and bulk viscosities.

Increasing the temperature leads to a decrease in surface viscosity. The surface viscosity increases with the bulk viscosity, and the variation follows a power law.

In the case of air-polymer systems, the surface is composed of macromolecular chains with a specific conformation in contact with air molecules. It is formed from the bulk, and the properties of the latter can have effects on the surface properties.

II.4.2.3. Interface responses

In this section, the DWR geometry was used to characterize the interfaces between high melt flow rate fluid subphases (PIB1-PDMS1 and PIB2-PDMS2) and the titanium biconical geometry for the interfaces between highly viscous subphases (PIB3-PDMS3, PIB4-PDMS4, PIB5-PDMS5, BF1-PDMS4 and BF2-PDMS5). (see Figure II-26)

In the case of the PIB2-PDMS2 system, the interface is purely viscous (Newtonian behavior). It is useful to indicate that no elastic modulus was detected. According to *Läuger et al*. [39], the absence of a measurable modulus of elasticity in the case of ultra-high melt flow rate liquids could be due to the torque sensitivity limit of the rheometer being reached. In these conditions, the inertia of the geometry and the instrument exceeds the response of the interface.

On one hand, we can observe that, for a fixed temperature, both the apparent and corrected interfacial viscosities increase when the viscosity of the subphases increases. On the other hand, the apparent and corrected interfacial moduli (and the interfacial viscosity) decrease when the temperature increases (the same observation can be made with the PIB1-PDMS1 interface). However, for PIB4-PDMS4 and BF1-PDMS4 the interfaces, the relationship between the apparent and the corrected interfacial magnitudes does not undergo the same trend. The apparent data obtained show that the interfacial viscous modulus G" decreases when the temperature increases, in contrast to the corrected values of the effects of the subphases when is subtracted (very low Boussinesq numbers). These interfaces remain Newtonian, but the interfacial viscosity increases due to the rise of the temperature. The same observation applies to the other interfaces (PIB3/PDMS3, PIB5/PDMS5 and BF2/PMDS5).

For the other fluid-fluid interfaces, all figures were presented in the Supporting Information. Table II-12 summarizes the interfacial viscosities of these systems.

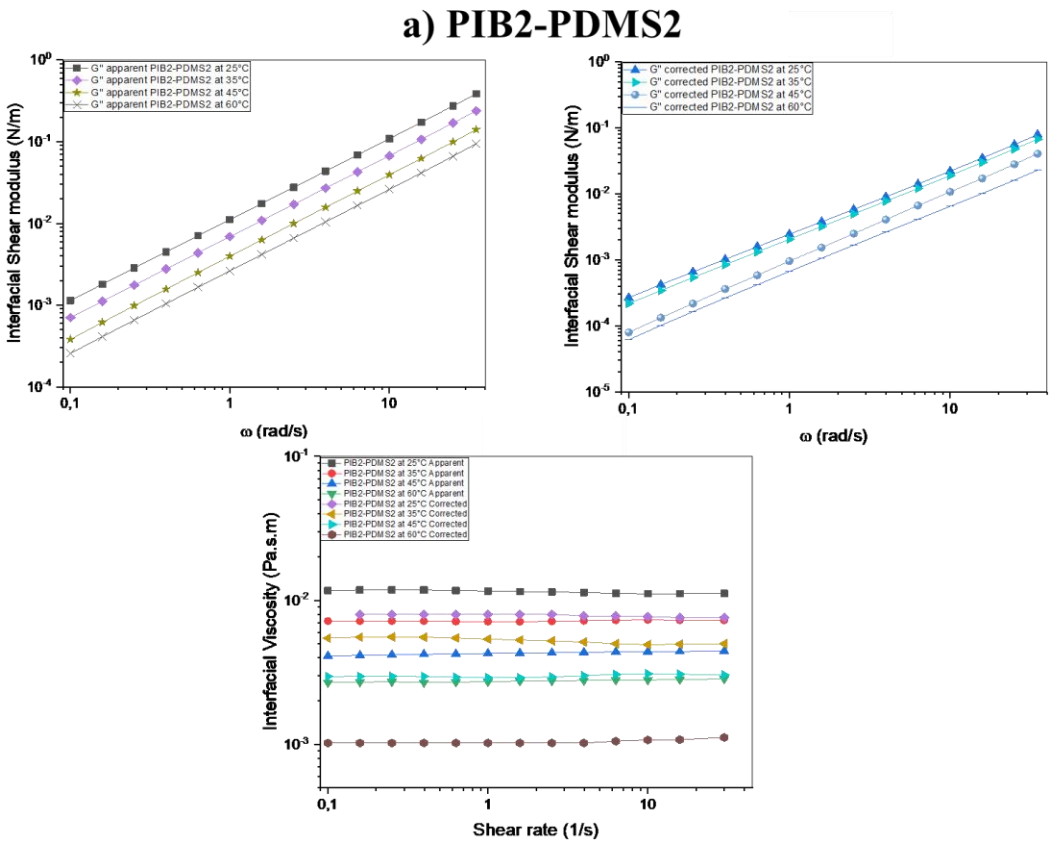

b) PIB3-PDMS3

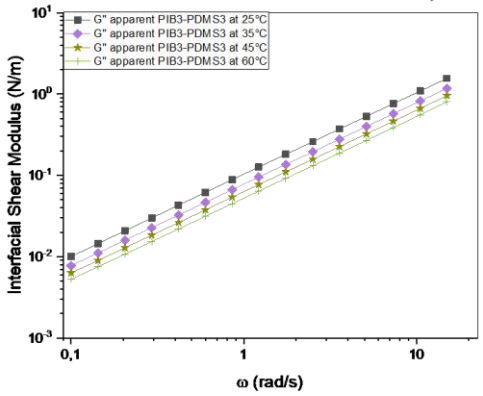

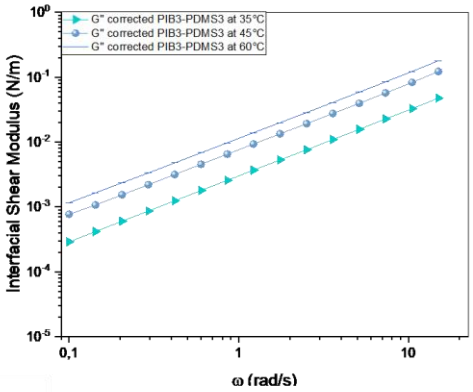

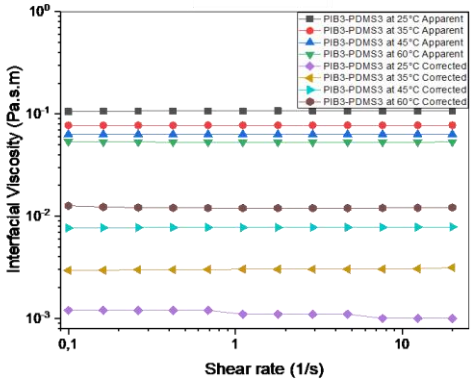

c) BF1-PDMS4

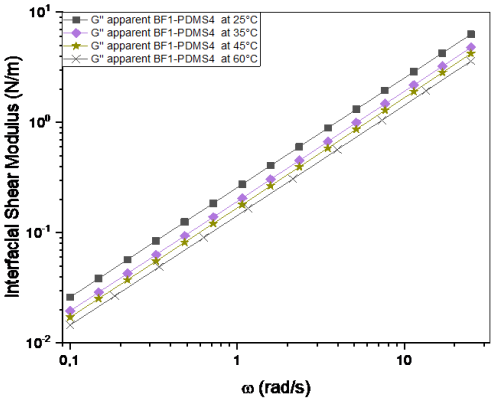

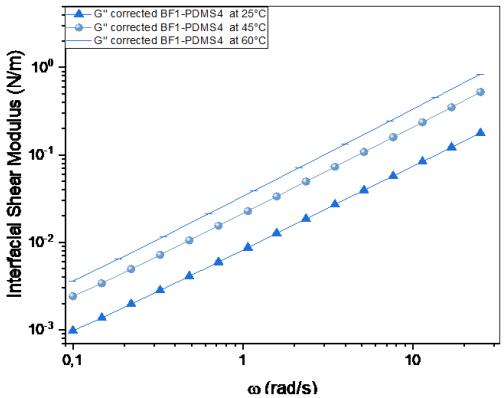

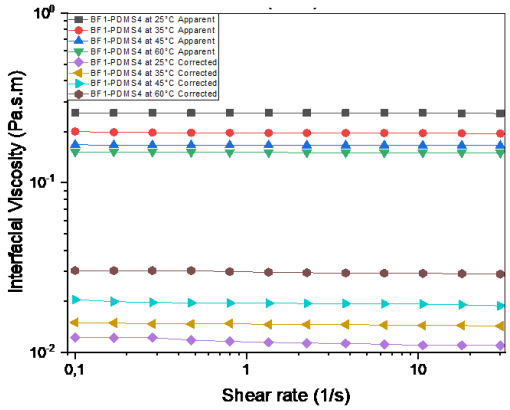

Figure II-26. Frequency sweep and the steady shear experiments of the PIB2-PDMS2 (a), PIB3-PDMS3 (b) and BF1-PDMS4 (c) interfaces.

Table II-12. Interfacial shear properties of the PIB-PDMS and BF-PDMS interfaces at 60°C.

Interface	Apparent interfacial viscosity (Pa.s.m) at 60°C	Boussinesq Number at 60°C	Corrected interfacial viscosity (Pa.s.m) at 60°C	Temperature effect on the interfacial viscosity
PIB1-PDMS1	$2.96.10^{-4}$	4.22	$4.72.10^{-5}$	↓↓↓↓
PIB2-PDMS2	$2.71.10^{-3}$	4.30	$1.02.10^{-3}$	↓↓↓↓
PIB3-PDMS3	$5.37.10^{-2}$	0.24	$1.26.10^{-2}$	↑↑↑↑
PIB4-PDMS4	0.13	0.21	$2.69.10^{-2}$	↑↑↑↑
PIB5-PDMS5	1.27	0.30	$5.47.10^{-1}$	↑↑↑↑
BF1-PDMS4	0.15	0.24	$3.04.10^{-2}$	↑↑↑↑
BF2-PDMSS5	1.17	0.30	$4.30.10^{-1}$	↑↑↑↑

From Table II-12, it can be seen that from a known molecular weight of the sub-phases, an increased temperature leads to increased interfacial viscosity, the macromolecules are long enough to diffuse from one phase to the other (Figure II-27). More the viscosity of the subphases is high, more the diffused chains are longer. Therefore, the interface became more and more “rigid”. Raising the temperature may lead to an increase in the kinetics of the diffusion. The small macromolecules migrate from one phase into the other by crossing the interface. In other words, the increased temperature makes it possible to boost the intra-entanglement at the interface.

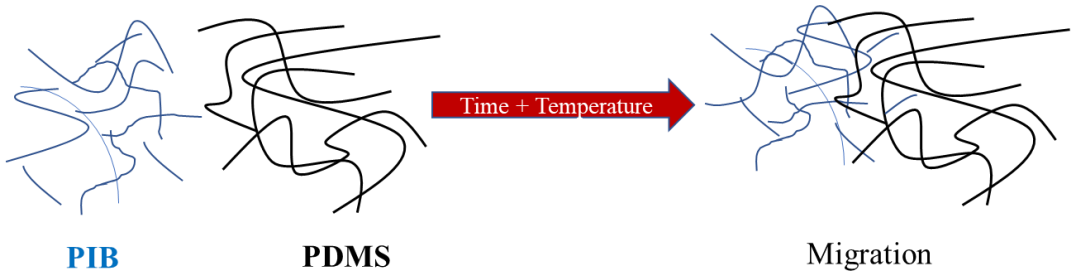

Figure II-27. Migration phenomena from the PIB to PDMS accross the interface

Similar observations were reported by Tufano *et al.* [40] in the case of PIB-PDMS systems. They studied the diffusion from the light subphase to the heavy subphase ($Mn_{PIB} < Mn_{PDMS}$) at the interface by measuring the evolution of interfacial tension as a function of the temperature [40]. Table II-13 summarizes the effect of the temperature on the interfacial tension in the case off the PIB-PDMS

systems considered in this study. The validation of this hypothesis will be checked in the next chapter using optical microscopy measurements.

Table II-13. Effect of temperature on the interfacial tension of the PDMS/PIB systems studied.

Interface	Interfacial tension at 25°C (mN/m)	Interfacial tension at 35°C (mN/m)	Interfacial tension at 45°C (mN/m)	Interfacial tension at 60°C (mN/m)
PIB2-PDMS2	2.15	2.3	2.4	4.2
PIB3-PDMS3	2.8	2.6	2.2	1.9
PIB4-PDMS4	2.9	2.6	2.5	2.1
PIB5-PDMS5	3.8	2.9	2.8	2.3
BF1-PDMS4	2.2	2.1	2.1	1.8
BF2-PDMS5	3.3	2.5	2.3	2.1

For the PIB2-PDMS2 system, the PIB2 drop becomes more and more spherical within the PDMS2 due to the temperature increase (figure II-28). The interface between the two subphases becomes less stable (which explains why the interfacial shear viscosity decreases with increasing temperature). On the contrary, for the other interfaces, the drop grows to be extended which increases the contact area between the subphases.

Figure II-28. Effect of the temperature on the diameter of a rising drop of PIB2 inside PDMS2.

II.4.3. Molten polymer systems investigation

II.4.3.1. Differential Scanning Calorimetry (DSC)

Figure II-29 presents the DSC spectra of the PEG and PCL semi-crystalline polymers during the cooling and heating steps. The crystallization and melting temperatures were observed to be very close. Therefore, the shear interfacial rheological properties of PEG-PCL molten systems were examined at temperatures higher than 80 °C to prevent the crystallization of the subphases.

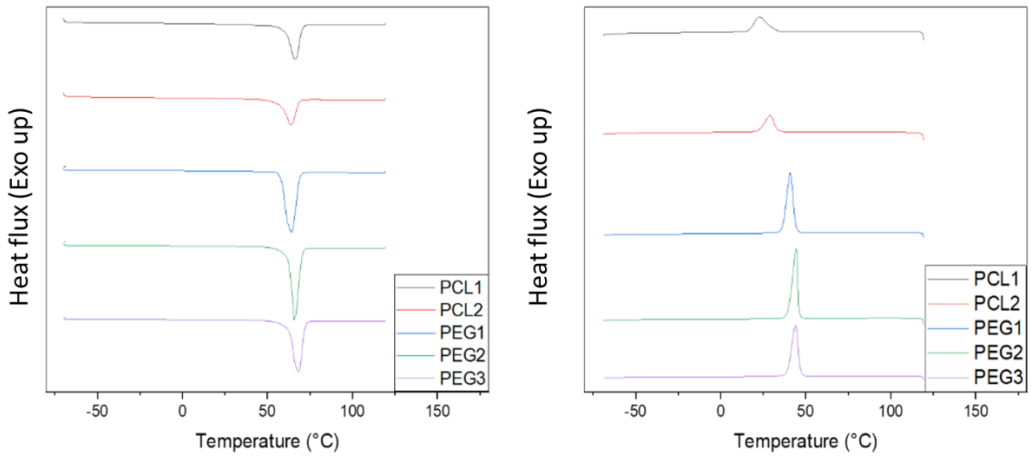

Figure II-29. Differential scanning calorimetry (DSC) thermograms for crystallization (right) and melting (left) for different PEG and PCL samples.

II.4.3.2. Scanning Electron Microscopy

Figure II-30 shows the SEM images of PEG- PCL blends of different grades. A nodular morphology is observed regardless of the viscosity ratio used which indicates once again the presence of a partially miscible polymer structure over the composition range studied [41].

a) PEG1-PCL1

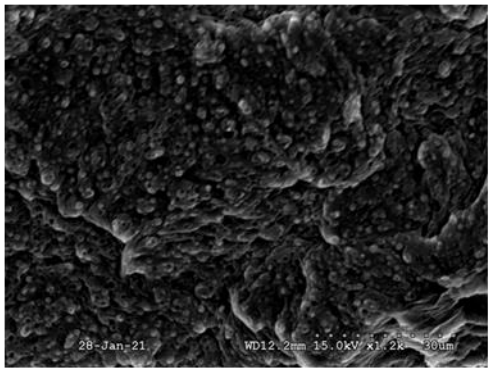

b) PEG2-PCL1

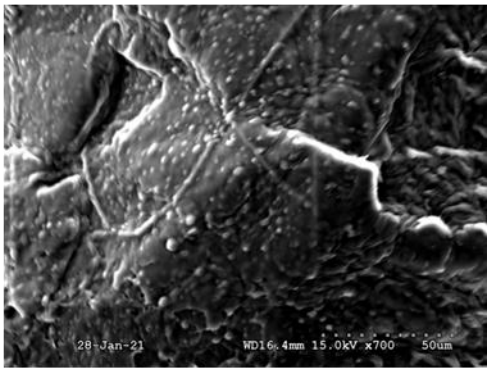

c) PEG3-PCL2

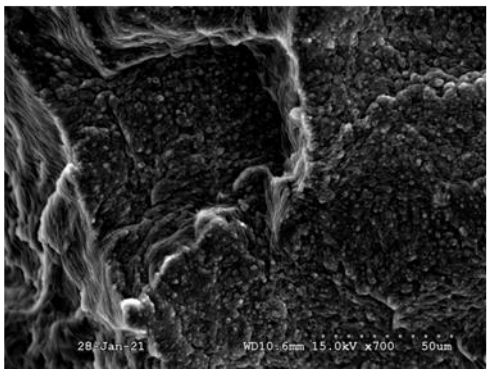

Figure II-30. Morphology corresponding of PEG-PCL extrudates.

II.4.3.3. Solubility parameters

For this system, the HSHiP software allowed to the distance Ra between the centres of the solubility spheres is equal to 3 $MPa^{1/2}$ which is lower than critical distance R_{0min}. Thus the PEG-PCL systems are partially miscible.

Table II-14. The theoretical solubility parameters of the PEG-PCL system obtained by HSHiP software.

	δ_D	δ_P	δ_H	Distance ($MPa^{1/2}$)
PEG	16	5	5	3
PCL	17	4	4	

II.4.3.4. Interfacial Shear rheology of molten polymer systems

In this section, interfaces in the molten state between two highly crystalline polymers (PEG-PCL systems) were investigated based on the interfacial shear rheology.

The bulk rheological curves (master curves at the reference temperature of 90°C) are depicted in Figures II-31 and II-32. It was observed that the two semi-crystalline polymers (PCL and PEG) are Newtonian in the shear rate region studied.

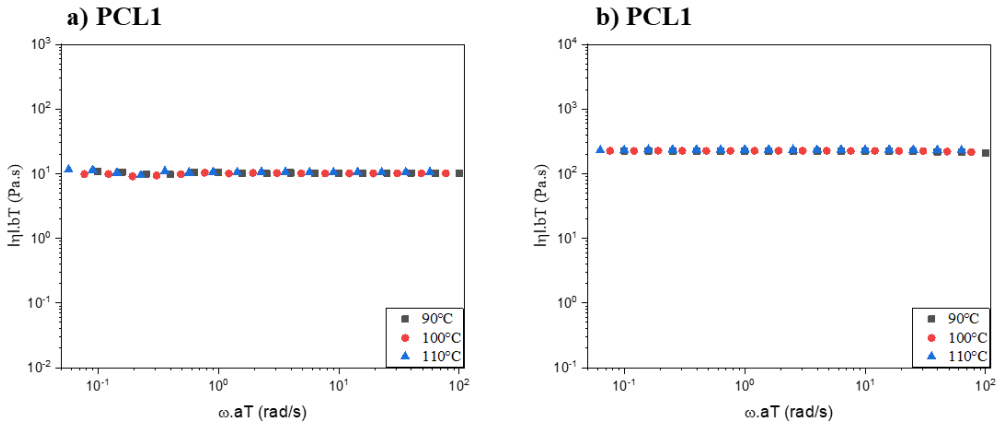

Figure II-31. Master curves of PCL1 (a) and PCL2 (b) at the reference temperature of 90°C.

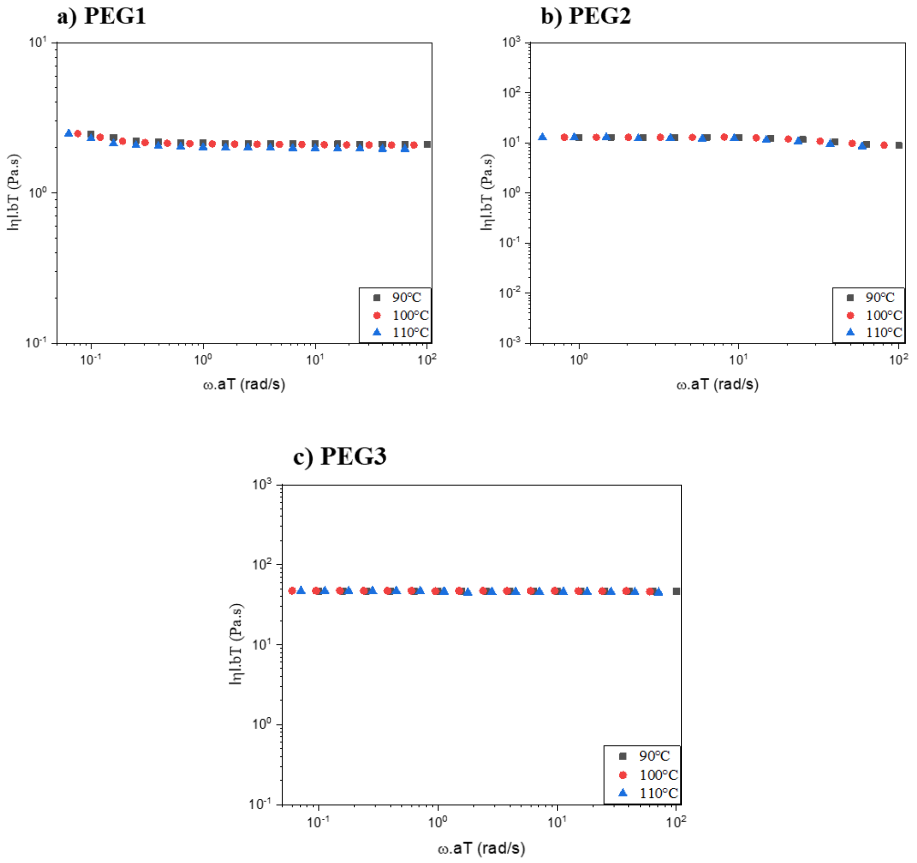

Figure II-32. Master curves of PEG1 (a), PEG2 (b) and PEG3 (c) at the reference temperature of 90°C.

Van-Gurp-Palmen plot of the different PCL and PEG in addition to the high viscous system PEG3-PCL2 (10/90 and 50/50wt%) were plotted and displayed in the supporting information section.

The interfacial properties of three different systems (PEG1-PCL1, PEG2-PCL1 and PEG3-PCL2) were studied from the steady shear experiments at 90 °C, 100 °C and 110°C (Figure II-33 and II-34).

Because of the high rigidity of their subphases, the interfacial shear properties of the PEG-PCL systems were examined using the titanium bicone. The steady flow tests show that all the interfaces are Newtonian. The apparent interfacial viscosities for each PEG-PCL system decrease when the temperature increases but different trends for the corrected values after correcting for the effects of the sub-phases.

For the PEG1-PCL1system, increasing the temperature leads to a decrease in the interfacial viscosity. Otherwise, the interfacial viscosity of the PEG2-PCL1 and PEG3-PCL2 systems increases when the temperature increases (the same observation can be made with the interfacial loss modulus). The actual results are similar to those found previously with PIB-PDMS systems. Because of the partial

miscibility between the PEG and the PCL and from a specific molecular weight, the interface might turn into a physical interphase.

An attempt was made to measure the interfacial tension between PCL and PEG at different temperatures using the pendant drop method. Unfortunately, these tests were unsuccessful for two essential reasons. The first reason was due to the difference in density between the two polymers which is almost zero, preventing the application of the Laplace law. The second reason was the refractive index difference, which was close, therefore inducing a low optical contrast.

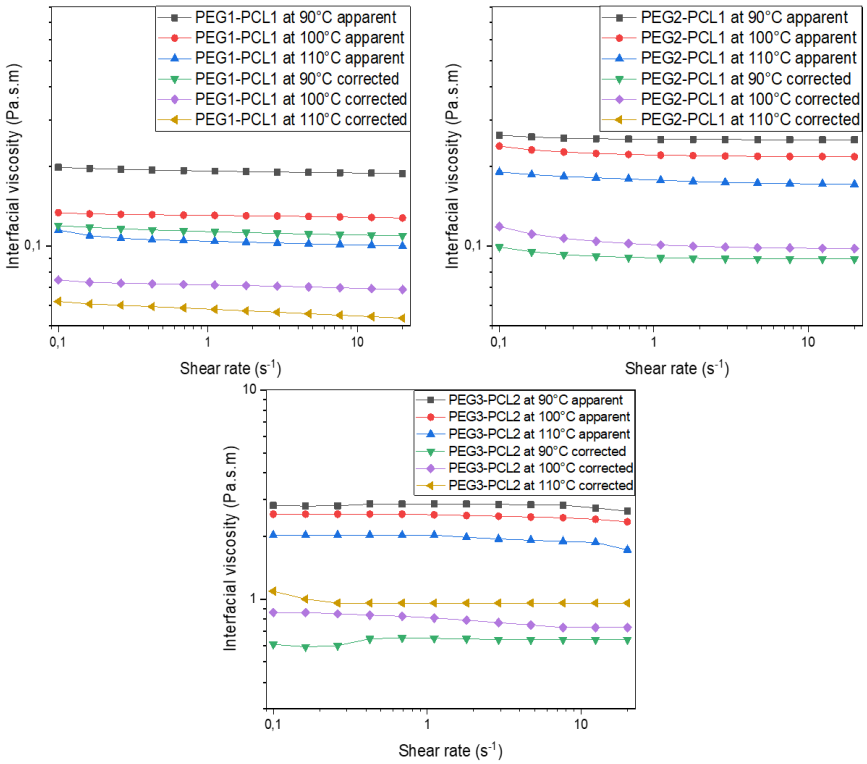

Figure II-33. Variation of the interfacial shear viscosity with the angular frequency of PEG-PCL systems.

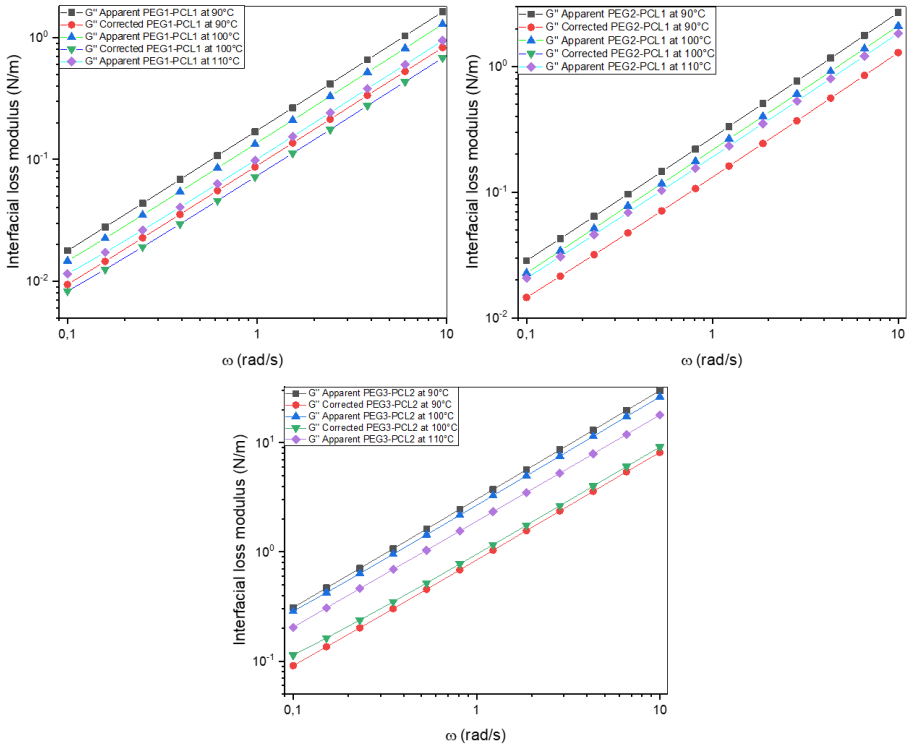

Figure II-34. Variation of the interfacial shear loss modulus with the angular frequency of the PEG-PCL systems studied.

Table II-15. Effect of the temperature on the interfacial tension of studied PEG-PCL systems.

Interface	Apparent interfacial viscosity (Pa.s.m) at 90°C	Boussinesq Number at 90°C	Corrected interfacial viscosity (Pa.s.m) at 90°C	Temperature effect on the interfacial viscosity
PEG1-PCL1	0.19	0.44	0.12	↓↓↓↓
PEG2-PCL1	0.26	0.36	0.10	↑↑↑↑
PEG3-PCL2	2.8	0.30	0.60	↑↑↑↑

II.5. Conclusions

The present work highlights the implementation of two rheological tools for characterizing the interfacial shear rheology of polymer systems. The measurements with the DWR setup showed a limiting subphase viscosity of 3 Pa.s when probing the interfaces from high melt flow rate liquids. Otherwise, a slip of the geometry with respect to the fixing rotation system was observed.

In the case of air/fluid surfaces, purely viscous behaviour was noticed. The corrected surface viscosity increased when the fluid bulk viscosity increased. As for the interfacial investigation of model PDMS-

PIB systems, the interface was purely viscous (Newtonian behavior). At a constant temperature, the more the viscosity of the subphases increased, the more the interfacial viscosity increased. On the other hand, for low-viscosity fluid systems, both the apparent and corrected interfacial moduli (and the interfacial viscosity) decreased when the temperature increased. However, when the interfaces were formed from a highly viscous fluid medium, the corrected interfacial viscosity underwent an opposite trend with the rise of the temperature indicating the formation of an interphase.

A similar tendency was noted for BF-PDMS model fluids. The presence of elasticity in Boger fluids does not affect their viscoelastic interfacial behavior. The measurements in the molten state of PEG-PCL systems using the newly developed biconical IRS showed that starting from a specific molecular weight, the interface turned into an interphase which inducing an increase in interfacial viscosity.

The results of this study could be transposed for the probing of other immiscible thermoplastic polymers that exhibit more complex interfaces such as in the presence of solid nanofillers, compatibilizers or multilayers.

References

[1] D. Renggli, A. Alicke, R. H. Ewoldt, and J. Vermant, "Operating windows for oscillatory interfacial shear rheology," *Journal of Rheology*, vol. 64, no. 1, pp. 141-160, 2020.

[2] J.-L. Grossiord and A. Ponton, *La mesure en rhéologie-des avancées récentes aux perspectives: des avancées récentes aux perspectives*. EDP Sciences, 2014.

[3] O. Soo-Gun and J. C. Slattery, "Disk and biconical interfacial viscometers," *Journal of Colloid and Interface Science*, vol. 67, no. 3, pp. 516-525, 1978.

[4] S. Derkach, J. Krägel, and R. Miller, "Methods of measuring rheological properties of interfacial layers (Experimental methods of 2D rheology)," *Colloid journal*, vol. 71, no. 1, pp. 1-17, 2009.

[5] P. Sánchez-Puga, J. Tajuelo, J. M. Pastor, and M. A. Rubio, "Dynamic measurements with the bicone interfacial shear rheometer: Numerical bench-marking of flow field-based data processing," *Colloids and Interfaces*, vol. 2, no. 4, p. 69, 2018.

[6] P. A. Rühs, C. Affolter, E. J. Windhab, and P. Fischer, "Shear and dilatational linear and nonlinear subphase controlled interfacial rheology of β-lactoglobulin fibrils and their derivatives," *Journal of Rheology*, vol. 57, no. 3, pp. 1003-1022, 2013.

[7] Y. Fan, S. Simon, and J. Sjöblom, "Interfacial shear rheology of asphaltenes at oil–water interface and its relation to emulsion stability: Influence of concentration, solvent aromaticity and nonionic surfactant," *Colloids and Surfaces A: Physicochemical and Engineering Aspects*, vol. 366, no. 1-3, pp. 120-128, 2010.

[8] L. M. Ligiero *et al.*, "Characterization of crude oil interfacial material isolated by the wet silica method. part 2: Dilatational and shear interfacial properties," *Energy & Fuels*, vol. 31, no. 2, pp. 1072-1081, 2017.

[9] S. Vandebril, A. Franck, G. G. Fuller, P. Moldenaers, and J. Vermant, "A double wall-ring geometry for interfacial shear rheometry," *Rheologica Acta*, vol. 49, no. 2, pp. 131-144, 2010.

[10] S. Barman and G. F. Christopher, "Simultaneous interfacial rheology and microstructure measurement of densely aggregated particle laden interfaces using a

modified double wall ring interfacial rheometer," *Langmuir,* vol. 30, no. 32, pp. 9752-9760, 2014.
[11] S. Costa, R. Höhler, and S. Cohen-Addad, "The coupling between foam viscoelasticity and interfacial rheology," *Soft Matter,* vol. 9, no. 4, pp. 1100-1112, 2013.
[12] L. Scriven, "Dynamics of a fluid interface equation of motion for Newtonian surface fluids," *Chemical Engineering Science,* vol. 12, no. 2, pp. 98-108, 1960.
[13] I. Delaby, B. Ernst, and R. Muller, "Drop deformation during elongational flow in blends of viscoelastic fluids. Small deformation theory and comparison with experimental results," *Rheologica Acta,* vol. 34, no. 6, pp. 525-533, Nov-Dec 1995, doi: 10.1007/bf00712313.
[14] D. Graebling, R. Muller, and J. Palierne, "Linear viscoelastic behavior of some incompatible polymer blends in the melt. Interpretation of data with a model of emulsion of viscoelastic liquids," *Macromolecules,* vol. 26, no. 2, pp. 320-329, 1993.
[15] D. Boger, "A highly elastic constant-viscosity fluid," *Journal of Non-Newtonian Fluid Mechanics,* vol. 3, no. 1, pp. 87-91, 1977.
[16] M. Verhoef, B. Van den Brule, and M. Hulsen, "On the modelling of a PIB/PB Boger fluid in extensional flow," *Journal of non-newtonian fluid mechanics,* vol. 80, no. 2-3, pp. 155-182, 1999.
[17] D. Merger and M. Wilhelm, "Intrinsic nonlinearity from LAOStrain—experiments on various strain-and stress-controlled rheometers: a quantitative comparison," *Rheologica Acta,* vol. 53, no. 8, pp. 621-634, 2014.
[18] A. Franck, "Measuring Structure of Low Viscosity Fluids in Oscillation Using a Rheometer with and without Separate Torque Transducer," *ANNUAL TRANSACTIONS-NORDIC RHEOLOGY SOCIETY,* vol. 11, pp. 95-100, 2003.
[19] J. D. Berry, M. J. Neeson, R. R. Dagastine, D. Y. Chan, and R. F. Tabor, "Measurement of surface and interfacial tension using pendant drop tensiometry," *Journal of colloid and interface science,* vol. 454, pp. 226-237, 2015.
[20] Y. Rotenberg, L. Boruvka, and A. Neumann, "Determination of surface tension and contact angle from the shapes of axisymmetric fluid interfaces," *Journal of colloid and interface science,* vol. 93, no. 1, pp. 169-183, 1983.
[21] H. CM, "Hansen solubility parameters: a user's handbook," *Florida: CRC,* 2007.
[22] M. D. de los Ríos and E. H. Ramos, "Determination of the Hansen solubility parameters and the Hansen sphere radius with the aid of the solver add-in of Microsoft Excel," *SN Applied Sciences,* vol. 2, no. 4, pp. 1-7, 2020.
[23] C. M. Hansen, "The universality of the solubility parameter," *Industrial & engineering chemistry product research and development,* vol. 8, no. 1, pp. 2-11, 1969.
[24] C. M. Hansen, "The three dimensional solubility parameter," *Danish Technical: Copenhagen,* vol. 14, 1967.
[25] R. Gallu, F. Méchin, F. Dalmas, J.-F. Gérard, R. Perrin, and F. Loup, "On the use of solubility parameters to investigate phase separation-morphology-mechanical behavior relationships of TPU," *Polymer,* vol. 207, p. 122882, 2020.
[26] A. Franck, "Double Wall Ring Geometry to Measure Interfa-cial Rheological Properties," in *APN031,* ed: TA Instruments, Germany, 2015, pp. 1-9.
[27] P. Bohr, H. Stettin, and J. Läuger, "Biconical geometries in rheometers: Exact solution for the flow field and implications for the design of measuring systems," *Review of Scientific Instruments,* vol. 90, no. 1, p. 015114, 2019.
[28] *Instruction Manual and Safety Information. Interfacial Rheology System,* Document Number B74IB056EN-C, 2019.
[29] S. Trinkle and C. Friedrich, "Van Gurp-Palmen-plot: a way to characterize polydispersity of linear polymers," *Rheologica Acta,* vol. 40, no. 4, pp. 322-328, 2001.

[30] S. Trinkle, P. Walter, and C. Friedrich, "Van Gurp-Palmen plot II–classification of long chain branched polymers by their topology," *Rheologica Acta,* vol. 41, no. 1-2, pp. 103-113, 2002.
[31] M. Van Gurp and J. Palmen, "Time-temperature superposition for polymeric blends," *Rheol. Bull,* vol. 67, no. 1, pp. 5-8, 1998.
[32] C. A. García-Franco, "A Note on the Elasticity of Polymer Melts Described by Primary Normal Stress Difference (N1)," in *Macromolecular Symposia*, 2013, vol. 325: Wiley Online Library, pp. 184-193.
[33] E. Mezger, "Loi de variation de la tension superficielle avec la température," 1946.
[34] G. Cazaux, "Faisabilité des procédés LCM pour l'élaboration de composites renfort continu à matrice thermoplastique polyamide," Le Havre, 2016.
[35] D. LeGrand and G. Gaines Jr, "The molecular weight dependence of polymer surface tension," *Journal of Colloid and Interface Science,* vol. 31, no. 2, pp. 162-167, 1969.
[36] Roger S. Porter, Julian F. Johnson, The status of non-Newtonian polymer flow, Polymer Engineering & Science, 10.1002/pen.760030105, **3**, 1, (18-20), 2004.
[37] Graessley, W. W., The entanglement concept in rheology, Advances in Polymer Science, 16 (1974).
[38] W. Tong, Y. Huang, C. Liu, X. Chen, Q. Yang, and G. Li, "The morphology of immiscible PDMS/PIB blends filled with silica nanoparticles under shear flow," *Colloid and Polymer Science,* vol. 288, no. 7, pp. 753-760, 2010.
[39] S. Nguyen, "Dynamique d'une interface en présence d'une singularité de contact solide/fluide," Paris Sud XI, 2005.
[40] C. Tufano, G. Peters, P. Van Puyvelde, and H. Meijer, "Transient interfacial tension and morphology evolution in partially miscible polymer blends," *Journal of colloid and interface science,* vol. 328, no. 1, pp. 48-57, 2008.
[41] K. Ragaert, G. Maeyaert, C. Martins, and L. Cardon, "Bulk compounding of PCL-PEO blends for 3D plotting of scaffolds for cardiovascular tissue engineering," *JOURNAL OF MATERIALS SCIENCE AND ENGINEERING,* vol. 3, no. 1, 2014.

Supporting Information (Chapter II):

Appendix 1: Van-Gurp Palmen plots

1) PCL

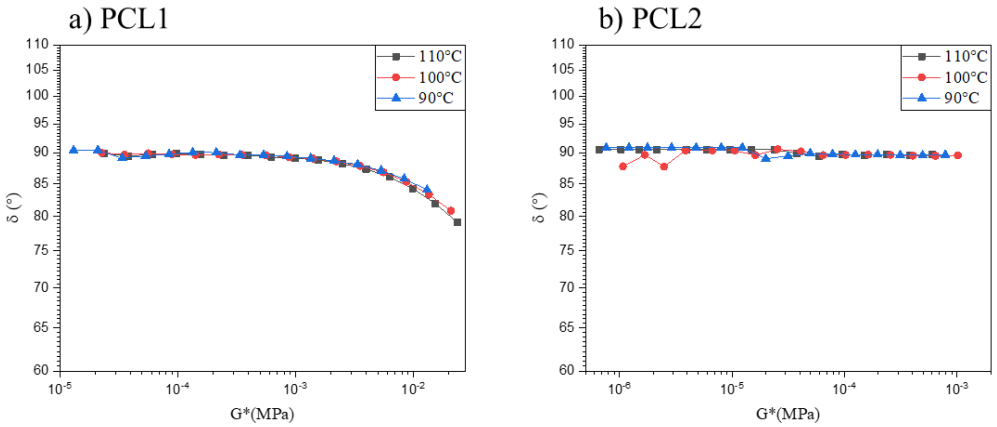

Figure SI.II-1. Variation of the phase-shift angle as a function of the complex modulus for PCL1 (a) and PCL2 (b) at 90, 100 and 110°C.

2) PEG

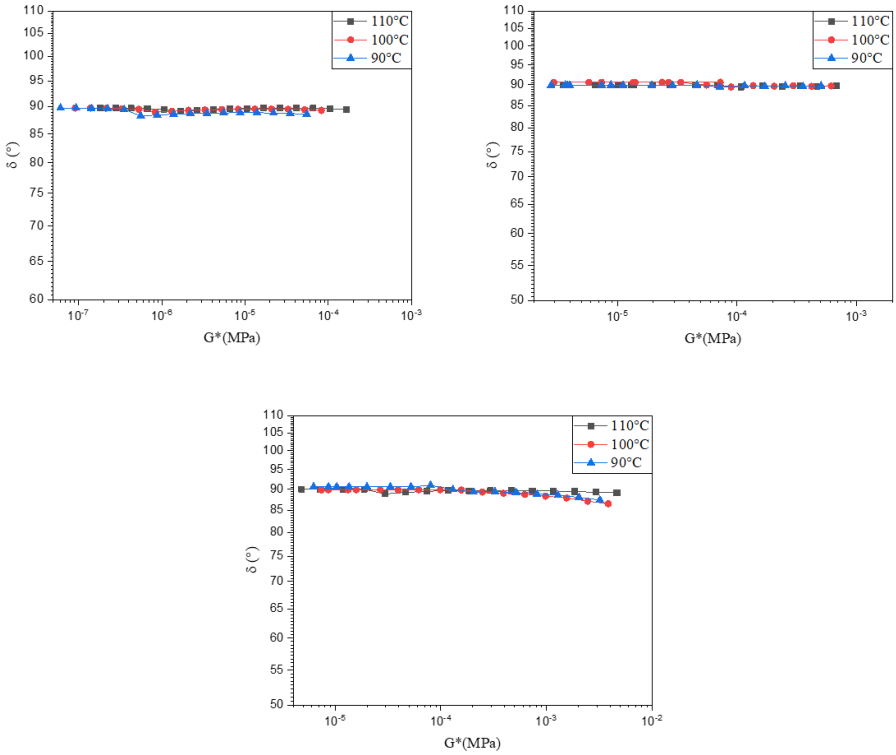

Figure SI.II-1. Variation of the phase-shift angle as a function of the complex modulus for PEG1 (a), PEG2 (b) and PEG (c) at 90, 100 and 110°C.

3) PCL-PEG blends

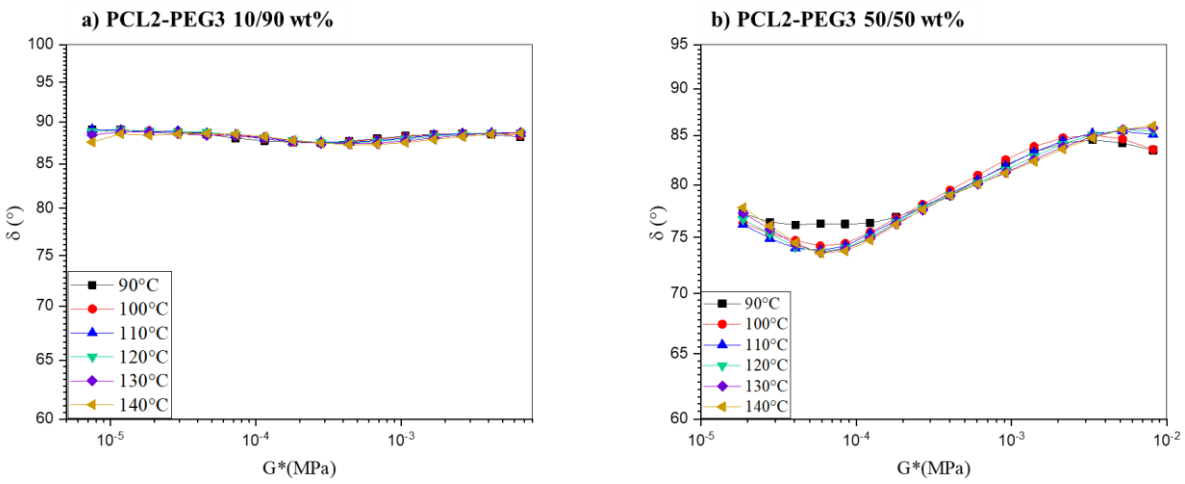

Figure SI.II-3. Variation of the phase-shift angle as a function of the complex modulus for PCL2-PEG3 blends at 90, 100, 110, 120, 130 and 140°C. (a) 10/90 wt% and (b) 50/50 wt%.

Appendix 2: Surface shear rheology of air-PDMS and air-PIB surfaces

- Air-PDMS surfaces

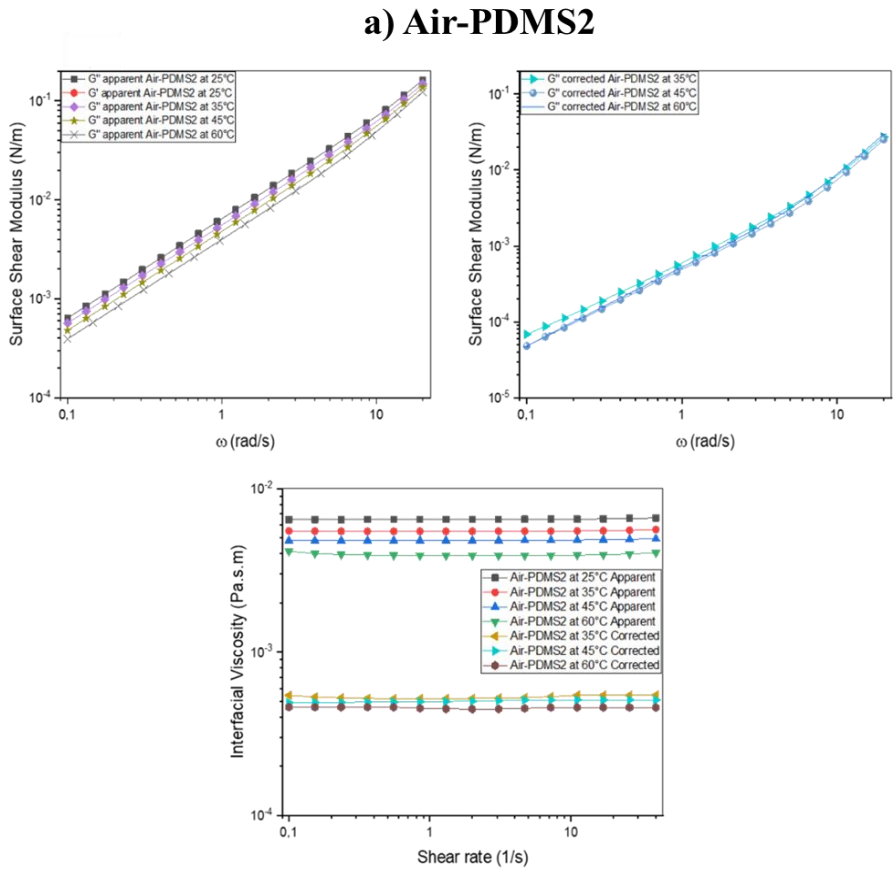

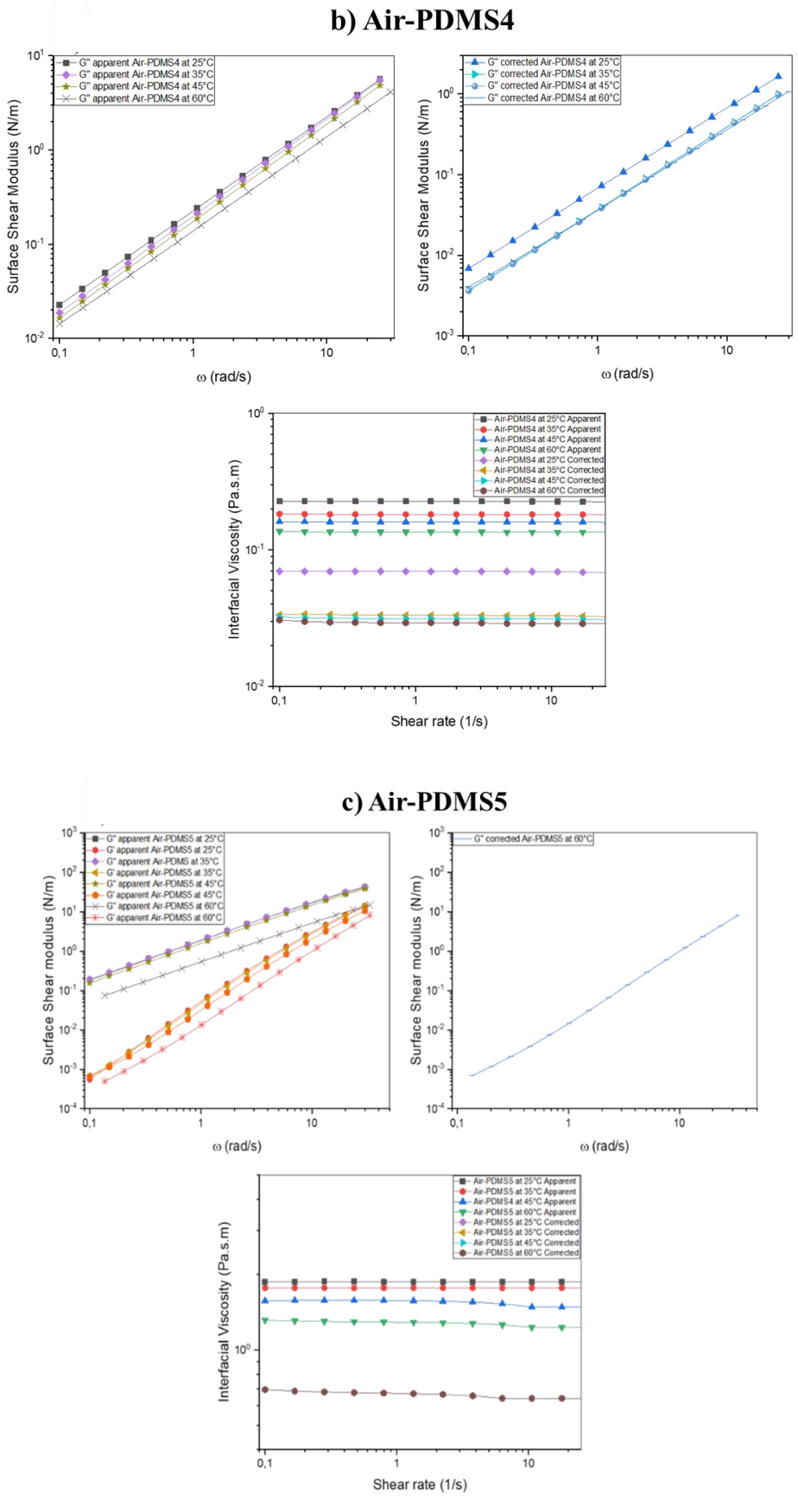

Figure SI.II-4. Frequency sweep and steady shear experiments of air-PDMS2 (a), air-PDMS4 (b) and air-PDMS5 (c) surfaces.

- Air-PIB surfaces

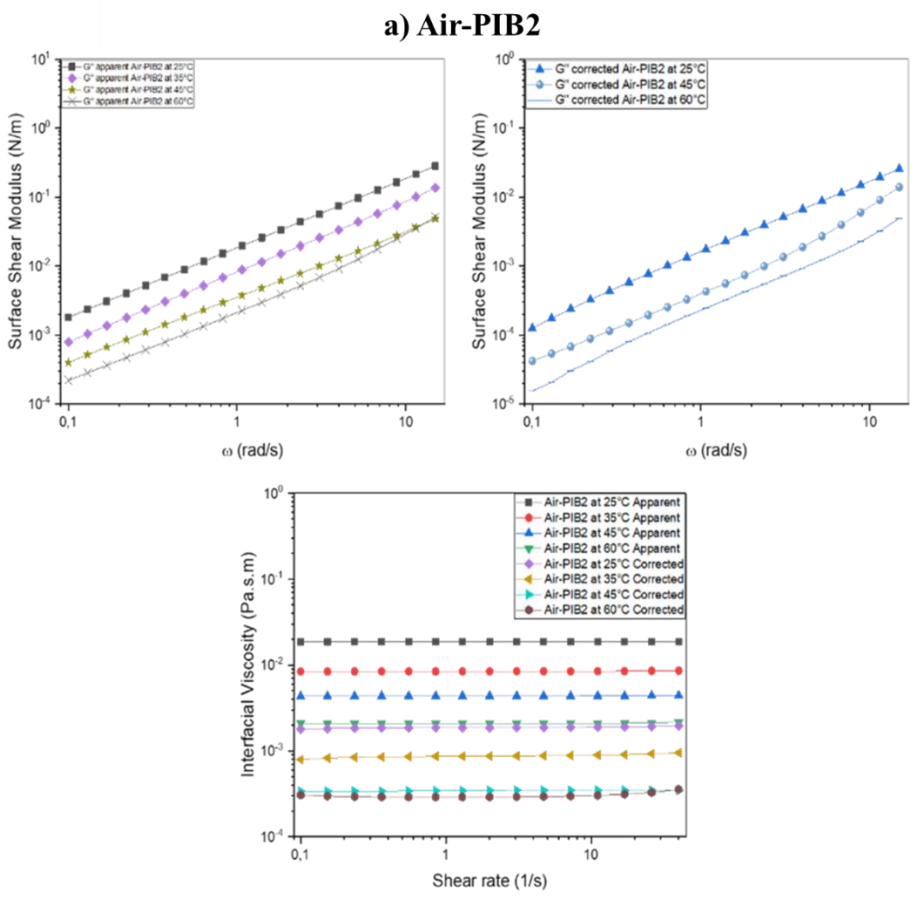

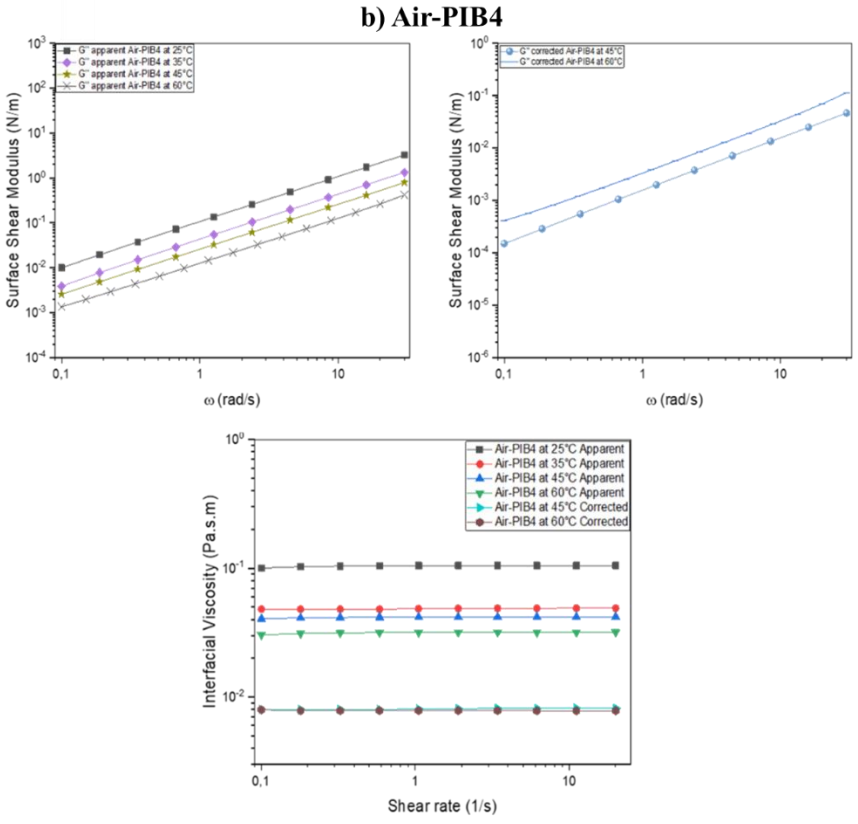

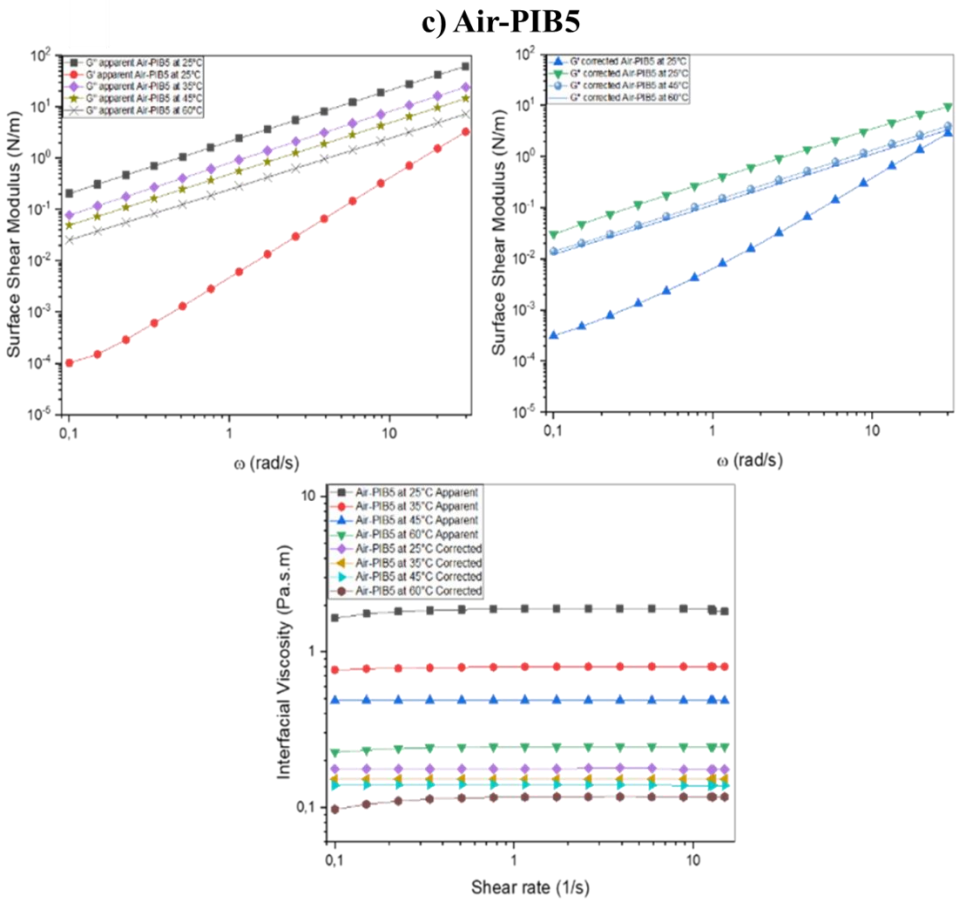

Figure SI.II-5. Frequency sweep and steady shear experiments of air-PIB2 (a), air-PIB4 (b) and air-PIB5 (c) surfaces.

Appendix 3: Interfacial shear rheology of PIB-PDMS and BF-PDMS interfaces

a) PIB1-PDMS2

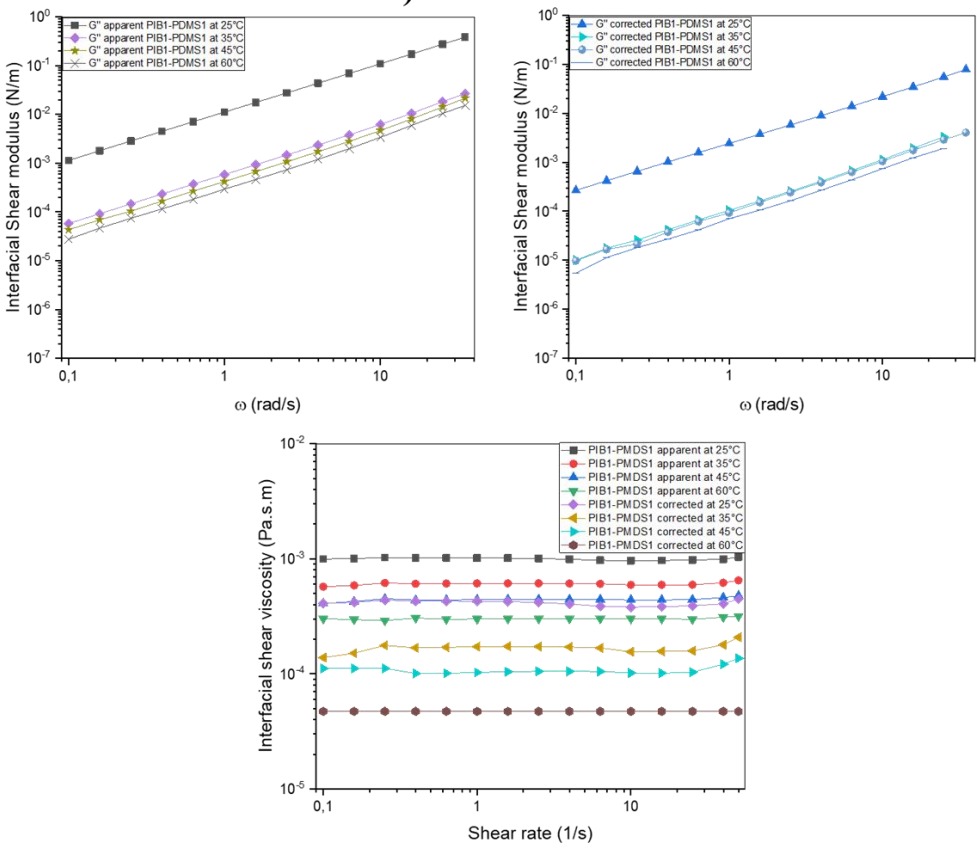

b) PIB4-PDMS4

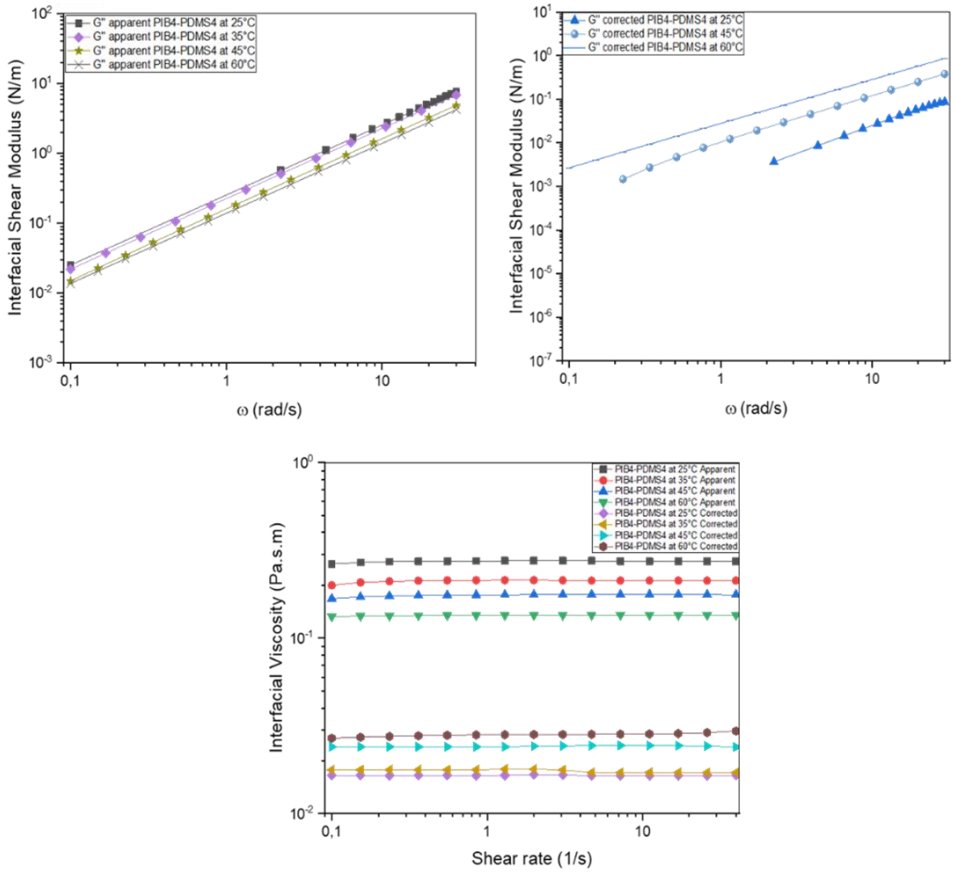

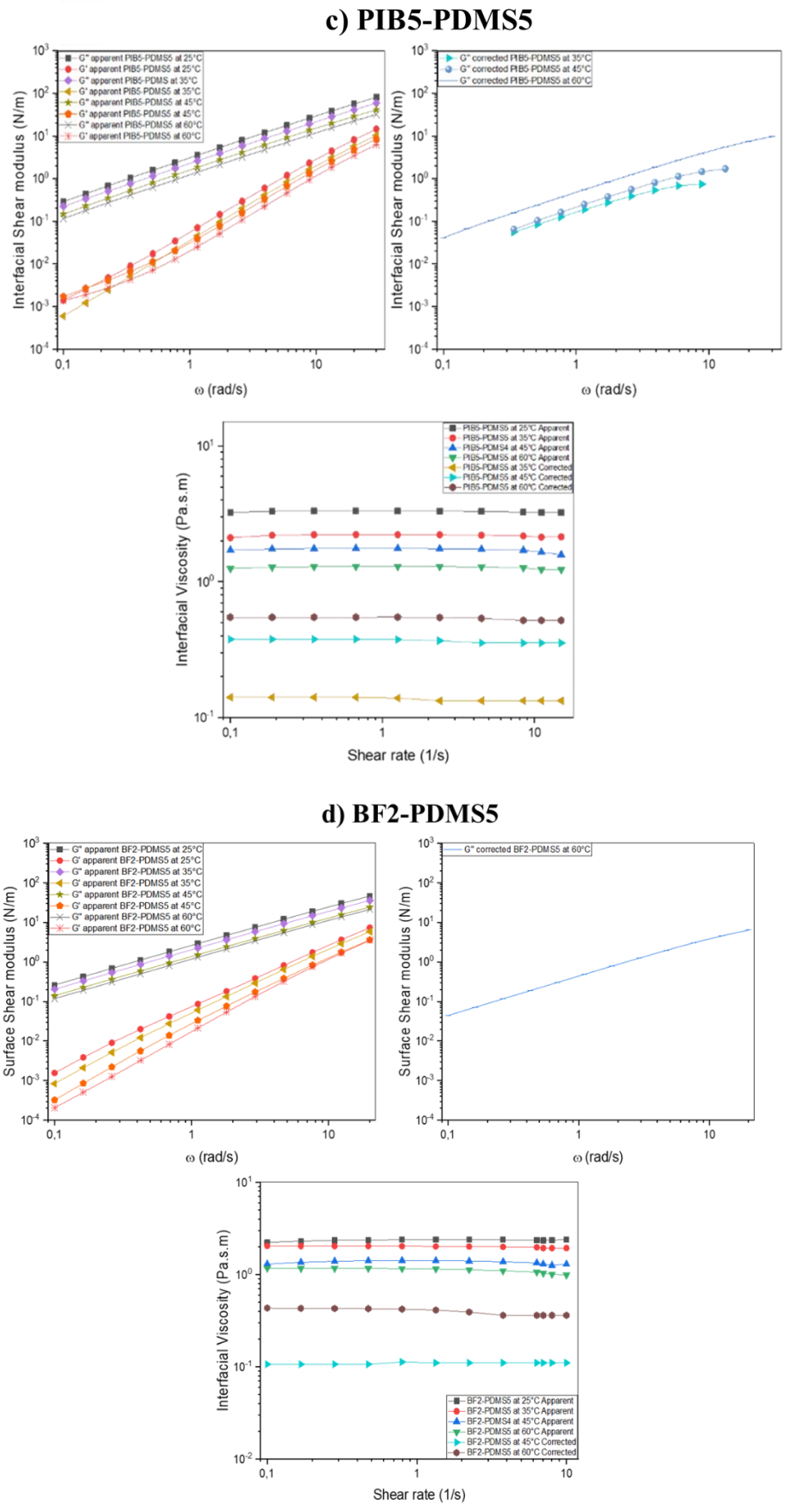

Figure SI.II-6. Frequency sweep and steady shear experiments of PIB1-PDMS1 (a), PIB4-PDMS4 (b), PIB5-PDMS5 (c) & BF2-PDMS5 (d) interfaces.

Chapter III. Probing the elongational rheological behaviour at interfaces of immiscible polymer melts using dilational tensiometry: Effect of viscosity and temperature on the interfacial properties

III.1. Abstract:

During polymer systems manufacturing processes, such as polymer blending or multilayer coextrusion, the elongational flow at interface is predominant. Nevertheless, direct interfacial rheological measurements in extension devoted to such polymer systems are not plentiful and are often based on indirect modelling methods. In the present chapter, interfacial dilational rheology testing based on the rising oscillating drop method was used to probe surface (and interfacial) properties of model Newtonian polymer melts: polydimethylsiloxane (PDMS) / polyisobutylene (PIB) systems. The interfacial properties in both oscillatory and static drop experiments were carefully corrected, considering the inertia and the contribution of the coexisting phase viscosities during the processing of the numerical data. The influence of molecular weight and temperature on the interfacial rheological responses was particularly examined. A new approach was developed to determine the dilational relaxation times (τ) of the studied polymer systems using a square pulse relaxation test. It was found that the evolution of (τ) with the temperature followed an Arrhenius behaviour. A comparison with capillary breakup extensional rheometry revealed similar overall values to those obtained with the pulse method. Finally, using interfacial shear rheology, we focused on the Trouton correlation between shear and dilational surface rheology, and a direct link between shear surface viscosities and elongational relaxation times was evidenced for the first time and over the entire viscosity range studied.

Keywords:

Interfacial dilational rheology, oscillating drop method, relaxation time, capillary breakup extensional rheometry.

III.2. Introduction

Multiphase systems constitute a topic of capital importance in biology, chemistry and material sciences. The interfacial or surface tension is the first criterion that one looks to evaluate when studying these systems. However, it is not the only surface or interfacial property worth considering. The tension gradient can provide information about the deformation resistance properties at the interface. For example, when surfactants or nanoparticles adsorb at liquid interfaces, they not only reduce the surface tension, but also confer intrinsic rheological properties to the corresponding interfaces.

When discussing the deformation of the interface (surface), we refer to the interfacial rheology in shear [1-3] as well as in dilatation/compression [4].

Interfacial or surface dilational rheology, which is the main subject of this chapter, has become a powerful tool to study the static and dynamic properties of surfaces and interfaces such as interfacial layers containing surfactants [5], polymers [6], proteins [7] or solid particles [8]. Understanding the properties of these complex interfaces (surfaces) is the main challenge faced when aiming to control many technological and natural processes involving multiphase systems such as polymer blends [9], multilayer coextruded polymers [10], overmolded parts, additively manufactured multimaterials, emulsions [11] or foams [12].

Furthermore, the close link that exists between the dynamic properties of complex interfaces as well as their adsorption mechanism makes dilational rheology one of the key tools for accessing the transport and kinetic processes involved in the physicochemical properties of a particular fluid/fluid system.

There are many experimental methods for studying interfacial dilational rheology, with all of them based on a disruption of the mechanical equilibrium at the interface and the analytical measurement of the interfacial response. Two methods are used to investigate dilational properties. The first one relies on the use of a Langmuir balance [13], which the principle was explained in the first chapter. The second method is the oscillating bubble/drop technique [14, 15], which consists in deforming a pendant drop (or a rising drop) at the end of a capillary in another liquid or gaseous phase. Interfacial rheology in situations of dilatation/compression evaluates the change occurring in the interfacial tension with respect to the variation of the area or the volume of the interface [16], whereas interfacial shear rheology measurements are performed using a constant interfacial area (Figure 1) [4].

In this work, we use a new type of interfacial rheological setup that enables the interfacial dilational rheology measurements to be extended to high viscosity polymer systems. Special emphasis has been placed on the effect of the temperature and the molecular weight of the two coexisting phases (PDMS and PIB) on the interfacial elastic modulus, particularly in the case of interfaces formed from polymer/air or polymer/polymer interfaces with an asymmetry in molecular weight.

Note that the main advantage of these polymers is that they are in the molten state at room temperature, and their refractive indices are sufficiently different (1.41 for PIB and 1.5 for PDMS) for one to observe PIB in PDMS and vice versa using dilational tensiometry. On the other hand, the higher-density component (PDMS) forming the matrix is highly incompatible with the rising droplet phase (PIB).

Furthermore, we have developed a new approach to access the characteristic elongational rheological times of air-polymer surfaces and polymer-polymer interfaces via a simple test called a "pulse" using the rising oscillating drop/bubble method. Additionally, the surface extensional properties measured with the capillary breakup extensional rheometer (CaBER) were investigated for comparison. Experimental difficulties encountered, possible artifacts and precautions necessary for reliable measurements are highlighted particularly in the presence of high molecular weight polymers. Finally, we aim to see if there is a correlation between the interfacial dilatational properties (via measured interfacial dilational relaxation times) and the interfacial shear properties (measured interfacial shear viscosities) in the air-PDMS and air-PIB interfaces following Trouton's relationship. Furthermore, PIB/PDMS combinations were chosen in such a way that they exhibit similar viscosities and close polydispersity indices. Therefore, the effect of the viscosity and polydispersity will not be discussed extensively hereafter.

III.3. Experimental

III.3.1. Materials and methods

III.3.1.1. Materials

The model fluids chosen were PDMS (polydimethylsiloxane) trimethylsiloxy terminated supplied from abcr and Alfa Aesar, and PIB (polyisobutene) supplied by INEOS. The used PDMS and PIB presented different molecular weights. Table III-1 shows the composition of each material.

Table III-1. Weight average molecular weight of the PDMS and PIB employed.

Material	**PDMS1**	**PDMS2**	**PDMS3**	**PDMS4**	**PDMS5**	**PIB1**	**PIB2**	**PIB3**
Mw (g/mol)	28000	63000	91700	117000	204000	1333	1440	3780

As explained in the first chapter, to well carry out interfacial dilational rheology using the oscillating drop method, the interfacial effect should be dominant comparing to the inertia and the viscous effects. In other words, the values of the Capillary ($\mathbf{Ca} = \frac{\Delta\eta\omega\Delta V}{\gamma R_c^2}$) and Weber ($\mathbf{We} = \frac{\Delta\rho\omega^2\Delta V^2}{\gamma R_c^3}$) numbers should be low. To do so, the above materials were used to prepare three PDMS and three PIB materials with a low viscosity difference ($\Delta\eta$ tending to zero in order to decrease Ca) at 25°C using the mixing law [17]. All of these materials were prepared by using an overhead stirrer with a wide speed

range. Table III-2 summarises the composition of each PDMS and PIB. Here, lv, mv and hv respectively denote low, medium and high viscosity systems.

Table III-2. Notation and composition of the studied PDMS and PIB.

Materials	PDMS lv	PDMS mv	PDMS hv	PIB lv	PIB mv	PIB hv
Compositions	78% PDMS1	89% PDMS2	100% PDMS5	100% PIB1	95.5% PIB2	93% PIB3
	22% PDMS2	11% PDMS4			4.6% PIB3	7% PIB2
Mw (g/mol)	31900[a]	93934[a]	204000[a]	1333[a]	1480[a]	3393[a]
Polydispersity index (MWD)	1.8[b]	1.6[b]	1.7[b]	2.1[a]	1.7[a]	1.8[a]

[a]Provided by supplier
[b]GPC based on polystyrene standards

It is interesting to indicate that all PIB and PDMS melts investigated in this study have the same viscosity (Isoviscosity) with different molecular weights. The PIB used in this this study are oligomers (M<Mc). The PDMS model fluids are entangled since they have an average weight molecular weight (Mw) higher than the critical molecular weight Mc. Indeed, as found in the chapter II, the Mc of PDMS is 28000 g/mol and 15200 g/mol for PIB, respectively [18-20].

The different polymer surfaces and polymer/polymer interfaces investigated in the present work are summarised in Table III-3.

Table III-3. Model polymer surfaces and interfaces studied.

Interface	PIB lv/PDMS lv		PIB mv/PDMS mv		PIB hv/PDMS hv	
Surface	Air/PDMS lv	Air/PIB lv	Air/PDMS mv	Air/PIB mv	Air/PIB hv	Air/PIB hv

III.3.1.2. Characterization methods

III.3.1.2.1. Bulk rheological measurements

To extract the rheological behaviour of the studied model fluids, a controlled-stress rheometer (DHR-2 Rheometer from TA Instruments, United States) with cone-plate geometry (diameter 40 mm, angle 1.994°) was used. The dynamic oscillatory measurements were performed using a frequency sweep (100 to 0.1 rad/s). All complex viscosity $|\eta^*|$ measurements were carried out at constant temperatures of 25, 45 and 60°C.

III.3.1.2.2. Interfacial tension measurements

The surface and interfacial tension measurements were performed at different temperatures using an automatic drop tensiometer (TRACKER-H from TECLIS Scientific, France). A drop of PIB was formed inside the PDMS ($\rho_{PDMS} > \rho_{PIB}$) using the rising drop configuration (Figure III-4). The detailed experimental protocol for this measurement was reported in the second chapter [18].

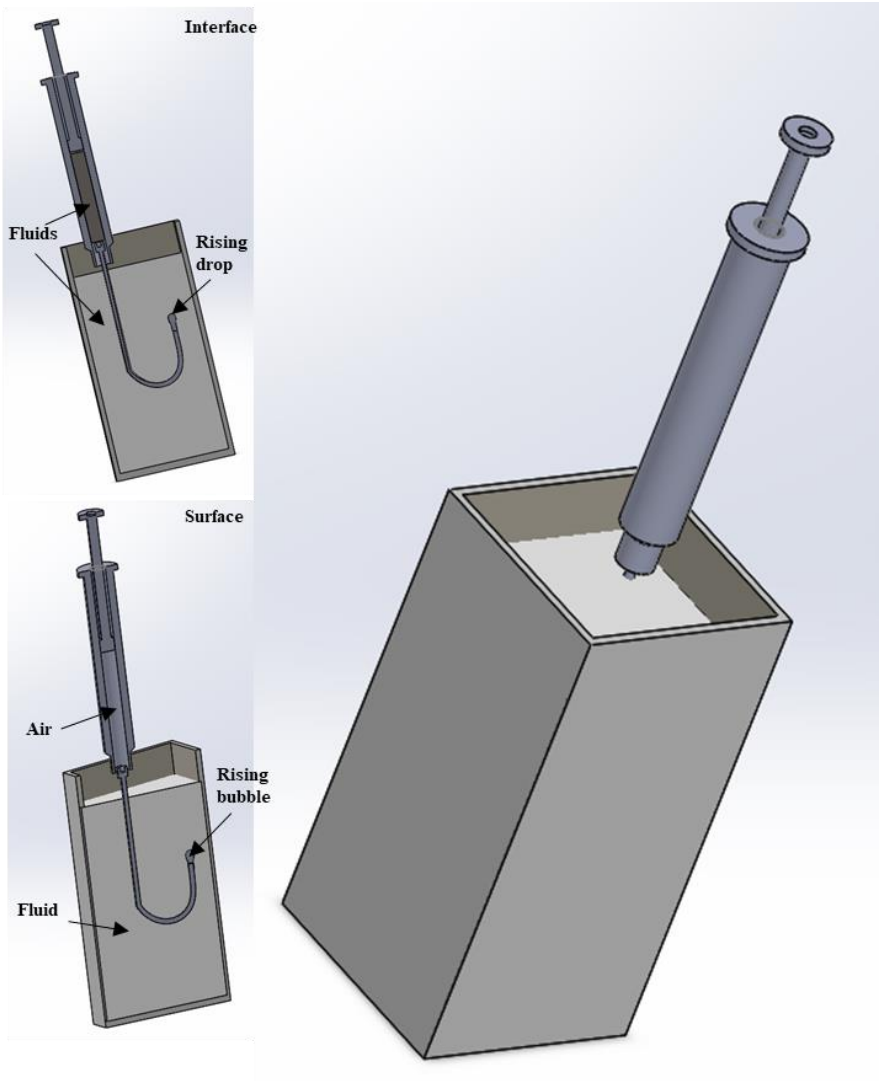

Figure III-1. Rising drop configuration. Sectional view of the cell (left) and cell in closed position (right).

III.3.1.2.3. Optical microscopy

In this section, we focus on the interface PIB/PDMS. A micrometric drop of PIB-hv is injected in PDMS-hv. The diameter of the drop was monitored over time using a polarized optical microscope (Zeiss, Germany) in isothermal conditions at 25 °C.

III.3.1.2.4. Interfacial dilational rheology

The interfacial dilational measurement was performed using the oscillating drop/bubble method on the TRACKER-H tensiometer from TECLIS Scientific (France). The drop/bubble was subjected to sinusoidal compression/dilation cycles using a mechanical motor. The viscoelastic modulus was determined at each frequency by analysing the shape of the drop as described previously. For the dynamic drop experiment, we started by defining the linear region with an amplitude sweep test [21], and then the frequency sweep was performed to determine the elastic and loss dilational moduli. The first step consisted in forming a drop of PIB (rising drop) inside the PDMS (receiving phase) and then waiting for the stationary state to be achieved (plateau γ(t)=constant). The next step was the amplitude sweep at the highest frequency (applied in the frequency sweep test). To minimise the capillary and Weber numbers, a syringe with a small volume (10 µL) was used to enable the application of a small amplitude ΔV, in addition to a needle with a high diameter (1 mm).

Surface and interfacial stress relaxation measurements

There are many experimental techniques for studying interfacial relaxations in air-polymer and polymer-polymer interfaces [22]. The oldest relaxation technique is wave damping [23], [24]. Miller et al. were the first to use the pendant drop method to initiate transient relaxation of aqueous solutions of surfactants and proteins. Here, we applied the "pulse" technique to study interfaces and surfaces of molten polymer systems. First, we began by reaching the equilibrium of the surface (or interfacial) tension, and then a constant amplitude was applied during a time $\Delta t = t_2 - t_1$. The evolution of the surface (or interfacial) tension makes it possible to characterise the relaxation of each surface or interface as a function of the temperature (Figure III-2).

The equation of this square variation of the drop volume noted V(t) is described by a Fourier series as expressed below:

$$\mathbf{V(t)=\frac{4\Delta V}{\pi}\sum_{n=1,3,5,\dots}^{\infty}\sin(n\omega t)} \qquad \textbf{(III-1)}$$

where $\mathbf{\Delta V}$ is the applied amplitude, ω is the frequency (ω=2π/T) and n is the number of the squares.

During one cycle (compression/dilatation), the applied square pulse disturbance is an expansion-relaxation-compression-relaxation cycle with amplitude ΔV applied to the surface or interface with initial volume V_0 as presented in Figure III-2. In the actual experiment, the dilatation and compression ramps were done at low flow rate (low frequencies), thus the intrinsic viscous contribution to the dilational properties can be neglected. Using the square pulse perturbations, an initial increase of the surface (or interfacial) tension was first observed, followed by a relaxation towards the stationary state value $\boldsymbol{\gamma_0}$. In the compression stage, the surface (or interfacial) tension $\boldsymbol{\gamma}$ decreased below its stationary value, and then at the end of the compression, the relaxation of $\boldsymbol{\gamma}$ towards the stationary value was noticed.

$$V(t)=\begin{cases} V_0 & t < t_1 \\ V_0 + \Delta V & t_1 < t < t_2 \\ V_0 - \Delta V & t > t_2 \end{cases} \qquad \text{(III-2)}$$

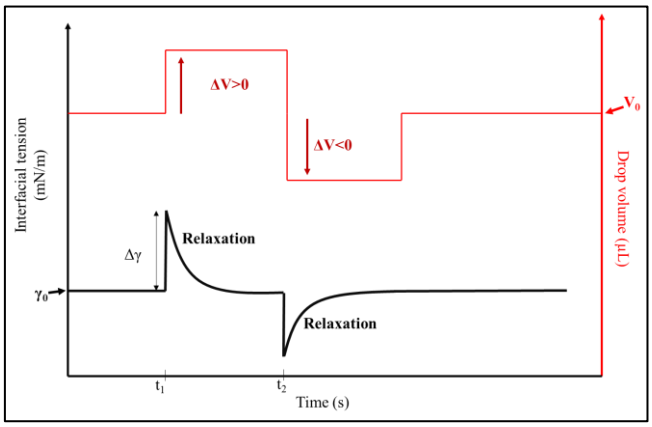

Figure III-2. Interfacial relaxation method or "pulse" technique used in this study.

III.3.1.2.5. Capillary breakup extensional rheometry (CaBER)

A capillary breakup extensional rheometer (CaBER) is conceptually based on the design of Bazilevsky et al. [25]. It is a rheological device that can quantify the elongational properties of low- to medium-viscosity fluids. A capillary bridge (a volume of fluid with a free surface, held by surface tension between two solid surfaces) is placed in an unstable situation that leads to its rupture into two distinct volumes of fluid (Figure III-3). This rupture is an elongational flow whose dynamics depend solely on the surface tension and the viscosity of the fluid. The recording of these dynamics (which can be very fast, in the order of few milliseconds) allows the extraction of the apparent elongational viscosity and the elongational relaxation time of the fluid.

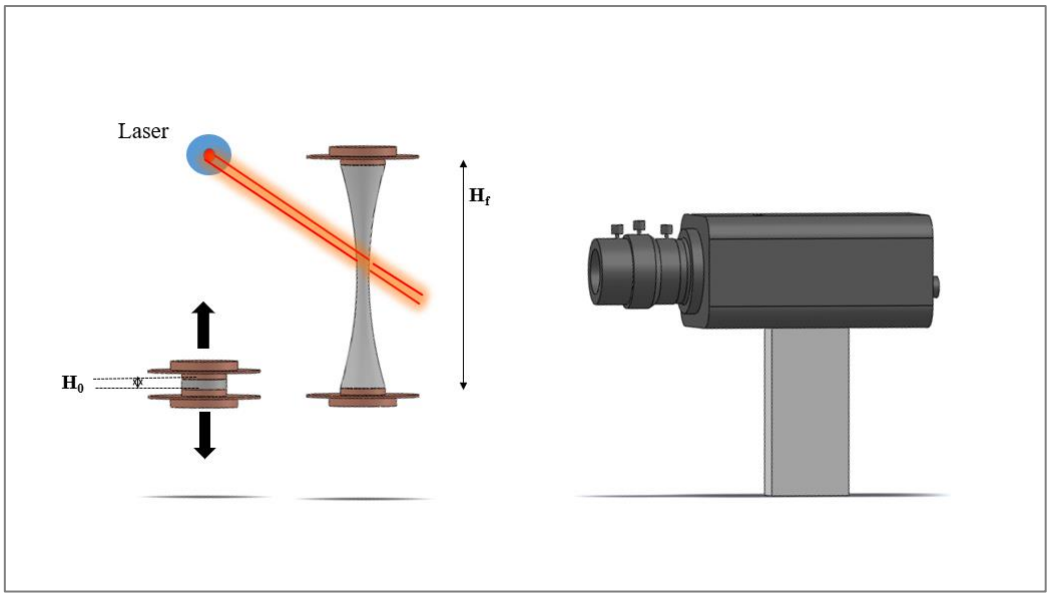

Figure III-3. Schematic representation of the CaBER instrument.

A Thermo Scientific™ HAAKE™ CaBER™ 1 capillary breakup extensional rheometer (United States) was used. A tiny droplet of the studied model fluid is placed between two parallel plates of diameter 4 mm, separated by an initial height H_0 of 500 µm. Then, one plate is moved using an extension velocity v_0 of 430 mm/s to a constant gap H_f of 40 mm. The experiment is recorded by a high-speed camera, Olympus i-SPEED 3, up to 5000 frames per second. The instrument also uses a laser micrometre to monitor the diameter at the midplane of the thinning filament, D(t).

It is essential to mention that the droplet must be homogeneous and must not contain any air bubbles; otherwise, the filament will break, and the extracted parameters will be incorrect. On the other hand, it is useful to mention that during the elongation and thinning of the filament, viscous forces tend to stabilise the cylindrical shape of the filament, whereas gravitational forces can drag the fluid below the mid-filament. The competition between viscous and gravitational forces can be estimated by the ratio of the Bond number to the capillary number, $\frac{B_0}{C_a} = \frac{\rho\, g\, D_0}{2\, \eta_0\, \dot{\varepsilon}}$, where ρ is the density of the fluid, g is the gravity constant and $\dot{\varepsilon}$ is the strain rate. In the present study, the $\frac{B_0}{C_a}$ ratio was calculated and found to be lower than 0.5, ensuring a viscous-dominated thinning mechanism [26].

The diameter versus time D(t) data, which represents the raw output of the CaBER, is then used to determine extensional rheological parameters. For a viscoelastic system, Anna and McKinley 2001 [27] and Naillon et al. [28] proposed the following fitting function:

$$\mathbf{D(t) = \alpha e^{-\frac{t}{3\tau}} - \beta t + \delta} \qquad \textbf{(III-3)}$$

where α, β, δ are the fitting parameters that have physical relevance, and τ is the elongational relaxation time.

If the surface tension γ of the system is known, the evolution of an apparent extensional viscosity η_E can easily be calculated (Equation III-4). The thinning of the filament is driven by the competition between capillarity and elasticity [27, 29, 30].

$$\eta_E = \frac{\gamma/R(t)}{\dot{\varepsilon}(t)} = \frac{-\gamma}{dD(t)/dt} \qquad \textbf{(III-4)}$$

where R(t) and $\dot{\varepsilon}(t)$ are, respectively, the filament radius and extension rate during time evolution.
The elongational relaxation time and the apparent elongational viscosity of the model fluids investigated (PDMS and PIB) were extracted with equation (III-3) and compared to the dilatational relaxation time obtained by the pulse method (dilational tensiometry).

III.3.1.2.6. Surface shear measurements

The interfacial shear properties of the surfaces were evaluated using the novel titanium biconical geometry designed by Anton Paar Research and Development Service (Stuttgart, Germany) (D: 68.28 mm, angle 5°) attached to an MCR 302 rheometer. The detailed experimental protocol for this measurement was reported in the second chapter [18].

III.4. Results

III.4.1. Bulk rheological measurements

In Figure III-4, the master curves of PDMS and PIB melts are depicted. It has been observed that all of the PDMS and PIB melt polymers present Newtonian behaviour for a frequency range lower than 1.6 Hz (10 rad.s^{-1}). The latter is greater than the maximum frequency (0.4 Hz) used during interfacial dilational measurements. On the other hand, the vertical (y-axis) shift factor (b_T) gives information about the temperature dependency of their densities. Indeed, the b_T values clearly show the high temperature sensitivity of PIB compared to PDMS. Therefore, the two phases have very similar viscosities at 25°C, but they do not exhibit the same tendency when the temperature is increased. The zero-shear viscosity and shift factor values of the different investigated PDMS and PIB are shown in Tables III-4 and III-5. It would be useful to recall that the main objective is to ensure a difference in viscosity of the coexisting phases that tends to low values during the dilational interfacial rheological experiments in order to minimise capillary and inertial effects (Δη tending to zero).

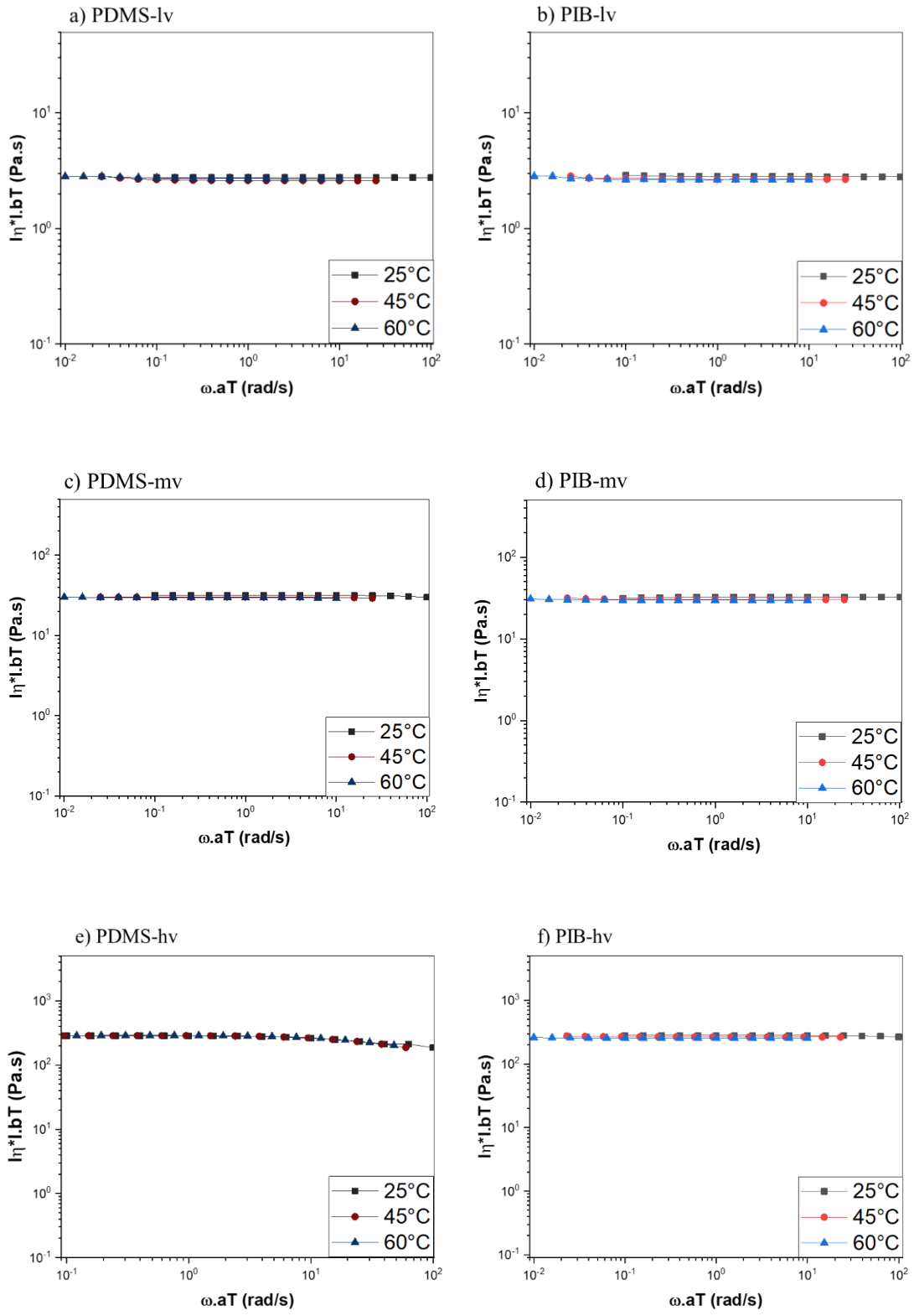

Figure III-4. Master curves of the different model fluids at $T_{reference}$ =25°C.

Table III-4. Zero-shear viscosity values of the different model fluids at 25°C.

Material	PDMS-lv	PDMS-mv	PDMS-hv	PIB-lv	PIB-mv	PIB-hv
η_0 (Pa.s)	2.8	31.7	284.8	2.9	32.0	281.0

Table III-5. Horizontal (x-axis) shift factor (a_T) and vertical (y-axis) shift factor (b_T) from the master curves of the shear viscosity measurements.

Polymer	a_T			b_T		
	25°C	45°C	60°C	25°C	45°C	60°C
PIB-lv	1	0.19	0.08	1	5.26	12.50
PIB-mv	1	0.23	0.09	1	4.34	11.11
PIB-hv	1	0.22	0.1	1	4.54	10.51
PDMS-lv	1	0.71	0.56	1	1.41	1.77
PDMS-mv	1	0.70	0.55	1	1.42	1.80
PDMS-hv	1	0.62	0.49	1	1.61	2.01

III.4.2. Interfacial tension measurements

The interfacial tension at equilibrium between PIB and PDMS was determined using the static experiment method. The volume of the drop of PIB was kept constant and the evolution of the interfacial tension was monitored until an equilibrium state (plateau) was reached. The range of Bond number values was between 0.3 and 0.5, whereas the Worthington number W_0 (see the details in first chapter) gives values in the 0.7 – 0.8 range, confirming the precision of the interfacial tension measurements.

The measurement was performed at 25, 45 and 60°C. Table III-6 summarises the interfacial tension at equilibrium for the studied interfaces.

Table III-6. Interfacial tension at equilibrium for the studied interfaces.

Interface	*Interfacial tension (mN/m) at 25°C*	*Interfacial tension (mN/m) at 45°C*	*Interfacial tension (mN/m) at 60°C*
PIB lv/PDMS lv	2.10±0.09	2.50±0.10	3.00±0.20
PIB mv/PDMS mv	3.20±0.02	2.80±0.12	2.4±0.03
PIB hv/PDMS hv	5.20±0.11	4.90±0.04	4.40±0.17

From Table III-6, it can be observed that interfacial tension between PDMS and PIB decreased with decreasing molecular weight. Legrand and Gaines [31] noticed the same trend using similar polymer systems. The authors developed the empirical formula given in equation (III-5) in order to model the dependency of the interfacial tension on the molar mass:

$$\gamma_{12} = \gamma_{12}^{\infty} - \left[\frac{k_1}{M_1^{2/3}}\right] - \left[\frac{k_2}{M_2^{2/3}}\right] \qquad \textbf{(III-5)}$$

where γ_{12}^{∞} is the equilibrium interfacial tension, k_1 and k_2 are constants and M_1 and M_2 are the molecular weight of the system components, respectively. Later, Vinckier et al. [32] used Legrand and Gaines's relationship to calculate the interfacial tension between different PIB/PDMS systems,

concluding that the interfacial tension increased when the molecular weight increased, which is once again consistent with our results.

On the other hand, from Table III-6, it can be observed that for the lowest viscosity system (PIB lv/PDMS lv), the interfacial tension increased slightly with the temperature. In the presence of higher viscosity polymers (PIB mv/PDMS mv and PIB hv/PDMS hv), however, the interfacial tension decreased with increasing temperature (Figure III-5). This phenomenon began starting from a specific molecular weight of subphases, as noted in second chapter, using similar PIB/PDMS polymer systems. Based on the interfacial shear rheology and the solubility parameter modelling, we proved that the transport phenomenon was responsible for the decrease in the interfacial tension. The interfacial shear viscosity increased for the high-viscosity polymer systems when the temperature was increased. This phenomenon that increases at high temperature was related to the short-chain components of broadly distributed samples migrating into the interface to reduce the interfacial tension and consequently the Gibbs energy of the entire system [18].

Wagner and Wolf [33] analyzed the variation of the interfacial tension γ versus temperature (T) of different PIB/PDMS systems with comparatively narrow molecular weight distributions (MWD). They found that the evolution of γ(T) depends on molecular weight. The authors argued based on the modeling of the solubility parameters that it was not trivial to interpret their experimental results by the Flory-Huggins interaction parameter since the two polymers are not miscible. Later, various studies investigated the effect of the temperature and molecular weight on the same PDMS/PIB polymer systems [34-36]. According to Ziegler et al. [36], in the case of apolar polymer systems (the case of PDMS/PIB) the interfacial properties are dependent on the average molecular weight and the polydispersity of both coexisting phases but also on the molecular weight difference, i.e., the asymmetry across the interface.

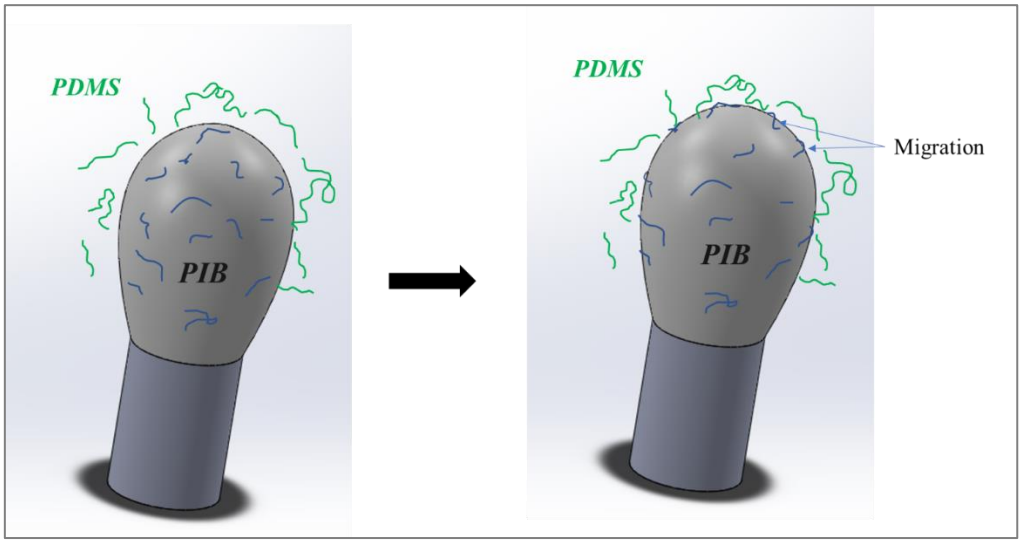

Figure III-5. Diagram representing the migration of short PIB chains into the interface of PIB/PDMS polymer systems.

III.4.3. Optical microscopy

Figure III-6 displays the variation of a high viscous PIB drop (PIB-hv) within PDMS-hv.

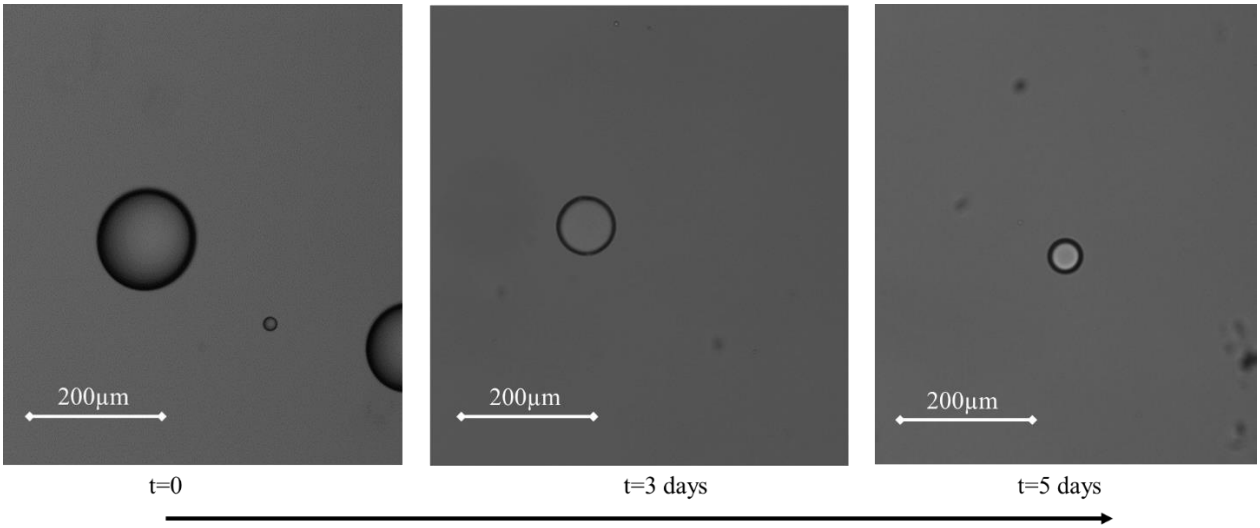

Figure III-6. Size evolution with time of PIB-hv drop injected into PDMS-hv matrix.

The diameter decreased during time. This is related to the diffusion of PIB chains from the drop to the PDMS matrix across the interface PIB/PDMS. The migration phenomenon took more time (a few days) due to the system high viscosity. The same observation was found in the work of Guido et al. [37]. The result from the optical microscopy confirms the second chapter's assumption. The rise of the interfacial shear viscosity, as well as the decrease in interfacial tension after heating the high molar weight systems, is explained by the fact that the PIB macromolecules could diffuse to the interface to play the role of a surfactant (decreasing the interfacial tension) as well as to rigidify the interface (increasing the interfacial shear viscosity).

III.4.4. Interfacial dilational measurements

It is important to mention that dimensionless numbers (Bond, Weber and capillary numbers) were carefully checked to correctly conduct such dilatational measurements for each PIB/PDMS system. The viscosity contrast ($\Delta\eta$) between PIB and PDMS phases was 0.1 Pa.s, the density difference ($\Delta\rho$) was 100 kg/m3, the radius of the nozzle was 0.5 mm, the interfacial tension was around 2.1 mN/m, the minimum and maximum frequencies used were 0.02 and 0.4 Hz respectively, the initial volume (V_0) of the drop was 4.8 µl and the ΔV amplitude was 0.3 µl. Table 7 displays the range values of each dimensionless number. The capillary number Ca was in the 10^{-4} to 10^{-1} range and We was around 10^{-8}, which is still very low (<<1). Therefore, viscous stress and inertia effects are sufficiently negligible.
On the other hand, the Bond number was calculated instantaneously by the tensiometer software according to the equation (15) and analysed immediately before each measurement launch. Values of Bd were found in the range between 0.3 and 0.5 for all experiments carried out in this study.

Figure III-7 shows the frequency sweeps at 25, 45 and 60°C. For all PIB/PDMS systems, the absence of the loss modulus was noticed. It is useful to mention that in our case, the probed interfaces are free (no particles or surfactants present on the interface), which induces small phase angle values between interface area oscillations and interfacial tension variations. This means that the storage modulus E' is much larger than the loss modulus E'' [16].

From Figure III-6, it was observed that at a constant temperature, the more the viscosity of the coexisting phases increased, the more the interfacial elastic modulus E' increased. For the lowest viscosity system (PIB lv/PDMS lv), the interfacial elastic modulus E' increased when the temperature decreased. However, by increasing the viscosity of the coexisting phases (PIB mv/PDMS mv), the opposite tendency was observed. The interfacial elastic modulus decreased when the temperature increased, which is in agreement with our observations during the static drop and the optical microscopic measurements, indicating a migration phenomenon (Dynamic interface) [18, 34]. No data are presented for the PIB hv/PDMS hv interface at 45 and 60°C. Due to the high difference in viscosities ($\Delta\eta$) of PIB hv and PDMS hv when the temperature was increased (Table III-5), high capillary and Weber numbers were obtained; as a result, the interfacial forces are not dominant and the measured droplets for these interfaces are not Laplacian (the drop profile does not follow the theoretical profile predicted by the Laplace equation). Therefore, no measurements could be carried out in this case, as it was not feasible to properly impose a sinusoidal volume or area variation (Figure III-8).

Table III-7. Calculated range of the capillary number (Ca) and the Weber number (We) in the dilatational oscillatory measurements.

Ca	We
10^{-4}-10^{-1}	$\approx 10^{-8}$

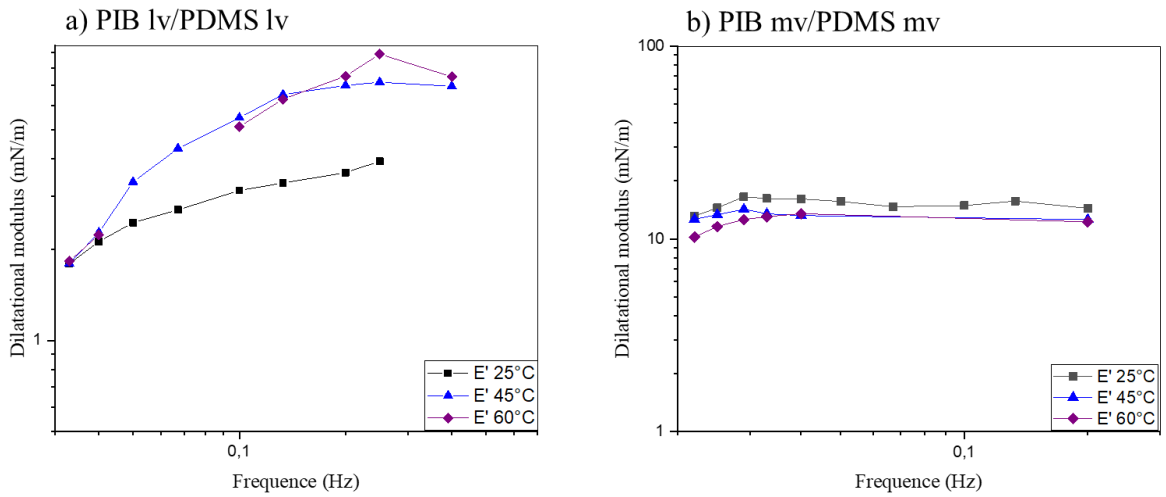

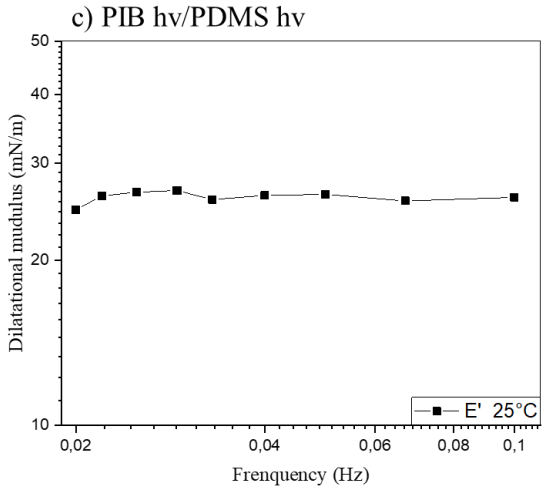

Figure III-7. Dilational frequency sweep experiment performed on the PIB/PDMS interfaces.

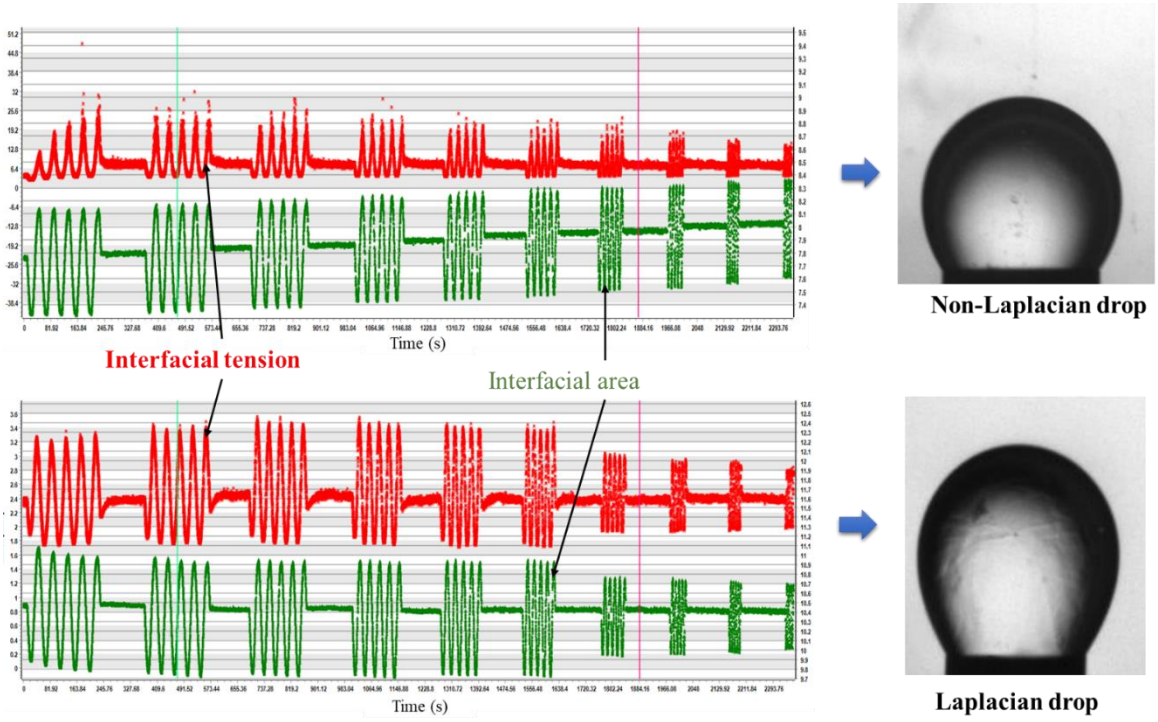

Figure III-8. Dilational frequency sweep experiment conducted on a Laplacian and non-Laplacian drop (pictures taken from the WINDROP software of the TRACKER apparatus).

III.4.5. Interfacial relaxation of PIB/PDMS systems

In this section, the relaxation of the surfaces and interfaces of PIB/PDMS polymer systems is examined. The response of the surface or interface is related to its temporal relaxation. The surface or interfacial tension decreased when a positive amplitude $+\Delta V$ was applied to return to the equilibrium state (γ_0). The temporal variation of the surface/interfacial tension was fitted using the Kohlrausch law [38]:

$$\gamma(t) = \gamma_0 + \Delta\gamma.\exp\left(\frac{-t}{3\tau}\right)^{\beta} \qquad \text{(III-6)}$$

where $\Delta\gamma$ is an amplitude factor (Figure III-2), τ is the characteristic relaxation time and β is the stretching parameter, which varies between 0 and 1 and describes the width of the relaxation time distribution [39]. In our case, the time-decay data of the relaxation processes of PIB/PDMS systems are better described in terms of a simple exponential function (β =1) (equation 7), implying that the tested polymers exhibit monodisperse relaxation characterizing the rheological model of Newtonian Maxwellian behaviour.

$$\gamma(t) = \gamma_0 + \Delta\gamma.\exp\left(\frac{-t}{3\tau}\right) \qquad \text{(III-7)}$$

This allows us to extract the values of the characteristic relaxation times of the surfaces and interfaces.
It is useful to mention that the Kohlrausch law has been widely used in the literature to model several time-decaying behaviours in the relaxation processes of polymers. For instance, Yousfi et al. [39] fitted the evolution of the scattering intensity with time in dPS/PBMA (deuterated polystyrene / polybutyl methacrylate) nanoblends using small angle neutron scattering (SANS) to extract the relaxation time of the dPS droplets in a PBMA matrix. Boyd et al. [40] fitted the dielectric data of PVAc (polyvinyl acetate) in the glass transition region using the Kohlrausch law to extract its relaxation kinetics.

III.4.5.1. Air/PDMS and air/PIB surfaces

Figures III-9 and III-10 show the decay of the surface tension γ with time for all PDMS and PIB surfaces at 25°C. This decay in $\gamma(t)$ may be related to a rearrangement of the macromolecules, or the end groups at the surface in contact with the air molecules, in order to decrease the surface tension and reach the equilibrium state described by γ_0 [41, 42]. From Figure III-11, one can observe that the dilational relaxation times of the surfaces increased with the viscosity of the coexisting phases, but they decreased when the temperature increased. Thus, the higher the viscosity, the longer the time required to create the new free surface. These results could have been predicted beforehand. Indeed, in chapter II, using similar PDMS and PIB polymers, they found that the surface shear viscosity increases linearly with the shear viscosity of the bulk, since the creation of the free surface starts from the bulk subphase [18].
Several studies that have investigated pure liquid surfaces or free polymer surface systems with no surface-active agent (surfactants, nanoparticles, etc.) as in the present work have confirmed the presence of variations in interfacial tension by dynamic interfacial tension measurements using the pendant drop technique [43, 44], by Wilhelmy plate force tensiometry [45, 46] and interfacial properties (interfacial moduli) measured by dilational rheology [47].
In the “dynamic relaxation” pulse mode, the tensiometer imposes square pulse variations of the drop volume and records the interfacial surface area variation as well as the results of the variation of the

interfacial tension. Compared to other methods that impose both elongation and shear stresses on the interface [48, 49], the square pulse method has the advantage of imposing pure contractions/expansions that allow a direct measurement of the dilatational properties of liquid/liquid or air/liquid interfaces. But it is of paramount importance to point out that our measurements were performed using a slow dilatation/compression rate ($\dot{\varepsilon} < 0.1\ s^{-1}$). In these conditions, viscous stresses are insignificant (small Capillary numbers), particularly in the case of low to medium viscosity polymers. Consequently, we expect that the characteristic elongational relaxation times deduced from the fit of the exponential decay of $\gamma(t)$ are related mainly to the dilatational properties of polymer-polymer and air-polymer interfaces rather than to bulk extensional rheology.

However, one may accept that these statements can be debatable in the case of high molecular weight melt surfaces (air/PDMShv and air/PIBhv systems) where $\Delta\eta$ is rather significant. Afterwards, the viscous forces are no longer negligible (high capillary numbers). Consequently, we expect that the characteristic elongational relaxation times deduced from the fit of $\gamma(t)$ of PDMShv and PIBhv are the result of the balance between the relaxation of the chains on the surface and the viscous force contribution. But it is quite difficult to deconvolute the two phenomena.

Jalbert et al. [50] measured the surface tensions of amine- and methyl-terminated poly(dimethylsiloxane) (PDMS) with molecular weights ranging from 1000 to 75 000 g/mol by pendant drop tensiometry. It has been reported that methyl chain ends of PDMS have low surface energy compared to that of the chain backbone. These low surface energy chains ("methyl ends") have an entropic preference and attraction to adsorb to the surface, which in turn was expected to cause the short chains of a polydisperse melt to segregate to the surface [51]. Moreover, Mahmoudi et al. [51] demonstrated that in the case of polydisperse melts, the chain-end segregation simultaneously induced an entropic enrichment of short chains at the surface, since they have more ends per unit volume.

Jalbert et al. [50] highlighted that the chain ends at the surface of a polymer melt control the evolution of surface tension γ with molecular weight. For the methyl-terminated polymer melts, γ increased with molecular weight. The end-group effect was confirmed a year later by Elman et al. [52] using neutron reflectivity.

In our study, we used polydisperse methylsiloxy-terminated PDMS melts. We suspect that the kinetics of transport of short chains and chain-ends connected to the chain backbone into the surface of a polymer melt of high Mw will be slower and will require more time to equilibrate compared to low Mw ones. These interpretations support why high molecular weight melts lead to longer dilational characteristic relaxation times. The latter reflect the rate of the chain-ends and short chains to move to the air/polymer interface.

The mobility of the macro-chains at the surface was also observed in the stability of foams using proteins [53]. Through the hydrophobicity of these macromolecules and their possible conformational reorganisation, rapid adsorption at the air/water interface is enabled, leading to the formation of an elastic adsorbed layer [53, 54]. Some studies have also highlighted the role that polysaccharides play

at the interfacial film regarding enhancement of the stability of foams, due to a thickening or gelling effect on the aqueous solution [55-57].

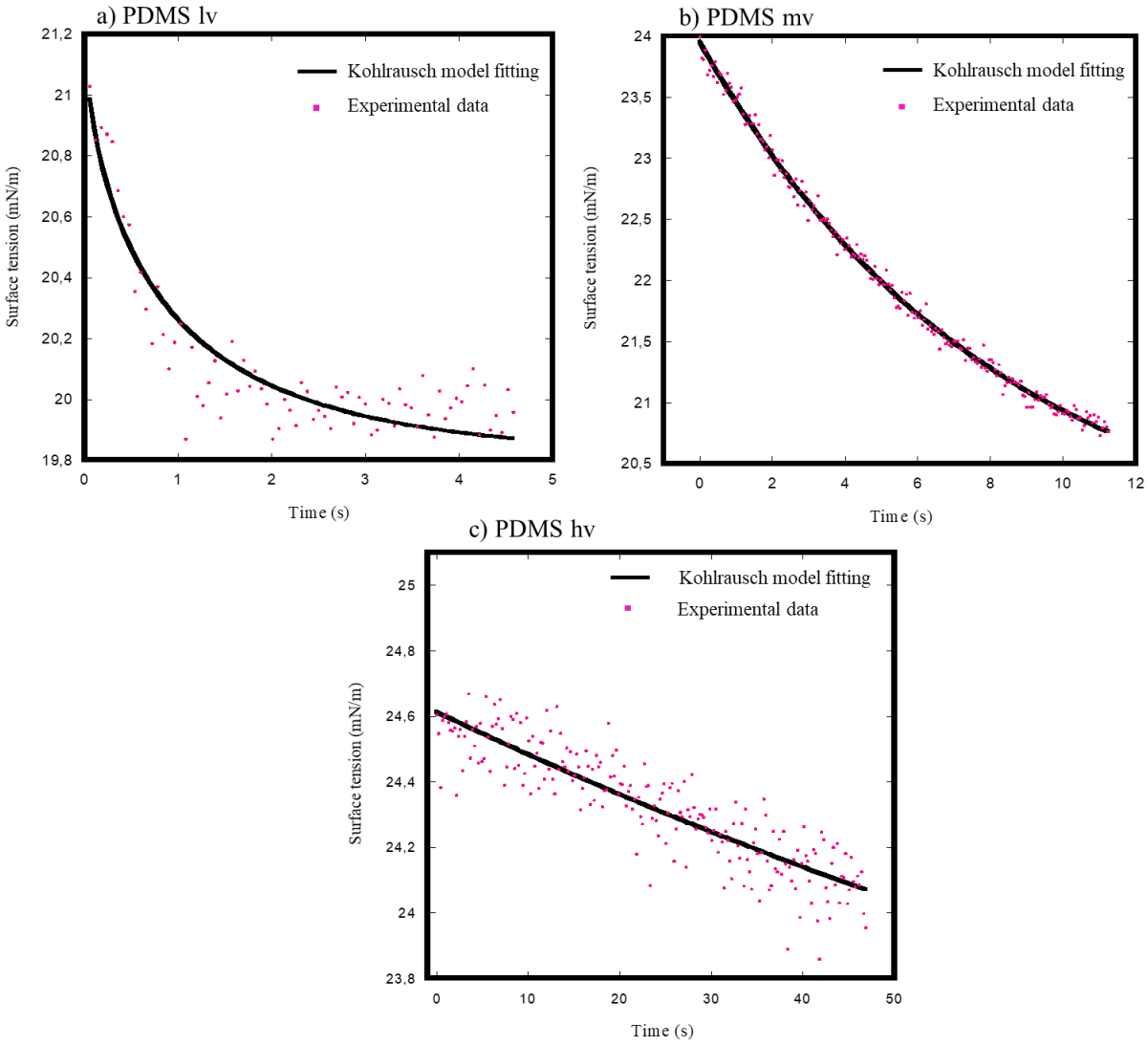

Figure III-9. Fitting of the variation of the surface tension as a function of time at 25°C of air/PDMS surfaces (a) PDMS lv, (b) PDMS mv and (c) PDMS hv. The dots represent the experimental relaxation measurements using the "pulse mode," and the continuous line is the fit using the Kohlrausch model.

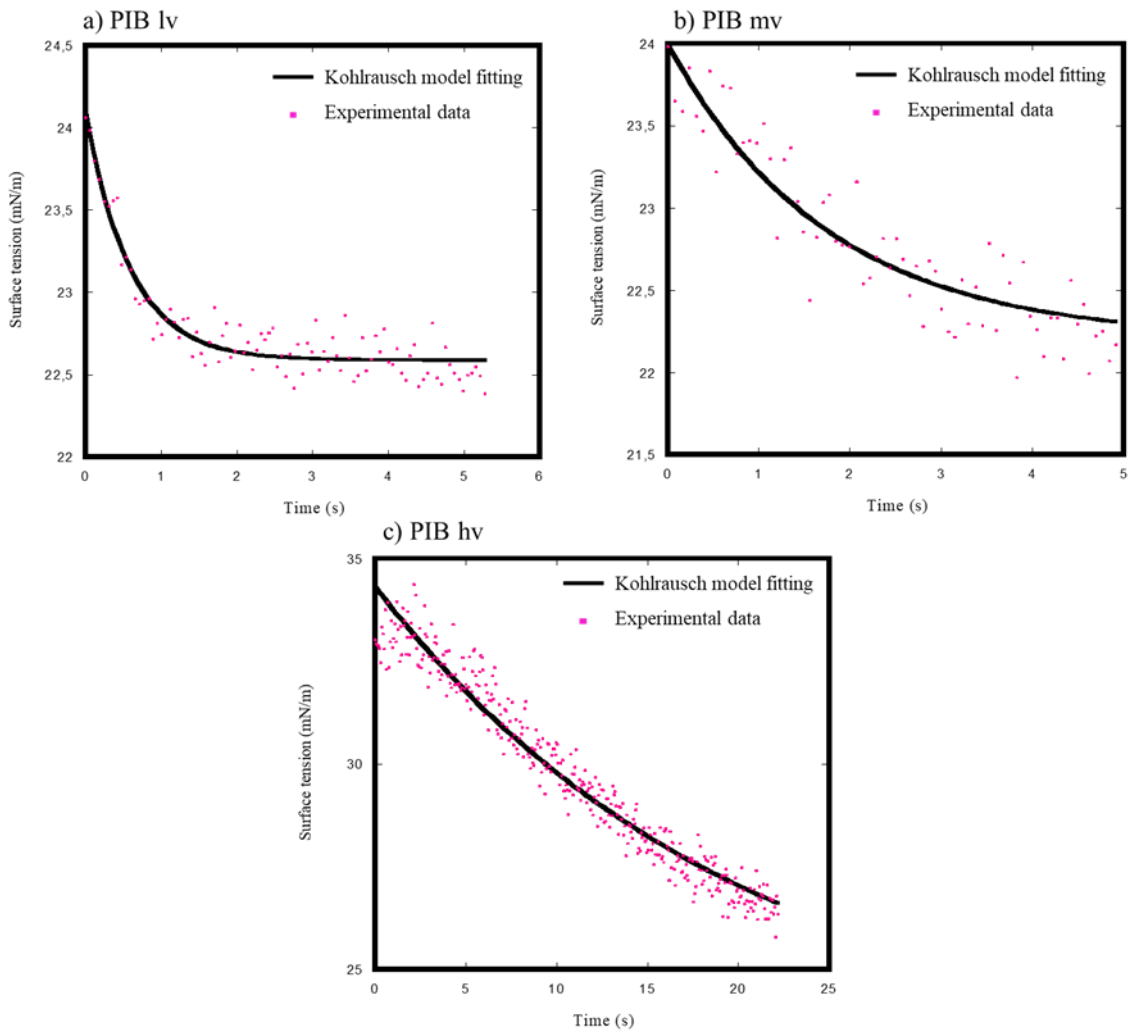

Figure III-10. Fitting of the variation of the surface tension as a function of time at 25°C of air/PIB surfaces (a) PIB lv, (b) PIB mv and (c) PIB hv. The dots represent the experimental relaxation measurements made using the "pulse mode," and the continuous line is the fit obtained using the Kohlrausch model.

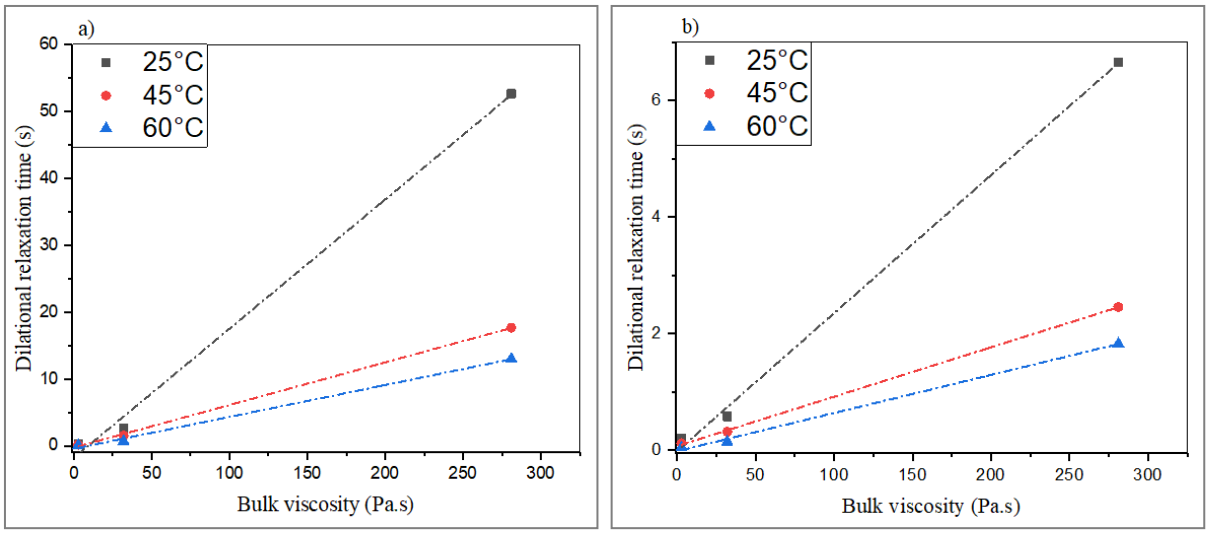

Figure III-11. Variation of the surface dilational relaxation times (in seconds) as a function of bulk viscosity at different temperatures for PDMS (a) and PIB (b).

We have also compared the evolution of the relaxation time of the studied surfaces with respect to temperature. For this purpose, Ln (τ) as a function of 1000/T was plotted. Figure III-11 shows this evolution for PIB and PDMS surfaces.

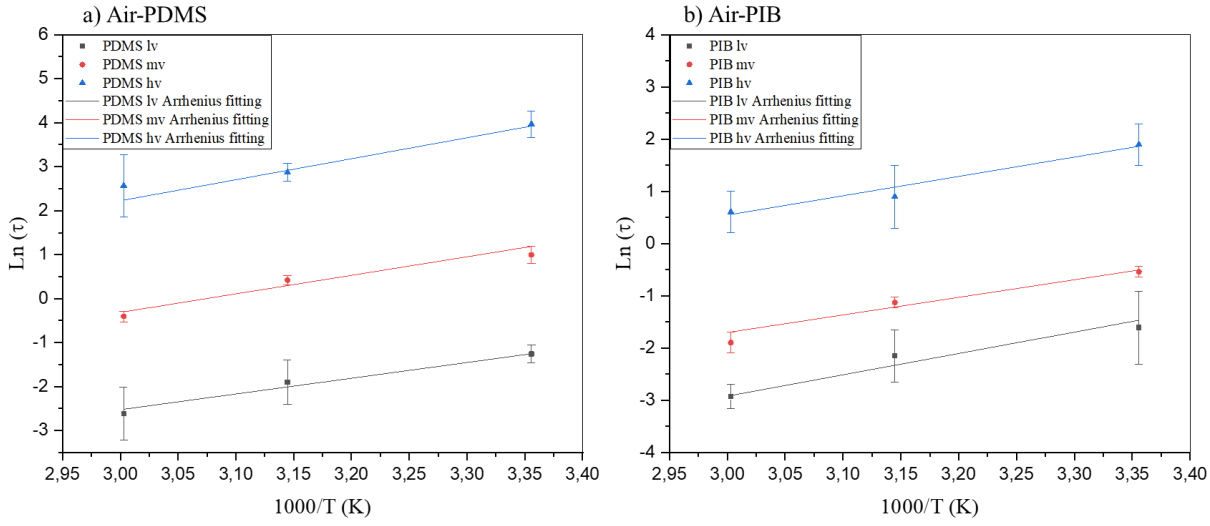

Figure III-12. Arrhenius plot of the relaxation time τ as obtained from fits of the surface relaxation test.

The variation of relaxation time with temperature (T in Kelvin) is calculated using an Arrhenius function (Equation III-8).

$$\tau = \tau_0 . \exp\left(\frac{E_a}{R.T}\right) \qquad \textbf{(III-8)}$$

where Ea is the activation energy (representing, in this case, the temperature sensitivity of the relaxation process), τ_0 is the pre-exponential factor and R is the universal gas constant.

Figure III-12 shows a linear evolution, demonstrating that the Arrhenius law fits these curves successfully. For all surfaces, regardless of the viscosity of the coexisting phases, we obtained an identical positive slope indicating that the activation energy is independent of the viscosity. These surface activation energies are higher than the bulk activation energy of PDMS (13 kJ/mol measured in this study) and are lower than the bulk activation energy of PIB (65 kJ/mol measured in this study).

Table III-8. Apparent activation energy of air/PDMS and air/PIB surfaces.

Sample	**PDMS lv**		**PDMS mv**	**PDMS hv**	**PIB lv**	**PIB mv**	**PIB lv**
Ea (kJ/mol)	31.3±3.2		32.1±4.5	33.7±1.2	30.4±5.2	31.3±1.9	31.1±3.2

III.4.5.2. PIB/PDMS interfaces

From Figure III-13, it can be seen that the decrease during pulse mode sometimes had additional small steps before contraction. In fact, a deformation transition (between dilatation and compression steps) takes a short time since it cannot be instantaneous. Indeed, if that is the case, the drop will not immediately follow the fast decrease of the volume (because of its inertia) and it will have an additional dilational deformation (not a Laplacian drop) [59].

It has been seen that regardless of the type of PIB/PDMS investigated, the interfacial relaxation is faster at high temperature than at low temperature, indicating a thermal dependency of the interfacial tension.

The time dependency of the interfacial tension during the pulse interface perturbations can be described according to the model of Shi et al. [60]. Immediately after the formation of a new interface between two immiscible polymer systems such as PDMS and PIB, which is constituted of broad molecular weight distribution chains, the interfacial tension decreases rapidly because of the preferential migration of the shorter chains into the interface. The effect of this favoured incorporation into the interface slows down as time proceeds. Therefore, a steady state is reached (Figure 13(a)), i.e., the interfacial tension becomes constant, as the rates of diffusion of short chains into the interface and out of it become identical [60]. On the other hand, in the presence of high molecular weight components (i.e., at low temperatures of measurement), the transport of shorter chains into the interface takes place so slowly that the stationary state cannot be reached, since it is higher than the imposed expansion/compression period time of the measurements (Figure 13(c)).

It is useful to mention that Shi et al. [60] measured the variation of the interfacial tension γ with time using the static pendant drop technique. In their experiments, they formed a drop and then followed the decrease in interfacial tension until equilibrium (when the calculated interfacial tension does not change with time) but without imposing any variation in drop volume (pulse) as exercised in our

study. They observed that γ decreased but with a large time scale (from minutes to several hours). They ascribed this drop in the interfacial tension to the molecular weight and polydispersity of the PIB and PDMS used. According to the authors, since the interfacial tension depends on the size of the chain components at the interface, the low molecular weight chains (especially PIB) can migrate into the interface, thus lowering the interfacial energy of the system. Since the PDMS/PIB systems used in our work are polydisperse, this transport effect might occur in our experiments as well.

Later, Peters et al. [47] used confocal Raman spectroscopy for the estimation of the thickness of the diffusion interfacial zone in PDMS/PIB systems and confirmed the migration and diffusion effect observed in the pendant drop technique by Shi et al. [60].

We note that with the increase of the average molecular weight of both phases (the case of the PDMShv/PIBhv system), the interfacial tension and the interfacial viscosity also increase [18], and thus substantially slow down the mobility and migration to the interface of entangled chains, as is observed from the shape of the change of γ with time (Figure III-13).

To conclude, most of these authors came to an agreement that short macromolecules of PIB can migrate from the bulk into the newly generated interface with PDMS. Since MwPIB<MwPDMS (Table III-2), the chain mobility of PIB will be higher, and they could diffuse into the interface. These short chains could act as a surfactant and lower the interfacial tension.

We suspect that the relaxation times determined by the pulse method correspond to long relaxation times of macromolecular chains (a few seconds), which are much higher than stretch time relaxations at the molecular scale (Rouse time ~ a few ms).

Peters et al. [47] assumed that the chain migration could occur also in dynamic shear experiments, but at time scales much shorter than for the pendant drop method.

According to several studies, the characteristic elongational relaxation times of interfaces are also higher than the relaxation times of droplet interfaces measured by dynamic shear rheology in the case of immiscible polymer blends [47, 60].

In this study, for all PDMS/PIB interfaces, the characteristic interfacial relaxation times increased with increasing viscosity of the coexisting phases, but these times decreased with increasing temperature (Table III-9). Interfacial relaxation times are higher than those of surfaces. This can be explained by the higher degrees of freedom of macromolecular chains at the surface compared to the interfaces. The relaxation shape of PIB hv/PDMS hv systems at 25 and 45 °C was slow, with the relaxation time tending to an infinite value. This phenomenon could be explained by the high viscosity of the PIB hv and PDMS hv polymers as explained above. Moreover, increasing the viscosity induced an increase in the volume of the drop (compression cycles), and a significant increase of the interfacial tension at high temperature was noticed. This is related to the significant difference in the viscosities of their coexisting phases Δη (Table III-5). The drop of PIB becomes more deformed in the continuous phase (PDMS), which leads to an imbalance at the interfaces. Thus, the drop is no longer Laplacian and the viscous and inertial effects are considerably more important.

Surprisingly, the characteristic dilational relaxation times of PIB/PDMS interfaces obtained in this work using the dilational pulse mode measurements were comparable to those measured on similar polymer systems by other authors using other techniques such as spinning drop extensiometry [61] and the retraction of deformed droplets [62].

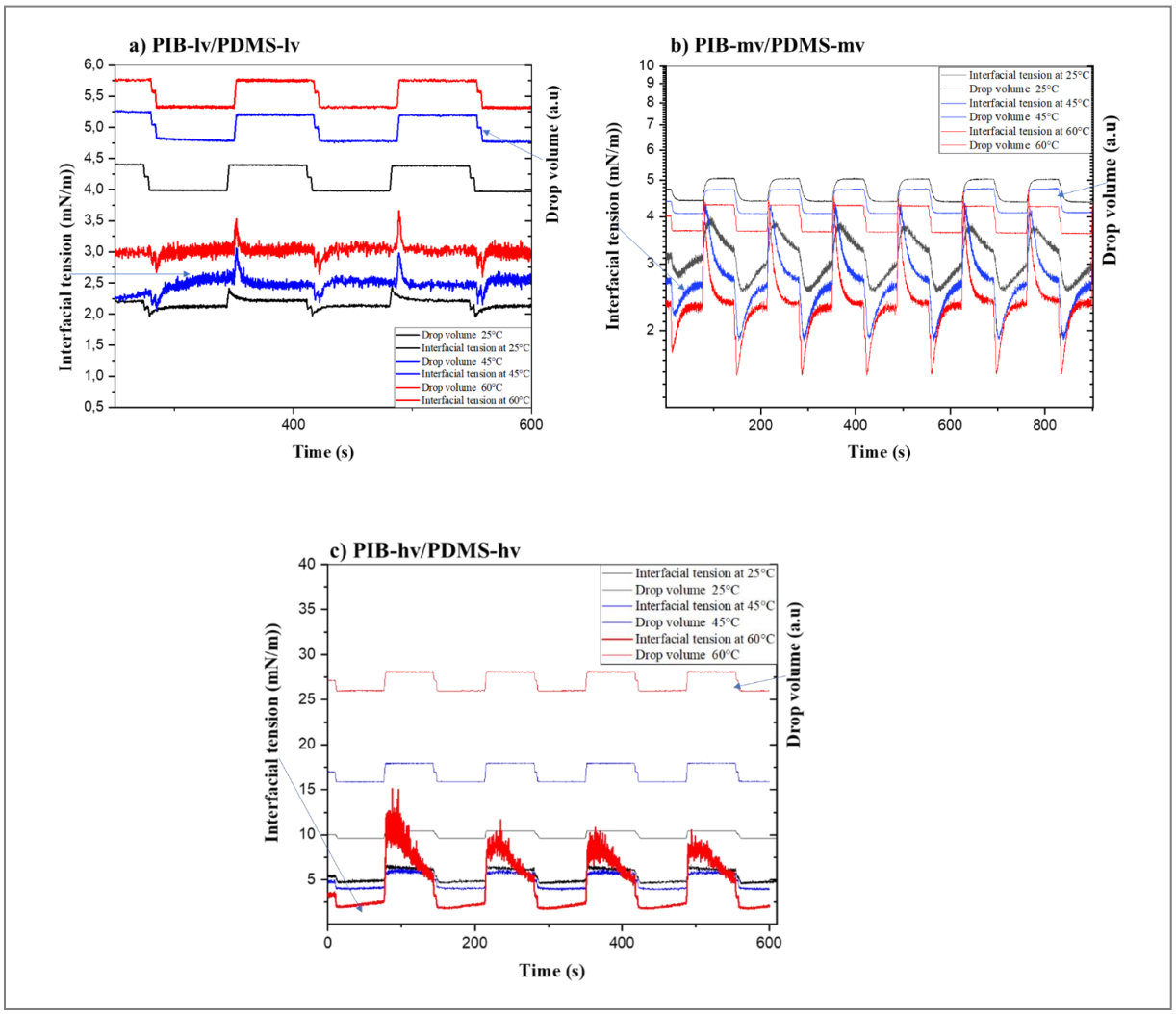

Figure III-13. Interfacial relaxation measurements conducted in pulse mode of (a) PIB lv/PDMS lv, (b) PIB mv/PDMS mv and (c) PIB hv/PDMS hv.

Table III-9. Variation of the interfacial relaxation times (in seconds) as a function of temperature.

Temperature (°C)	PIB lv/PDMS lv	PIB mv/PDMS mv	PIB hv/PDMS hv
25	1.37± 0.02	7.90±1.2	infinite
45	0.84±0.15	5.00±0.85	infinite
60	0.63±0.09	3.34±0.58	51.76±5.98

Compared to the air/PDMS and air/PIB surfaces, the PDMS/PIB interfaces presented a relatively low activation energy value (18 kJ/mol for interfaces versus 31 kJ/mol for surfaces). This result suggests

that chain motion at the interface between PIB and PDMS is different compared to PDMS and PIB surfaces.

Table III-10. Apparent activation energy of PIB/PDMS interfaces.

Sample	**PIB lv/PDMS lv**	**PIB mv/PDMS mv**
Ea (KJ/mol)	18.2±1.8	20.2±0.9

The apparent activation energy varies slightly with increasing source and receiving phase viscosities. Knowing that the relaxation time of the PIB hv/PDMS hv system was obtained at 60°C and assuming that the activation energy is very close to the other systems, the relaxation times at 25 and 45°C can be determined by extrapolation. Table III-11 shows an estimation of these relaxation times.

Table III-11. Variation of the PIB hv/PDMS hv interfacial relaxation times (in seconds) as a function of temperature.

Temperature (°C)	PIB hv/PDMS hv
25	≈ 116.70
45	≈ 71.90
60	51.76

III.4.6. Capillary breakup extensional rheometry (CaBER)

There are two ways to extract the evolution of the filament diameter. The first way is by using the recording movie (Figure III-14) of the filament thinning until the breakup - in other words, by using image software to post-analyse the saved pictures in order to extract D(t).

The second way is to use the laser micrometre to measure the diameter of a filament during the experiment. This latter method was used here to extract D(t).

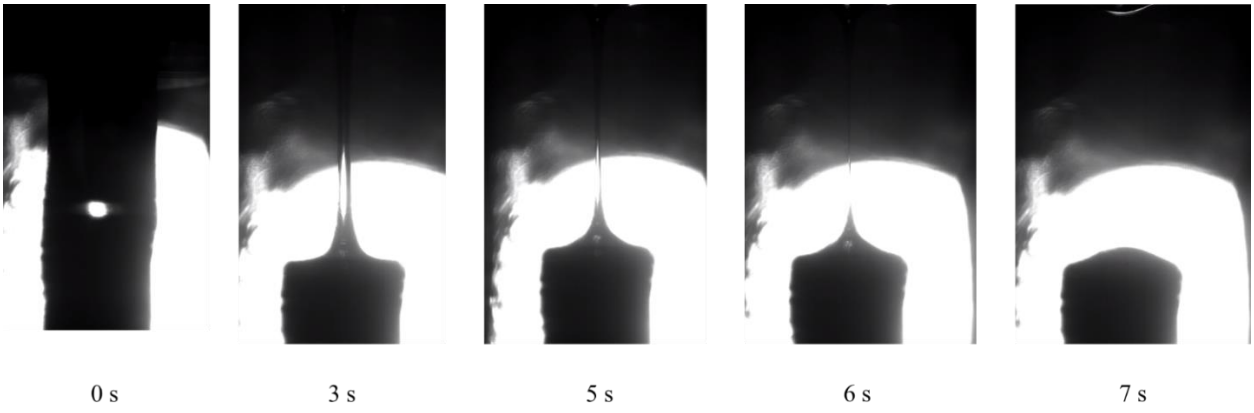

Figure III-14. Sequence of images of capillary breakup for a PIB filament.

Figure III-15 shows the evolution of the stretched filament diameter as a function of time for PIB and PDMS at 25°C. The diameter of the filament decreases during the experiment time. The raw diameter data were fitted using equation (26) to determine the elongational relaxation time of PIB and PDMS (Figures III-16 and III-17).

It should be noted that the fit of the data did not include the initial data just after the initial step-stretch; this evolution of the diameter near t=0 is dependent on the initial elongation rate. Miller et al. [29] demonstrated that most of the CaBER experiments were conducted on surfactant wormlike micelle solutions and immiscible polymer blends, to obtain a relaxation time that is insensitive to step-stretch conditions.

As mentioned in Figure III-15, there is no data about the PDMS hv. For this model fluid, we failed to form a filament and to study the evolution of its diameter. The filament broke immediately after applying the initial constant step-stretch. This might be explained by the distribution of the molar weight that could be bimodal. It can be related to the presence of a narrow peak for the long macromolecules and a wide one for the short macromolecules. Molar mass measurements are in progress to validate these postulates.

Table III-12 summarises the variation of the elongational relaxation times with the temperature for all the bulk viscosities of the coexisting phases. We can clearly observe that the elongational relaxation times for both PIB and PDMS increase with the molar weight of the bulk and decrease with temperature. For low-viscosity fluids and at high temperatures (PDMS lv and PIB lv), the breakup of the filament is instantaneous, and the saved data are minimal (only three or four points): the data are not enough for the fit to be carried out.

Wagner et al. [63] suspected in the case of highly entangled PS melts that premature breakage of the filament during the stretching step could happen when the elongation rate $\dot{\varepsilon}$ is significantly larger than the inverse of the Rouse stretch time "τ_R" of the polymer chain, i.e., an extension process time scale much faster than "τ_R". Feng et al. [64] demonstrated the same finding using polyisoprene (PI) melts with various weight average molecular weights (Mw). They found that in the presence of high molar mass polyisoprene melts (Mw > 430K), high extension rates make the filament break quickly compared to PIs with low Mw. The authors suggested that chain scission due to finite extensibility effects is the cause of the filament rupture. However, elucidation of this phenomenon still represents a challenge, and there is currently no consensus for the description of the underlying physics in such melt polymer systems [65].

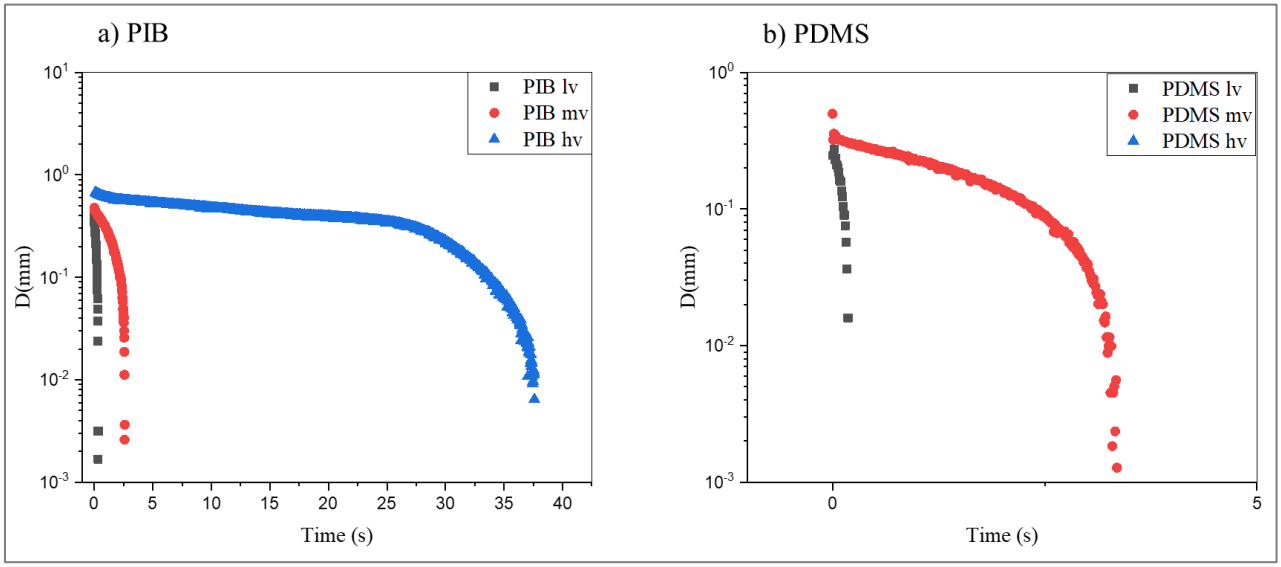

Figure III-15. Evolution of the stretched filament diameter as a function of time, for PIB (a) and PDMS (b) at 25°C.

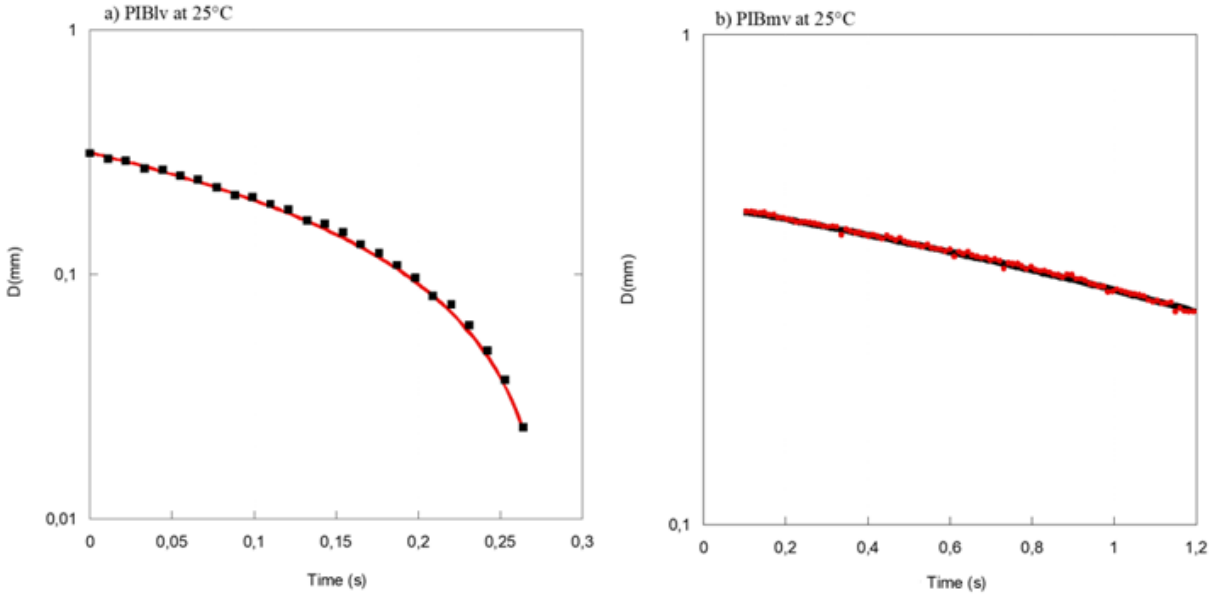

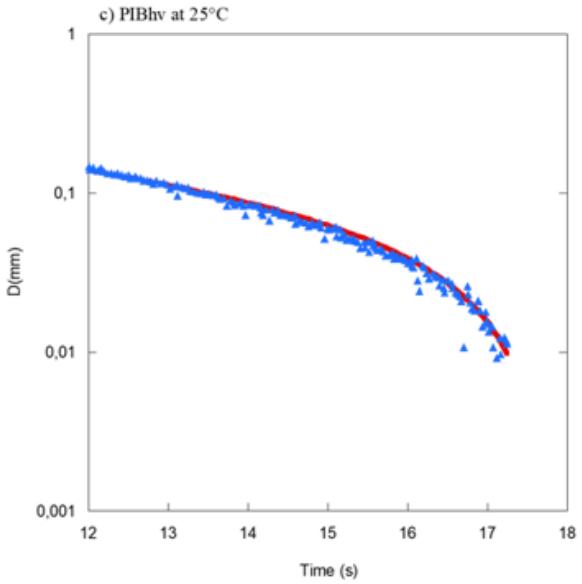

Figure III-16. Fitting of the variation of the filament diameter as a function of time of PIB at 25°C. (a) PIB lv, (b) PIB mv and (c) PIB hv.

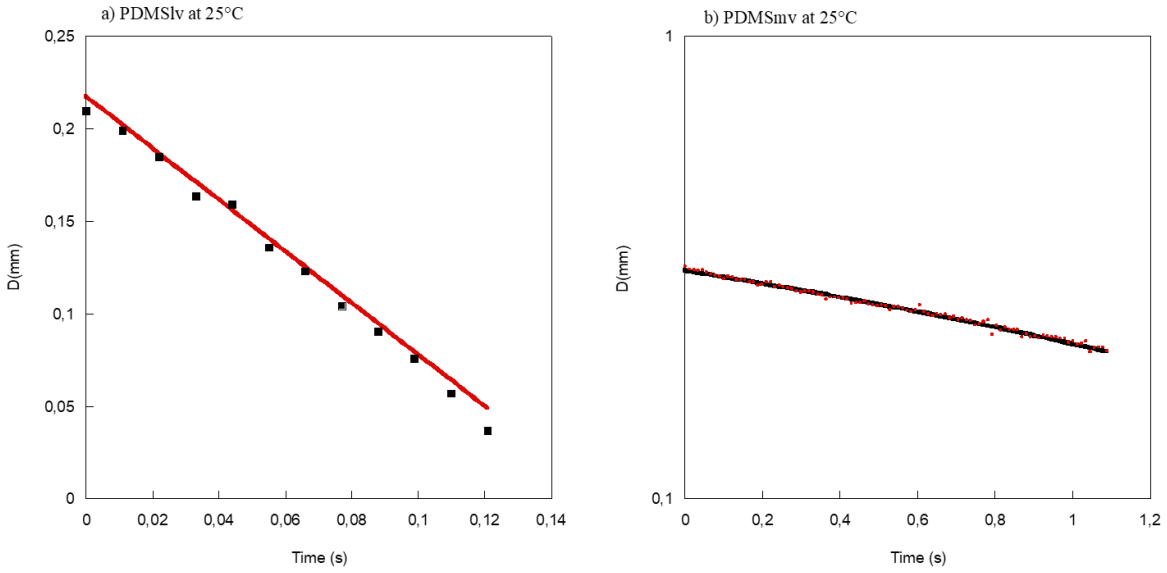

Figure III-17. Fitting of the variation of the filament diameter as a function of time of PDMS at 25°C. (a) PDMS lv and (b) PDMS mv.

Table III-12. Variation of the surface relaxation times (in seconds) as a function of temperature.

T (°C)	PDMS-lv	PDMS-mv	PDMS-hv	PIB-lv	PIB-mv	PIB-hv
25	0.290±0.03	2.20±0.10	------	0.18±0.01	0.52±0,090	6.94±1,70
45	0.160±0.02	1.54±0.02	------	0.09±0.02	0.28±0,006	2.36±0,25
60	------	0.65±0.01	------	------	0.13±0,005	1.96±0,03

It is worth pointing out that in CaBER experiments, the normal stress (viscous force effect) happens simultaneously with the capillary forces in the visco-capillary thinning domain. Nonetheless, in all our measurements with CaBER, the relaxation times have been extracted in the elasto-capillary thinning region where the viscous effect is insignificant [27]. Therefore, the calculated elongational relaxation times are mainly related to the capillary stress effect in analogy with tensiometry experiments. From Figure III-18, one can see that the extensional relaxation times obtained from CaBER measurements are very close to the dilational relaxation times obtained with the "pulse" method (several seconds in both cases depending on the viscosity and molecular weight of the polymer). It might be probable that the preferential migration of short chains into the bulk during thinning manifests itself in the same way for the polymer filament as in the rising or pendant drop.

This is not the case when compared to relaxation measurements carried out with other techniques. Recently, Rahman et al. [15], using a Wilhelmy plate force tensiometer, measured the variation of the bulk relaxation time of different liquids with viscosities ranging from 1 mPa.s to 1 Pa.s. The relaxation time was defined as the time to attain the equilibrium of the surface tension γ during its decay. The latter was measured with the help of a force sensor connected to the vertical Wilhelmy plate. Interestingly, they found a power law dependency between the viscosity and the relaxation time. Highly viscous fluids take much more time to attain the equilibrium compared to low-viscosity liquids. However, it should be noted that the dilatational interfacial relaxation times measured by the pulse relaxation technique of the present work are much shorter than the bulk relaxation times obtained by the Wilhelmy plate force tensiometer. For example, Rahman et al. showed a relaxation time of 54 s in the case of the liquid with 1 Pa.s, while in our case PDMS or PIB with 2.8 Pa.s gave a dilatational interfacial relaxation time of 0.3 s or 0.2 s, respectively.

We note that at a specific temperature and due to the difference in their average molecular weights, the characteristic elongational relaxation time of PIBlv is lower than that of PDMSlv, although they have the same melt viscosity since MwPIB < MwPDMS. The same trend was observed when comparing PDMSmv and PIBmv, or PDMShv with PIBhv.

Recently, several authors [66-68] have tried to study the extensional behavior using CaBER of PEO solutions (in solvents) with varying molecular weights in combination with time-dependent surface tension measurements. In all cases, they found that the surface tension decreases with time after a new, fresh interface is created. They explained that with time, polymer from the bulk diffused and adsorbed to the interface and reduced the surface tension. Their data showed that the higher molecular weight PEO took a longer time to approach equilibrium than the more mobile polymers. On the other hand, it was ascertained that the values of extensional relaxation times extracted from CaBER measurements for the PEO solutions are seen to increase with molecular weight, in qualitative agreement with data from the dynamic surface tension (DST). However, the authors argued that DST alone cannot explain the difference in the shape of the curves in the capillary thinning process of CaBER experiments.

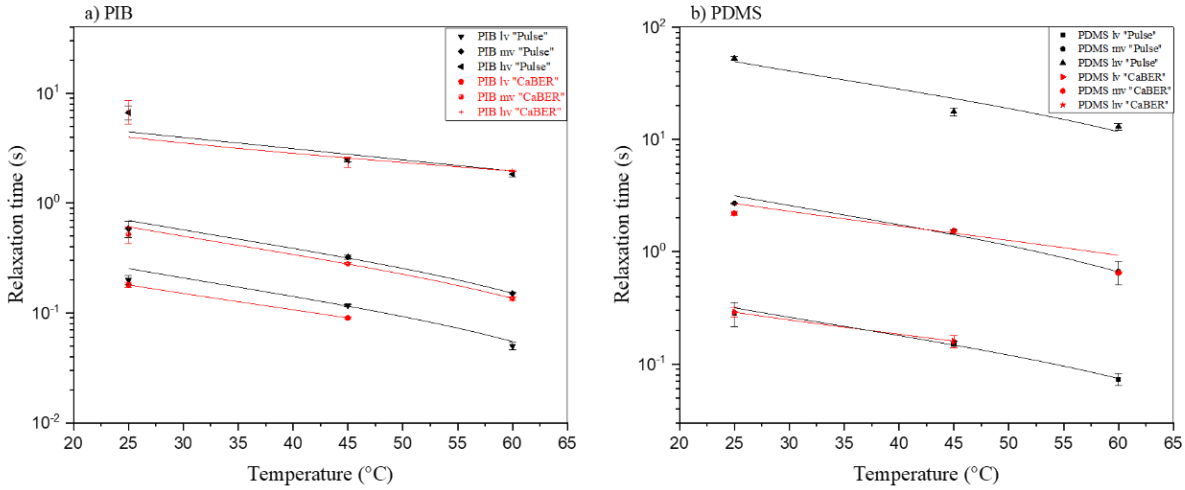

Figure III-18. Elongational relaxation times measured by the pulse method and CaBER technique.

The evolution of the apparent elongational viscosity as a function of time for the model fluids at 25°C is also carried out and depicted in Figure III-19. The elongational viscosity passed through a transient stage before reaching a steady terminal regime. Using the latter, a Trouton ratio (Tr) of around 3 was found for the PDMS and PIB melted polymers, which confirms the reliability of measurements obtained with CaBER.

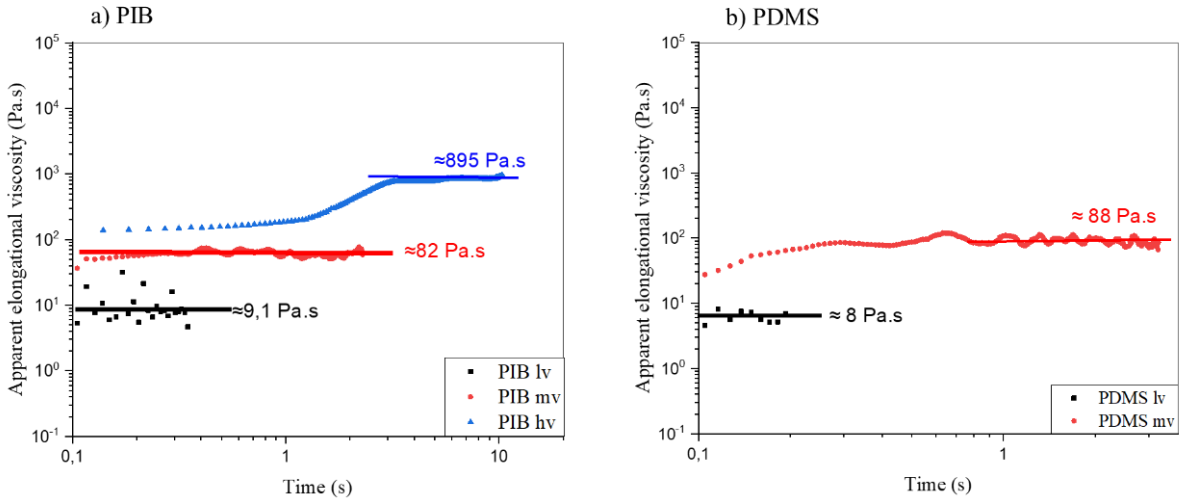

Figure III-19. Evolution of the apparent elongational viscosity as a function of time, for PIB (a) and PDMS (b) at 25°C.

III.4.7. Surface shear rheology

In the interfacial shear measurements, the corrected surface shear viscosities were determined for low Boussinecq values (B_0 < 1) to reach true surface viscosity values. In this work, the calculated Boussinesq numbers were in the range of 0.2 to 0.6.

Zero-shear surface viscosities of air/PIB and air/PDMS are summarised in Table III-13.

Table III-13. Zero-shear surface viscosities of air/PIB and air/PDMS as a function of temperature.

	Surface viscosity (Pa.s.m)		
Surfaces/Temperature	25°C	45°C	60°C
Air/PIB lv	$2.3.10^{-3}$	$8.6.10^{-4}$	$7.8.10^{-4}$
Air/PIB mv	$2.4.10^{-2}$	$9.9.10^{-3}$	$7.7.10^{-3}$
Air/PIB hv	$2.0.10^{-1}$	$1.7.10^{-1}$	$1.2.10^{-1}$
Air/PDMS lv	$8.6.10^{-4}$	$6.6.10^{-4}$	$4.8.10^{-4}$
Air/PDMS mv	$9.8.10^{-3}$	$3.5.10^{-2}$	$3.2.10^{-2}$
Air/PDMS hv	$8.8.10^{-2}$	$5.7.10^{-1}$	$3.9.10^{-1}$

All the surfaces were Newtonian at the studied shear rate. Moreover, the surface viscosity of air/PIB and air/PDMS increased with the viscosity of the subphases.

Velandia et al. [69] found the same tendency when they studied the link between interfacial and bulk viscoelasticity in reverse Pickering emulsions. For both bulk and interfaces, they demonstrate, using the Double Wall Ring (DWR) [2], that elastic modulus increases with the silica content, according to a power-law dependency.

We also compared the zero-shear surface viscosities obtained by interfacial shear rheology with the elongational relaxation times acquired by the pulse relaxation test. Figure III-20 shows the variation of the relaxation times with the zero-shear surface viscosities of air/PIB and air/PDMS.

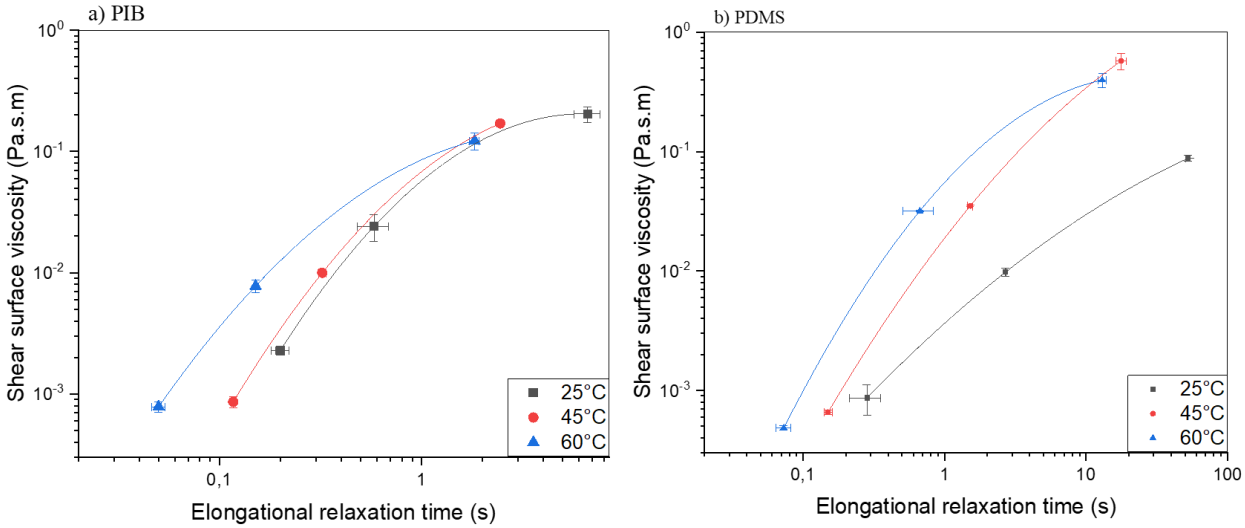

Figure III-20. Evolution of the relaxation times with the zero-shear surface viscosities of air/PIB (a) and air/PDMS (b) systems.

One can show that zero-shear surface viscosities of the studied surfaces increase with the elongational relaxation time. Furthermore, since this tendency follows a power-law dependency, we suspect the existence of a direct relationship between the interfacial shear and elongational properties in our air/PIB and air/PDMS systems, described generally by an interfacial or surface Trouton ratio.

Verwijlen et al. [48] defined the interfacial Trouton ratio Tr_s. Similarly to bulk fluids, Tr_s is defined as the ratio between the surface dilational η_d and the surface shear viscosity η_s:

$$Tr_s = \frac{\eta_d}{\eta_s} \qquad \textbf{(III-9)}$$

In our published article [18], we have shown a linear correlation between the bulk viscosity and the surface viscosity in the case of free surfaces of PDMS and PIB, i.e., air/PIB and air/PDMS. A similar power law tendency between the viscosity and relaxation time has been noticed by other authors [46, 67]. These observations require further study with the use of viscoelastic interfaces allowing reliable interfacial dilational viscosity measurements and will be the subject of an article in the near future.

III.5. Conclusions

In this chapter, the rising oscillating drop method has been used to probe the dilational rheological properties of PDMS/PIB ***free*** interfaces. The effects of molecular weight and temperature have been taken into account. To prevent inertial and capillary effects, a number of material and experimental precautions were carefully respected. During the static and dynamic experiments, the creation of an interphase was evidenced in the case of coexisting phases with a high molecular weight. Then, the characteristic dilational relaxation times of the studied surfaces and interfaces were extracted using the new pulse relaxation method. The empirical Kohlrausch formula was used to fit experimental data showing the evolution of surface or interfacial tension with time, and the Arrhenius law was applied to validate the temperature dependency of the relaxation time. It was observed that the surface and interfacial relaxation times increased with the melt viscosity of the polymer and decreased with temperature. For the PIB/PDMS interfaces probed at high temperatures, however, the oscillating drop/bubble method and the relaxation test did not provide exploitable experimental data due to the presence of high Weber and capillary numbers caused by the significant viscosity differences of the coexisting phases. Capillary breakup extensional rheometry (CaBER) was used to probe the elongational rheological properties of model fluids. Thanks to the fit of D(t), elongational relaxation times were determined. The latter were comparable to the characteristic dilational times obtained with the pulse relaxation method. Finally, the possibility of a Troutonian correlation between shear and dilational surface rheology was discussed, and a direct link between zero-shear surface viscosities and relaxation elongational times was highlighted.

The original method developed in this study could be applied to a wide range of polymer melts and fluids and to even more complex polymeric systems.

III.6. References

[1] J. C. Slattery, L. Sagis, and E.-S. Oh, *Interfacial transport phenomena*. Springer, 2007.

[2] S. Vandebril, A. Franck, G. G. Fuller, P. Moldenaers, and J. Vermant, "A double wall-ring geometry for interfacial shear rheometry," *Rheologica Acta*, vol. 49, no. 2, pp. 131-144, 2010.

[3] D. Renggli, A. Alicke, R. H. Ewoldt, and J. Vermant, "Operating windows for oscillatory interfacial shear rheology," *Journal of Rheology*, vol. 64, no. 1, pp. 141-160, 2020.

[4] S. Derkach, J. Krägel, and R. Miller, "Methods of measuring rheological properties of interfacial layers (Experimental methods of 2D rheology)," *Colloid journal*, vol. 71, no. 1, pp. 1-17, 2009.

[5] L. Lai, P. Mei, X. M. Wu, L. Cheng, Z. H. Ren, and Y. Liu, "Interfacial dynamic properties and dilational rheology of sulfonate gemini surfactant and its mixtures with quaternary ammonium bromides at the air–water interface," *Journal of Surfactants and Detergents*, vol. 20, no. 3, pp. 565-576, 2017.

[6] H.-Q. Sun, L. Zhang, Z.-Q. Li, L. Zhang, L. Luo, and S. Zhao, "Interfacial dilational rheology related to enhance oil recovery," *Soft Matter*, vol. 7, no. 17, pp. 7601-7611, 2011.

[7] E. M. Freer, K. S. Yim, G. G. Fuller, and C. J. Radke, "Shear and dilatational relaxation mechanisms of globular and flexible proteins at the hexadecane/water interface," *Langmuir*, vol. 20, no. 23, pp. 10159-10167, 2004.

[8] B. Noskov and A. Bykov, "Dilational rheology of monolayers of nano-and micropaticles at the liquid-fluid interfaces," *Current opinion in colloid & interface science*, vol. 37, pp. 1-12, 2018.

[9] T. Dadouche, M. Yousfi, C. Samuel, M. F. Lacrampe, and J. Soulestin, "(Nano) Fibrillar morphology development in biobased poly (butylene succinate-co-adipate)/poly (amide-11) blown films," *Polymer Engineering & Science*, vol. 61, no. 5, pp. 1324-1337, 2021.

[10] H. Zhang, K. Lamnawar, and A. Maazouz, "Fundamental studies of interfacial rheology at multilayered model polymers for coextrusion process," in *AIP Conference Proceedings*, 2015, vol. 1664: AIP Publishing LLC, p. 100008.

[11] J. Lei, Y. Gao, Y. Ma, K. Zhao, and F. Du, "Improving the emulsion stability by regulation of dilational rheology properties," *Colloids and Surfaces A: Physicochemical and Engineering Aspects*, vol. 583, p. 123906, 2019.

[12] H. Wang, X. Wei, Y. Du, and D. Wang, "Experimental investigation on the dilatational interfacial rheology of dust-suppressing foam and its effect on foam performance," *Process Safety and Environmental Protection*, vol. 123, pp. 351-357, 2019.

[13] B. S. Murray and P. V. Nelson, "A novel Langmuir trough for equilibrium and dynamic measurements on air− water and oil− water monolayers," *Langmuir*, vol. 12, no. 25, pp. 5973-5976, 1996.

[14] K. Lunkenheimer and G. Kretzschmar, "Neuere Ergebnisse der Untersuchung der Elastizität von löslichen Adsorptionsschichten nach der Methode der pulsierenden Blase," *Zeitschrift für Physikalische Chemie*, vol. 256, no. 1, pp. 593-605, 1975.

[15] O. Del Rıo and A. Neumann, "Axisymmetric drop shape analysis: computational methods for the measurement of interfacial properties from the shape and dimensions of pendant and sessile drops," *Journal of colloid and interface science*, vol. 196, no. 2, pp. 136-147, 1997.

[16] J. Lucassen and M. Van den Tempel, "Longitudinal waves on visco-elastic surfaces," *Journal of Colloid and Interface Science*, vol. 41, no. 3, pp. 491-498, 1972.

[17] N. Grizzuti, G. Buonocore, and G. Iorio, "Viscous behavior and mixing rules for an immiscible model polymer blend," *Journal of Rheology*, vol. 44, no. 1, pp. 149-164, 2000.

[18] Y. El Omari, M. Yousfi, J. Duchet-Rumeau, and A. Maazouz, "Interfacial rheology testing of molten polymer systems: Effect of molecular weight and temperature on the interfacial properties," *Polymer Testing*, vol. 101, p. 107280, 2021.

[19] Roger S. Porter, Julian F. Johnson, The status of non-Newtonian polymer flow, Polymer Engineering & Science, 10.1002/pen.760030105, **3**, 1, (18-20), 2004.

[20] Graessley, W. W., The entanglement concept in rheology, Advances in Polymer Science, 16 (1974).

[21] E. Becker, W. Hiller, and T. Kowalewski, "Experimental and theoretical investigation of large-amplitude oscillations of liquid droplets," *Journal of Fluid Mechanics,* vol. 231, pp. 189-210, 1991.
[22] G. Serrien, G. Geeraerts, L. Ghosh, and P. Joos, "Dynamic surface properties of adsorbed protein solutions: BSA, casein and buttermilk," *Colloids and surfaces,* vol. 68, no. 4, pp. 219-233, 1992.
[23] R. Miller, G. Loglio, U. Tesei, and K.-H. Schano, "Surface relaxations as a tool for studying dynamic interfacial behaviour," *Advances in colloid and interface science,* vol. 37, no. 1-2, pp. 73-96, 1991.
[24] R. Miller, R. Sedev, K.-H. Schano, C. Ng, and A. Neumann, "Relaxation of adsorption layers at solution/air interfaces using axisymmetric drop-shape analysis," *Colloids and surfaces,* vol. 69, no. 4, pp. 209-216, 1993.
[25] A. Bazilevsky, V. Entov, and A. Rozhkov, "Liquid filament microrheometer and some of its applications," in *Third European Rheology Conference and Golden Jubilee Meeting of the British Society of Rheology*, 1990: Springer, pp. 41-43.
[26] G. H. McKinley and A. Tripathi, "How to extract the Newtonian viscosity from capillary breakup measurements in a filament rheometer," *Journal of Rheology,* vol. 44, no. 3, pp. 653-670, 2000.
[27] S. L. Anna and G. H. McKinley, "Elasto-capillary thinning and breakup of model elastic liquids," *Journal of Rheology,* vol. 45, no. 1, pp. 115-138, 2001.
[28] A. Naillon, C. de Loubens, W. Chèvremont, S. Rouze, M. Leonetti, and H. Bodiguel, "Dynamics of particle migration in confined viscoelastic Poiseuille flows," *Physical Review Fluids,* vol. 4, no. 5, p. 053301, 2019.
[29] E. Miller, C. Clasen, and J. P. Rothstein, "The effect of step-stretch parameters on capillary breakup extensional rheology (CaBER) measurements," *Rheologica acta,* vol. 48, no. 6, pp. 625-639, 2009.
[30] F. van Berlo, R. Cardinaels, G. Peters, and P. Anderson, "Towards a universal shear correction factor in filament stretching rheometry," *Rheologica Acta,* vol. 60, no. 11, pp. 691-709, 2021.
[31] D. LeGrand and G. Gaines Jr, "Immiscibility and interfacial tension between polymer liquids: dependence on molecular weight," *Journal of Colloid and Interface science,* vol. 50, no. 2, pp. 272-279, 1975.
[32] I. Vinckier, P. Moldenaers, and J. Mewis, "Relationship between rheology and morphology of model blends in steady shear flow," *Journal of Rheology,* vol. 40, no. 4, pp. 613-631, 1996.
[33] M. Wagner and B. Wolf, "Interfacial tension between polyisobutylene and poly (dimethylsiloxane): influence of chain length, temperature, and solvents," *Macromolecules,* vol. 26, no. 24, pp. 6498-6502, 1993.
[34] C. Tufano, G. Peters, P. Van Puyvelde, and H. Meijer, "Transient interfacial tension and morphology evolution in partially miscible polymer blends," *Journal of colloid and interface science,* vol. 328, no. 1, pp. 48-57, 2008.
[35] M. Gabriele, R. Pasquino, and N. Grizzuti, "Effects of Viscosity-Controlled Interfacial Mobility on the Coalescence of Immiscible Polymer Blends," *Macromolecular Materials and Engineering,* vol. 296, no. 3-4, pp. 263-269, 2011.
[36] V. E. Ziegler and B. A. Wolf, "Interfacial tensions from drop retraction versus pendant drop data and polydispersity effects," *Langmuir,* vol. 20, no. 20, pp. 8688-8692, 2004.
[37] S. Guido, M. Simeone, and M. Villone, "Diffusion effects on the interfacial tension of immiscible polymer blends," *Rheologica acta,* vol. 38, no. 4, pp. 287-296, 1999.
[38] R. S. Anderssen, S. A. Husain, and R. Loy, "The Kohlrausch function: properties and applications," *Anziam journal,* vol. 45, pp. C800-C816, 2003.
[39] M. Yousfi, L. Porcar, P. Lindner, F. Boué, and Y. Rharbi, "A novel method for studying the dynamics of polymers confined in spherical nanoparticles in nanoblends," *Macromolecules,* vol. 42, no. 6, pp. 2190-2197, 2009.
[40] R. H. Boyd, F. Liu, J. Runt, and J. Fitzgerald, "Dielectric spectroscopy of semicrystalline polymers," *Dielectric spectroscopy of polymeric materials,* pp. 107-136, 1997.

[41] C. Quintero, C. Noïk, C. Dalmazzone, and J. Grossiord, "Formation kinetics and viscoelastic properties of water/crude oil interfacial films," *Oil & Gas Science and Technology-Revue de l'IFP*, vol. 64, no. 5, pp. 607-616, 2009.
[42] J. A. Kleingartner, H. Lee, M. F. Rubner, G. H. McKinley, and R. E. Cohen, "Exploring the kinetics of switchable polymer surfaces with dynamic tensiometry," *Soft Matter*, vol. 9, no. 26, pp. 6080-6090, 2013.
[43] J. Jůza, "Surface Tension Measurements of Viscous Materials by Pendant Drop Method: Time Needed to Establish Equilibrium Shape," in *Macromolecular Symposia*, 2019, vol. 384: Wiley Online Library, p. 1800150.
[44] D. Kwok, L. Cheung, C. Park, and A. Neumann, "Study on the surface tensions of polymer melts using axisymmetric drop shape analysis," *Polymer Engineering & Science*, vol. 38, no. 5, pp. 757-764, 1998.
[45] B. B. Sauer and N. V. Dipaolo, "Surface tension and dynamic wetting on polymers using the Wihelmy method: Applications to high molecular weights and elevated temperatures," *Journal of colloid and interface science*, vol. 144, no. 2, pp. 527-537, 1991.
[46] M. R. Rahman, A. Deng, S.-A. Hussak, A. Ahmed, T. Willers, and P. R. Waghmare, "On the effect of relaxation time in interfacial tension measurement," *Colloids and Surfaces A: Physicochemical and Engineering Aspects*, vol. 574, pp. 239-244, 2019.
[47] G. W. Peters, A. N. Zdravkov, and H. E. Meijer, "Transient interfacial tension and dilatational rheology of diffuse polymer-polymer interfaces," *The Journal of chemical physics*, vol. 122, no. 10, p. 104901, 2005.
[48] T. Verwijlen, D. Leiske, P. Moldenaers, J. Vermant, and G. Fuller, "Extensional rheometry at interfaces: Analysis of the Cambridge Interfacial Tensiometer," *Journal of Rheology*, vol. 56, no. 5, p. 1225, 2012.
[49] T. Verwijlen, P. Moldenaers, and J. Vermant, "A fixture for interfacial dilatational rheometry using a rotational rheometer," *The European Physical Journal Special Topics*, vol. 222, no. 1, pp. 83-97, 2013.
[50] C. Jalbert, J. T. Koberstein, I. Yilgor, P. Gallagher, and V. Krukonis, "Molecular weight dependence and end-group effects on the surface tension of poly (dimethylsiloxane)," *Macromolecules*, vol. 26, no. 12, pp. 3069-3074, 1993.
[51] P. Mahmoudi and M. Matsen, "Entropic segregation of short polymers to the surface of a polydisperse melt," *The European Physical Journal E*, vol. 40, no. 10, pp. 1-9, 2017.
[52] J. Elman, B. Johs, T. Long, and J. Koberstein, "A neutron reflectivity investigation of surface and interface segregation of polymer functional end groups," *Macromolecules*, vol. 27, no. 19, pp. 5341-5349, 1994.
[53] E. Dickinson, "Milk protein interfacial layers and the relationship to emulsion stability and rheology," *Colloids and Surfaces B: Biointerfaces*, vol. 20, no. 3, pp. 197-210, 2001.
[54] E. A. Foegeding, P. Luck, and J. P. Davis, "Factors determining the physical properties of protein foams," *Food hydrocolloids*, vol. 20, no. 2-3, pp. 284-292, 2006.
[55] D. Langevin, "Polyelectrolyte and surfactant mixed solutions. Behavior at surfaces and in thin films," *Advances in Colloid and Interface Science*, vol. 89, pp. 467-484, 2001.
[56] R. v. Klitzing and H.-J. Müller, "Film stability control," *Current opinion in colloid & interface science*, vol. 7, no. 1-2, pp. 42-49, 2002.
[57] I. Schmidt, B. Novales, F. Boué, and M. A. Axelos, "Foaming properties of protein/pectin electrostatic complexes and foam structure at nanoscale," *Journal of colloid and interface science*, vol. 345, no. 2, pp. 316-324, 2010.
[58] C. Roland and P. Santangelo, "Effect of temperature on the terminal relaxation of branched polydimethysiloxane," *Journal of non-crystalline solids*, vol. 307, pp. 835-841, 2002.
[59] M. Molaei and J. C. Crocker, "Interfacial microrheology and tensiometry in a miniature, 3-d printed Langmuir trough," *Journal of colloid and interface science*, vol. 560, pp. 407-415, 2020.
[60] T. Shi, V. E. Ziegler, I. C. Welge, L. An, and B. A. Wolf, "Evolution of the interfacial tension between polydisperse “immiscible” polymers in the absence and in the presence of a compatibilizer," *Macromolecules*, vol. 37, no. 4, pp. 1591-1599, 2004.

[61] D. Joseph *et al.*, "A spinning drop tensioextensometer," *Journal of Rheology,* vol. 36, no. 4, pp. 621-662, 1992.
[62] P. Siahcheshm, F. Goharpey, and R. Foudazi, "Droplet retraction in the presence of nanoparticles with different surface modifications," *Rheologica Acta,* vol. 57, no. 11, pp. 729-743, 2018.
[63] M. H. Wagner, E. Narimissa, and Q. Huang, "On the origin of brittle fracture of entangled polymer solutions and melts," *Journal of Rheology,* vol. 62, no. 1, pp. 221-233, 2018.
[64] Y. Feng *et al.*, "Exploring rheological responses to uniaxial stretching of various entangled polyisoprene melts," *Journal of Rheology,* vol. 63, no. 5, pp. 763-771, 2019.
[65] S.-Q. Wang, "Melt rupture unleashed by few chain scission events in fully stretched strands," *Journal of Rheology,* vol. 63, no. 1, pp. 105-107, 2019.
[66] D. Sachsenheimer, B. Hochstein, H. Buggisch, and N. Willenbacher, "Determination of axial forces during the capillary breakup of liquid filaments–the tilted CaBER method," *Rheologica acta,* vol. 51, no. 10, pp. 909-923, 2012.
[67] A. Zell, S. Gier, S. Rafai, and C. Wagner, "Is there a relation between the relaxation time measured in CaBER experiments and the first normal stress coefficient?," *Journal of non-newtonian fluid mechanics,* vol. 165, no. 19-20, pp. 1265-1274, 2010.
[68] L. E. Rodd, T. P. Scott, J. J. Cooper-White, and G. H. McKinley, "Capillary break-up rheometry of low-viscosity elastic fluids," *Applied Rheology,* vol. 15, no. 1, pp. 12-27, 2005.
[69] S. F. Velandia *et al.*, "Exploring the link between interfacial and bulk viscoelasticity in reverse Pickering emulsions," *Colloids and Surfaces A: Physicochemical and Engineering Aspects,* vol. 624, p. 126785, 2021.

Chapter IV. Interfacial rheology for probing the in-situ chemical reaction at interfaces of molten polymer systems

IV.1. Abstract

The design of new functional materials from immiscible polymers or multi-layered structures using reactive compatibilisation is an efficient approach that has been extensively employed in a wide range of applications. The adhesion/interfacial properties in these multiphase polymeric systems depend on the extent of reaction occurring at the interface. However, probing in-situ interfacial reactions in the molten state has proved challenging. In this study, interfacial shear rheology is used for the first time to directly probe the reaction at the interface between maleic anhydride-grafted polyethylene (PEgMA) and aminopropyl-terminated polydimethylsiloxane (PDMS-(PropNH$_2$)$_2$) used as model reactive polymer systems. First, the extent of reaction was checked using differential scanning calorimetry (DSC) and dynamic rheology coupled with fast-scan FTIR spectroscopy. Then the reaction at the interface was investigated using interfacial shear rheology based on a newly homemade, lightweight biconical setup. Thereafter, the time evolution of the interfacial tension with the progress of interfacial reaction was assessed using the pendant drop method. It has been demonstrated that the molecular weight of the aminated PDMS and the temperature of the medium markedly affect the rate of melt reaction at the interface and related interfacial rheological properties. Interestingly, the ability to assess the reactions at the interface in PEgMA/PDMS-(PropNH$_2$)$_2$ systems, even with low concentrations of reactive functionalities, demonstrates that interfacial rheology is a suitable, sensitive probe that could be applied to other reactive polymer systems, allowing better control of the resulting physical properties.

Keywords: Interfacial shear rheology, dynamic interfacial tension, interface, interphase, reaction kinetics.

IV.2. Introduction

Polymers are now among the most frequently used materials in a variety of fields such as electronics, aeronautics, the automotive sector, biomedical applications, etc. They are often manufactured with other polymers and additives in the molten state in order to design new products with novel functional properties. Blends [1] and multilayers [2] are some interesting examples of these multiphase polymer systems. Understanding their interfacial phenomena is crucial in controlling their mechanical [3], optical [4] and rheological properties [5, 6]. In the case of molten polymer systems, the adhesion between polymer constituents during processing is provided by interdiffusion at the interfaces and the corresponding interphase formation induced by the interfacial reaction. Thus, the study of polymer systems with a chemical reaction at the interface has been a topic of great interest in academic and industrial studies over the last decades. The knowledge acquired makes it possible to control the formation processes of these reactive systems as well as understand the mechanisms involved, for instance, in reactive extrusion [7, 8], multilayer coextrusion [6, 9, 10] and injection over-moulding [11].

PDMS/polyolefin is one of the polymer systems that have attracted the most attention in recent years. It can combine the valuable properties obtained separately in polyolefin and PDMS and therefore present strong potential in a wide range of applications, especially those related to polyolefin processing. Wu et al. [12] demonstrated the potential for using maleic anhydride-grafted polypropylene (PP-g-MA) as an effective compatibilizer for the enhancement of mechanical, morphological and foaming properties of PP/PDMS blends. Peng et al. [13] confirmed that the addition of 0.5–3 wt % of PDMS into PA66 made it possible to obtain PA66/PDMS blend fibres with excellent mechanical properties and reduced hot shrinkage.

In reactive polymer blends, the equilibrium interfacial tension induced by reactive compatibilization is often estimated indirectly using the deformed drop retraction method (DDRM) [14]. The interfacial tension in reactive polymer blends is also assessed from blend rheology using theoretical predictions such as the Palierne, Lee and Park, Honerkamp and Weese or Choi-Schowalter models [15]. However, the droplet sizes depend on several parameters such as blend composition, matrix viscosity, melt density, shear rate and temperature [14]. This makes the deduction of interfacial tension from these techniques somewhat irrelevant and often not very reproducible [16].

The investigation of interfacial reaction kinetics in reactively blended polymers or multilayers is indirectly probed by dynamic rheology through following the viscoelastic modulus with time [17, 18]. Macosko et al. [19] have observed that the kinetics of reaction in (MA)-grafted PMMA / PS-NH_2 multilayers made by coextrusion (640 layers) is dependent on the mode of flow used in rheological tests. The reaction rate was higher in oscillatory shear mode than in the steady shear. The authors suggested that this may be related to the frequency of contact between chain ends in the interfacial

region or to fluctuations in the interfacial thickness. Nonetheless, in all of these studies, the contribution of the interface to the dynamic bulk modulus was difficult to quantify, complexifying the interpretation of the rheological results.

Interfacial rheology is currently used to probe the interfacial properties of multiphase liquid systems such as emulsions [20], foams [21] and blends [22]. We remind that depending on the kind of deformation, two parts can be defined. The first method is interfacial shear rheology, in which a shear geometry is placed at the interface and deforms it to assess the interfacial viscoelastic modulus and the interfacial viscosity. The most common geometries are the double-walled ring (DWR) [23] and the bicone [24]. The second method is interfacial dilatational rheology, in which the interface is compressed or stretched using the oscillating drop [25], Langmuir trough [26] or oscillating spinning drop [27] technique.

The study of reactive two-phase liquid systems at room temperature using interfacial rheology has been the subject of various reports; one can cite the case of emulsion stabilisation with reactive and non-reactive surface agents [28]. The process is usually started with a diffusion followed by an adsorption/desorption and then a reaction at the interface. However, studies of the interfacial rheology of molten polymer systems are not abundant due to the difficulties accompanying experimental measurements. The first attempt was carried out by El Omari et al. [29], who highlighted the interfacial diffusion of non-reactive model polymer melts and semi-crystalline polymer systems using a new high-temperature biconical setup.

For all these reasons, studying the interfacial melt rheology of reactive polymer/polymer systems may be very attractive and of paramount importance, allowing direct probing of the interfaces despite some experimental difficulties involved in carrying out these measurements for polymer melts.

Today, various tools make it possible to directly probe the reaction between two polymer systems. On can cite the fluorescent labelling technique [30], neutron reflectometry [31, 32], forward recoil spectrometry (FRES) [33] and sum frequency generation (SFG) vibrational spectroscopy [34]. However, these characterisation methods do not assess the rheological properties of the interface, and they are sensitive only for high concentrations of reactive functionalities [35].

In this chapter, the interfacial rheological behaviour and the reaction kinetics in both reactive and non-reactive low-viscosity molten polymer systems were investigated using two different methods: interfacial shear rheology and dynamic interfacial tension measurements. First of all, polydimethylsiloxane, trimethylsiloxy terminated was used as a non-reactive polymer. Then two functionalised polymers were chosen as reactive systems. The first one has amino functions (polydimethylsiloxane, aminopropyl terminated), and the second has a maleic anhydride function (polyethylene-grafted maleic anhydride). The effects of the temperature of the medium and the molecular weight of the aminated PDMS on the reaction kinetics were highlighted. The rheological properties of the interfacial layer formed were also evaluated.

IV.3. Theoretical background

In this section, the thermodynamic aspect of the creation of an interface or interphase is described. Then, we briefly summarise the phenomena that take place at the interface, such as interdiffusion and interfacial reaction.

IV.3.1. Thermodynamic aspect

The formation of an interface is a thermodynamic process, and its thickness can be used to evaluate the interactions between two polymers. It is rarely robust and varies around a few nanometres depending on the nature of the interactions, molecular weight, temperature and time.

From a thermodynamic point of view, when an interface is created, it costs energy for a molecule to remain at the interface [36]. In a system composed of two phases, 1 and 2, and an interface **int**, we can define the internal energy U as:

$$\mathbf{U = U_{int} + U_1 + U_2} \qquad \textbf{(IV-1)}$$

where U_{int} is the internal energy resulting from the presence of an interface,

and U_1 and U_2 are the internal energies of polymers 1 and 2.

The variation of internal energy is given as follows:

$$\mathbf{dU = \mu_1 dn_1 + \mu_2 dn_2 + TdS - pdV + \gamma dA} \qquad \textbf{(IV-2)}$$

where $\mu_i n_i$ is the chemical work, μ_i is the chemical potential of the polymer i, and n_i is the number of moles of polymer i,

$\mu_i = kT\ln(a_i)$ (k is the Boltzmann constant and a_i is the activity of polymer i),

T is the temperature and S is the entropy,

and pdV and γdA are the mechanical work.

The Gibbs free energy is expressed as follows:

$$\mathbf{G = \mu_1 dn_1 + \mu_2 dn_2 + U + pdV - TS} \qquad \textbf{(IV-3)}$$

which gives:

$$\mathbf{dG = \mu_1 dn_1 + \mu_2 dn_2 - SdT - Vdp - \gamma dA} \qquad \textbf{(IV-4)}$$

At constant temperature T, pressure p and number of moles n_i, the interfacial tension γ is defined by:

$$\gamma = \left.\frac{\partial G}{\partial A}\right|_{T,P,ni} \qquad \textbf{(IV-5)}$$

Based on this expression, the interfacial tension depends on the temperature, the pressure and the composition of each polymer. On the other hand, the system will spontaneously minimise the area of the interface to minimise its energy.

When two polymers are placed in contact with each other and heated to a temperature above their glass transition temperature Tg, macromolecular movements become accessible. The thickness of the interface increases over time, which is not the case if these two polymers are completely immiscible (positive Gibbs free energy) and the penetration of the chain ends of one phase into the other is not favoured; therefore, the chains repel each other, and the interfacial tension, in this case, is high.

IV.3.2. Interfacial phenomena at the polymer/polymer interface

IV.3.2.1. Interdiffusion process

Relevant models for interfacial diffusion have been established in the literature [18, 37, 38]. Interfacial diffusion is a phenomenon that reflects the molecular dynamics at the interface of polymer chains. It is based on models that describe the motion of a single chain or an entangled chain [39, 40], under or without shear [41]. This process depends on the Brownian movements of the chains (which are related to their densities), the rheological behaviour of the polymers and experimental parameters such as contact time and temperature [42].

The mutual diffusion kinetics could also be significantly influenced by the miscibility of the diffused chains expressed by the Flory-Huggins interaction parameter χ [43], which may accelerate or suppress the diffusion kinetics. Therefore, the mutual diffusion between different polymer chains is far more complicated than the self-diffusion of the same chains [44, 45]. In the case of the interdiffusion of polymers of different chemical nature, the diffusion is dominated by the excess enthalpy and entropy of segment-segment mixing [46], and an expression for the mutual diffusion coefficient D_m of polymers A and B can be given by [46]:

$$\boldsymbol{D_m = 2(\chi_s - \chi)\varphi_A\varphi_B D_T = (\frac{\varphi_A}{N_B} + \frac{\varphi_B}{N_A} - 2\chi\varphi_A\varphi_B)D_T} \qquad \textbf{(IV-6)}$$

$$\boldsymbol{\chi_s = \frac{1}{2}(\frac{1}{N_A\varphi_A} + \frac{1}{N_B\varphi_B})} \qquad \textbf{(IV-7)}$$

where χ_s is the interaction parameter at the spinodal of the A/B mixture, D_T is a transport coefficient, χ is the Flory-Huggins interaction parameter, and φ_i and N_i represent the volume fraction and the weight-average degree of polymerisation of component i, respectively.

Note that $\boldsymbol{\varphi_A + \varphi_B = 1}$.

Jones et al. [47] have experimentally determined that the thermodynamic interaction χ influences the interfacial reaction kinetics. For polymer bilayers formed from anhydride-grafted poly(methyl methacrylate) with complementary amine functional polymers (PS-NH_2, PB-NH_2 and PDMS-$(NH_2)_2$), the reaction rate increased as χ decreased. The latter appeared to be determined not by the movement

of the reactive chains through a chemically similar bulk phase, but rather by the movement of reactive chains in a relatively narrow interfacial region [47].

IV.3.2.2. Interdiffusion/reaction duality at the interface

The creation of a reactive interface implies that each polymer contains functions capable of reacting in situ and reversibly with the antagonistic function of the other polymer. Hence, a copolymer occupies the interface (Figure IV-1). If the polymers are immiscible, their coexistence area gradually reduces. The reaction is then confined between the two sub-phases and does not extend into the volume. Therefore, the kinetics of the interfacial reaction is different from that of the bulk reaction [33, 48]. Several researchers such as Fredrickson [37] and O'Shaughnessy [49] have examined the physical aspects of the interfacial reaction, in the absence of flow and especially in the presence of low concentrations of functionalised chains in each phase. They suggested theoretically that the reaction kinetics between two functionalised, low molecular weight polymers is controlled either by the interfacial reaction or by the chain diffusion phenomenon [33]. This is referred to as a diffusion-controlled response (DC regime), as opposed to a reaction-controlled response (RC regime). However, their experimental results were not sufficiently accurate to provide validation of such a theoretical prediction.

Later, Macosko et al. [19], working with reactive multilayer coextruded polymers, experimentally showed that reaction timescales are typically of the order of hours and that the interfacial reaction rate could not be adequately described by the theories of Fredrickson and O'Shaughnessy. They concluded that the interfacial reaction is not a diffusion-controlled reaction but is reaction-limited [33].

Similar results were noted later by Chi et al. [35] using dynamic interfacial tension measurements to probe the kinetics of interfacial reaction between carboxylic-terminal polybutadiene (PBd-COOH) and amino-terminal polydimethylsiloxane (PDMS-NH_2). The authors confirmed that the interfacial reaction is reaction-limited rather than a diffusion-controlled reaction. On the other hand, using FTIR and dynamic rheology, Scot and Macosko investigated the melt reaction between styrene-maleic anhydride copolymer with two different amine-terminated polymers (butadiene-acrylonitrile copolymer and polyamide 11). They demonstrated that the reaction kinetics includes contributions due to both interdiffusion and chemical reaction.

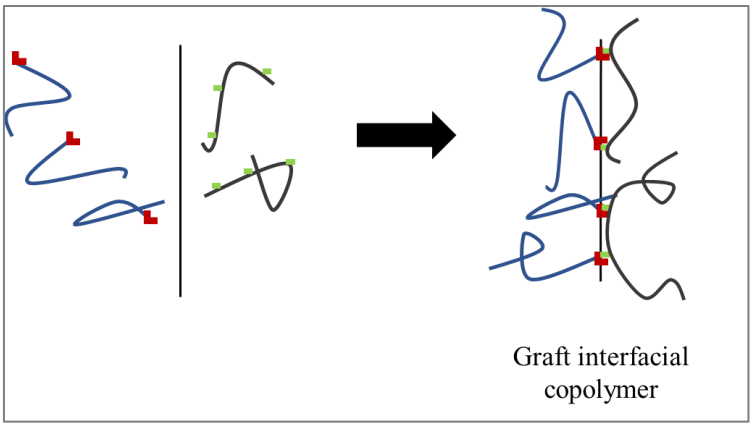

Figure IV-1. Schematic representation of interfacial diffusion/reaction.

IV.4. Experimental

IV.4.1. Materials

In the present work, we used aminopropyl-terminated polydimethylsiloxane with 0.05% aminopropyl pendant groups on the chain (Gelest, United States); polydimethylsiloxane, trimethylsiloxy terminated (Alfa Aesar, United States); and maleic anhydride-grafted polyethylene containing 0.5 wt.% maleic anhydride grafts (Sigma Aldrich, United States). The characteristics of each material are listed in Table IV-1.

Table IV-1. Characteristics of the studied materials.

Material	Polydimethylsiloxane, trimethylsiloxy terminated	Polydimethylsiloxane, aminopropyl terminated		Polyethylene-grafted maleic anhydride
Notation	PDMS	PDMS1-$(PropNH_2)_2$	PDMS2-$(PropNH_2)_2$	PEgMA
Chemical formula	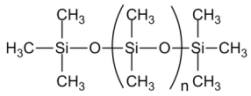	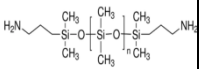	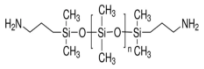	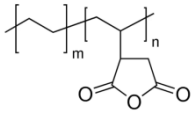
Molar weight Mw (g/mol)	63000[a]	64868[a]	145145[a]	6650[b]
Polydispersity index	1.82[a]	2.13[a]	1.93[a]	2.40[b]

[a]SEC measurements at 23°C in toluene.
[b]SEC measurements at 160°C in trichlorobenzene.

The reaction between maleic anhydride and amine-based polymer systems is called an amidation/imidation reaction [50-52] (Figure IV-2). This reaction has been successfully used for the

compatibilisation of blends and multilayers [17, 47, 52, 53], the amination of polyolefins [54], encapsulation [55] and surface modification [56]. According to Scott and Macosko [51], at typical melt processing temperatures, the reaction between anhydride and amine first creates an amic acid intermediate (amide salt) and then proceeds to imide formation. However, the amidation stage is expected to be rapid compared to the imidization step, which is slow. Therefore, the reaction kinetics from amine/anhydride to amide intermediate and to cyclic imide could be approximated by the kinetics of the amide to imide transformation. This would make it possible to separate the chemical reaction kinetics from the diffusion kinetics.

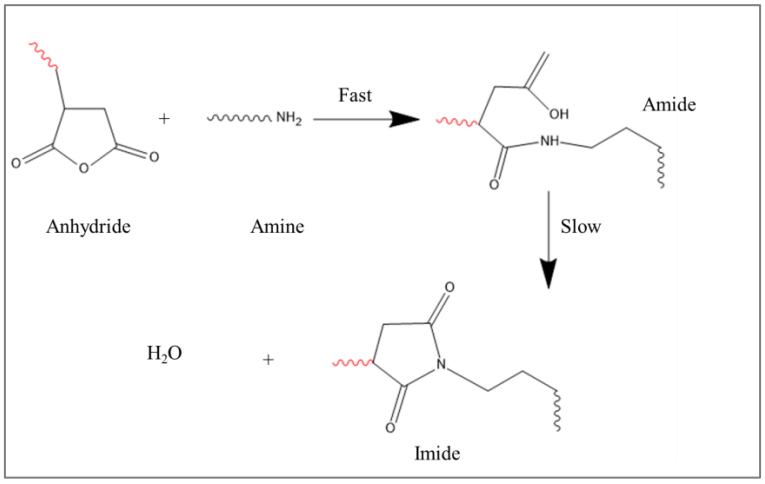

Figure IV-2. Schematic representation of the amidation/imidation reaction between a multifunctional amine and a maleic anhydride reactive group.

IV.4.2. Characterisation methods

IV.4.2.1. Differential scanning calorimetry (DSC)

Differential scanning calorimetry (DSC Q10 from TA Instruments) was used first to measure the melting and crystallisation temperatures of PEgMA and the glass transition temperature (Tg) of PDMS and PDMS-$(PropNH_2)_2$. The following cycle was applied in the DSC apparatus under a nitrogen environment: heating from -70°C to 250°C at 10°C/min, cooling from 250°C to -70°C and finally a second heating ramp under the same conditions.

To measure the reaction enthalpy (ΔH) for a reactive melt blending system, a mixture of 50/50 wt% of PDMS-$(PropNH_2)_2$/PEgMA was heated from -70°C to 250°C at 5, 10 and 20°C/min, with cooling from 250°C to -70°C and finally a second heating ramp under the same conditions to check if the chemical reaction went to completion in the first cycle. ΔH was determined by integration of the area under the exothermic peak.

IV.4.2.2. Thermogravimetric analysis (TGA)

Thermogravimetric analysis (TGA) was performed on a Q500 thermogravimetric analyser (TA instruments). The samples were heated from 30 to 600°C at 10°C/min under nitrogen flow. We also measured the weight variation at the isothermal of 200°C for 2 hours to verify the thermal stability of PDMS, PDMS-$(PropNH_2)_2$ and PEgMA.

IV.4.2.3. Bulk rheological measurements

An ARES-G2 rheometer from TA Instruments with a parallel-plate geometry (of diameter 25 mm) was used to determine the rheological properties of the different bulk phases: PDMS, PDMS-$(PropNH_2)_2$ and PEgMA. Frequency sweeps were performed from 100 to 0.1 rad.s^{-1}. The complex viscosity modulus ($|\eta^*|$) was measured at different temperatures: 120, 130 and 140°C. Time sweep tests at a steady shear rate of 5 s^{-1} for two hours were also performed to examine the thermal stability window of different molten polymers investigated in this study.
Thereafter, inside a disposable 40 mm parallel-plate cup geometry, a mixture composed of 50/50 wt% PDMS-$(PropNH_2)_2$/PEgMA and PDMS/PEgMA was sheared at 5 s^{-1} to study the kinetics of a possible reaction occurring with the evolution of time. The effect of temperature was also studied (at 120, 130 and 140°C).

IV.4.2.4. Rheology coupled to fast-scan FTIR spectroscopy

Fourier transform infrared spectroscopy (FTIR) coupled with rheology makes it possible to pursue in real time the kinetic evolution of the reactive system. The simultaneous combination of these two methods in a single instrument, rather than separate analyses, allows the rheological response to be linked to the structural changes taking place at the molecular scale and, in particular, to the vibration of the functional groups in the bonds. These experiments enable the correlation of the measured viscosity with the rates of the chain reaction. To this end, a 50/50 wt% mixture of PDMS-(Prop-(NH_2))$_2$ and PEgMA was quickly placed in the measuring cell, which had been previously heated to the set temperature. The acquisition speed of the FTIR spectrometer is extremely fast to probe the onset of the reaction at the same time as the rheological tests. This system, known as RHEONAUT, involves the combination of a Thermo Scientific Haake MARS III type rheometer, equipped with a parallel-plate (20 mm) geometry with a transparent window, and a Nicolet IS10 FTIR spectrophotometer with a unique acquisition system. Infrared spectra in the mid-infrared range (400-4000 cm^{-1}) were recorded at a resolution of 4 cm^{-1}. Each spectrum represented a collection of 32 scans. This module consists of a single-reflection diamond optical unit (Figure IV-3) combined with an electrical heater allowing studies on molten polymers up to 400°C. The in-situ infrared data are

collected in attenuated total reflection (ATR) mode. The beam propagates through the crystal to the crystal/sample interface, where it undergoes reflection/absorption and exits the crystal. It is then focused back to the detector by means of mirrors and lenses.

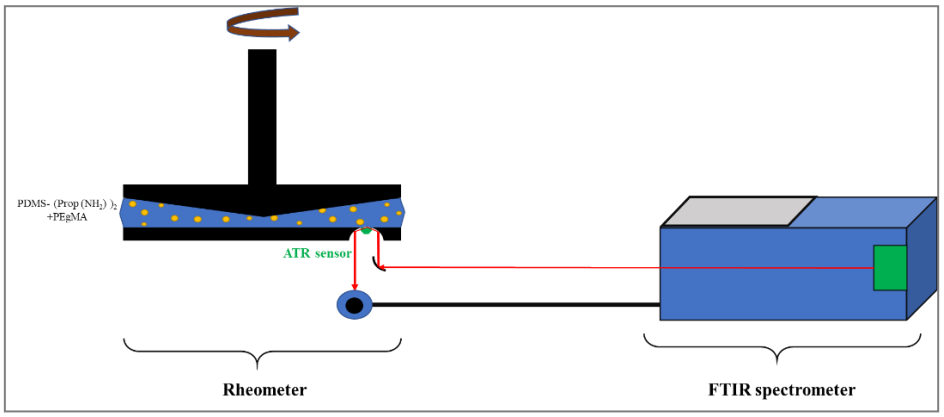

Figure IV-3. Schematic representation of dynamic rheology coupled to fast-scan FTIR.

IV.4.2.5. Interfacial measurements

IV.4.2.5.1. Interfacial shear rheology (ISR)

We studied the interfacial shear properties of the reactive and non-reactive interfaces using the novel biconical setup attached to an MCR 302 rheometer (Figure IV-4). (Titanium bicone (D: 68.28 mm, angle 5°) with a high-temperature interfacial cell) [29].

In this study, a Boussinesq number between 0.2 and 0.6 was obtained. A steady shear rate of 1 s^{-1} was applied in all experiments. The effect of the temperature was investigated as well.

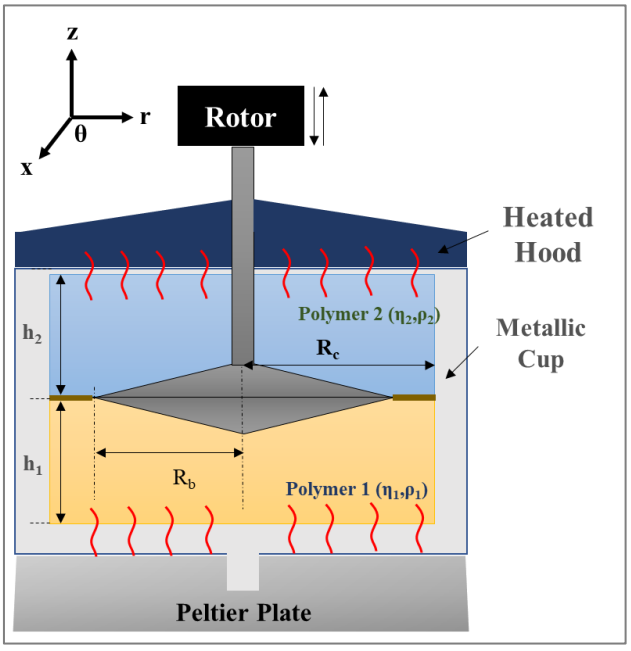

Figure IV-4. Schematic diagram of the biconical interfacial setup.

IV.4.2.5.2. Interfacial tension measurements

The interfacial tension measurements were performed at different temperatures (120,130 and 140°C) using an automatic drop tensiometer (TRACKER-H from TECLIS Instruments, France). We used a newly home-designed stainless steel syringe to resist high temperatures. It was equipped with a U-shaped needle to form a rising drop inside the continuous phase (Figure IV-5). From the digital analysis of a melting drop, the profile was acquired by a high-speed CCD camera, and characteristic parameters of the interfaces (area, volume, interfacial tension) were determined in real time. Following the variation of interfacial tension with time can enable the probing of polymer-polymer interfaces in order to characterise the kinetics of an interfacial response at the drop scale. In this work, we chose to use polymer systems of relatively low melt viscosities, to avoid long measurement times for interfacial tensions.

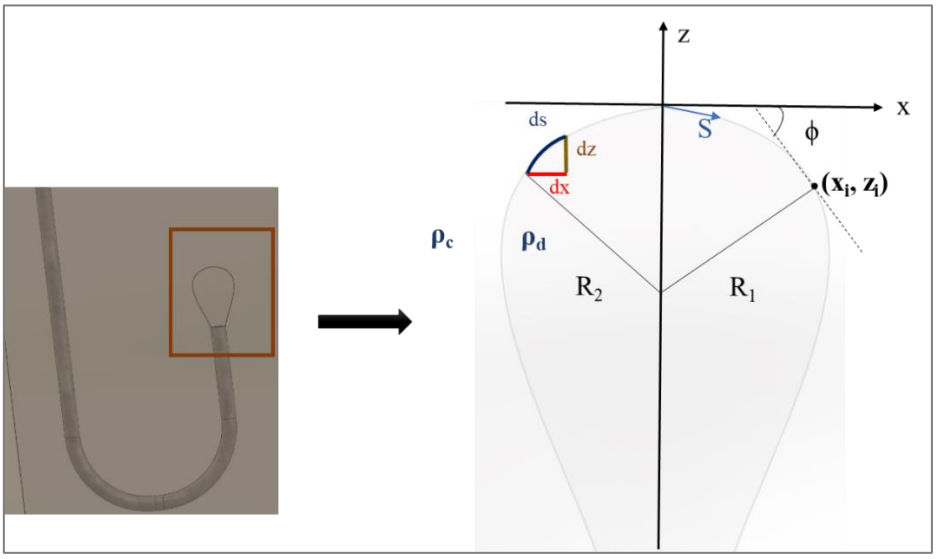

Figure IV-5. Schematic diagram of the characteristics of the rising drop.

In this study, the Bond number B_d values varied between 0.3 and 0.6.

IV.5. Results

IV.5.1. Thermal properties of reactive and non-reactive polymer systems (DSC)

The reaction between the amino group and the maleic anhydride function is exothermic. Figures IV-6 and IV-7 display the non-isothermal DSC scans of the samples at different heating/cooling rates. For both PDMS1-$(PropNH_2)_2$/PEgMA and PDMS2-$(PropNH_2)_2$/PEgMA, we observed an exothermic peak

around 200°C during the first cycle. This peak was shifted towards higher or lower temperatures when we respectively increased or decreased the heating rate. However, the reaction enthalpy ΔH_{react} obtained by integrating the area under the exothermic peak was the same (11.2 J/g) regardless of the heat flow rate applied. In addition, this exothermic peak was not detected during the second heating cycle. This suggests that the reaction between maleic anhydride and amino groups was finished at the end of the first heating step, which is explained by the chemical function's stoichiometric ratio (more maleic anhydride function than amino function). A PDMS/PEgMA non-reactive system sample was also tested, and there was no exothermic reaction (Figure IV-8).

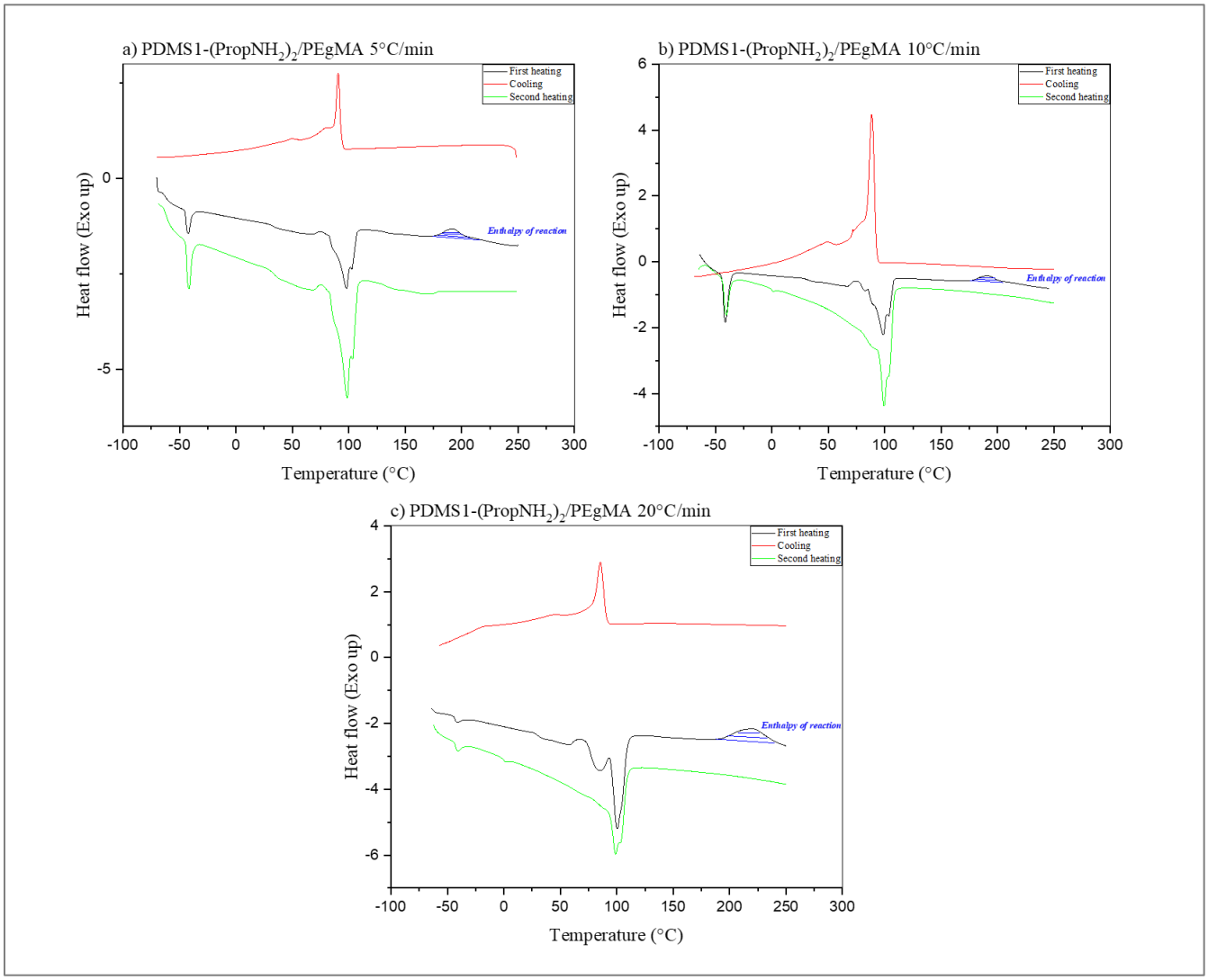

Figure IV-6. A series of DSC curves for PDMS1-$(PropNH_2)_2$/PEgMA at different heating/cooling rates. a) 5°C/min, b) 10°C/min and c) 20°C/min.

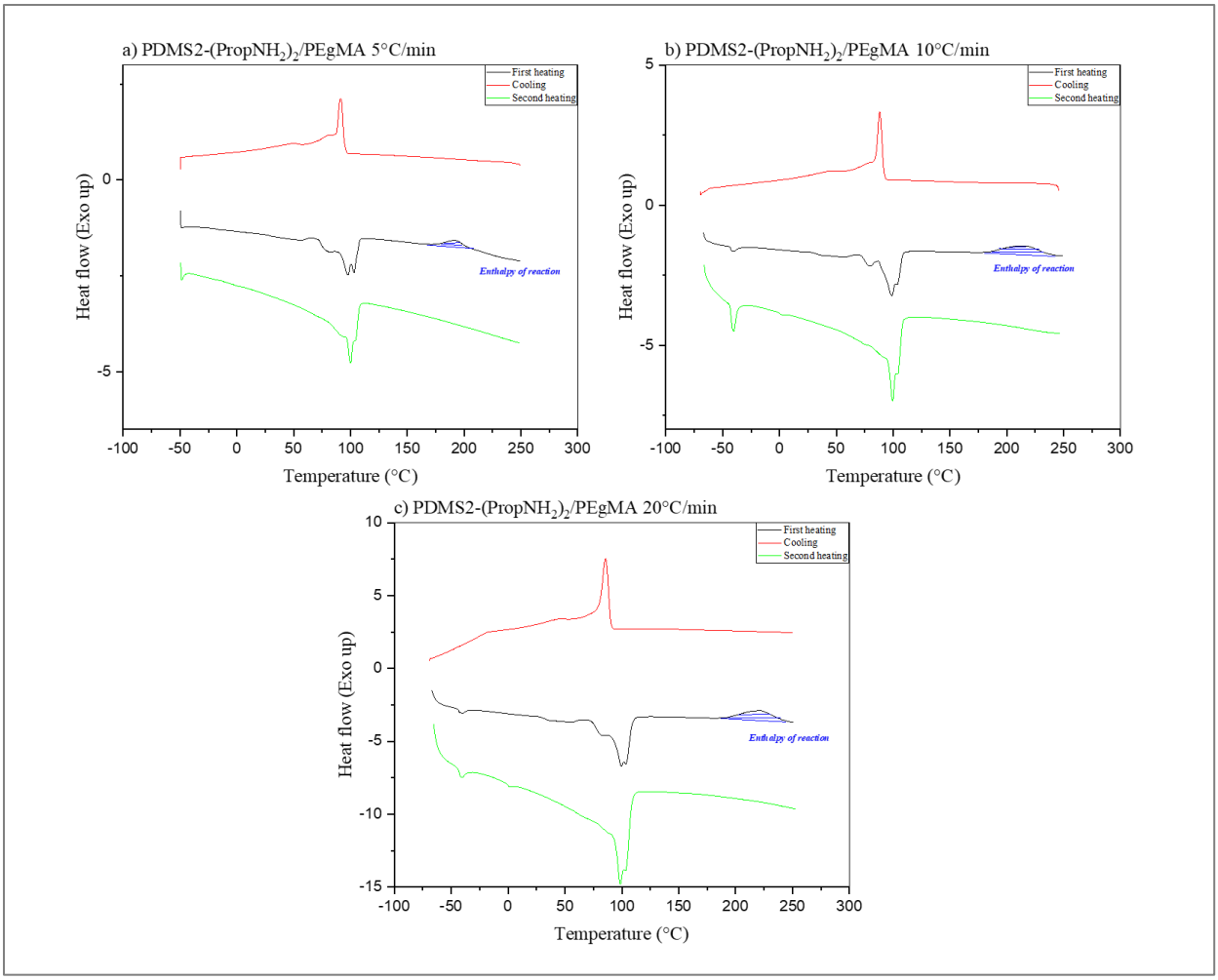

Figure IV-7. A series of DSC curves for PDMS2-(PropNH$_2$)$_2$/PEgMA at different heating/cooling rates. a) 5°C/min, b) 10°C/min and c) 20°C/min.

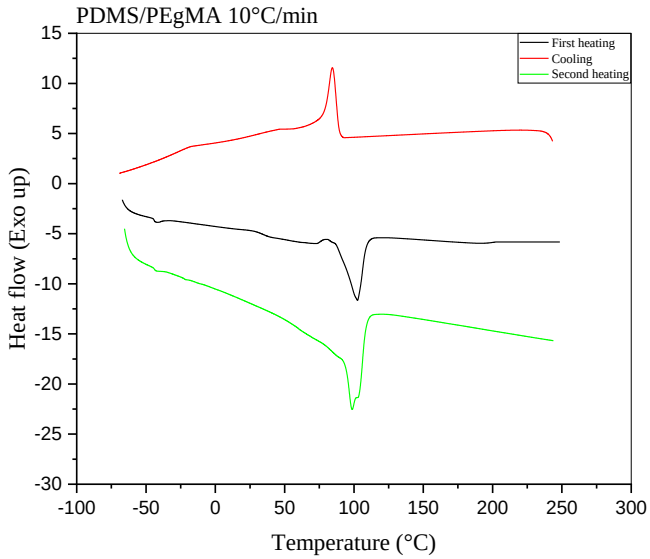

Figure IV-8. DSC curve for PEgMA at heating/cooling rates of 10°C/min.

We also compared these DSC curves with each pristine material (Figure IV-9), and no peaks were revealed in the investigated temperature region. The glass transition temperature of PDMS (an amorphous material) and the melting and crystallisation temperatures of PEgMA (a semi-crystalline material) are provided in Table IV-2.

Table IV-2. Thermal characteristics of the studied polymers over the first heating cycle.

	PDMS	PDMS1-(PropNH$_2$)$_2$	PDMS1-(PropNH$_2$)$_2$	PEgMA
Tg (°C)	-42.2	-38.3	-37.1	-105.4
Tm (°C)	-	-	-	110.1
Tc (°C)	-	-	-	87.2

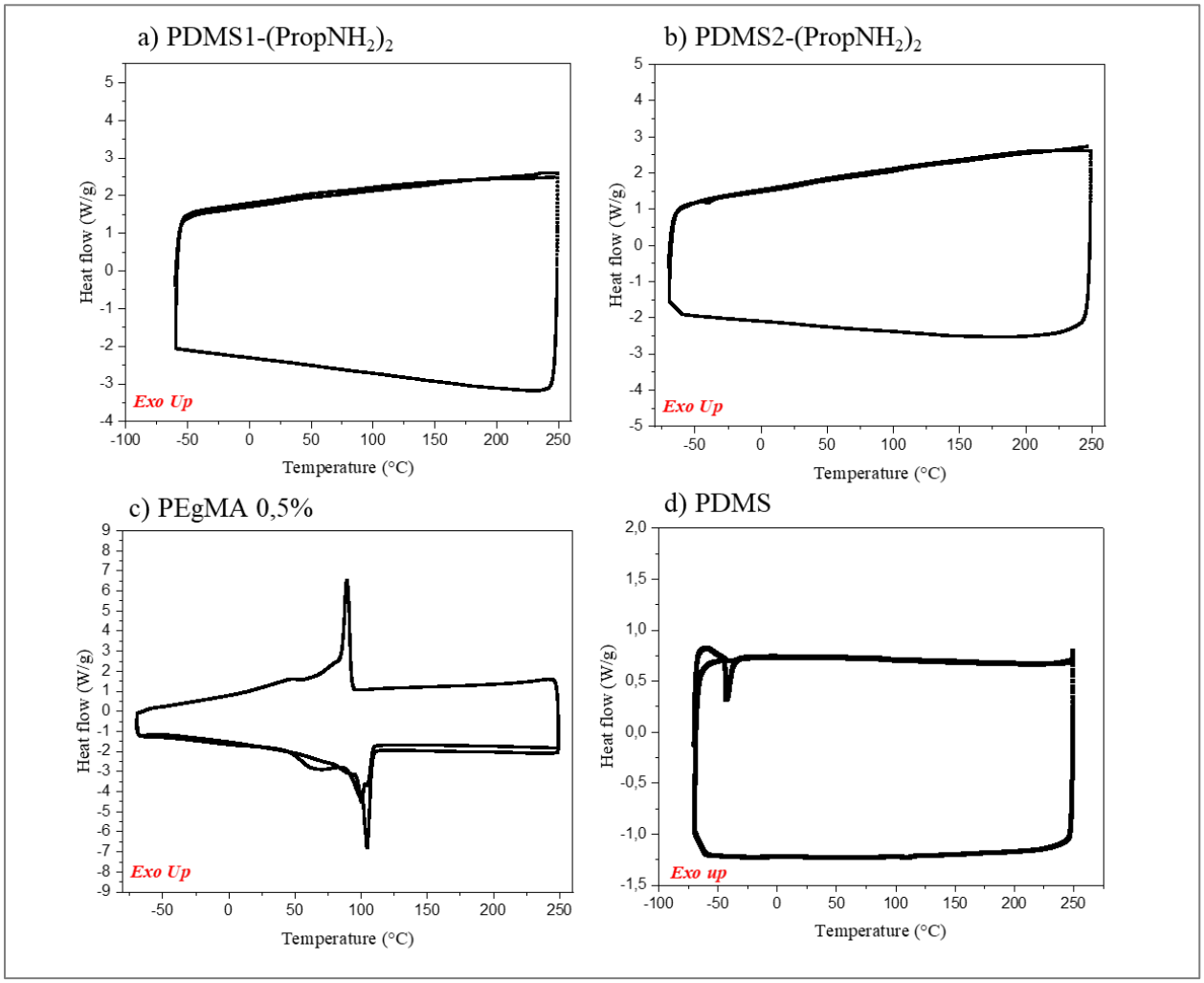

Figure IV-9. A series of DSC curves for PDMS1-(PropNH$_2$)$_2$ (a), PDMS2-(PropNH$_2$)$_2$ (b), PEgMA (c) and PDMS (d) at heating/cooling rates of 10°C/min.

IV.5.2. Fast-scan FTIR analyses at the molten state

First, PDMS-(PropNH_2)$_2$ and PEgMA were analysed. As shown in the IR spectra (Figure IV-10), most characteristic peaks correspond to C-C, Si-O, C-H and C-C bonds for PDMS-(PropNH_2)$_2$, and C-C, C-H, C-O and C=O for PEgMA are present. The intensity of the maleic anhydride bond peaks (1710 and 1780 cm^{-1}) is small because of the low maleic anhydride content (0.5 wt%). However, the peaks of the N-H stretch at 3200 cm^{-1} and C-N stretch at 1280 cm^{-1} were not detected for PDMS-(PropNH_2)$_2$. After melt mixing these components, the chemical reaction was initiated. The viscosity of the reactive melt blends increased with the shear time, as shown in the dynamic rheology section.

Nevertheless, following the appearance/disappearance of the characteristic IR bond peaks was not straightforward. Due to the low amounts of maleic anhydride (0.5 wt%) and amine (0.05 wt%), most of the characteristic peaks in the region of interest were not identified for each material nor for the product of the reaction (Figure IV-11). As a result, FTIR spectroscopy was not sensitive enough to observe the difference in the intensities of the peaks. This shows the limit of this technique for following a reaction in the case of a low concentration of reactive functions.

The chemical reaction between maleic anhydride and amine was studied in the literature by different authors using FTIR spectroscopy [57-59]. Hameed et al. [58] investigated reactions of low molecular weight, highly functionalised maleic anhydride-grafted polyethylene with polyetherdiamine. The FTIR spectra showed that significant absorbances due to anhydride were present before the reaction (1715, 1780 and 1860 cm^{-1}), corresponding to the PEgMA before the melt blending with polyetherdiamine. The final product after reaction was also analysed by FTIR. A decrease in absorbance at 1860 cm^{-1} and the disappearance of absorbances at 1780 and 1715 cm^{-1} due to the consumption of MA and the development of new absorbances at 1700, 1770, 1550, and 1645 cm^{-1} suggested a significant reaction between MA and amine. New absorbances at 1700 and 1770 cm^{-1} were ascribed to the formation of imide. The same result should be found when increasing the percentage of maleic anhydride and amine function for our products. Nonetheless, due to the rapidity of the reaction with these highly reactive systems, it is very difficult to follow the reaction using interfacial shear rheology or interfacial tension measurements, which is the main subject of the present work.

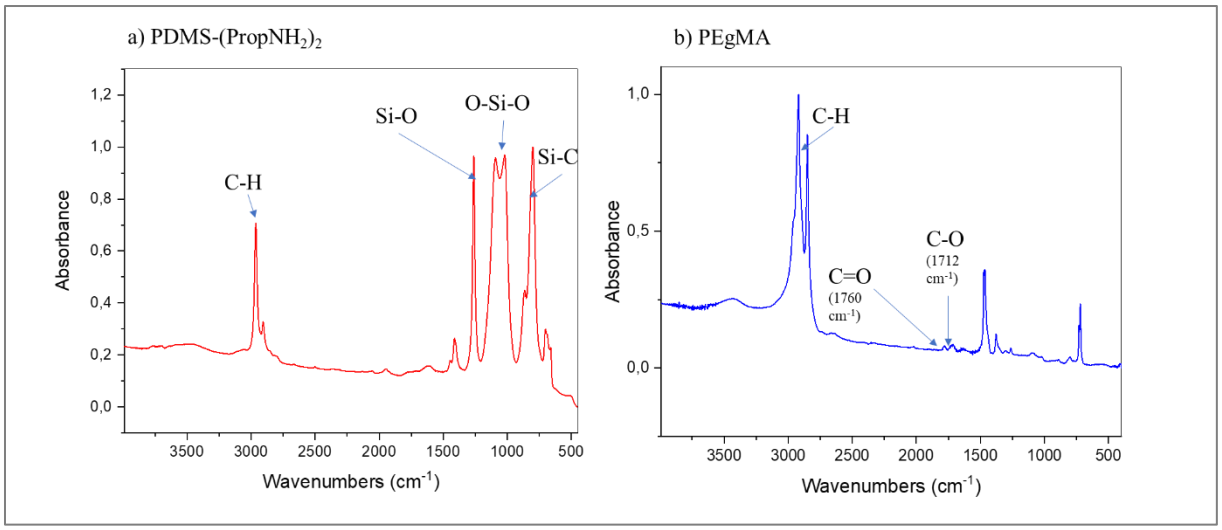

Figure IV-10. FTIR spectra of PDMS-(PropNH$_2$)$_2$ (a) and PEgMA (b).

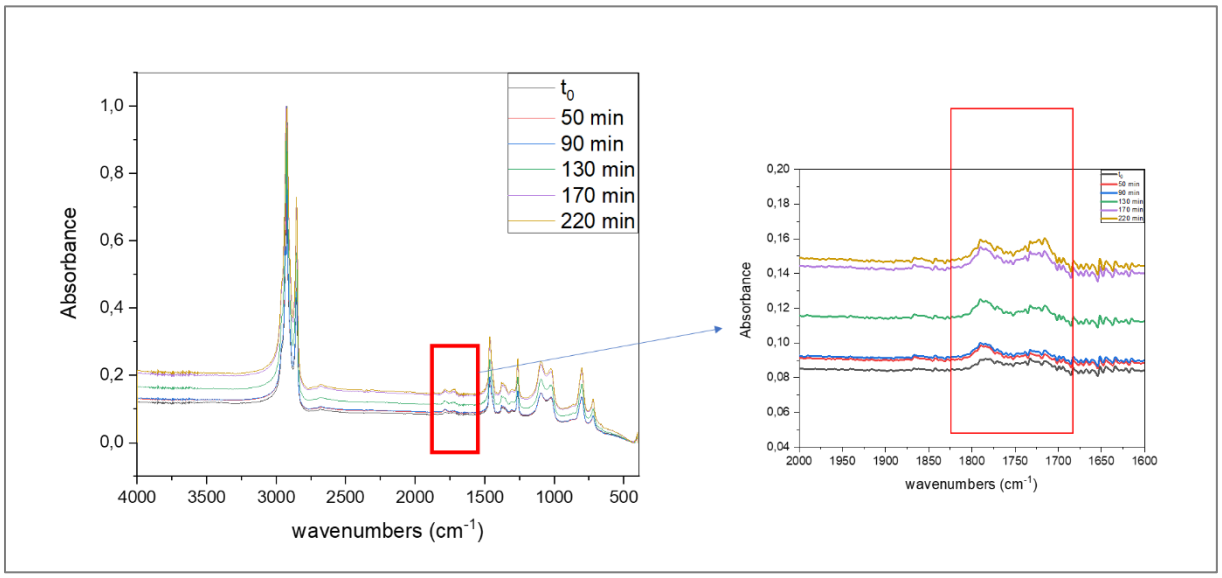

Figure IV-11. (left) FTIR spectra at 140 °C of the PDMS-(PropNH$_2$)$_2$/PEgMA blend at different scanning times. (right) A magnification zoom in the 1680-1820 cm^{-1} zone.

In this work, the investigation of the melt reaction in highly reactive functional PDMS-(PropNH$_2$)$_2$/PEgMA systems used as controls was also performed using FTIR analyses. A reactive polymer blend system composed of 50/50 wt% PDMS-(Prop(NH$_2$)$_2$) with 3.2% aminopropyl functions (reference: Gelest DMS-A11) and PEgMA (reference: Clariant Licocene® PE MA 4351) with 7.0 wt% maleic anhydride grafts was prepared by melt blending at 180°C for 90 min under a steady shear of 5 s^{-1} on an ARES-G2 rheometer (parallel plate, D = 40 mm). Figure VI-12 shows the FTIR spectra of pure PDMS-(Prop(NH$_2$)$_2$), pure PEgMA and the PDMS-(Prop(NH$_2$)$_2$)/PEgMA blend in the 800–4000 cm^{-1} range. One can observe the presence of significant absorbance peaks (1710, 1782 and 1862 cm^{-1}) due to anhydride, corresponding to the pure PEgMA before the reaction with PDMS-(Prop(NH$_2$)$_2$). The final PDMS-(Prop(NH$_2$)$_2$)/PEgMA blend after the melt reaction shows the disappearance of the absorbance peak at 1862 cm^{-1} and a decrease in absorbances at 1782 and 1710

cm^{-1} due to the consumption of maleic anhydride species. In addition, we note the appearance of new absorbance peaks at 1542, 1579 and 1665 cm^{-1} that suggest the occurrence of a significant reaction between maleic anhydride and amine. New absorbances at 1702 and 1775 cm^{-1} are attributed to the formation of imide.

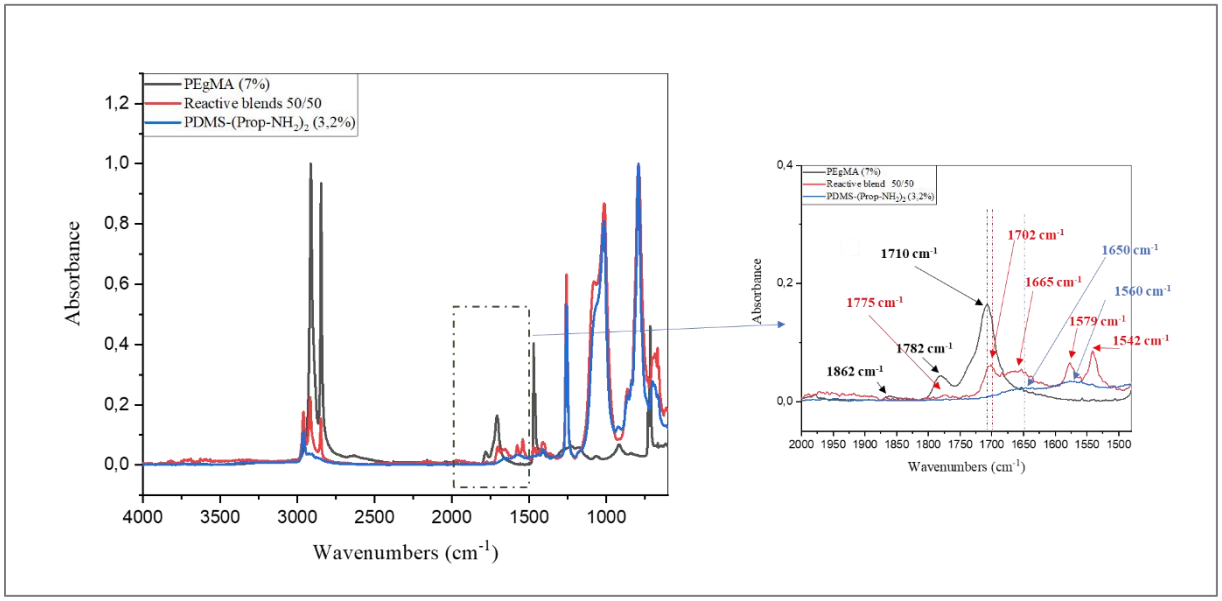

Figure IV-12. (left) FTIR spectra at 25°C of PDMS-(PropNH$_2$)$_2$(3.2%), PEgMA (7%) and the reactive blend. (right) A magnification zoom in the 2000-1500 cm^{-1} zone.

IV.5.3. Thermogravimetric analyses of the studied polymer systems

Thermogravimetric analysis (TGA) is a complementary technique that can determine the decomposition temperature and thermal stability during an isothermal measurement. The evolution of weight as a function of temperature is presented in Figure IV-13, and the decomposition temperatures are summarised in Table IV-3.

Table IV-3. Decomposition temperature of the studied materials.

Material	PDMS1-(PropNH$_2$)$_2$	PDMS2-(PropNH$_2$)$_2$	PEgMA	PDMS
Decomposition temperature (°C)	322.1	341.2	350.8	311.5

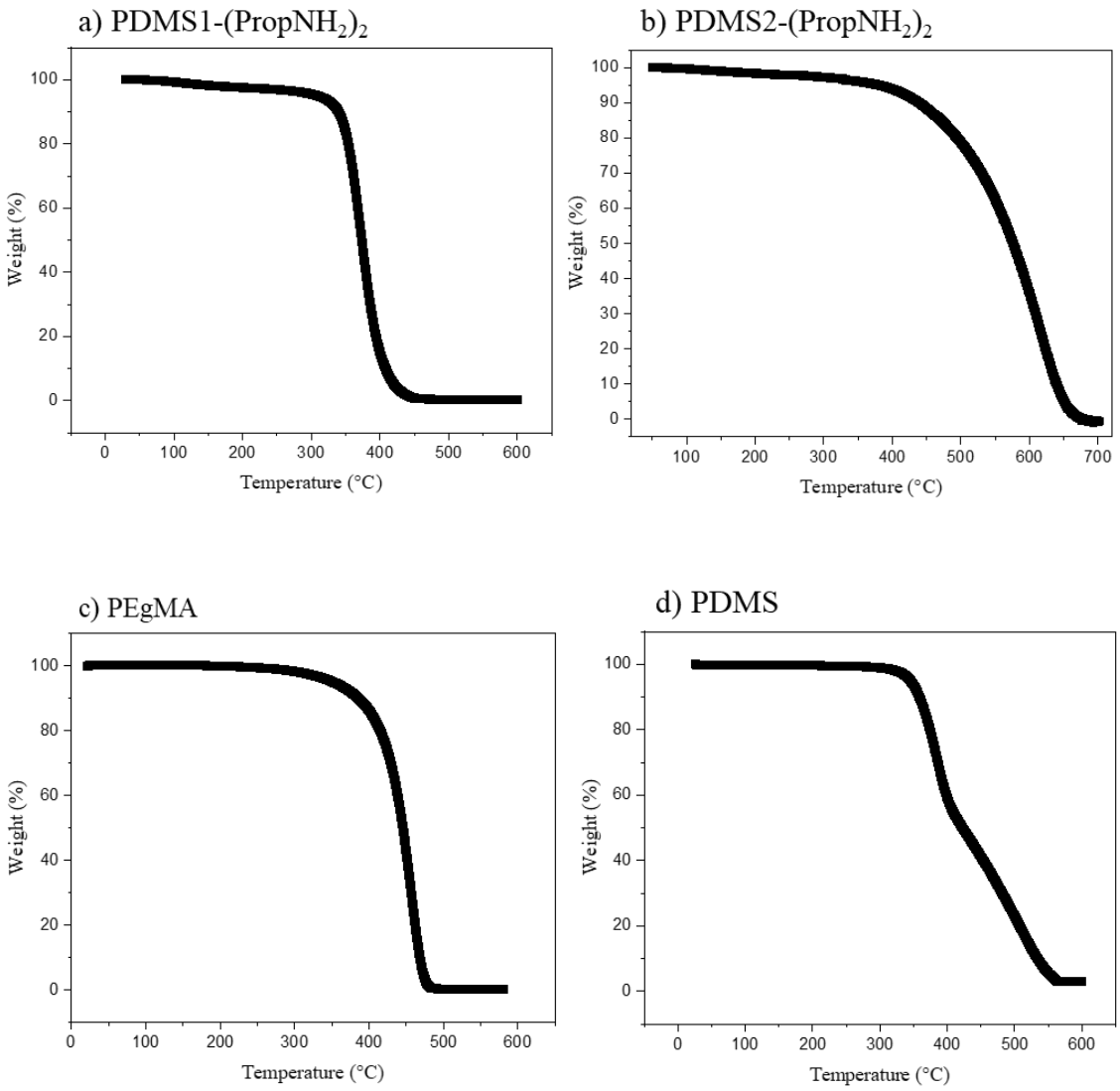

Figure IV-13. TGA curves of PDMS1-(PropNH$_2$)$_2$ (a), PDMS2-(PropNH$_2$)$_2$ (b), PEgMA (c) and PDMS (d).

Other tests were carried out to examine the thermal stability of each material at a constant temperature of 200°C for two hours. Figure IV-14 shows the evolution of weight as a function of time. The studied polymers display good thermal stability, and the weight loss is lower than 3% at the end of the experiment. This information is important for quantifying the degradation while measuring interfacial tension, as seen in the next section.

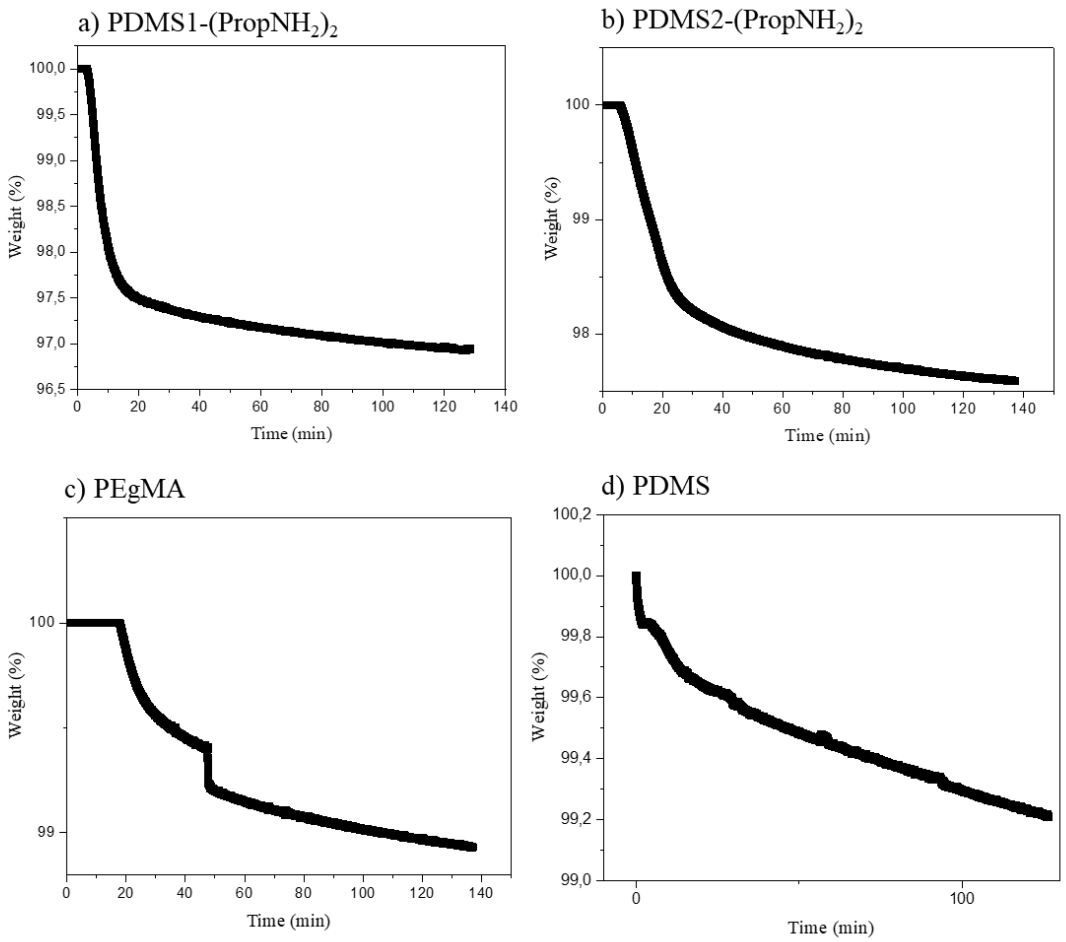

Figure IV-14. TGA curves of PDMS1-(PropNH$_2$)$_2$ (a), PDMS2-(PropNH$_2$)$_2$ (b), PEgMA (c) and PDMS (d) at 200°C for two hours.

IV.5.4. Bulk rheological properties of the studied polymer systems

In this section, rheological measurements were used for many purposes. First, we determined the zero-shear viscosity of the pristine materials, which enables a correction for the contribution of the sub-phases in the interfacial shear rheological measurements. Figure IV-15 shows the master curves of the studied polymers. Both of the functionalised PDMS (PDMS1-(PropNH$_2$)$_2$ and PDMS2-(PropNH$_2$)$_2$) are Newtonian at low frequency. However, they exhibit a slight shear-thinning after 30 rad/s. PEgMA-0.5wt% and PDMS are Newtonian in the studied frequency range. Table IV-4 summarises the zero-shear viscosity η_0 of each polymer at 130°C.

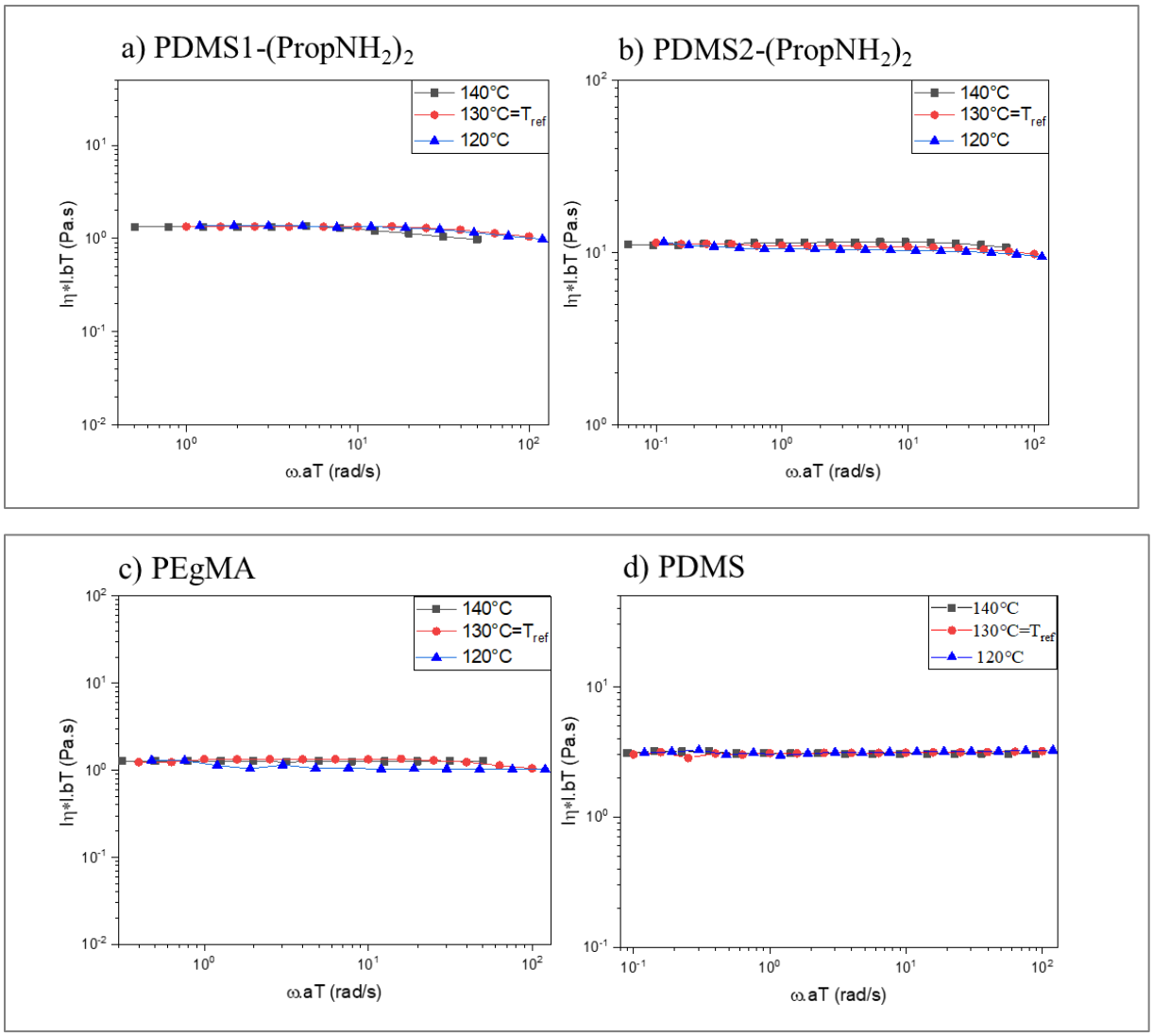

Figure IV-15. Frequency sweep curves of PDMS1-(PropNH$_2$)$_2$ (a), PDMS2-(PropNH$_2$)$_2$ (b), PEgMA (c) and PDMS (d).

Table IV-4. Zero-shear viscosity of the studied materials at 130 °C.

Material	PDMS1-(PropNH$_2$)$_2$	PDMS2-(PropNH$_2$)$_2$	PEgMA	PDMS
η_0 (Pa.s)	1.8	12.5	1.3	3.2

Thereafter, the rheological tool was used to check the thermal stability of different molten polymers. This characterisation is essential before studying the melt reactivity of the defined polymer systems. The material needs to be thermally stable during the measurement of interfacial shear viscosity. Figure IV-16 displays the evolution of the viscosity of the studied polymers at 140°C while applying a constant shear rate of 5 s^{-1} for 7200 s. It can be seen that their viscosities remained constant over time.

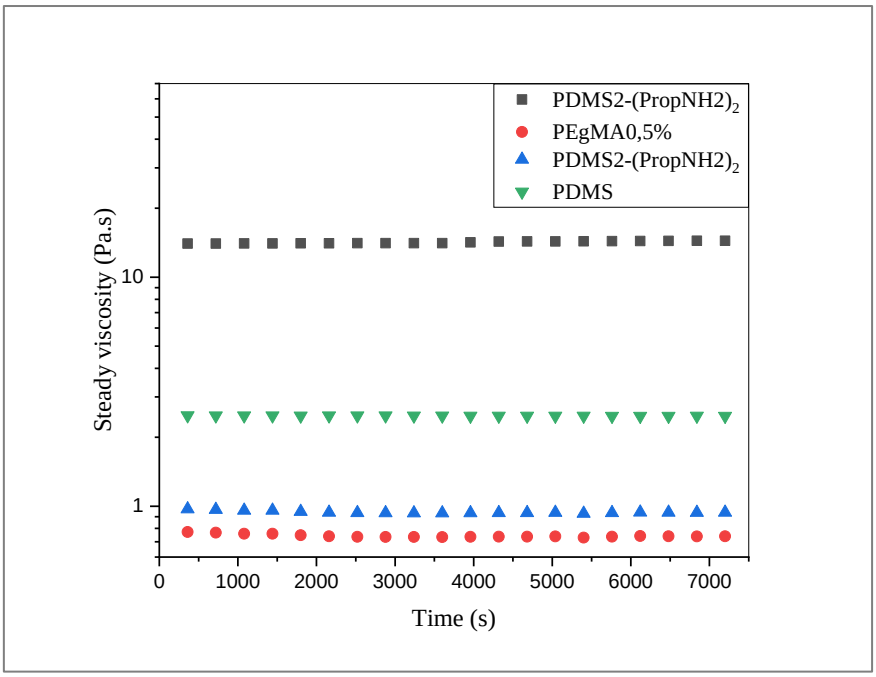

Figure IV-16. Thermal stability of the studied materials.

The kinetics of the reaction between functionalised PDMS and the PEgMA was carried out by mixing them in-situ in the lower parallel cup plate at a constant shear rate of 5 s^{-1}. Figure IV-17 shows that the viscosity of the blend increased significantly and then reached a plateau. This rise in viscosity is related to the chemical reaction between PDMS-$(PropNH_2)_2$ and PEgMA, resulting in a more viscoelastic compound [19]. The reaction became faster when the temperature increased. For the PDMS1-$(PropNH_2)_2$/PEgMA, we reached a high blend viscosity value compared to the one obtained with the high-viscosity PDMS2-$(PropNH_2)_2$/PEgMA reactive system, where the equilibrium melt viscosity was lower. This could be explained by the slow mobility of the PDMS2-$(PropNH_2)_2$ due to its high molecular weight. Furthermore, it is important to remember that the rheometer is not a perfect mixer that ensures a total homogenous chemical reaction between the two phases, especially when the viscosity ratio is high (PDMS2-$(PropNH_2)_2$ and PEgMA). We also studied the evolution of the viscosity of the PDMS/PEgMA blend as a control. As shown in Figure IV-17, the viscosity of the PDMS/PEgMA blend is almost constant over time, which proves that no reaction takes place between unfunctionalised PDMS and PEgMA.

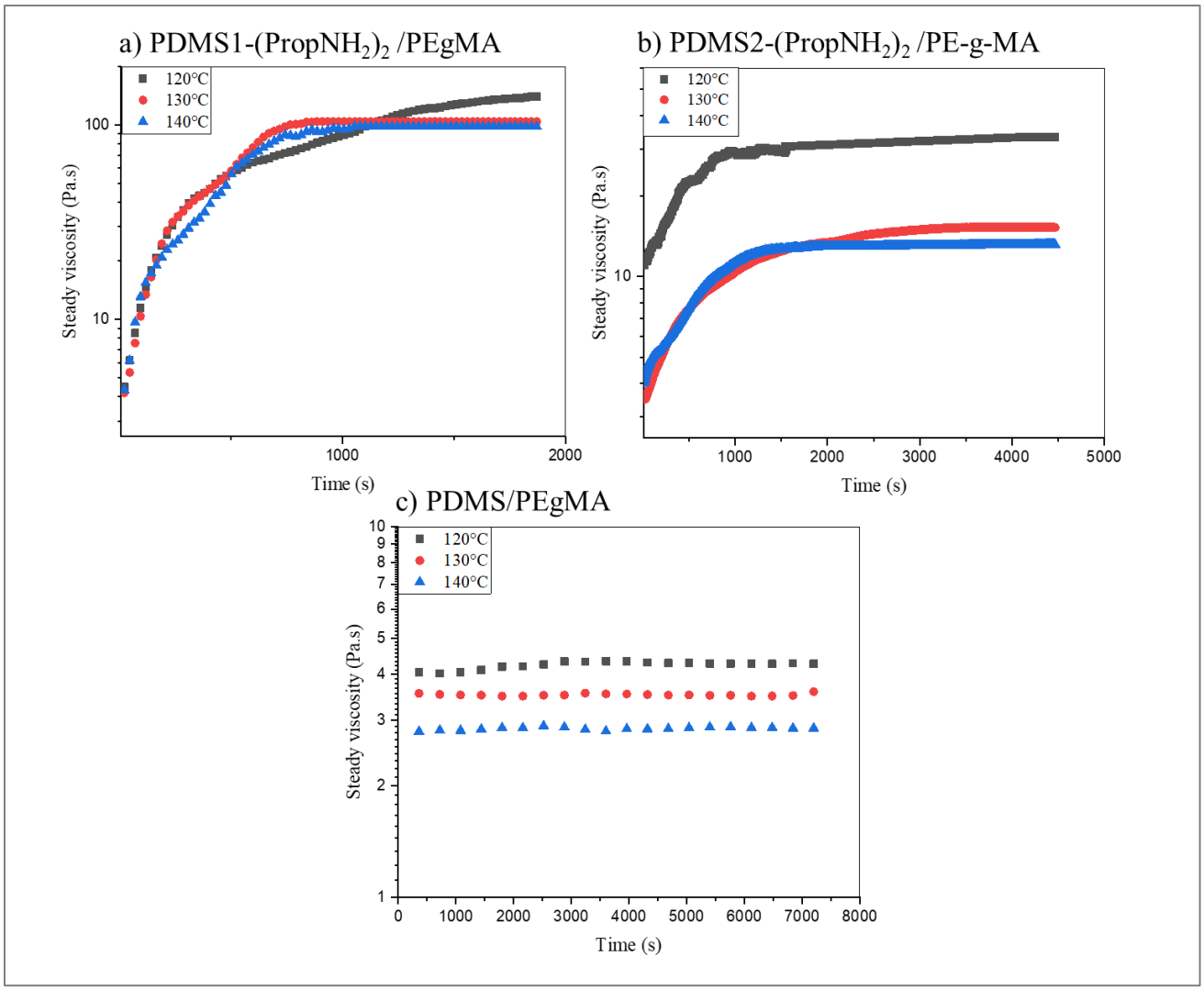

Figure IV-17. Steady time sweep of reactive and non-reactive systems: a) PDMS1-$(PropNH_2)_2$/PEgMA, b) PDMS2-$(PropNH_2)_2$/PEgMA and c) PDMS/PEgMA at 120, 130 and 140°C.

IV.5.5. Interfacial rheological properties of reactive and non-reactive polymer systems

IV.5.5.1. Interfacial shear rheological properties

Interfacial shear rheology is a sensitive method used to reveal any change in the viscoelastic properties of the interface. To the best of our knowledge, studies investigating high-temperature interfacial shear rheology applied to reactive polymer systems are non-existent. In this work, we tried to probe this kind of interface using our interfacial rheological tool. Figure IV-18 exhibits the variation of the steady interfacial shear viscosity as a function of time while applying a low constant shear rate of 1 s^{-1}. The calculated Boussinesq number in our experiments varied from 0.2 to 0.6, so the values of the interfacial shear viscosity presented here are the values after correction for the contribution of bulk sub-phases.

For reactive systems, interfacial shear viscosity increased, and the interface between PDMS-$(PropNH_2)_2$ and PEgMA became more viscoelastic. This is linked to the formation of an interfacial layer between the sub-phases with a solid-like rheological behaviour (Figure IV-18). The kinetics of this rise in interfacial viscosity is directly dependent on the molecular weight and the temperature. The plateau was reached rapidly by increasing the temperature and decreasing the viscosity of the PDMS-$(PropNH_2)_2$ phase. These two parameters control the interdiffusion of the small chains towards the interface, thereby delaying or accelerating the first stage of the interfacial reaction. The diffusion of the chains controls the kinetics at the interface over a short time period, because the reaction between the amine group and the maleic anhydride is known to be extremely fast, especially the first step to form the amide function [50]. Nevertheless, the kinetics becomes too slow (almost a plateau) at long reaction times, which corresponds to the imidization step of the reaction [51].

To define the reaction's order, the apparent conversion X(t) [60, 61] of the in situ formed copolymers at the interface could be defined as:

$$\mathbf{X(t)=}\frac{\boldsymbol{\eta_{int}(t)-\eta_{int}(t=0)}}{\boldsymbol{\eta_{int}(t=t_{final})-\eta_{int}(t=0)}} \qquad \textbf{(IV-8)}$$

Where η_{int} (t=0), η_{int} (t) and η_{int} ($t=t_{final}$) are the initial interfacial viscosities at t=0, the interfacial viscosities at t and the final interfacial viscosities. As shown in the figure VI-19, the variations of -Ln (1-X(t)) for both systems are linear (equation IV-9). We talk about first order reaction. The slope of these lines increases with the temperature and decreases with the viscosity.

$$\mathbf{-Ln\left(1-X(t)\right)=kt} \qquad \textbf{(IV-9)}$$

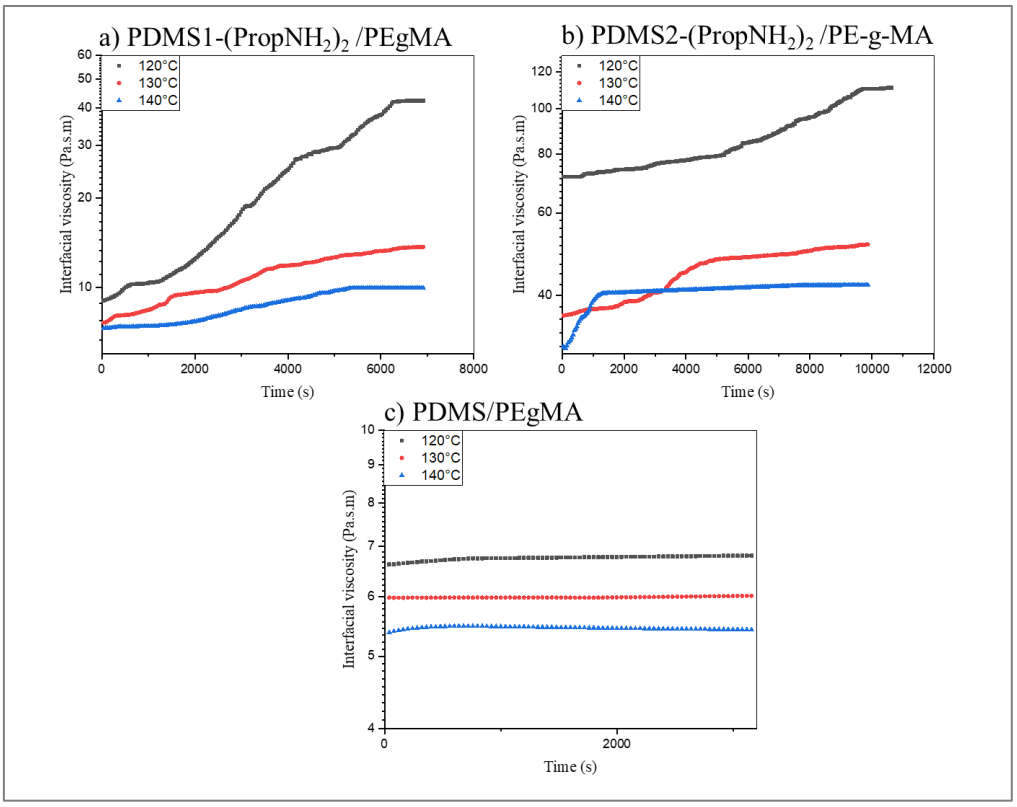

Figure IV-18. Steady interfacial shear viscosity of reactive and non-reactive systems: a) PDMS1-$(PropNH_2)_2$/PEgMA, b) PDMS2-$(PropNH_2)_2$/PEgMA and c) PDMS/PEgMA at 120, 130 and 140°C.

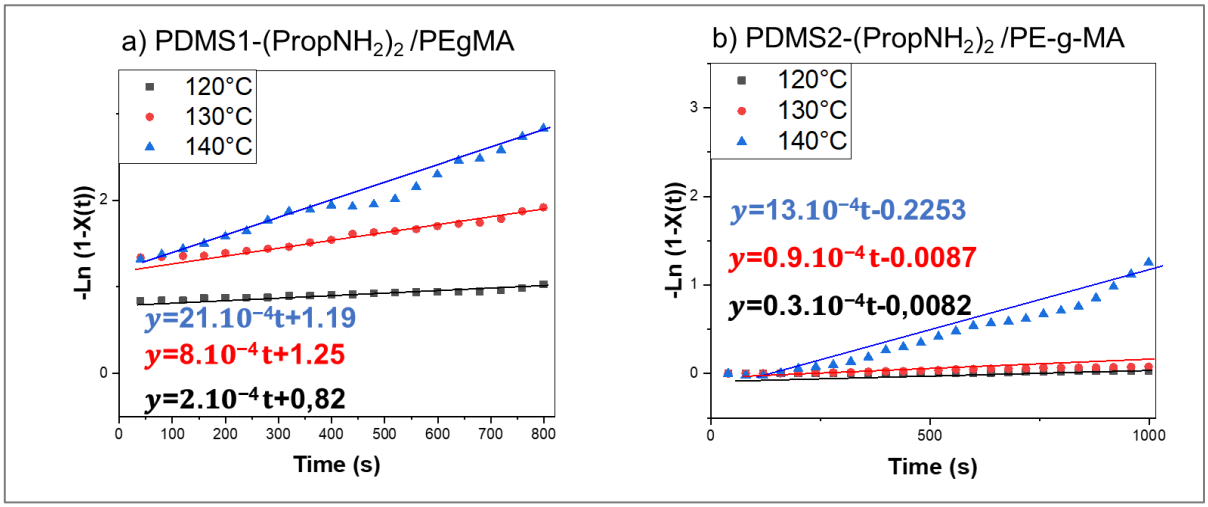

Figure IV-19. The conversion as a function of the reaction time according to first-order kinetics given by Eq. IV-9 of reactive systems: a) PDMS1-$(PropNH_2)_2$/PEgMA and b) PDMS2-$(PropNH_2)_2$/PEgMA.

It is also relevant to note that when the PE-g-PDMS graft copolymer (Figure IV-20) forms at the interface with increasing reaction time, energy develops at the interface, which acts as a barrier to chain interdiffusion until the interface is saturated (Figure IV-21). This energy is generated by the orientation/location of the chain ends of each homopolymer at the interface. It is a function of the

molecular weight of the copolymer. The residual homopolymers must thus adopt a stretched configuration of low entropy in order to cross the copolymer brush at the interface. The higher this activation energy, the longer the chains [62].

The interfacial shear viscosity (ηint) in the case of the non-reactive PDMS/PEgMA interfaces reached a steady-state value within a short time (about 4 min). We observed that η_{int} decreased when the temperature increased. This was expected for a non-reactive immiscible polymer system such as PDMS/PEgMA [63].

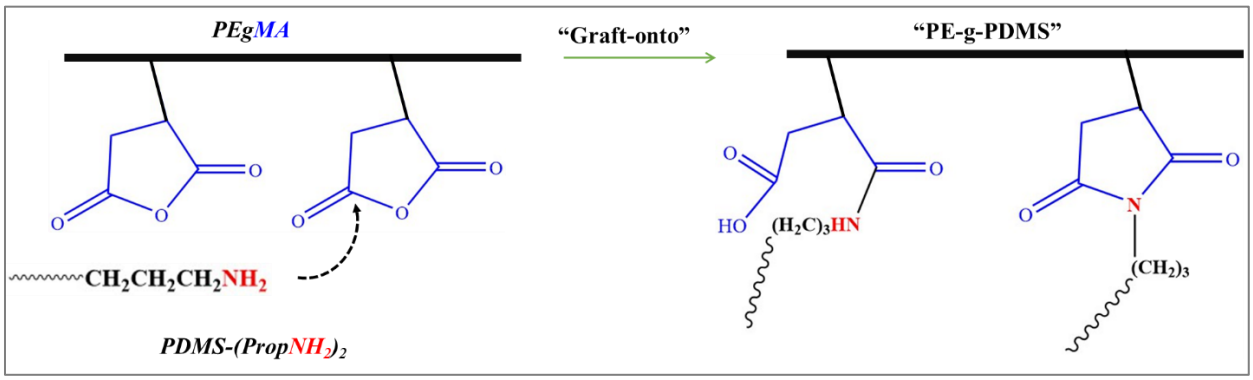

Figure IV-20. Formation of PE-g-PDMS copolymer by a graft-onto mechanism.

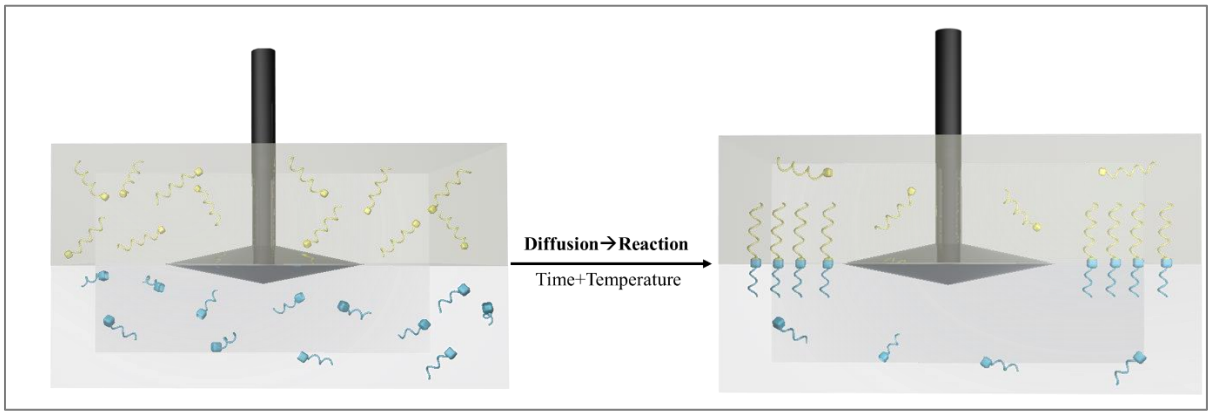

Figure IV-21. Schematic diagram of the diffusion/reaction phenomena at the interface within the biconical setup.

The diffusion at the interface was already studied by Pandit et al. [64] using the bicone to highlight the formation of a surface biofilm of an aqueous solution of bacteria, proteins, DNA and polysaccharides. By following the variation of the surface elastic modulus G', they demonstrated that the interface becomes more elastic after several hours.

As previously mentioned for the reactive PDMS-(PropNH_2)$_2$/PEgMA systems, the interface will be saturated after the diffusion/reaction phenomena. However, the measurement was carried out in the steady shear mode. Thus, applying a constant rotation might be responsible for creating an interfacial layer that hangs on and climbs up the axis of the biconical geometry against the force of gravity

(Figure IV-22). This is due to the Weissenberg effect [65], which indicates that the interfacial layer is viscoelastic. The interfacial shear viscosity will continue to rise until the reaction between the entire sub-phases is completed.

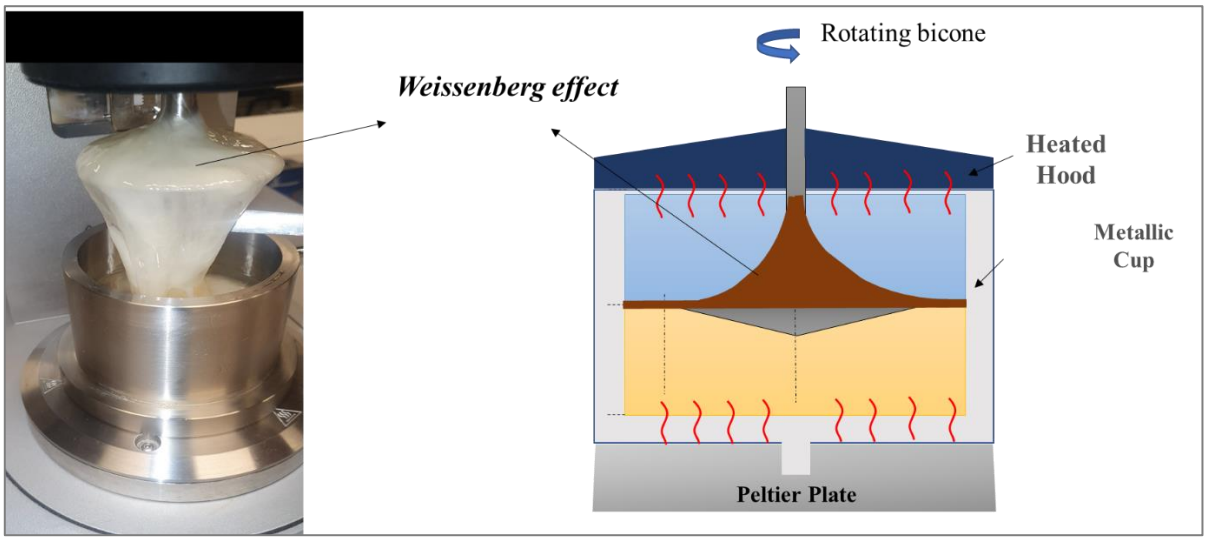

Figure IV-22. Weissenberg effect observed at the PDMS2-$(PropNH_2)_2$/PEgMA interface at 140°C.

This interfacial layer was collected, and its rheological properties were studied. To do this, a dynamic frequency sweep was performed. It has been seen that the interfacial layer presents a solid-like behaviour. The elastic modulus G' is higher than the loss modulus G" in the studied frequency range, and the material presents a high viscosity with shear-thinning behaviour compared to the PEgMA and PDMS1-$(PropNH_2)_2$ (Figure IV-23). The interfacial reaction leads to the formation of a cross-linked network that is more elastic than the pristine polymer phases. Similar rheological behaviour was observed by DeLeo et al. [66] when investigating the interfacial reaction between amine-functional polydimethylsiloxane and maleic anhydride-functional polyisoprene. They showed that the interface formed exhibited a solid-like behaviour.

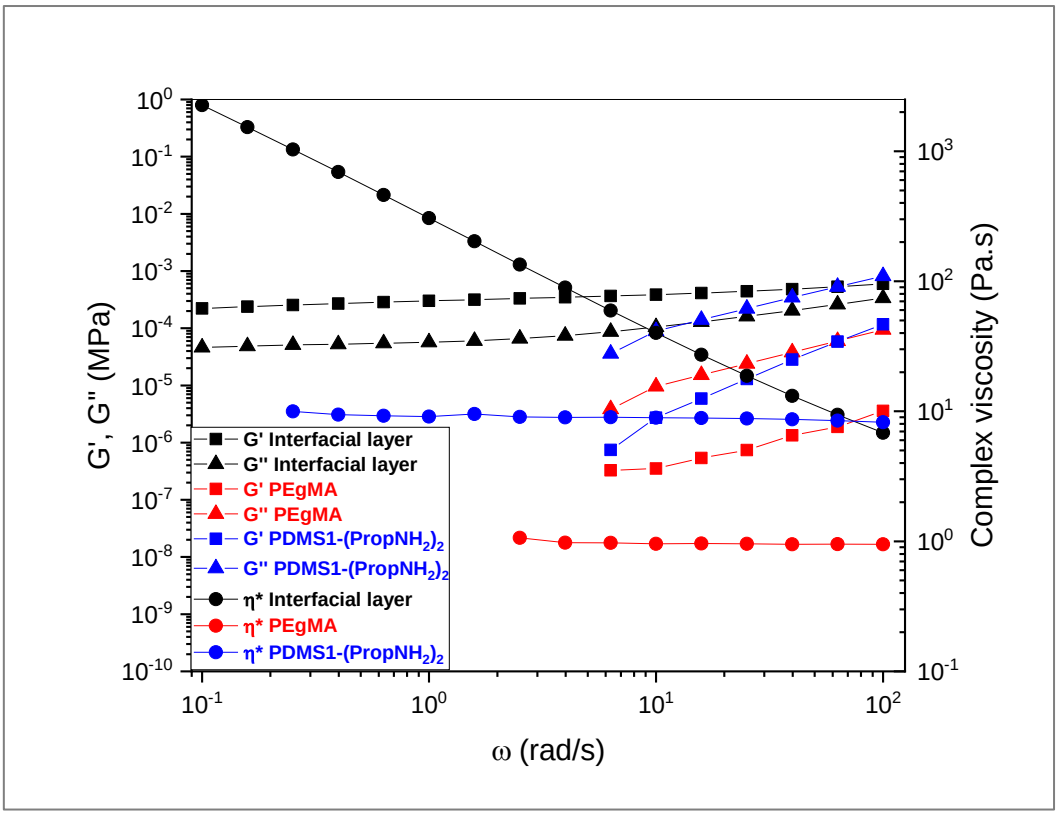

Figure IV-23. Frequency sweep of the interfacial layer (blue), PEgMA (red) and PDMS1-(PropNH$_2$)$_2$ (black) at 140°C.

IV.5.5.2. Dynamic interfacial tension

The variation of the surface/interfacial tension over time is mainly the result of interfacial phenomena such as adsorption or desorption of an entity at the interface, which will lead to a decrease (adsorption) or an increase (desorption) of the surface/interfacial tension. The occurrence of a chemical reaction at the interface leads to the formation of a chemical component that will compatibilise the two phases, consequently decreasing their interfacial tension [63].

Here we measure the evolution of interfacial tension during the time while the drop volume is constant. Figure IV-24 shows the interfacial tension of the reactive and non-reactive polymer systems. For reactive PDMS-(PropNH$_2$)$_2$/PEgMA interfaces, the interfacial tension decreased, tending towards a small value. This is related to the diffusion of short chains towards the interfaces, followed by a chemical reaction. These two processes continue until the interface is saturated through the formation of an interfacial layer (copolymer) responsible for reducing the interfacial tension and enabling the compatibilisation of the two coexisting phases (Figure IV-25). However, after a sufficiently long time, the drop tends to break away from the capillary and change into a non-Laplacian drop. The kinetics of the diffusion/reaction duality became faster after increasing the temperature. Nevertheless, it decreased after increasing the molar mass of PDMS-(PropNH$_2$)$_2$ since the macromolecules became longer. Therefore, the diffusion/reaction might be slower.

On the other hand, the interfacial tension of non-reactive PDMS/PEgMA systems reached an equilibrium value within one minute and then stayed constant. We note that the interfacial tension decreased when the temperature increased, and when the equilibrium state was reached, the drop remained hanging on to the capillary, as opposed to what was observed in PDMS-(PropNH$_2$)$_2$/PEgMA reactive systems.

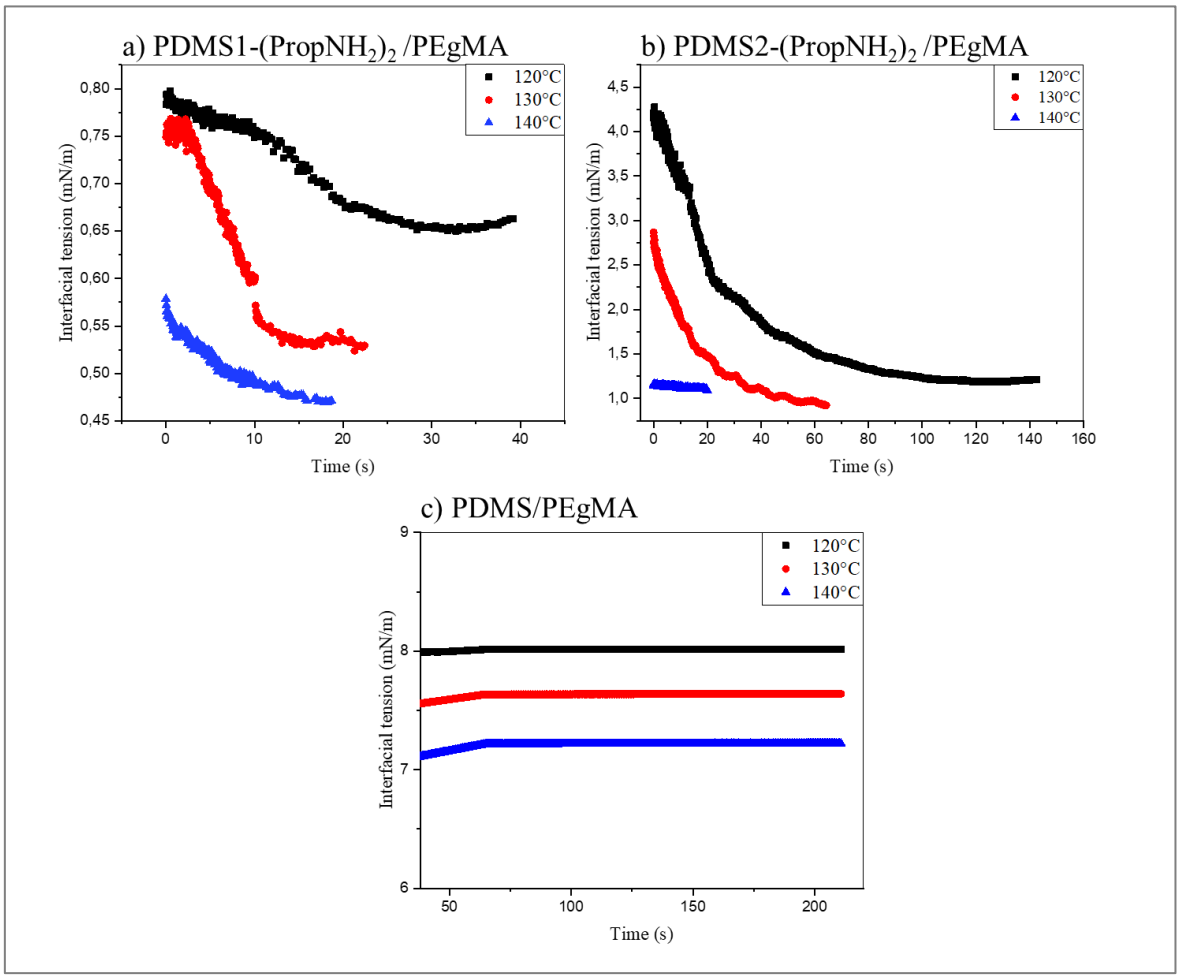

Figure IV-24. Evolution of the dynamic interfacial tension of reactive and non-reactive systems: a) PDMS1-(PropNH$_2$)$_2$/PEgMA, b) PDMS2-(PropNH$_2$)$_2$/PEgMA and c) PDMS/PEgMA at 120, 130 and 140°C.

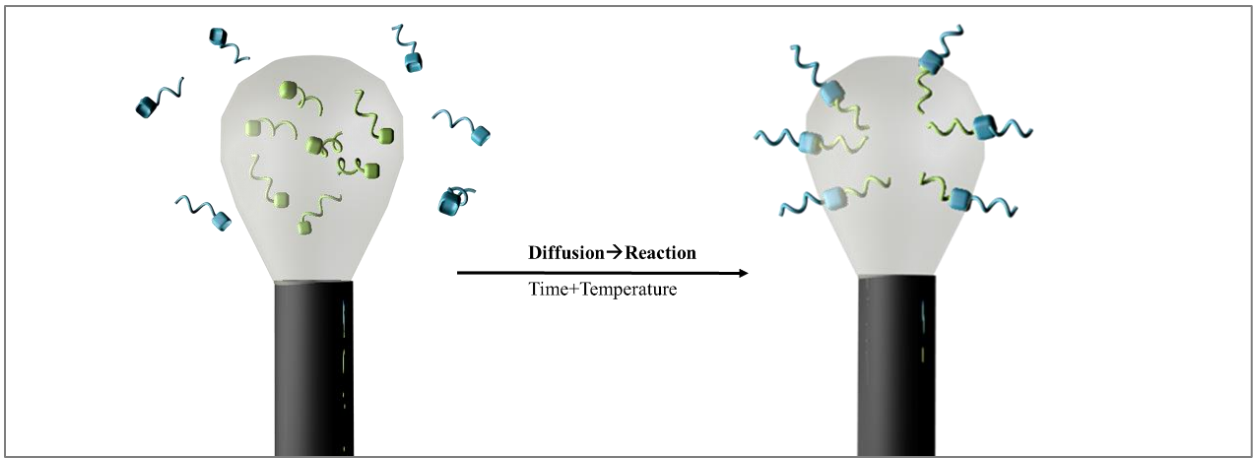

Figure IV-25. Schematic diagram of the diffusion/reaction phenomena at the interface drop/continuous phase.

Measuring interfacial tension to prove the existence of a chemical reaction at the interface has been studied elsewhere. Giustiniani et al. [67] investigated the relationship between the interfacial properties and the stability of poly(ethylene glycol) PEG/MHDS siloxane copolymer emulsions by forming a polymer at the interface to prevent droplet coalescence. They used a PEG-soluble cross-linking agent that diffuses at the interface to react with the MHDS, thereby decreasing the interfacial tension. The polymerisation continues until the interface is saturated and the interfacial tension reaches a constant value. The effect of the concentration of the cross-linking agent on the interfacial tension has also been studied.

Chi et al. [35] studied the kinetics of copolymer formation at the interface between two immiscible polymers (polydimethylsiloxane (PDMS) and polybutadiene (PBd)) using two types of end-functionalised reactive chains (amino-terminated PDMS and carboxyl-terminated PBD). They measured changes in interfacial tension during the reaction and deduced the concentration of the reaction product at the interface by applying the Gibbs adsorption equation, which is justified for an insignificant degree of conversion of reactants in either phase and also when all reactant concentrations remain effectively constant. The variation of copolymer concentration with time was found to obey a single-exponential growth model at low copolymer coverage, indicating first-order reaction kinetics. However, at high PDMS-NH_2 concentrations, the model captured only the initial growth and later deviated from the experimental data at longer times. According to the authors, this deviation may be related to chain-chain interactions that become progressively rate limiting as the interface approaches saturation [35].

IV.6. Conclusions

In this chapter, the focus was on the study of reactive interfaces. Polydimethylsiloxane, aminopropyl terminated and polyethylene-grafted maleic anhydride (PEgMA) with relatively low melt viscosities

were chosen as model molten reactive polymer systems. The effect of molecular weight and temperature on the interfacial reaction kinetics was highlighted. It was shown that the melt viscosity of the reactive blends increased during steady shear flow and reached a plateau when the reaction was finished, while the viscosity of the non-reactive blends remained almost constant. Furthermore, the DSC spectra demonstrated the presence of the reaction by detecting an exothermic peak for reactive systems. However, FTIR spectroscopy was not sensitive enough to prove that the reaction took place, due to the low molar content of the reactive functions in the PEgMA and PDMS-(Prop(NH_2)$_2$) used.

It was clearly evidenced that the increase of the interfacial viscosity was attributed to the reaction at the interface occurring during the interfacial shear solicitations. Interfacial tension measurements also demonstrated that the reaction at the interface was responsible for the decrease in interfacial tension until the drop became detached from the needle.

This work describes an effective approach based on interfacial rheology that could be applied to study the melt reaction at the interface of other molten polymer systems usually encountered in different industrial areas, including twin-screw reactive extrusion, over-moulding or reactive multilayer coextrusion. This would make it possible to predict the interfacial adhesion and possible defects/instabilities during the processing of multiphase polymer blends or multilayer structures.

The main strength of the specific interfacial characterisation tools used in this study was their ability to straightforwardly probe reactive polymer interfaces and investigate the reaction/diffusion phenomena in-situ, which are explorations that long represented a major scientific and technological challenge.

References

[1] M. Yousfi, C. Samuel, J. Soulestin, and M.-F. Lacrampe, "Rheological Considerations in Processing Self-Reinforced Thermoplastic Polymer Nanocomposites: A Review," *Polymers*, vol. 14, no. 3, p. 637, 2022.

[2] G. Yu *et al.*, "Producing Microlayer Pipes and Tubes through Multiplication Coextrusion and Unique Annular Die: Simulation and Experiment," *Industrial & Engineering Chemistry Research*, vol. 60, no. 50, pp. 18408-18420, 2021.

[3] M. Yousfi, J. Soulestin, S. Marcille, and M.-F. Lacrampe, "In-situ nano-fibrillation of poly (butylene succinate-co-adipate) in isosorbide-based polycarbonate matrix. Relationship between rheological parameters and induced morphological and mechanical properties," *Polymer*, vol. 217, p. 123445, 2021.

[4] W. Zhang, Z. Gui, C. Lu, S. Cheng, D. Cai, and Y. Gao, "Improving transparency of incompatible polymer blends by reactive compatibilization," *Materials Letters*, vol. 92, pp. 68-70, 2013.

[5] M. Yousfi, S. Livi, and J. Duchet-Rumeau, "Ionic liquids: A new way for the compatibilization of thermoplastic blends," *Chemical Engineering Journal*, vol. 255, pp. 513-524, 2014, doi: 10.1016/j.cej.2014.06.080.

[6] G. Jiang, H. Wu, and S. Guo, "Reinforcement of adhesion and development of morphology at polymer–polymer interface via reactive compatibilization: A review," *Polymer Engineering & Science*, vol. 50, no. 12, pp. 2273-2286, 2010.

[7] C.-C. Huang and F.-C. Chang, "Reactive compatibilization of polymer blends of poly (butylene terephthalate)(PBT) and polyamide-6, 6 (PA66): 1. Rheological and thermal properties," *Polymer*, vol. 38, no. 9, pp. 2135-2141, 1997.

[8] K. C. Chiou and F. C. Chang, "Reactive compatibilization of polyamide-6 (PA 6)/polybutylene terephthalate (PBT) blends by a multifunctional epoxy resin," *Journal of Polymer Science Part B: Polymer Physics*, vol. 38, no. 1, pp. 23-33, 2000.
[9] K. Lamnawar and A. Maazouz, "Rheology and morphology of multilayer reactive polymers: effect of interfacial area in interdiffusion/reaction phenomena," *Rheologica Acta*, vol. 47, no. 4, pp. 383-397, 2008.
[10] R. Zhao and C. W. Macosko, "Slip at polymer–polymer interfaces: Rheological measurements on coextruded multilayers," *Journal of rheology*, vol. 46, no. 1, pp. 145-167, 2002.
[11] E. Lafranche, S. Macedo, P. Ferreira, and C. I. Martins, "Thin wall injection-overmoulding of polyamide 6/polypropylene multilayer parts: PA6/PP-g-ma interfacial adhesion investigations," *Journal of Applied Polymer Science*, vol. 138, no. 17, p. 50294, 2021.
[12] Q. Wu, C. B. Park, N. Zhou, and W. Zhu, "Effect of temperature on foaming behaviors of homo-and co-polymer polypropylene/polydimethylsiloxane blends with CO2," *Journal of cellular plastics*, vol. 45, no. 4, pp. 303-319, 2009.
[13] W. Peng, Y. Qian, T. Zhou, S. Yang, J. Jin, and G. Li, "Influence of Incorporated Polydimethylsiloxane on Properties of PA66 Fiber and Its Fabric Performance," *Polymers*, vol. 11, no. 11, p. 1735, 2019.
[14] W. Yu, M. Bousmina, and C. Zhou, "Determination of interfacial tension by the retraction method of highly deformed drop," *Rheologica acta*, vol. 43, no. 4, pp. 342-349, 2004.
[15] S. Jose, S. Thomas, I. Aravind, and J. Karger-Kocsis, "Rheology of multiphase polymer blends with and without reactive compatibiliser: Evaluation of interfacial tension using theoretical predictions," *International Journal of Plastics Technology*, vol. 18, no. 2, pp. 223-240, 2014.
[16] P. Xing, M. Bousmina, D. Rodrigue, and M. Kamal, "Critical experimental comparison between five techniques for the determination of interfacial tension in polymer blends: model system of polystyrene/polyamide-6," *Macromolecules*, vol. 33, no. 21, pp. 8020-8034, 2000.
[17] H. Asthana and K. Jayaraman, "Rheology of reactively compatibilized polymer blends with varying extent of interfacial reaction," *Macromolecules*, vol. 32, no. 10, pp. 3412-3419, 1999.
[18] K. Lamnawar, A. Baudouin, and A. Maazouz, "Interdiffusion/reaction at the polymer/polymer interface in multilayer systems probed by linear viscoelasticity coupled to FTIR and NMR measurements," *European Polymer Journal*, vol. 46, no. 7, pp. 1604-1622, 2010.
[19] C. W. Macosko, H. K. Jeon, and T. R. Hoye, "Reactions at polymer–polymer interfaces for blend compatibilization," *Progress in Polymer Science*, vol. 30, no. 8-9, pp. 939-947, 2005.
[20] J. Lei, Y. Gao, Y. Ma, K. Zhao, and F. Du, "Improving the emulsion stability by regulation of dilational rheology properties," *Colloids and Surfaces A: Physicochemical and Engineering Aspects*, vol. 583, p. 123906, 2019.
[21] H. Wang, X. Wei, Y. Du, and D. Wang, "Experimental investigation on the dilatational interfacial rheology of dust-suppressing foam and its effect on foam performance," *Process Safety and Environmental Protection*, vol. 123, pp. 351-357, 2019.
[22] S. Vandebril, J. Vermant, and P. Moldenaers, "Efficiently suppressing coalescence in polymer blends using nanoparticles: role of interfacial rheology," *Soft Matter*, vol. 6, no. 14, pp. 3353-3362, 2010.
[23] S. Vandebril, A. Franck, G. G. Fuller, P. Moldenaers, and J. Vermant, "A double wall-ring geometry for interfacial shear rheometry," *Rheologica Acta*, vol. 49, no. 2, pp. 131-144, 2010.
[24] O. Soo-Gun and J. C. Slattery, "Disk and biconical interfacial viscometers," *Journal of Colloid and Interface Science*, vol. 67, no. 3, pp. 516-525, 1978.
[25] A. Yeung and L. Zhang, "Shear effects in interfacial rheology and their implications on oscillating pendant drop experiments," *Langmuir*, vol. 22, no. 2, pp. 693-701, 2006.
[26] L. A. Pugnaloni, R. Ettelaie, and E. Dickinson, "Brownian dynamics simulation of adsorbed layers of interacting particles subjected to large extensional deformation," *Journal of colloid and interface science*, vol. 287, no. 2, pp. 401-414, 2005.
[27] J. M. Zamora, R. Marquez, A. M. Forgiarini, D. Langevin, and J.-L. Salager, "Interfacial rheology of low interfacial tension systems using a new oscillating spinning drop method," *Journal of colloid and interface science*, vol. 519, pp. 27-37, 2018.

[28] A. Giustiniani, W. Drenckhan, and C. Poulard, "Interfacial tension of reactive, liquid interfaces and its consequences," *Advances in Colloid and Interface Science,* vol. 247, pp. 185-197, 2017.
[29] Y. El Omari, M. Yousfi, J. Duchet-Rumeau, and A. Maazouz, "Interfacial rheology testing of molten polymer systems: Effect of molecular weight and temperature on the interfacial properties," *Polymer Testing,* vol. 101, p. 107280, 2021.
[30] P. Bosch, F. Catalina, T. Corrales, and C. Peinado, "Fluorescent probes for sensing processes in polymers," *Chemistry–A European Journal,* vol. 11, no. 15, pp. 4314-4325, 2005.
[31] M. L. Coote, D. H. Gordon, L. R. Hutchings, R. W. Richards, and R. M. Dalgliesh, "Neutron reflectometry investigation of polymer–polymer reactions at the interface between immiscible polymers," *Polymer,* vol. 44, no. 25, pp. 7689-7700, 2003.
[32] M. Hayashi *et al.*, "Interface between a polysulfone and polyamide as studied by combined neutron reflectivity and small-angle neutron scattering techniques," *Macromolecules,* vol. 33, no. 22, pp. 8375-8387, 2000.
[33] J. S. Schulze, J. J. Cernohous, A. Hirao, T. P. Lodge, and C. W. Macosko, "Reaction kinetics of end-functionalized chains at a polystyrene/poly (methyl methacrylate) interface," *Macromolecules,* vol. 33, no. 4, pp. 1191-1198, 2000.
[34] B. Li *et al.*, "Probing molecular behavior of carbonyl groups at buried nylon/polyolefin interfaces in situ," *Langmuir,* vol. 36, no. 38, pp. 11349-11357, 2020.
[35] C. Chi, Y. Hu, and A. Lips, "Kinetics of interfacial reaction between two polymers studied by interfacial tension measurements," *Macromolecules,* vol. 40, no. 18, pp. 6665-6668, 2007.
[36] A. W. Neumann, R. David, and Y. Zuo, *Applied surface thermodynamics*. CRC press, 2010.
[37] G. H. Fredrickson and S. T. Milner, "Time-dependent reactive coupling at polymer− polymer interfaces," *Macromolecules,* vol. 29, no. 23, pp. 7386-7390, 1996.
[38] A. D. Litmanovich, N. A. Platé, and Y. V. Kudryavtsev, "Reactions in polymer blends: interchain effects and theoretical problems," *Progress in polymer science,* vol. 27, no. 5, pp. 915-970, 2002.
[39] P.-G. de Gennes, "Reptation of a polymer chain in the presence of fixed obstacles," *The journal of chemical physics,* vol. 55, no. 2, pp. 572-579, 1971.
[40] M. Doi and S. Edwards, "Dynamics of concentrated polymer systems. Part 4.—Rheological properties," *Journal of the Chemical Society, Faraday Transactions 2: Molecular and Chemical Physics,* vol. 75, pp. 38-54, 1979.
[41] M. Bousmina, H. Qiu, M. Grmela, and J. Klemberg-Sapieha, "Diffusion at polymer/polymer interfaces probed by rheological tools," *Macromolecules,* vol. 31, no. 23, pp. 8273-8280, 1998.
[42] G. Agrawal *et al.*, "Interdiffusion of polymers across interfaces," *Journal of Polymer Science Part B: Polymer Physics,* vol. 34, no. 17, pp. 2919-2940, 1996.
[43] C. Hu, X. Chen, J. Chen, W. Zhang, and M. Q. Zhang, "Observation of mutual diffusion of macromolecules in PS/PMMA binary films by confocal Raman microscopy," *Soft Matter,* vol. 8, no. 17, pp. 4780-4787, 2012.
[44] H. Qiu and M. Bousmina, "New technique allowing the quantification of diffusion at polymer/polymer interfaces using rheological analysis: Theoretical and experimental results," *Journal of Rheology,* vol. 43, no. 3, pp. 551-568, 1999.
[45] H. Qiu and M. Bousmina, "Determination of mutual diffusion coefficients at nonsymmetric polymer/polymer interfaces from rheometry," *Macromolecules,* vol. 33, no. 17, pp. 6588-6594, 2000.
[46] R. J. Composto, J. W. Mayer, E. J. Kramer, and D. M. White, "Fast mutual diffusion in polymer blends," *Physical review letters,* vol. 57, no. 11, p. 1312, 1986.
[47] T. D. Jones, J. S. Schulze, C. W. Macosko, and T. P. Lodge, "Effect of thermodynamic interactions on reactions at polymer/polymer interfaces," *Macromolecules,* vol. 36, no. 19, pp. 7212-7219, 2003.
[48] B. O'shaughnessy and U. Sawhney, "Polymer reaction kinetics at interfaces," *Physical review letters,* vol. 76, no. 18, p. 3444, 1996.

[49] B. O'Shaughnessy and D. Vavylonis, "Reactive polymer interfaces: how reaction kinetics depend on reactivity and density of chemical groups," *Macromolecules,* vol. 32, no. 6, pp. 1785-1796, 1999.
[50] N. Dharmarajan, S. Datta, G. Ver Strate, and L. Ban, "Compatibilized polymer blends of isotactic polypropylene and styrene—maleic anhydride copolymer," *Polymer,* vol. 36, no. 20, pp. 3849-3861, 1995.
[51] C. Scott and C. Macosko, "Model experiments for the interfacial reaction between polymers during reactive polymer blending," *Journal of Polymer Science Part B: Polymer Physics,* vol. 32, no. 2, pp. 205-213, 1994.
[52] H. K. Jeon, J. Zhang, and C. W. Macosko, "Premade vs. reactively formed compatibilizers for PMMA/PS melt blends," *Polymer,* vol. 46, no. 26, pp. 12422-12429, 2005.
[53] S. J. Park, B. K. Kim, and H. M. Jeong, "Morphological, thermal and rheological properties of the blends polypropylene/nylon-6, polypropylene/nylon-6/(maleic anhydride-g-polypropylene) and (maleic anhydride-g-polypropylene)/nylon-6," *European polymer journal,* vol. 26, no. 2, pp. 131-136, 1990.
[54] Q. W. Lu, C. Macosko, and J. Horrion, "Melt amination of polypropylenes," *Journal of Polymer Science Part A: Polymer Chemistry,* vol. 43, no. 18, pp. 4217-4232, 2005.
[55] L. M. Croll and H. D. Stöver, "Formation of Tectocapsules by Assembly and Cross-linking of Poly (divinylbenzene-a lt-maleic anhydride) Spheres at the Oil− Water Interface," *Langmuir,* vol. 19, no. 14, pp. 5918-5922, 2003.
[56] U. Schmidt, S. Zschoche, and C. Werner, "Modification of poly (octadecene-alt-maleic anhydride) films by reaction with functional amines," *Journal of applied polymer science,* vol. 87, no. 8, pp. 1255-1266, 2003.
[57] N. McManus, S. H. Zhu, C. Tzoganakis, and A. Penlidis, "Grafting of ethylene–ethyl acrylate–maleic anhydride terpolymer with amino-terminated polydimethylsiloxane during reactive processing," *Journal of applied polymer science,* vol. 101, no. 6, pp. 4230-4237, 2006.
[58] T. Hameed, D. K. Potter, and E. Takacs, "Reactions of low molecular weight highly functionalized maleic anhydride grafted polyethylene with polyetherdiamines," *Journal of applied polymer science,* vol. 116, no. 4, pp. 2285-2297, 2010.
[59] M. Fan *et al.*, "Facile synthesis and applications of polypropylene/polydimethylsiloxane graft copolymer," *Polymers for Advanced Technologies,* vol. 30, no. 5, pp. 1226-1233, 2019.
[60] Fan Xie; Chixing Zhou; Wei Yu; Defeng Wu. Study on the reaction kinetics between PBT and epoxy by a novel rheological method, European Polymer Journal, 41(9), 2171–2175, 2005.
[61] Khalid Lamnawar; Anne Baudouin; Abderrahim Maazouz. Interdiffusion/reaction at the polymer/polymer interface in multilayer systems probed by linear viscoelasticity coupled to FTIR and NMR measurements. European Polymer Journal, 2010.
[62] Z. Song and W. E. Baker, "Chemical reactions and reactivity of primary, secondary, and tertiary diamines with acid functionalized polymers," *Journal of Polymer Science Part A: Polymer Chemistry,* vol. 30, no. 8, pp. 1589-1600, 1992.
[63] J. Nasrollah Gavgani, F. Goharpey, S. Velankar, and R. Foudazi, "Suppressing droplet coalescence and aggregation in immiscible homopolymer blends by interfacially cross-linked compatibilizers," *Journal of Rheology,* vol. 62, no. 5, pp. 1217-1231, 2018.
[64] S. Pandit *et al.*, "The exo-polysaccharide component of extracellular matrix is essential for the viscoelastic properties of Bacillus subtilis biofilms," *International journal of molecular sciences,* vol. 21, no. 18, p. 6755, 2020.
[65] K. Weissenberg, "A continuum theory of rhelogical phenomena," 1947.
[66] C. L. DeLeo and S. S. Velankar, "Morphology and rheology of compatibilized polymer blends: Diblock compatibilizers vs crosslinked reactive compatibilizers," *Journal of Rheology,* vol. 52, no. 6, pp. 1385-1404, 2008.
[67] A. Giustiniani, P. Guégan, M. Marchand, C. Poulard, and W. Drenckhan, "Generation of Silicone Poly-HIPEs with Controlled Pore Sizes via Reactive Emulsion Stabilization," *Macromolecular rapid communications,* vol. 37, no. 18, pp. 1527-1532, 2016.

Chapter V. Conclusions and Perspectives

The present thesis project has studied polymer/polymer interfaces in the molten state using interfacial rheology, a direct method for probing the interfaces and surfaces of multiphase polymeric systems. This work focused on free surfaces/interfaces with and without an interfacial chemical reaction.

In the first chapter, a general overview was given. The historical background and the theoretical aspects of interfacial rheology were discussed in detail. As in bulk rheology, an interface can be deformed, either by shear force, in which the interfacial area remains constant, or by elongation, in which the interfacial area changes. Interfacial shear and dilational devices were described, and the possibility of their use on molten polymer systems was critiqued. Performing direct measurements on polymer melts requires careful precaution. Thus, it is important to quantify some primordial numbers such as the Boussinesq number, which represents the ratio between interfacial and bulk effects; the capillary number, which is a ratio of interfacial and viscous effects; and the Weber number, which is the ratio of interfacial and inertial forces. Particular modifications/adaptations to the actual devices need to be carried out. A heating system is essential to broaden the range of polymers studied, as well as robust shear geometry to deform viscous polymer interfaces. In addition, the use of lightweight fixtures is essential to increase their sensitivity while performing experiments within the limits of current rheometers. The methodology of correcting the contribution of the subphases from the apparent interfacial data was also presented. Some pioneering works were cited for each technique, which made it possible to position this project in the context of the literature and demonstrate its originality.

In the second part of this work, the interfacial shear rheology of molten polymer systems was examined. PIB/PDMS and PCL/PEG systems were studied using a DWR and a novel interfacial setup. The measurements with the DWR fixture showed a limiting subphase viscosity range (around 3 Pa.s) when the interfaces were probed at a medium/high shear rate. Otherwise, due to the fragility of the geometry, mechanical deformation of the ring could occur. Because of the high viscosity of the polymers, the bicone was chosen to investigate high-viscosity polymer surfaces and interfaces. However, this geometry is not sensitive enough to probe interfaces. Therefore, the stainless steel-based bicone was replaced by a lighter titanium bicone, which reduced its inertia. Thereafter, the interfacial rheology cell was equipped with an actively heated Peltier-temperature-controlled hood to perform interfacial rheology measurements up to 200 °C. The effects of molecular weight and temperature were highlighted. The measured apparent interfacial shear properties in both oscillatory and steady flow modes were corrected to deduce the contribution of the bulk subphases during the treatment of

the numerical data. As the studied surfaces and interfaces are free (no mineral or organic compound is placed at the surface or interface), we found that the interfacial properties depend on the bulk properties (molar weight and temperature). In the case of surfaces, purely viscous behaviour was noticed. The corrected surface viscosity increased with the bulk viscosity. As for the interfacial investigation of model PDMS/PIB systems, the interface was purely viscous (Newtonian behaviour). It was observed that at a constant temperature, the more the viscosity of the subphases increased, the more the interfacial viscosity increased. For low-viscosity polymer systems, the apparent and corrected interfacial moduli (and the interfacial viscosity) decreased when the temperature increased. However, when the interfaces were formed from a highly viscous fluid medium, the corrected interfacial viscosity followed the opposite trend, with a rise in temperature indicating the occurrence of a diffusion phenomenon across the interface. Coupling interfacial shear rheology with the modelling of the Hansen solubility parameters and the interfacial tension measurement allowed us to demonstrate the presence of an interdiffusion (migration to the interface) of the short chain subphases (PIB phase) starting at a specific molecular weight. These observations were consistent with various literature reports.

Chapter III was dedicated to studying the dilational interfacial properties of PIB/PDMS systems using the oscillating drop method. First, the interfacial properties in both oscillatory and static drop experiments were carefully corrected, considering the inertial and viscous effects of the coexisting phases by evaluating the capillary and Weber numbers. The influence of molecular weight and temperature on the interfacial rheological responses was particularly examined. The more the viscosity of the bulk increased, the more the interfacial tension and dilational modulus increased. In addition to these measurements, optical microscopy results demonstrated the interdiffusion phenomena from the PIB to the PDMS across the interface by flowing the diameter temporal evolution of an injected PIB drop within a PDMS matrix.

Second, the surface and interfacial relaxation tests were performed using a square pulse relaxation method. The empirical Kohlrausch formula was used to fit experimental data showing the evolution of surface or interfacial tension with time. It was found that the evolution of the relaxation time with the temperature followed an Arrhenius behaviour. A comparison with capillary breakup extensional rheometry was also investigated. By fitting the variation in filament diameter over time, elongational relaxation times and apparent extensional viscosities were extracted. It was concluded that the overall values and tendencies with the viscosity and temperature of relaxation times (from Caber tests) were similar to those obtained with the pulse method.

Finally, using interfacial shear rheology, we focused on the correlation between shear and dilational surface rheology, and a direct link between shear surface viscosities and elongational relaxation times was evidenced based on the Trouton model.

In the last chapter, reactive interfaces were studied. Interfacial shear rheology was used to directly probe the reaction at the interface between maleic anhydride-grafted polyethylene (PEgMA) and aminopropyl-terminated poly(dimethylsiloxane) (PDMS-(PropNH_2)$_2$) with a low content of the reactive chemical functions. First, the extent of reaction was checked using differential scanning calorimetry (DSC) (by detecting the exothermic peak) and dynamic rheology coupled with fast-scan FTIR spectroscopy (by following the evolution of the viscosity as well as the intensity of the characteristic IR peaks of the reactive chemical functions). However, FTIR spectroscopy was not sensitive enough to follow the reaction due to the low concentration of reactive functions. Then the interfacial reaction was investigated using the biconical setup, as was the time evolution of the interfacial tension using the pendant drop method (by following the variation of the interfacial shear viscosity and interfacial tension with time). From the results, it was highlighted that the reaction kinetics was controlled by the diffusion process, because the amine/anhydride reaction is known to be fast. Additionally, it was evidenced that the molecular weight of the aminated PDMS and the temperature of the medium affected the rate of melt reaction at the interface.

Perspectives

This work could be transposed to other applications in which two polymers meet and create an interface (polymer blends, overmolded polymer parts, multilayers, etc.). Therefore, many projects will be studied in the near future.

- Polymer foaming

Studying surface rheology could be useful to understand the stability of polymer foams. Interfacial tension is another parameter that we should control to achieve a good foaming morphology of molten polymers. The foaming of poly (Lactic Acid) (PLA) in supercritical CO_2 and a thermodynamic approach will be investigated. The modified PLA using a chain extender agent, as well as the reactivity, will be followed using tensiometry and interfacial shear rheology. Then, the effect of matrix viscosity, pressure and temperature on the interfacial tension of a PLA/scCO_2 systems will be investigated. This project is in progress, and it will be the subject of an upcoming publication.

- Stability of Pickering emulsions

The stability of oil/water emulsions using polymer particles is another research project under way in collaboration with the LAGEPP laboratory of Claude Bernard Lyon 1 University.

- Ionic liquid / polymer interactions at the interface

Recently, it has been proven through various studies carried out at the IMP@INSA laboratory that ionic liquids (ILs) could be used as a structuring agent, compatibilising agent or reactive agent in different polymer matrices (thermoplastics and thermosetting). The interfacial

rheology tools developed in this thesis can be applied to these particular multiphase polymer systems to probe the ionic interactions at the interfaces between polymers and ILs.

FOLIO ADMINISTRATIF

THESE DE L'INSA LYON, MEMBRE DE L'UNIVERSITE DE LYON

NOM : EL OMARI DATE de SOUTENANCE : 02/12/2022

Prénom: Younes

TITRE: **Interfacial rheology of polymers in the molten state/ experimental and fundamental aspects**

NATURE : Doctorat Numéro d'ordre : 2022LYSEI0109

Ecole doctorale : ED34

Spécialité : Matériaux

RESUME :

Les travaux de cette thèse portent sur la rhéologie interfaciale en cisaillement et en dilatation/compression de systèmes polymères. Dans un premier temps, notre choix a porté sur l'étude de systèmes modèles à base de PIB (polyisobutylene) et PDMS poly (dimethylsiloxane). Ces polymères présentent l'avantage d'être liquides à température ambiante. Les propriétés de surface et d'interfaces ont été sondées à l'aide d'une nouvelle cellule interfaciale développée pendant ce projet. Elle présente l'avantage relatif de réaliser des mesures à des températures élevées pouvant atteindre 200°C. L'effet de la masse molaire et de la température sur les propriétés interfaciales ont été étudiées selon les régimes, permanent et oscillatoire. Ces études ont été transposées ensuite sur des polymères semi- cristallins fondus tels que le PEG poly (éthylène glycol) et le PCL poly(caprolactone). Dans un deuxième temps, nous avons étudié et analysé les propriétés rhéologiques interfaciales en élongation des systèmes modèles, au moyen de la rhéologie interfaciale en dilatation / compression en utilisant la méthode de la goutte pendante oscillante. De plus, la relaxation des surfaces / interfaces a été sondée par la méthode de « pulse », d'une part, et en utilisant un rhéomètre extensionnel à rupture capillaire (CaBER), d'autre part. Les grandeurs rhéologiques interfaciales en élongation/compression des systèmes modèles de différentes masses molaires et sous différentes températures ont été obtenues. Elles ont ensuite été comparées à celles mesurées en cisaillement et analysées selon le rapport de Trouton interfacial. Dans la dernière partie de la thèse, nous avons montré que la rhéologie interfaciale en cisaillement permet de sonder les réactions chimiques aux interfaces d'un système polymère fondu : PEgMA, Poly (Ethylène Greffé Anhydride Maléique) / PDMS-$(PropNH_2)_2$, Poly (DiMethyl Siloxane, terminé Amino Propyle). En outre, l'étude de la tension interfaciale dynamique a permis le suivi de la cinétique de la réaction interfaciale des systèmes réactifs de différentes masses molaires et à différentes températures. Enfin les études de rhéologie interfaciale s'avèrent très pertinentes pour sonder *in-situ* les interfaces et/ou interphases de systèmes polymères liquides. Les méthodologies ainsi établies et utilisées sont très innovantes et font sauter des verrous scientifiques et technologiques majeurs.

MOTS-CLÉS : Surface, interface, rhéologie interfaciale, bicone, goutte pendante oscillante, CaBER.

Laboratoire de recherche : Ingénierie des matériaux polymères IMP UMR 5223

Directeur de thèse : Pr. MAAZOUZ Abderrahim

Président de jury :

Composition du jury :

Dr. Nadia El Kissi (Présidente de Jury) ; Dr. Philippe Marchal (Examinateur) ; Pr. Lazhar Benyahia (Rapporteur) ; Pr. Patrick Anderson (Rapporteur) ; Prof. Abderrahim Maazouz (Directeur de Thèse) ; Pr. Jannick Duchet-Rumeau (Co-Directrice de thèse) ; Dr. Mohamed Yousfi (Co-Encadrant)